

Pretreatment of Lignocellulosic Biomass Using Novel Methodologies

Muhammad Nauman Ahmad Khan

Doctor of Philosophy

ASTON UNIVERSITY

September 2024

©Muhammad Nauman Ahmad Khan, 2024

Muhammad Nauman Ahmad Khan asserts his moral right to be identified as the author of this thesis

This copy of the thesis has been supplied on the condition that anyone who consults it is understood to recognise that its copyright belongs to its author and that no quotation from the thesis and no information derived from it may be published without appropriate permission or acknowledgement.

Abstract

Lignocellulose fractionation is a critical step in biorefineries to convert cellulose, hemicellulose, and lignin into sustainable fuels and chemicals. Conventional acid hydrolysis causes equipment corrosion, acid recovery challenges, excessive wastewater, and toxic by-products. To overcome this, solid acid ion exchange resins were investigated for the fractionation of lignocellulosic feedstocks in water and in ionic liquids. Characterisation of raw materials and pulp fractions via thermogravimetric analysis, X-ray diffraction, and other analytical techniques was used to evaluate its efficiency.

After 2 hours at 110 °C in water, the highest cellulose retention (53 to 55 wt.%) and hemicellulose reduction (23 to 18 wt.%) for *miscanthus x giganteus* (MxG) was observed with the commercial resin Amberlyst 70 (IER70) at a 1:8 mass ratio resin to biomass. When compared to equivalent proton concentrations of HCl and H₂SO₄, IER70 transformed better crystalline cellulose to amorphous forms achieving the largest changes in cellulose thermal degradation (10 °C).

In the presence of triethylammonium hydrogen sulphate (IL-TS), IER70 enhanced the crystalline cellulose transformation to amorphous cellulose, reducing the cellulose peak degradation temperature from 269 °C to 257 °C. When compared to other six commercial ion exchange resins, IER70 overperformed them, due to its higher acid strength (117 kJ mol⁻¹) and thermo-mechanical stability.

The combination of IER70 with IL-TS was tested using three different feedstocks: MxG (high cellulose), brewery spent grains (low hemicellulose) and pine bark (high lignin). It was found this combination is most efficient for cellulose-rich biomasses, due to its stronger cellulose depolymerisation effect.

In conclusion, IER70 enhanced biomass hydrolysis and fractionation in the presence of water and ionic liquids. Its solid form can reduce conventional hydrolysis issues (equipment corrosion and complex neutralisation and recovery steps). Thus, IER70 can enhance the pretreatment efficiency and enhance the feasibility of producing renewable chemicals and fuels from lignocellulosic biomass.

Keywords: Lignocellulosic biomass, homogenous catalysis, heterogeneous catalysis, ionic exchange resins, ionic liquids

Acknowledgements

I wanted to convey my gratitude to my supervisor, Dr Marta Granollers Mesa, for her continuous direction and substantial encouragement during my PhD studies at the Energy and Bioproducts Research Institute (EBRI) at Aston University. I want to thank my co-supervisors, Dr Paula Blanco-Sanchez and Dr Amin Osatiashtiani, for their assistance and guidance during my research. I am grateful to former and current colleagues at EBRI for their support and collaborative opportunities that have enriched my research knowledge, particularly to Dr Alfred F. Castane, Dr Daniel J. Nowakowski, and Dr Jude A. Onwudilli.

I want to express my gratitude to Dr Scott Banks and Dr Jinesh C. Manayil for their time, guidance, and support in training me in various analytical methods, which enabled me to complete my experimental work.

I want to express my gratitude to the College of Engineering and Physical Sciences at Aston University for my studentship, which enabled me to conduct this research at the Energy and Bioproducts Research Institute (EBRI), and for the additional assistance from the COVID-19 Hardship Fund to mitigate delays caused by the University closure and varying restrictions over the past 18 months.

Lastly, I would like to express my gratitude to my mentor, Professor Dr Yassir Taha Makkawi, for all the support and encouragement he gave me when I was a student at various higher education institutions. His knowledge and experience have been instrumental in developing my enthusiasm for specialising as a chemical engineer in the field of bioenergy.

Table of Contents

Abstract	2
Acknowledgements	3
Table of Contents	4
List of Tables	8
List of Figures	11
List of Equations	15
List of Abbreviations	16
1. Introduction	18
1.1. Biorefinery Concept	19
1.2. Lignocellulosic biomass	20
1.2.1. <i>Cellulose</i>	22
1.2.2. <i>Hemicellulose</i>	23
1.2.3. <i>Lignin</i>	24
1.3. Lignocellulosic Biomass Pretreatment Methodologies	27
1.4. Chemical Pretreatment Methods	29
1.4.1. <i>Acid Pretreatment</i>	30
1.4.2. <i>Alkali Pretreatment</i>	31
1.4.3. <i>Organo-Solv</i>	33
1.4.4. <i>Solid Acid catalysts</i>	34
1.5. Advanced Pretreatment Methods using Ionic Liquids	40
1.5.1. <i>Some classifications of ILs</i>	40
1.5.2. <i>ILs for Biomass Pretreatment</i>	41
1.6. Mains findings, main research gaps and research objectives	46
2. Material and Methods	48
2.1. Chemicals	49
2.1.1. <i>Biomass feedstock</i>	49
2.1.2. <i>Ion Exchange Resins (IERS)</i>	49
2.1.3. <i>Ionic Liquids (ILs)</i>	49
2.1.4. <i>Synthesis of Fibre Detergent Solutions</i>	49
2.1.5. <i>Feedstock preparation</i>	49
2.1.6. <i>Miscanthus x giganteus grass (Feedstock 1)</i>	50
2.1.7. <i>Pine Bark Wood (Feedstock 2)</i>	50

2.1.8. <i>Brewery Spent Grains (Feedstock 3)</i>	50
2.2. <i>Characterisation of IERs</i>	50
2.2.1. <i>Acid Capacity</i>	50
2.2.2. <i>Swelling Degree</i>	50
2.3. <i>Synthesis and Characterisation of Ionic Liquids (IL)</i>	51
2.3.1. <i>Synthesis of Triethylamine hydrogen sulphate [TEA][HSO₄] (TS)</i>	51
2.3.2. <i>Synthesis of Triethylamine acetate [TEA][OAc] (TA)</i>	51
2.3.3. <i>Water Content</i>	52
2.4. <i>Feedstock and Pulp Characterisation</i>	53
2.4.1. <i>Compositional analysis</i>	53
2.4.2. <i>Thermogravimetric Analysis (TGA) and Proximate Analysis</i>	53
2.4.3. <i>Ultimate Analysis and Higher Heating Value (HHV)</i>	55
2.4.4. <i>Attenuated Total Reflectance-Fourier Transformation Infrared Spectroscopy (ATR-FTIR)</i>	57
2.4.5. <i>X-ray Diffraction (XRD)</i>	58
2.4.6. <i>Scanning Electron Microscopy-Energy Dispersive X-ray (SEM-EDX)</i>	60
2.5. <i>Experimental setup for reaction and purification</i>	60
2.5.1. <i>Reaction set-up and procedure</i>	60
2.5.2. <i>Product Washing</i>	61
3. Evaluation of Ionic Exchange Resins for Acid Hydrolysis	63
3.1. <i>Introduction</i>	64
3.2. <i>Effect of Ion Exchange Loading on Acid Hydrolysis</i>	66
3.2.1. <i>Compositional-Proximate-Ultimate analyses</i>	66
3.2.2. <i>Thermogravimetric analysis (TGA)</i>	69
3.2.3. <i>X-ray Diffraction (XRD)</i>	73
3.2.4. <i>Attenuated Total Reflection Fourier Transformation Infrared (ATR-FTIR) Spectroscopy</i>	74
3.3. <i>Comparison of hydrolysis with solid IERs and mineral acids</i>	78
3.3.1. <i>Compositional-Proximate analyses</i>	78
3.3.2. <i>Thermogravimetric analysis (TGA)</i>	79
3.3.3. <i>X-ray Diffraction (XRD)</i>	82
3.3.4. <i>Attenuated Total Reflection Fourier Transformation Infrared (ATR-FTIR) Spectroscopy</i>	83
3.4. <i>Conclusions</i>	86
4. Evaluation of Ionic Exchange Resin and Ionic Liquid mixtures for lignocellulosic biomass fractionation	87
4.1. <i>Introduction</i>	88
4.2. <i>Preliminary experiments of IL (TS) + IER70 using mesh baskets</i>	89

4.2.1. Scanning Electron Microscopy-Energy Dispersive X-Ray (SEM-EDX).....	89
4.3. Ionic liquid system (TA) with and without IER70 for MIS16.....	91
4.3.1. Proximate and Ultimate analyses	91
4.3.2. Thermogravimetric analysis (TGA)	93
4.3.3. X-ray Diffraction (XRD).....	94
4.3.4. Attenuated Total Reflection Fourier Transformation Infrared (ATR-FTIR) Spectroscopy.....	96
4.4. Ionic liquid system (TS) with and without IER70 for MIS16.....	98
4.4.1. Proximate and ultimate analyses	98
4.4.2. Thermogravimetric analysis (TGA)	100
4.4.3. X-ray Diffraction (XRD).....	102
4.4.4. Attenuated Total Reflection Fourier Transformation Infrared (ATR-FTIR) Spectroscopy.....	104
4.5. Conclusions	108
5. Evaluation of triethyl ammonium hydrogen sulphate with different Ionic Exchange Resins and lignocellulosic feedstocks	110
5.1. Introduction	111
5.2. Ionic Liquid TS80 with different Ion Exchange Resins	112
5.2.1. Proximate and Ultimate analyses	112
5.2.2. Thermogravimetric analysis (TGA)	114
5.2.3. X-ray Diffraction (XRD).....	117
5.2.4. Attenuated Total Reflection Fourier Transformation Infrared (ATR-FTIR) Spectroscopy.....	119
5.3. Comparison of Lignocellulosic Materials	122
5.3.1. Proximate and Ultimate analyses	122
5.3.2. Thermogravimetric analysis (TGA)	123
5.3.3. X-ray Diffraction (XRD).....	125
5.3.4. Attenuated Total Reflection Fourier Transformation Infrared (ATR-FTIR) Spectroscopy.....	127
5.4. Effect of TS80 and IER70 for different lignocellulosic materials (MIS48, BSG48 and PB48)	128
5.4.1. Proximate and ultimate analyses	128
5.4.2. Thermogravimetric analysis (TGA)	130
5.4.3. X-ray Diffraction (XRD).....	132
5.4.4. Attenuated Total Reflection Fourier Transformation Infrared (ATR-FTIR) Spectroscopy.....	134
5.5. Conclusions	137
6. Conclusions and Recommendations for Future Work	139
6.1. Conclusions	140
6.2. Recommendations for Future Work.....	141
References	143

Appendices	179
Appendix 1 (Literature Review)	180
Appendix 2 (Material and Methods)	187
Appendix 3 (Evaluation of Ionic Exchange Resins for Acid Hydrolysis)	189
Appendix 4 (Evaluation of Ionic Exchange Resin and Ionic Liquid mixtures for lignocellulosic biomass fractionation)	197
Appendix 5 (Evaluation of Triethyl ammonium hydrogen sulphate with different Ionic Exchange Resins and Lignocellulosic Feedstocks)	202

List of Tables

Table 1.1. Chemical composition of different lignocellulosic biomasses [14,16–19].	21
Table 1.2. Lignocellulosic Biomass pretreatment technologies with different methodologies [57,58].	28
Table 1.3. Pretreatment methods and related advantages, limitations, and disadvantages [53,59–64].	30
Table 1.4. Classification of Acidic catalysts [70].	31
Table 1.5. Comparison of different alkaline pretreatment [93].	32
Table 1.6. Comparison of catalytical properties and activities of solid acid catalyst for hydrolysis.	34
Table 3.1. Summary of nomenclature for samples in chapter 3.	65
Table 3.2. Chemical composition (wt.%) of raw material and pretreated pulp.	66
Table 3.3. Proximate analysis (wt.%) of raw material and pretreated pulp.	67
Table 3.4. Ultimate analysis (wt.%) of raw material and hydrolysed pulp.	68
Table 3.5. Crystallinity Index (<i>CrI</i>) and crystallite size of untreated MIS48 and pretreated pulp.	74
Table 3.6. Functional groups of organic compounds identified in FTIR with corresponding absorption ranges [247].	75
Table 3.7. Chemical composition (wt.%) of biomass (MIS48) and pulp after acid hydrolysis IER35, IER70 and mineral acids.	78
Table 3.8. Proximate analysis (wt.%) of MIS48 and pulps obtained from after acid hydrolysis using IERs and equivalent proton concentration of mineral acids.	79
Table 3.9. Crystallinity Index (<i>CrI</i>) and crystallite size of pulp.	83
Table 4.1. Summary of nomenclature for samples in chapter 4.	89
Table 4.2. SEM-EDX elemental analysis of M48 treated with IL-TS (60 wt.%) in the absence or presence of two baskets of IER70. ND = Not detected.	90
Table 4.3. Proximate analysis (wt.%) of raw material (MIS16) and pulp treated with two concentrations of IL-TA (40 and 80 wt.%) and the absence or presence of 0.25 g of IER70.	92
Table 4.4. Crystallinity Index (<i>CrI</i>) and crystallite size of untreated MIS16 and pretreated pulp.	96
Table 4.5. Proximate analysis (wt.%) of raw material (MIS16) and pulp from IL-TS-IER70 treatment with two concentrations of TS (40 and 80wt.%) and the absence or presence of 0.25 g of IER70.	98
Table 4.6. Ultimate analysis (wt.%) of raw material (MIS16) and the pretreated pulp for the IL-TS-IER70 system.	99
Table 4.7. <i>CrI</i> , the crystallite size of untreated MIS16, and pulp with IL-TS-IER70 at different IL concentrations with and without IER70.	104
Table 4.8. Relative crystallinity index (Relative <i>CrI</i>) and lateral order index (LOI) of untreated MIS48 and pretreated pulp.	106

Table 5.1. Summary of terminologies for samples.....	112
Table 5.2. Proximate analysis (wt.%) of raw material (MIS48) and pulp for TS80 with different IERs.	113
Table 5.3. Ultimate analysis (wt.%) of raw material (MIS48) and pulp for TS80 with different IERs..	113
Table 5.4. Crystallinity index (<i>Crl</i>) and crystallite size of pulp treated with TS80 and different IERs.	119
Table 5.5. Proximate analysis (wt.%) of different raw materials.....	123
Table 5.6. Ultimate analysis (wt.%) of different raw materials.....	123
Table 5.7. Crystallinity Index (<i>Crl</i>) and crystallite size for different raw materials.	127
Table 5.8. Proximate analysis (wt.%) of raw materials after TS80-IER70 treatment.	129
Table 5.9. Ultimate analysis (wt.%) of raw materials after TS80-IER70 treatment.	130
Table 5.10. <i>Crl</i> , crystallite size for different raw materials (MIS48, BSG48, PB48), and pulp after TS80- IER70 treatment.....	134
Table A1.1. Principles of Green Chemistry [6].....	180
Table A1.2. Proximate analysis for Miscanthus and Spent Grains [17–19,277,283,436–440].	184
Table A1.3. Elemental analysis for miscanthus and Spent Grain [18,19,277,283,285,437–441].	184
Table A1.4. Literature on the use of different IL for different lignocellulosic materials. ND: Not defined in the paper, H: High, M: Medium, L: Low, and V: Vary.....	186
Table A2.1. Physiochemical properties of macro-reticular ionic exchange resins [393,461–463].	187
Table A2.2. ATR-FTIR operational parameters	187
Table A2.3. XRD operational parameters.....	188
Table A3.1. Ultimate analysis for IER70 fresh, ethanol washed-dry, and after pretreatment.	189
Table A3.2. Higher heating value (HHV) of raw material and pretreated pulp.....	189
Table A3.3. pH of 20 mL Deionize water for different number of baskets.	189
Table A3.4. TGA-DTG for raw material-pulp-treated IER under an inert atmosphere.	191
Table A3.5. TGA-DTG for raw material-pulp treated IER under oxidative atmosphere.	191
Table A3.6. Crystallinity Index (<i>Crl</i>) using area deconvolution and peak fit values.	192
Table A3.7. ATR-FTIR spectral wavenumber and band assignment.....	193
Table A3.8. Crystallinity Index (<i>Crl</i>) using area deconvolution and peak fit values.	193
Table A4.1. Ultimate analysis (wt.%) of raw material (MIS16) and pulp for IL-TA-IER70.....	197
Table A4.2. TGA-DTG peak temperatures-mass loss for raw material-pulp treated IL-TA-IER70 under inert conditions.....	199
Table A4.3. TGA-DTG peak temperatures-mass loss for raw material-pulp treated IL-TA-IER70 under air.	199
Table A4.4. TGA-DTG peak temperatures-mass loss for raw material-pulp treated IL-TS-IER70 inert conditions.....	201

Table A4.5. TGA-DTG peak temperatures-mass loss for raw material-pulp treated IL-TS-IER70 under air.	201
Table A5.1. TGA-DTG peak temperatures-mass loss for raw material-pulp treated TS80 treatment with different IERs under inert conditions.	204
Table A5.2. TGA-DTG peak temperatures-mass loss for raw material-pulp treated TS80 treatment with different IERs under oxidative conditions.	204
Table A5.3. TGA-DTG shoulders-mass loss for raw material-pulp treated TS80 treatment with different IERs under oxidative conditions.	205
Table A5.4 Proximate analysis (wt.%) of raw materials for different particle size ranges.	207
Table A5.5. Ultimate analysis (wt.%) of raw materials and different particle size ranges.	207
Table A5.6. TGA-DTG peak temperatures-mass loss for different lignocellulosic materials particle size <106 µm under nitrogen.	210
Table A5.7. TGA-DTG peak temperatures-mass loss for lignocellulosic materials particle size 425-800 µm and <106 µm under air.	210
Table A5.8. XRD diffractograms for lignocellulosic materials in different particle size ranges.	212
Table A5.9. TGA-DTG peak temperatures-mass loss under inert conditions for lignocellulosic materials, treated with TS80 and IER70 for materials.	215
Table A5.10. TGA-DTG peak temperatures-mass loss under oxidative conditions for lignocellulosic materials, treated with TS80 and IER70 for materials.	216

List of Figures

Figure 1.1. Biorefinery schematic representation for the production of chemicals adapted from [5]. ...	20
Figure 1.2. Plant cell wall structure consisting of cellulose, Hemicellulose and lignin adapted from [15].	21
Figure 1.3. Cellulose structure, dashed lines show hydrogen bonds adapted from [27]......	22
Figure 1.4. The major hemicellulose component arabinoxylan adapted from [41].	23
Figure 1.5. The chemical structure of lignin adapted from [46].	25
Figure 1.6. Chemical structures of monolignols and the derived lignin units.	26
Figure 1.7. Different lignin-carbohydrate complexes bonds in lignocellulosic biomass adapted from [48,49].	27
Figure 1.8. Schematic for conversion of biomass to fuel-modified [53].	29
Figure 1.9. Combined cellulose conversion and product separation by IER. Reprinted with permission from [108].	37
Figure 1.10. Functionality in ion exchange resins [133].	39
Figure 1.11. Ions exchange among the solid and solution phases of IERs [147] Legend: X ⁺ , fixed cation.	40
Figure 1.12. Structure of if imidazolium-based protic and aprotic IL adapted from [152].	41
Figure 1.13. The dissolution mechanism of cellulose in ionic liquids adapted from [155].	42
Figure 1.14. General schematic for Biomass fractionation with IL adapted from [161].	42
Figure 2.1. Triethylamine mixed with sulfuric acid in an ice bath.	51
Figure 2.2. Triethylamine is mixed with acetic acid under a closed system.	52
Figure 2.3. Schematic diagram of the TGA-DSC adapted from [236].	54
Figure 3.1. DTG curves for biomass and pulp obtained under inert conditions zoomed in 200-600 °C temperature range. Effect of IER loading from 0 to 4 baskets: (a) IER70; (b) IER35.	69
Figure 3.2. Thermograms under air for MIS48 and Pulp pretreated pulp with different amounts of IER. (a) TGA for IER70; (b) TGA for IER35; (c) DTG for IER70; (d) DTG IER35.	71
Figure 3.3. XRD diffractograms of untreated MIS 425-800 and cellulose pulp after hydrolysis.	73
Figure 3.4. ATR-FTIR wavelength range 2000-400 cm ⁻¹ spectra MIS48, blank and pulps obtained after treatment with different amounts of IER70.	76
Figure 3.5. ATR-FTIR spectral wavelength range 2000-400 cm ⁻¹ for MIS48, blank and pulps treated with different amounts of IER35.	77
Figure 3.6. DTG curves under inert conditions for biomass and pulp, comparing hydrolysis using two baskets of IER or mineral acids with equivalent proton concentration: (a) IER70 and equivalent mineral acids; (b) IER35 and equivalent mineral acids.	80

Figure 3.7. TGA-DTG curves under oxidative conditions for biomass and pulp, comparing hydrolysis for two baskets of IER with an equivalent proton concentration of mineral acid.	81
Figure 3.8. XRD diffractograms of MIS48 and pulp samples via hydrolysis using IER and mineral acids. (a) IER70 and equivalent mineral acids; (b) IER35 and equivalent mineral acids.	82
Figure 3.9. ATR-FTIR spectral wavelength range 2000-400 cm^{-1} for MIS48, Pulp treated with IER70, and dilute acid hydrolysis.	84
Figure 3.10. ATR-FTIR spectral wavelength range 2000-400 cm^{-1} for MIS48, Pulp treated with IER35, and dilute acid hydrolysis.	85
Figure 4.1. DTG curves of raw material and pulp treated with two concentrations of IL-TA (40 and 80 wt.%) and the absence or presence of 0.25 g of IER70. (a) under inert; (b) under air.	93
Figure 4.2. XRD diffractogram of raw material and pulp treated with IL-TA and the absence or presence of 0.25 g of IER70. (a) IL-TA 40 wt.%; (b) IL-TA 80 wt.%.	95
Figure 4.3. ATR-FTIR from 2000-400 cm^{-1} for of raw material and pulp treated with two concentrations of IL-TA (40 and 80 wt.%) and the absence or presence of 0.25 g of IER70.	97
Figure 4.4. DTG curves for biomass, IL-TS-IER70, (a) under inert and (b) under air treatment at different IL concentrations.	100
Figure 4.5. XRD diffractograms for biomass and pulp treated with IL-TS-IER70 with and without IER70 for IL-TS (a) 40 wt.% and (b) IL-TS 80 wt.%.	103
Figure 4.6. ATR-FTIR for the biomass and pulp samples treated with IL-TS-IER70 ranged from 2000 – 400 cm^{-1} at different IL concentrations.	105
Figure 5.1. DTG curves under inert conditions for raw material and pulp treated with TS80 and different IERs: (a) IER00, (b) IER15, (c) IER35, (d) IER45, (e) IER70, (f) IER482, (g) IER252, and (h) IER275.	116
Figure 5.2. XRD diffractograms for raw material-pulp treated with TS80 and different IERs. (a) Amberlyst IERs and (b) Purolite IERs.	118
Figure 5.3. ATR spectra for raw material-pulp treated TS80 treatment with different Amberlyst IERs.	120
Figure 5.4. ATR spectra for raw material-pulp treated with TS80 and different Purolite IERs.	121
Figure 5.5. DTG curves under inert (a) and air (b) for different lignocellulosic materials.	124
Figure 5.6. XRD diffractogram for different lignocellulosic materials.	126
Figure 5.7. ATR spectra for different raw materials.	128
Figure 5.8. DTG curves for different raw materials under an inert environment for different raw materials and pulps treated with TS80-IER70. (a) MIS48, (b) BSG48 and (c) PB48.	131
Figure 5.9. XRD diffractogram for different raw materials (MIS48, BSG48, PB48), pulp after TS80-IER70 treatment (a) MIS48, (b) BSG48 and (c) PB48.	133

Figure 5.10. ATR-FTIR for MIS48, pulp after TS80-IER70 treatment.	135
Figure 5.11. ATR-FTIR for BSG48, pulp after TS80-IER70 treatment.	136
Figure 5.12. ATR-FTIR for PB48, pulp after TS80-IER70 treatment.	136
Figure A1.1. Main monomers of hemicellulose adapted from [434].	182
Figure A1.2. The major hemicellulose component in hardwoods adapted from [41].	182
Figure A1.3. The major hemicellulose component in softwoods adapted from [41].	182
Figure A1.4. Lignin linkages: ether bonds, carbon-carbon bonds and other linkages [435].	183
Figure A1.5. Common cations used ILs along with their structures adapted from [342,442,443].	185
Figure A1.6. Common anions used ILs along with their structures adapted from [342,374,443].	185
Figure A3.1. TGA and DTG thermograms under an inert environment for MIS48 and the pretreated pulp with different IER loadings: (a) IER70 TGA; (b) IER70 DTG; (c) IER35 TGA; (d) IER35 DTG.	190
Figure A3.2. XRD diffractogram: Original after background subtracted, deconvoluted, and peak fit. F1(X), F3(X) and F4(X) deconvolution of crystalline peaks, F2(X) and F5(X) deconvolution of amorphous peaks, and FIT fitting curve.	192
Figure A3.3. ATR spectral wavelength range 4000-400 cm^{-1} for MIS48 and IER70 treated pulp.	194
Figure A3.4. ATR spectral wavelength range 4000-400 cm^{-1} for MIS48 and IER35 treated pulp.	194
Figure A3.5. Thermogravimetric analysis of biomass and pulp under inert conditions. Comparative of hydrolysis for two baskets of IER with mineral acid hydrolysis using equivalent proton concentration: (a) TGA IER70 and equivalent, (b) TGA IER35 and equivalent, (c) DTG IER70 and equivalent, and (d) DTG IER35 and equivalent.	195
Figure A4.1. EDX colour mapping for pulp, after IL-TS60-IER00-0B: S (Sulphur), Si (Silica), Ca (calcium), and pulp.	197
Figure A4.2. EDX colour mapping for pulp, after IL-TS60-IER70-2B: S (Sulphur), Si (Silica), Ca (calcium), (Fe) Iron, (Mo) Molybdenum (Cr) chromium and pulp. (* Baskets dissolved)	197
Figure A4.3. TGA-DTG curves under inter conditions for biomass, pulp treated with IL-TA-IER70, (a, c) under nitrogen and (b, d) under air at different IL concentrations.	198
Figure A4.4. TGA-DTG curves under inter conditions for biomass, pulp treated with IL-TS-IER70, (a, c) under nitrogen and (b, d) under air at different IL concentrations.	200
Figure A5.1. Comparison of TGA-DTG curves for raw material, benchmark pulp obtained from pretreatment with only TS80, and pulps obtained from pretreatment with TS80 + different Amberlyst IERs. (a) TGA under inert conditions, (b) TGA in air, (c) DTG for inert conditions and (d) DTG under air.	202
Figure A5.2. Comparison of TGA-DTG curves for raw material, benchmark pulp obtained from pretreatment with only TS80, and pulps obtained from pretreatment with TS80 + different Purolite IERs. (a) TGA under inert conditions, (b) TGA in air, (c) DTG for inert conditions and (d) DTG under air. .	203

Figure A5.3. ATR spectral wavelength range 4000-400 cm^{-1} for raw material-pulp treated TS80 treatment with different Amberlyst IERs.	206
Figure A5.4. ATR spectral wavelength range 4000-400 cm^{-1} for raw material-pulp treated TS80 treatment with different Purolite IERs.	206
Figure A5.5. TGA-DTG curves under inert (a, c) and air (b, d) conditions for different lignocellulosic materials particle size 425-800 μm	208
Figure A5.6. TGA-DTG curves under nitrogen (a, c) and air (b, d) conditions for lignocellulosic materials with particle sizes <106 μm	209
Figure A5.7. XRD diffractogram for lignocellulosic materials with different particle sizes 425-800 μm , <106 μm , MIS (a), BSG (b) and PB (c).	211
Figure A5.8. ATR wavelength range 3900-400 cm^{-1} for MIS106 and MIS48.	212
Figure A5.9. ATR wavelength range 3900-400 cm^{-1} for BSG106 and BSG48.	213
Figure A5.10. ATR wavelength range 3900-400 cm^{-1} for PB16 and PB48.	213
Figure A5.11. ATR wavelength range 2000-400 cm^{-1} for raw materials particle size <106 μm	214
Figure A5.12. TGA-DTG curves under inert conditions for lignocellulosic materials, treated with TS80-IER70 for materials M48 (a, d), BSG48 (b, e) and PB48 (c, f).	215
Figure A5.13. TGA-DTG curves under oxidative conditions for lignocellulosic materials, treated with TS80 and IER70 for materials M48 (a, d), BSG48 (b, e) and PB48 (c, f).	216
Figure A5.14. ATR-FTIR for MIS48, pulp TS-IER70 treatment range 3900-400 cm^{-1}	217
Figure A5.15. ATR-FTIR for BSG48, pulp TS80-IER70 treatment range 3900-400 cm^{-1}	217
Figure A5.16. FTIR-ATR for PB48, pulp TS80-IER70 treatment range 3900-400 cm^{-1}	218

List of Equations

Equation 2.1. Swelling Degree	51
Equation 2.2. Karl Fisher titration stoichiometry	52
Equation 2.3. Fixed carbon calculation.....	55
Equation 2.4. HHV using elemental composition percentages.	57
Equation 2.5. Bragg's law equation.....	59
Equation 2.6. Segal equation for the calculation of the crystallinity index	59
Equation 2.7. Crystallinity calculation using the Gaussian function.	59
Equation 2.8. Scherrer equation for the calculation of the crystallite size	60

List of Abbreviations

Abbreviation	Description
AC	Ash Content
ADF	Acid Detergent Fiber
ADL	Acid Detergent Lignin
AILs	Aprotic Ionic Liquids
ASTM	American Society for Testing and Materials
ATR	Attenuated Total Reflectance
ATR-FTIR	Attenuated Total Reflectance-Fourier Transformation Infrared
BSG	Brewery Spent Grains
CRM	Cellulose-rich material
CTAB	Cetyl trimethyl ammonium bromide
DAH	Dilute Acid Hydrolysis
DTG	Derivative Thermogravimetric
DTG _{max}	Maximum mass loss rate in Thermogravimetric analysis
DVB	Divinylbenzene
EDTA	Ethylenediaminetetraacetic Disodium Salt
FC	Fixed Carbon
FTIR	Fourier Transformation Infrared
FWHM	Full Width Half Maximum Value
GHG	Greenhouse Gases
HHV	Higher Heating Value
IERs/PRs	Ionic Exchange Resins/Polymeric Resins
ILs	Ionic Liquids
IR	Infrared
KF	Karl Fischer Titrator
MC	Moisture Content
NDF	Neutral Detergent Fiber
PB	Pine Bark
PILs	Protic Ionic Liquids
SEM-EDX	Scanning Electron Microscopy-Energy Dispersive X-ray
TA	Triethylammonium Acetate
TCD	Thermal Conductivity Detector
TGA	Thermogravimetric Analysis

TS	Triethylammonium Hydrogen Sulphate
VC	Volatile Content
XRD	X-ray Diffraction

Chapter 1. Introduction

1.1. Biorefinery Concept

The biorefinery concept is based on creating a process that emulates what the conventional petroleum refinery does but uses renewable carbon sources as raw materials. However, as biorefinery differs from petroleum refinery in terms of raw materials, it also differs in the process steps to manufacture the required products, which range from different chemicals, energy carriers and materials. Ultimately, the main goal of the biorefinery is to run a process that can take over the conventional refinery in a sustainable manner through a circular economy strategy, where carbon materials produced should be recovered and recycled [1]. Biorefinery implementation is critical to achieving a sustainable and bio-based economy.

Biorefinery can produce sustainable alternative products to conventional refineries that rely on fossil fuels, but it needs to be economically feasible and reduce the environmental impact compared to conventional refineries [2]. This can be achieved by generating valuable products derived from organic materials and reducing carbon emissions through specific processes such as thermochemical, biochemical and chemical [3]. In summary, the effective transformation of lignocellulosic biomass into a range of value products and bioenergy can reduce greenhouse gas (GHG) emissions and reliance on fossil resources [4]. Biorefineries can use several raw materials, such as food crops, lignocellulosic biomass, algae, and genetically modified biomass, promoting the efficient use of resources and the concepts of a circular economy [5]. A successful biorefinery should follow the principles of green chemistry mentioned in Appendix A1 Table A1.1 [6].

Biorefinery includes two main steps: primary refining and secondary refining. Primary refining includes conditioning and pretreatment to separate components in the raw materials. Secondary refining includes the conversion of platform chemicals into precursors, separation for further processing, and final product [7,8]. Among these different stages of a biorefinery, pretreatment is crucial in establishing the feasibility of the whole process. This stage depends on the material used as a carbon source and the conversion route used in the refinery.

Lignocellulosic biomass is one of the most abundant types of material. It can come from plants, also known as lignocellulosic feedstock (forest, agriculture and their waste and any industry processing plants such as the paper and food industry). The lignocellulosic materials are complex and are comprised of carbohydrate polymers (cellulose and hemicellulose) and aromatic polymers (lignin) [9]. These materials, through biorefinery, can be converted into value-added/end-user products [10] to produce current petrochemical derivatives such as chemicals, fuels, plastics, and synthetic materials [11]. In a biorefinery, an efficient pretreatment step is crucial to separate biomass fractions. Each fraction from lignocellulosic material can be converted to value-added chemicals, as shown in Figure 1.1 as an

overview. If the pretreatment step is not successfully done, the feasibility of a biorefinery gets compromised.

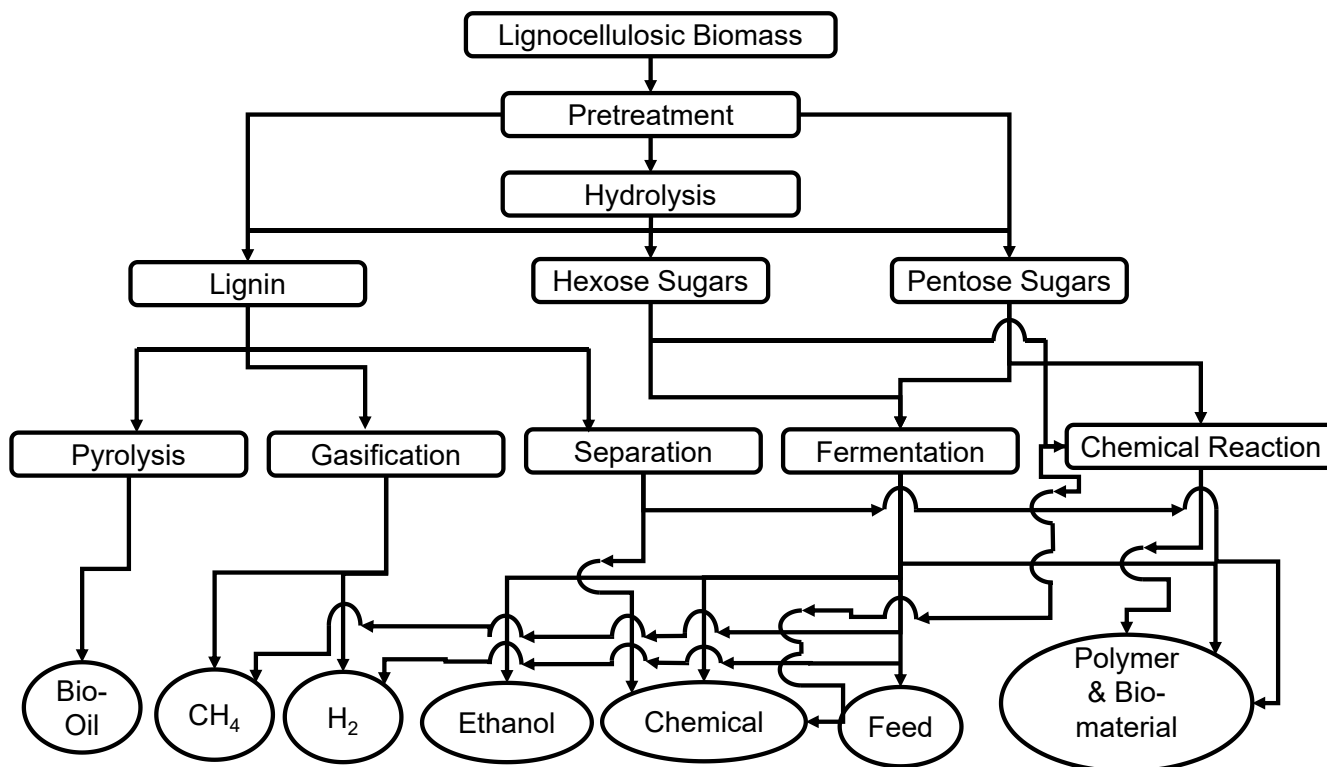


Figure 1.1. Biorefinery schematic representation for the production of chemicals adapted from [5].

Before discussing the various pretreatment technologies for lignocellulosic materials, it is essential to understand the building blocks that compose lignocellulosic materials. Therefore, the following section will provide a detailed overview of the main components of lignocellulosic materials, their structural insights, and how they are connected.

1.2. Lignocellulosic biomass

Lignocellulosic biomass is an abundant and promising source for the manufacture of biochemicals and biofuels [12]. The term "lignocellulosic" originates from lignin, a complex polymer that provides structural support to plants and cellulose. The cell wall consists of carbohydrates (hemicellulose, cellulose) and lignin, presented in Figure 1.2. The chemical structures of different pentose and hexose carbohydrates are presented in Appendix A1 Figure A1.1. The range of cellulose, hemicellulose, and lignin content in lignocellulosic biomass varies depending on the type of biomass. Typically, cellulose constitutes about 40-50 wt.% of the biomass, hemicellulose accounts for 20-35 wt.%, and lignin makes up 15-25 wt.% [13,14].

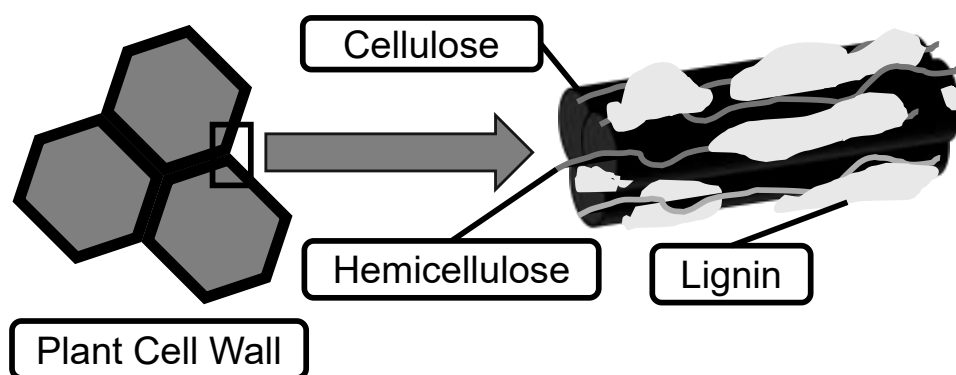


Figure 1.2. Plant cell wall structure consisting of cellulose, hemicellulose and lignin adapted from [15].

Lignocellulosic biomass can be divided into three categories based on component composition: hardwood, softwood, and herbaceous. All three lignocellulosic materials have different ranges of major components: cellulose, hemicellulose, and lignin, as shown in Table 1.1.

In softwood, bark cellulose ranges from 18-38 wt.%, hemicellulose 15-33 wt.%, and lignin 30-60 wt.%. For hardwood materials, cellulose content is in the higher range of 43-47 wt.%, with lower ranges of hemicellulose and lignin 25-35 wt.% and 16-24 wt.%, respectively, compared to softwood. For herbaceous biomass such as cereal straw, cellulose is around 33-38 wt.%, hemicellulose 26-32 wt.%, and lignin 17-19 wt.% [14].

Table 1.1. Chemical composition of different lignocellulosic biomasses [14,16–19].

Raw Material	Cellulose (wt.%)	Hemicellulose (wt.%)	Lignin (wt.%)
Poplar wood	49.7	24.1	23.6
Poplar wood (Hard)	42.7	21.7	26.9
Willow (Hard)	44.3	22.6	25.1
Pine Bark (Soft)	21.9	18.3	40.7
Spruce Bark (Soft)	29.7	13.9	45.1
Miscanthus Giganteus (Nov)	50.3	24.8	12.0
Miscanthus Giganteus (Feb)	52.1	25.8	12.6
Miscanthus Sinesis (Nov)	47.6	33.0	9.2
Miscanthus Sinesis (Feb)	52.2	30.6	9.3

Furthermore, the physiochemical composition of any lignocellulosic biomass is influenced by natural factors such as the type of soil [20,21], regional location [22], and climate change of the local land where the raw material was planted and harvested [23]. For example, properties of soil which can significantly influence the physiochemical properties of lignocellulosic material are following: nutrient availability and uptake, pH and mineral composition, organic matter content, and water availability [24–26]. Other than natural factors, there are human factors such as the time of plantation and harvest, the use of pesticides and herbicides during growing lignocellulosic biomass, and storage before using them in a chemical process. For example, delaying harvest time significantly influences lignocellulosic biomass component

composition, increasing lignin and cellulose and decreasing hemicellulose contents over the winter season [27]. To see the difference in other properties, such as proximate and ultimate analysis, due to regional changes for similar materials, see Appendix A1 Table A1.1 and Table A1.2.

1.2.1. Cellulose

Cellulose has a relatively simple structure, as shown in Figure 1.3 in comparison to the other two components, and consists of a minimum of ten thousand β -D-glucose units bond through glycosidic (β -1 \rightarrow 4) linkage with molecular formula represented as $(C_{12}H_{20}O_{10})_n$ where n is the number of β -D-glucose units [28]. Cellulose has both crystalline and amorphous regions. Crystalline regions are ordered and have compact structures; however, amorphous regions have a loose arrangement of cellulose chains with high reactivity and accessibility during any pretreatment [29].

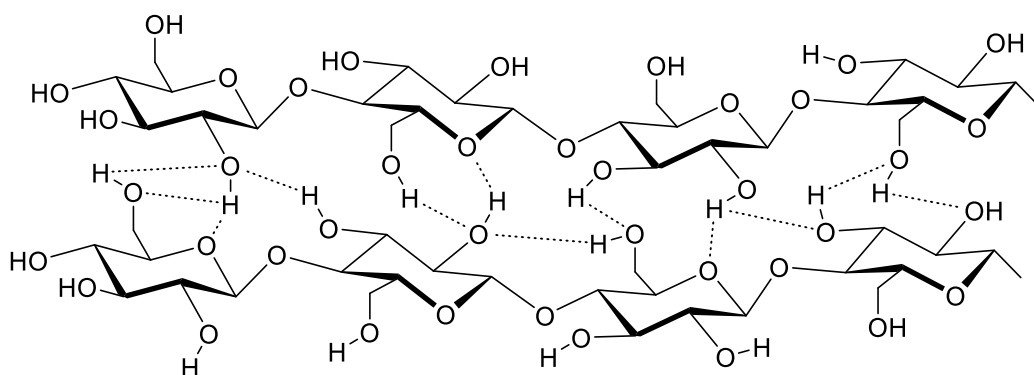


Figure 1.3. Cellulose structure, dashed lines show hydrogen bonds adapted from [30].

Cellulose exists as long thread-like fibres called microfibrils packed together to form cellulose fibrils [31] by hydrogen bonding between their hydroxyl groups. Microfibrils are composed of crystalline cellulose connected by amorphous sections. The diameter of each microfibril ranges from 2 to 10 nm, while its length varies from 100 nm to a few micrometres, depending on the source [32]. As an illustration, in wood, the cellulosic fibres have a length of 1-2 μ m and a width of approximately 3.5 nm [32]. The microfibrils consist of 30-40 chains of cellulose [32]. As cellulose's number of glucose units increases, its degree of polymerisation increases, making lignocellulosic biomass more recalcitrant to any pretreatment method because highly organised structures are more resistant to chemical and enzymatic attacks [33]. Due to the crystalline structure of cellulose, its typical thermal degradation ranges between 280-360 $^{\circ}$ C [34]. Fractionation of cellulose in any lignocellulosic material is necessary to lower its thermal stability and break the long, rigid polymeric chain into simpler glucose monomer units. This ultimately enhances cellulose accessibility, which is crucial for effective enzymatic hydrolysis and subsequent transformation into useful products like biofuels and chemicals [35].

Cellulose can exist in various allomorphs due to changes in molecular arrangement and hydrogen bonding [36,37]. Natural cellulose exists in the crystalline state known as cellulose I, with each glucose unit forming eight hydrogen bonds. In contrast, amorphous cellulose has 5.3 hydrogen bonds [38]. For example, Cellulose I has inter- and intramolecular hydrogen bonding at O₃H-O₅ and O₆H-O₃, respectively, while O₂H-O₆ (which are also linked in cellulose I) and O₆H-O₂ are reported to be intra- and intermolecular hydrogen bonding for cellulose II [39].

In summary, cellulose in any lignocellulosic material cannot directly produce biofuels in a biorefinery. The depolymerisation of cellulose is one of the critical steps in producing glucose, which can be further transformed into high-value products chemically or biologically, such as 5-HMF, levulinic acid, lactic acid and others.

1.2.2. Hemicellulose

Hemicellulose, with a generic formula of (C₅H₈O₄)_n, has an amorphous and random structure consisting of branched chains with a lower polymerisation degree in comparison to cellulose [40]. Due to the amorphous structure, hemicellulose thermal degradation range (220-315 °C) is lower than cellulose [41]. Hemicellulose major components include branched hydrocarbon chains made with the following sugars: pentose and hexose with residues such as D-glucose, L-arabinose, D-galactose, D-mannose, and D-glucuronic acid and D-galacturonic acids [42] (see these building blocks in Appendix A1 Figure A1.1). Hemicellulose composition, structure, and percentage of the material depend on the biomass type. Hemicellulose typically has a rod-like structure with branches and side chains folded back onto the main chain by hydrogen bonding. This elongated form enhances their ability to engage with cellulose, leading to a strong connection that provides significant stability to the cell matrix [43].

Hemicellulose structures in herbaceous crops have arabinoxylan as the main component, as shown in Figure 1.4. It contains β-(1-4)-linked xylose units, with α-(1-2)- and α-(1-3)-linked arabinose units [44].

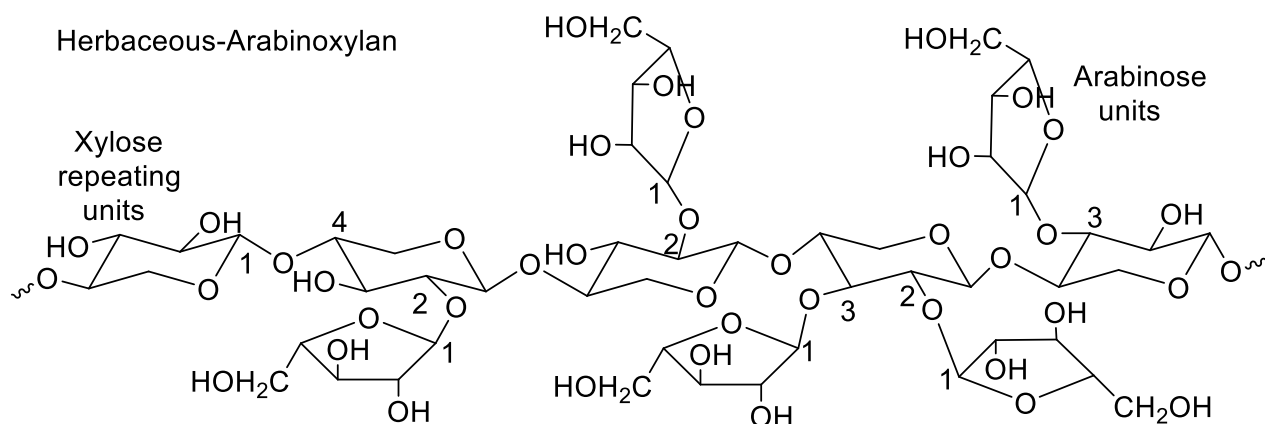


Figure 1.4. The major hemicellulose component arabinoxylan adapted from [45].

However, in the case of softwood, the major hemicellulose component is O-acetyl-galactoglucomannan. The backbone consists of a random distribution of β -(1-4)-linked mannose and glucose units with α -(1-6)-linked galactose units attached to the mannose and glucose units, as shown in Appendix A1 Figure A1.3. Moreover, in hardwoods, the major hemicellulose component is O-acetyl-4-O-methylglucuronoxyran, along with one-tenth of backbone units are substituted at C-2 with (1-2)-linked 4-O-methyl glucuronic acid, and about 70% of the xylo-pyranose backbone is a hydroxyl group that is acetylated at C-2 or C-3 as shown in Figure A1.2 [45]. The structural variations of hemicellulose between herbaceous and woody biomass are essential for determining plant cell walls' mechanical characteristics, digestibility, and usefulness. For example, in woody biomass, the xylan backbone can take on a two-fold screw shape, facilitating intimate interaction with cellulose microfibrils and so augmenting structural stiffness [46]. In contrast, the more branching and diverse hemicelluloses in herbaceous biomass result in a less stiff structure, perhaps enhancing enzymatic accessibility [47].

Hemicellulose acts as a bridge between cellulose and other components in biomass. The cohesion of secondary cell walls relies on the interaction between xylan and cellulose microfibrils through hydrogen bonding [48]. Xylan can extend the cellulose crystal structure, acting as a transitional phase between stiff crystalline microfibrils and more flexible polysaccharide phases [49]. Including hemicellulose components in lignocellulosic materials has diverse biomechanical effects, with glucomannans increasing rigidity and xylans favouring flexibility and elongation [46]. In summary, Hemicellulose is more susceptible to hydrolysis than other constituents of lignocellulosic biomass, such as cellulose and lignin, owing to its amorphous and less crystalline configuration.

1.2.3. Lignin

Lignin (Figure 1.5) is a complex and highly branched polymer with a three-dimensional structure of 4-propenyl-2-methoxy phenol, 4-propenyl phenol, and 4-propenyl- 2,5-dimethoxy phenol. The main lignin building blocks are p-hydroxyphenyl, guaiacyl, and syringyl (Figure 1.6) [50].

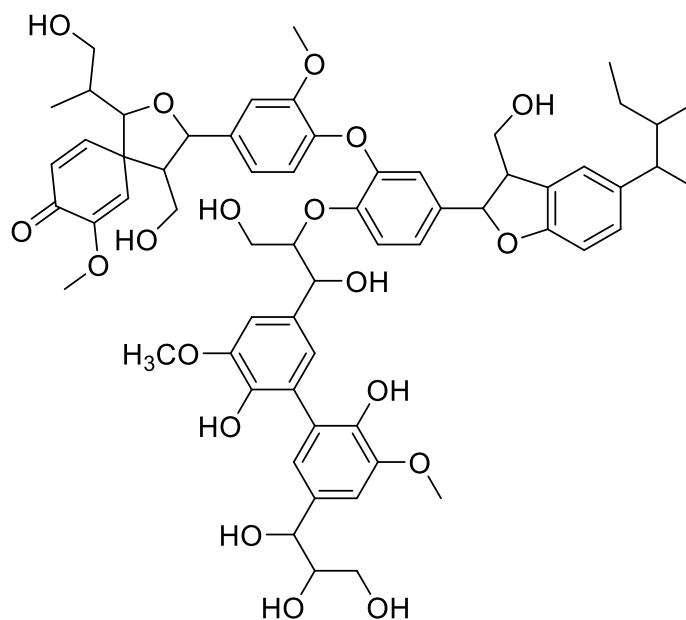


Figure 1.5. The chemical structure of lignin adapted from [51].

Depending on the source of the lignin, the ratio of these subunits differs. For example, softwoods possess more lignin with more guaiacyl units [52]. In contrast, hardwoods have a more even distribution of syringyl and guaiacyl lignin units [52]. On the other hand, herbaceous lignin includes an even distribution of all p-hydroxyphenyl, guaiacyl, and syringyl units. These building blocks are interconnected through multiple connections, mostly ether bonds such as aryl- or phenyl ether and carbon-carbon bonds, as shown in Appendix A1 Figure A1.4.

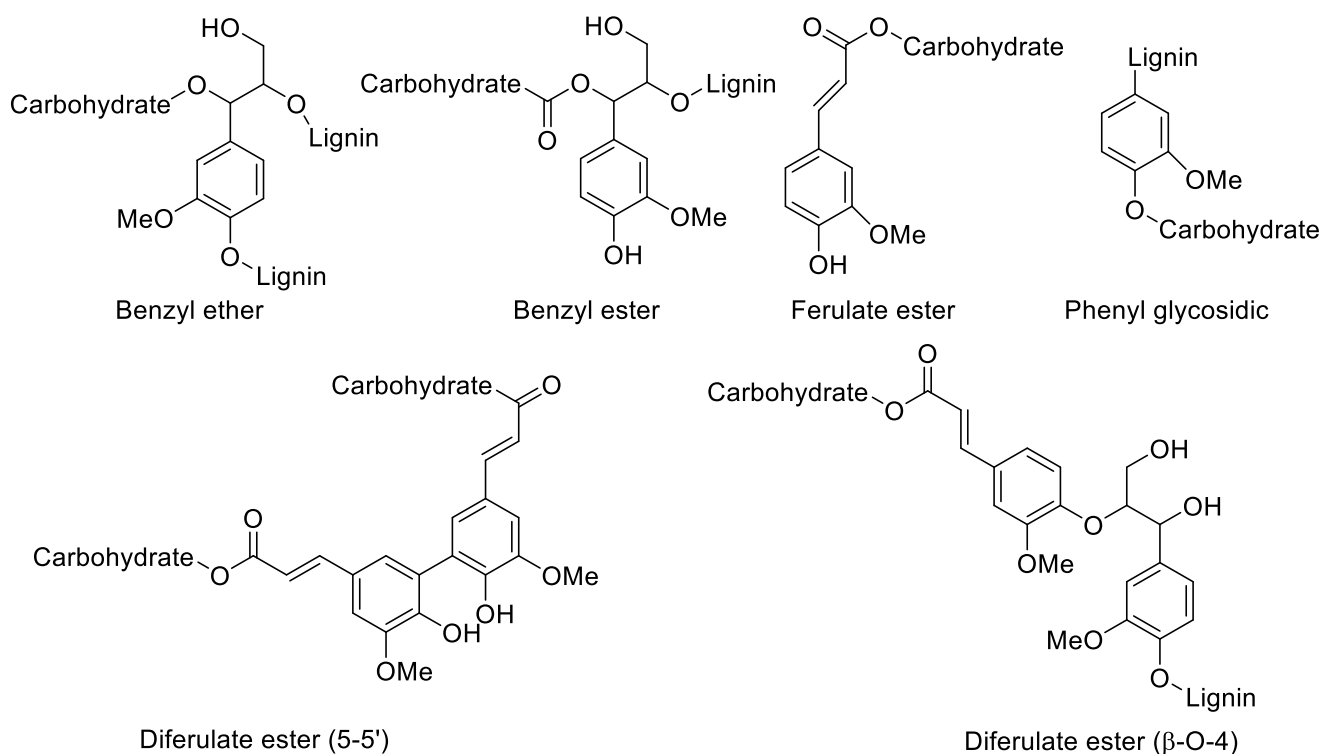


Figure 1.7. Different lignin-carbohydrate complexes bonds in lignocellulosic biomass adapted from [53,54].

These lignin-carbohydrate complexes play a vital role in the lignocellulosic material in resistance to fractionate during any processes as it is reported that all lignin moieties in softwood and 47-66 wt.% of lignin moieties in hardwood are chemically bonded to carbohydrates [55]. Lignin-carbohydrates complexes can impede biomass dissolution during pretreatment, causing a significant obstacle in biomass fractionation.

In summary, this section shows how comprehending biomass's unique structural and compositional properties is essential to maximising its use in sustainable energy and material manufacturing. Considering all this information and the large availability of lignocellulosic biomass worldwide, the present work is focused on studying novel pretreatment routes for lignocellulosic feedstocks. Therefore, the following section explains the current and more advanced methodologies for chemical pretreatment of lignocellulosic biomass.

1.3. Lignocellulosic Biomass Pretreatment Methodologies

The primary purpose of any lignocellulosic biomass pretreatment is to remove lignin and retain hemicellulose, reduce cellulose crystallinity, and change surface morphology. Lignocellulosic biomass can be utilised to make second-generation biofuels, bio-sourced chemicals, and materials as an alternative to fossil fuels. However, biomass structural properties: cellulose surface area, degree of

polymerisation, cellulose crystallinity, pore size and volume and chemical factors: composition of cellulose, lignin, and hemicellulose make it a recalcitrant material to be used as it is [33,56,57].

After the pretreatment process, the treated material should have the following characteristics: avoid the need for size reduction, preserve hemicellulose fractions, increase the yield of sugars, avoid carbohydrates degradation or loss, as well as the generation of by-products such as inhibitors in the post-hydrolysis processes, easy extraction of lignin components from hydrolysate and the process to be cost-effective for recycling and regeneration of pretreatment reagents [58,59].

Hydrolysis is one of the common technologies used in woody biomass pretreatment. The process can be either chemical/biological or a combination of both methods. Hydrolysis is defined as the depolymerisation of polysaccharides in lignocellulosic biomass via hydration into monosaccharide carbohydrates [60]. For example, glucose can be produced from the enzymatic hydrolysis of corn [10] and also after acid hydrolysis of lignocellulosic materials [61].

Regardless of the combination of different pretreatment methods in a biorefinery, lignocellulosic biomass pretreatment technologies are divided into four main categories: physical, chemical, biological, and physicochemical, as shown in Table 1.2.

Table 1.2. Lignocellulosic biomass pretreatment technologies with different methodologies [62,63].

Pretreatment category	Methodologies
Physical/Thermal	Milling, grinding, Microwave (MW), Ultrasound (SN), Pyrolysis
Chemical	Organo-Solv, Ionic liquids, Acid, Alkali
Physio-chemical	Steam explosion, Wet oxidation, Liquid hot water, Ammonia fibre explosion
Biological	Fungi (Brown, White, Soft rot), Bacterial, Archaeal

Lignocellulosic materials differ a lot in physiochemical properties, as mentioned earlier. For example, softwood and its residue are much more recalcitrant than herbaceous or energy crops. So, finding the optimal general pretreatment process for all lignocellulosic raw materials is difficult. The fundamental pathway for biomass to fuel production via pretreatment can be seen in Figure 1.8.

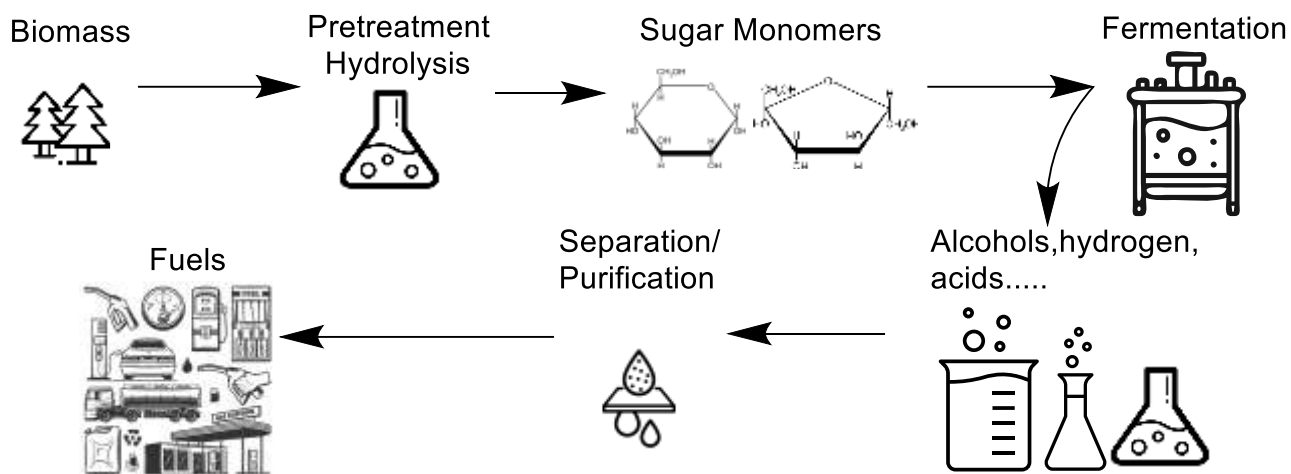


Figure 1.8. Schematic for conversion of biomass to fuel-modified [58].

Furthermore, other factors such as proposed application and production of the end product, availability of raw material, techno-economic feasibility, and environmental impact are required to be taken into consideration when selecting a pretreatment method [5]. The present work focuses on chemical pretreatment methodologies. Therefore, the following section expands on the different chemical pretreatments reported in the literature.

1.4. Chemical Pretreatment Methods

Chemical pretreatment is a process that utilises acids, alkalis, or organic solvents to break down the intricate composition of biomass. This process dissolves hemicellulose and partially eliminates lignin, ultimately enhancing cellulose accessibility for enzymatic hydrolysis. This approach is favoured because it effectively improves biomass digestibility, mostly under moderate conditions, as opposed to physical or biological pre-treatments. Chemical pretreatment can be customised to focus on specific biomass constituents, enabling more precise and effective processing. Table 1.3. summarises the main advantages and disadvantages/limitations of each one of them.

Table 1.3. Pretreatment methods and related advantages, limitations, and disadvantages [58,64–69].

Pretreatment method	Advantages	Limitations and disadvantages
Acid hydrolysis	Removal of lignin with hemicellulose solubilisation, improve sugar yield, short reaction period, low reagent cost	Monomer sugar degradation at high temperatures, inhibitors formation, corrosion of operating system, high equipment cost
Alkali hydrolysis	Substantial lignin removal, significant removal of hemicellulose infiltrate, ability to recover lignin in modified form, reduce cellulose crystallinity, low reactant cost, combine with acid pretreatment for pure cellulose with the lower formation of by-products, increase accessible surface area	Less biomass recovery, harsh chemical conditions, formation of salts which incorporate into the regenerated structure, require neutralisation, recovery step, and higher residence time, sugar degradation minimum
Organosolv	Obtain pure cellulose, lignin, and hemicellulose, a significant yield of sugar from biomass, a catalyst that can be used to reduce the severity of operating conditions	High capital cost, influence on environment, production of inhibitors, solvent recovery required, high operational cost, need washing step
Ionic liquid	Lignin removal high, a significant decrease in cellulose crystallinity, able to work at high temperatures, non-volatile in nature, properties can be adjusted, reusability, environment-friendly, able to hydrolyse biomass at ambient conditions	High cost, solvent recovery required, a tendency to denture enzyme, complex synthesis, for selective solvent design require various types of anions and cations

1.4.1. Acid Pretreatment

Acid hydrolysis is one of the most common processes used in biorefineries to treat lignocellulosic biomass for cellulose and hemicellulose conversion to mono-sugars. Acid hydrolysis is divided into two kinds of processes based on operational parameters: first, the Scholler process using dilute acid (0.5 wt.% H₂SO₄) [62], temperature around 170-210 °C, the pressure under 20 bar and processing time 45 minutes produce mono-sugars around 50 wt.% [61].

Second, the Bergius process [70] using concentrated acid (72 wt.% H₂SO₄ or 41 wt.% HCl or 77-83 wt.% H₃PO₄), room temperature, and short processing time produce a high yield of mono-sugar [71]. Under acidic conditions, hemicellulose dissolution is maximum. At low pH, most of the hemicellulose is removed from the solid material and converted into compounds such as furfural and 5-hydroxymethylfurfural (5-HMF), which are furan aldehydes generated from sugar dehydration [5]. Additionally, acetates from hemicellulose and several acids and phenolics from lignin are produced during dilute acid hydrolysis [72,73]. The presence of these compounds increases in the hydrolysate as the severity of acid pretreatment increases and has a strong negative influence on ethanol fermentation [74]. Similarly, compounds such as levulinic acid (LA) from agricultural waste/woody biomass could be

produced; however, forming solid humins is a potential drawback of the process [10]. Acid pretreatment with biomass can be classified into three categories based on acid classification: concentrated mineral acid, dilute acid, and organic acid, and each of them has its advantages and disadvantages [75], as shown in Table 1.4.

Table 1.4. Classification of Acidic catalysts [75].

Acidity concentration level and type	Operational Parameters	Pros	Cons
Concentrated Mineral acid	>30% (w/v) for many hours (hrs) at room/moderate temperature (temp.)	<ul style="list-style-type: none"> No requirement for enzyme Both pressure and temp. low 	<ul style="list-style-type: none"> chemical toxicity and corrosiveness high cost
Dilute Mineral acid	0.5-5% (w/v) few minutes (mins) at high temp.	<ul style="list-style-type: none"> rapid rate reaction Combined severity factor influence 	<ul style="list-style-type: none"> High temp. Inhibitor creation
Dilute Organic acid	0.5-5% (w/v) few mins at high temp.	<ul style="list-style-type: none"> Toxic less Fewer inhibitors creation 	<ul style="list-style-type: none"> Catalyst costly Efficacy

Dilute acid hydrolysis pretreatment [76] for lignocellulosic biomass could be achieved at an industrial scale, as proved by [77,78]. Acid hydrolysis can be combined with other pretreatment techniques in two stages as follows: concentrated acid with subsequent alkali treatments [79], hot water and dilute acid [80], two-step acid hydrolysis treatment [81]. For example, dilute acid and dilute alkali effectively fractionated empty fruit bunches (EFB) through lignin removal (53.6 wt.%) and hemicellulose hydrolysis (53.6 wt.%) [82]. Depending on biomass type and acid concentration, dilute or concentrated [83] optimum process parameters will be changed [84–86].

Regardless of the type of the process, there will always be shortcomings of acid pretreatment, such as equipment corrosion and degradation over time, hydrolysed neutralisation, treatment and disposal of the waste stream, acid recovery, and detoxification before any post-process such as fermentation. Detoxification of acid hydrolysate can be done through different techniques, such as evaporation [87], liquid/liquid extraction [88], activated charcoal [89], resin [90], electro dialysis [91] and combination of different techniques [92]. Even though the cost of reagents such as sulfuric acid or hydrochloric acid is low, process drawbacks do not regard the process to be cost-effective and eco-friendly [61].

1.4.2. Alkali Pretreatment

The alkali system is conducted at low temperatures, although the pretreatment time is defined in hours or days rather than minutes or seconds [93] with limitations such as producing irrecoverable salts or

their absorption into treated biomass. In the basic pretreatment process, lignocellulosic biomass has two types of reactions, solvation and saponification, causing biomass structure to swell, decrease in polymerisation degree, solubilisation, redistribution, and condensation of lignin [59]. Alkali-based pretreatment could be achieved through the use of different base reagents, such as ammonium hydroxide (NH₄OH), potassium hydroxide (KOH), ammonia (NH₃), sodium hydroxide (NaOH), calcium hydroxide (Ca(OH)₂), and ammonium sulphite ((NH₄)₂SO₃), depending on the severity of the process for lignocellulosic agricultural residues [94]. The comparison of different alkaline treatments is shown in Table 1.5. When compared to the acid process, alkali treatment is more effective in solubilising lignin while having a slight effect on cellulose and hemicellulose [95], resulting in increased cellulose digestibility in less severe conditions [96] and less degradation of sugars [97].

Table 1.5. Comparison of different alkaline pretreatment [98].

Description Process	Ammonia (NH ₃)	Sodium Hydroxide (NaOH)	Sodium Carbonate (Na ₂ CO ₃)	Calcium Hydroxide (Ca(OH) ₂)
Pressure	High	Low	Low	Low
Temperature	High	Low	High	Low
Chemical loading	~ 15-30 wt.% aq. or gas	1-5 wt.%	5-15 wt.%	0.1 g Ca(OH) ₂ /g solid
Recovery process	Evaporation, high-pressure equipment	Kraft process expensive	Partial Kraft process, less expensive	CO ₂ , carbonating, less expensive
Corrosiveness	High	High	Medium	Low

Comparing different alkaline pretreatment methods, for instance, lime [99], aqueous ammonia [100], and others, NaOH alkali treatment is considered to be the most cost-effective for biofuel production [101]. Further, an alkali treatment is used for de-lignification; however, a similar treatment does not work if the lignin composition is higher in the wood. For example, with soaking aqueous ammonia pretreatment, enzymatic digestibility with agricultural waste rice straw and barley straw was 85 wt.% and 95 wt.%, respectively. However, with Eucalyptus residue and Pinus Rigida, enzymatic digestibility was relatively low, within the range of 3.2-8.3 wt.% [102]. Alkali pretreatment has several advantages over acid pretreatment, such as high selectivity for delignification, retention of carbohydrates, no need for detoxification, and higher fermentation efficiency due to the absence of inhibitors [98]. However, using alkali pretreatment in biorefinery is not a very attractive choice because of the operational parameters such as temperature (80-150 °C), water requirement (solid to liquid ratio 1:10 to 1:20), time (hours to days), and costs of reagent (alkaline reagents costs more as compared acid reagents). For a successful alkaline pretreatment, it should have feasible techno-economic analysis and integration with biomass biorefineries [59].

1.4.3. Organo-Solv

The basic objective of organic solvent pretreatment is to separate all three lignocellulosic biomass components, breaking the linkage between lignin and hemicellulose bonds and then into a major macromolecular fraction.

Organosolv, as indicated by the name, are organic solvents, for example, alcohols (ethanol, methanol), acetic acid, tetrahydrofuran, acetone, and γ -valerolactone that can be derived from renewable resources [103]. For example, organic solvents such as γ -valerolactone from levulinic acid [104] and tetrahydrofuran from 1,4-butanediol and furfural [105] can be produced from biomass-derived compounds. During organosolv, a small amount of acid can be used that will act as a catalyst and solubilise lignin and hemicellulose fractions, making cellulose accessible for enzymatic hydrolysis [106–108]. Using organic solvents has advantages over conventional pretreatment technologies. For example, macromolecule fractions of lignin obtained from organosolv [109] have a less modified sulphur-free structure than the obtained from kraft lignin through alkali pretreatment [110].

These renewable organic solvents can be generated in a biorefinery and used for biomass pretreatment; however, the fractionation techniques using these bio-organic solvents are novel, so more research is required for commercialisation [111]. Commercialising an organic solvent pretreatment operation as part of a biorefinery has a lot of challenges, such as solvent recovery and high process costs, susceptibility to fossil fuel processes, and operational integration with other parts of a biorefinery. To have an organosolv pretreatment facility, operating conditions should be optimised to have maximum product yields for all three streams of cellulose, lignin, and hemicellulose fractions in a continuous process for different biomass feedstocks [112].

Considering the above factors, using organic solvents could be a potential choice for lignocellulosic fractionation in a biorefinery. However, the process requires ongoing research and development to address existing constraints and enhance overall process efficiency and economics.

Due to the anisotropic physiochemical properties of lignocellulosic materials, there can be no standard pretreatment methodology for them. Due to this, optimum pretreatment technology should be adaptive to different raw materials, such as softwood, hardwood, energy crops, and agricultural residues, based on their physical properties and chemical composition. Biomass pretreatment processing in a biorefinery can be a big operation with sub-operations suitable for different biomass raw materials. Pretreatment for lignocellulosic biomass in a biorefinery is integral and can be a starting point in a typical industry to produce biofuel for woody biomass. Without it, biorefinery will be a non-functional part of the bio-industry.

1.4.4. Solid Acid catalysts

Solid acid catalysts provide a lot of advantages, like high selectivity, long catalytic life, and simplicity of recovery, reuse, and separation. They also have a lot of potential for efficiently converting lignocellulosic biomass into biofuels. They can also be used to replace a variety of traditional liquid acids and bases for hydrolysis and pretreatment [113]. Table 1.6 represents the hydrolysis of different raw materials using different solid catalysts.

Table 1.6. Comparison of catalytical properties and activities of solid acid catalyst for hydrolysis.

Catalyst	Biomass	Assisting Pretreatment	Temp. (°C)	Time (hr)	TRS* Yield (%)	Ref.
HSO ₃ -ZSM-5	Corn Cob	Extraction	120	6	54.1	[114]
Biochar-SO ₃ H	Cord grass	-	100	6	30.0	[115]
Amberlyst 15	<i>Eucheuma cottonii</i>	-	120	1.5	24.5	[116]
Lignin	Sugarcane bagasse	-	140	3	65.0	[117]
SnO ₂ -Co ₃ O ₄ /C-Biochar	Corn Cob	-	180	2.8	83.3	[118]
MSF-copolymer-SO ₃ H	Banana fibres	[BMIM]Cl	110	1	61.0	[119]
Lignin-SO ₃ H	Rice straw	[BMIM][Cl]	140	3	63.4	[120]
AL-Py-450	Japanese cedarwood	Milling-HCl	210	1	47.1 ^a	[121]
C-SO ₃ H	Corn Cob	-	140	6	78.1 ^b	[122]
Fe ₃ O ₄ -SBA-SO ₃ H	Corn Cob	-	150	3	45.0	[123]
PCM-SO ₃ H	Rice straw	[BMIM]Cl	150	2	35.5	[124]
Fe ₃ O ₄ @C-SO ₃ H	Palmyra peel	Ultrasonication	125	1	97.6	[125]
Fe ₃ O ₄ @C-SO ₃ H	Corn cob	Ultrasonication	135	1	90.0	[125]

*TRS (Total reducible sugars); (a) Glucose, (b) Xylose.

Solid acid catalysts are not always enough to achieve maximum reducible sugar yield. Any other pretreatment technology should assist the hydrolysis of any lignocellulosic material using the catalyst. For example, the raw material should be treated with different treatments (alkali [120], ultrasonication [125], ionic liquid [124]) before using a solid acid catalyst for hydrolysis. The detailed literature concludes that solid acid catalysts enhance biomass hydrolysis efficiency; however, the performance of the catalyst is dependent on different factors.

The efficacy of solid acid catalysts is determined by their specific surface area, pore size, pore volume, active site concentration, and acidic type. To lower the degree of crystallinity of cellulose or transform it to a less crystalline structure, solid catalysts for cellulose hydrolysis should have a high number of Bronsted acid sites, a good affinity for the reactant substrates, and good thermal stability. Furthermore, solid catalyst composition, porosity, presence of water to have ions in the liquid phase from the catalyst, and reactor specifications could make it probable for hydrolysis of lignocellulosic biomass on a practical level [113]. Using acid solid catalysts will always have some challenges during biomass conversion

processes compared to homogenous systems. The following sections discuss various solid acid catalysts.

1.4.4.1. Zeolites

Zeolites are minerals composed of microporous aluminosilicates that can act as solid catalysts in converting biomass components into valuable compounds. Zeolites possess a porous structure capable of accommodating a diverse range of cations. These cations are weakly attached to the surface of the zeolite and can be discharged into a solution, displaying various catalytic activities. H-form zeolites are extensively utilised as acid catalysts because of their shape-selective capabilities in chemical processes. The acidity of the catalyst is determined by the atomic ratio of Si/Al. The number of Brønsted acid sites is directly proportional to the amount of Al atoms. Therefore, the higher the ratio of Al/Si, the greater the acidity of the catalyst [126].

Even though zeolites can be used to catalysed cellulose depolymerisation to value-added products, there are challenges: low catalytical activity sites, instability in aqueous system at high temperature [127] [128], promote undesired side reactions, leading to lower selectivity towards the target product [129,130], coke formation [131] and framework collapse at high temperatures [132]. These challenges need to be addressed before using H-form zeolites for biomass conversion processes at an industrial scale.

1.4.4.2. Carbon Based Solid Acids

Carbon-based catalysts are made from carbon-rich materials (sucrose [133], cellulose, biochar [115]), activated carbon that has been functionalised with acidic groups, often sulfonic acid ($-\text{SO}_3\text{H}$) group. Synthesis of these catalysts can be achieved using biomass waste materials such as lignosulfonate (water-soluble lignin derivative generated as a by-product during the sulphite pulping process of wood pulp manufacture), a byproduct of the paper industry [120]. One of the advantages of this carbon base catalyst is that it can be incorporated with different metals, such as iron [124] to make them magnetic or addition of heavy metals such as cobalt [118] to catalysts acidity.

Carbon-based solid catalysts may be utilised with ionic liquids to improve biomass conversion [119,120]. Nevertheless, solid acid catalysts possess certain drawbacks. Their catalytic activity may diminish with repeated usage, and they may encounter diffusion restrictions due to the heterogeneous nature of the reaction, particularly with bigger biomass molecules [134]. Moreover, although ecologically advantageous, synthesising certain solid acid catalysts from biomass waste may necessitate several stages and meticulous regulation of synthesis parameters to attain the appropriate characteristics [125]. Carbon-based solid acid catalysts are effective for generating value-added products from carbohydrates; however, utilising lignocellulosic materials presents a considerable barrier to separating

the catalyst post-hydrolysis. To utilise these solid catalysts for biomass hydrolysis, they must be readily separable from the pretreated raw material.

1.4.4.3. Ionic Exchange Resins for biomass pretreatment

Ionic Exchange Resins (IERs) are made of crosslinking hydrocarbon chains with one another through the polymerisation process and can be used as solid catalysts for lignocellulosic pretreatment. IERs are made up of a functionalised polymeric matrix. Most IERs are made of polystyrene or acrylic polymer, serving as a structural material, and then undergo chemical treatment for binding functional groups to ion exchange sites located throughout the matrix [135,136]. The IERs manufacturing process is a polymerising monomer (styrene or methyl acrylates) mixed with a certain amount of crosslinking monomer divinyl benzene (DVB). The mixture is dispersed in water in a stirred tank reactor and agitated to produce small droplets of suspended monomer mix. The mixture is then polymerised in the presence of catalysts, which create a solid three-dimensional sphere with a certain degree of porosity. Once the polymeric matrix is made, functional groups are added to the styrene backbone of the polymer to make the resin reactive, which could act as ions in a water mixture [137].

IER catalysts provide a lot of advantages, like high selectivity, long catalytic life, and simplicity of recovery, reuse, and separation. They also have a lot of potential for efficiently converting lignocellulosic biomass into biofuels. They can also be used to replace a variety of traditional liquid acids for hydrolysis and pretreatment [113]. IERs have advantages over conventional acidic catalysts used for hydrolysis because of their ionic nature, which makes catalyst alteration possible, for example, substituting suitable species with metal ions working as a homogeneous catalyst. Furthermore, IERs can be used in a regulated manner in several reaction steps for combination or sequential actions [138].

Compared to other types of solid catalysts, IERs such as cationic-exchange resin work as both a catalyst and a membrane to allow product permeability during hydrolysis, as shown in Figure 1.9. The inhibitory chemicals would be eliminated by IERs, which would benefit the succeeding fermentation process. However, at elevated temperatures above 150 °C, macro reticular resins lack thermal stability, which further creates problems of catalyst recycling and leaching due to a large number of acid ions, such as sulphates, in the liquid phase [113]. Nonetheless, these solid acid materials are interesting to further explore for hydrolysis.

IER stability must be high enough to be used as a catalyst. For example, in strong oxidising agents such as chromic or nitric acid, IERs start degrading quickly, and slow degradation occurs in the presence of oxygen and chlorine, which is catalytically induced. Due to this, in IERs, metal ions such as iron, copper, and manganese should be minimalised in oxidising solutions [139].

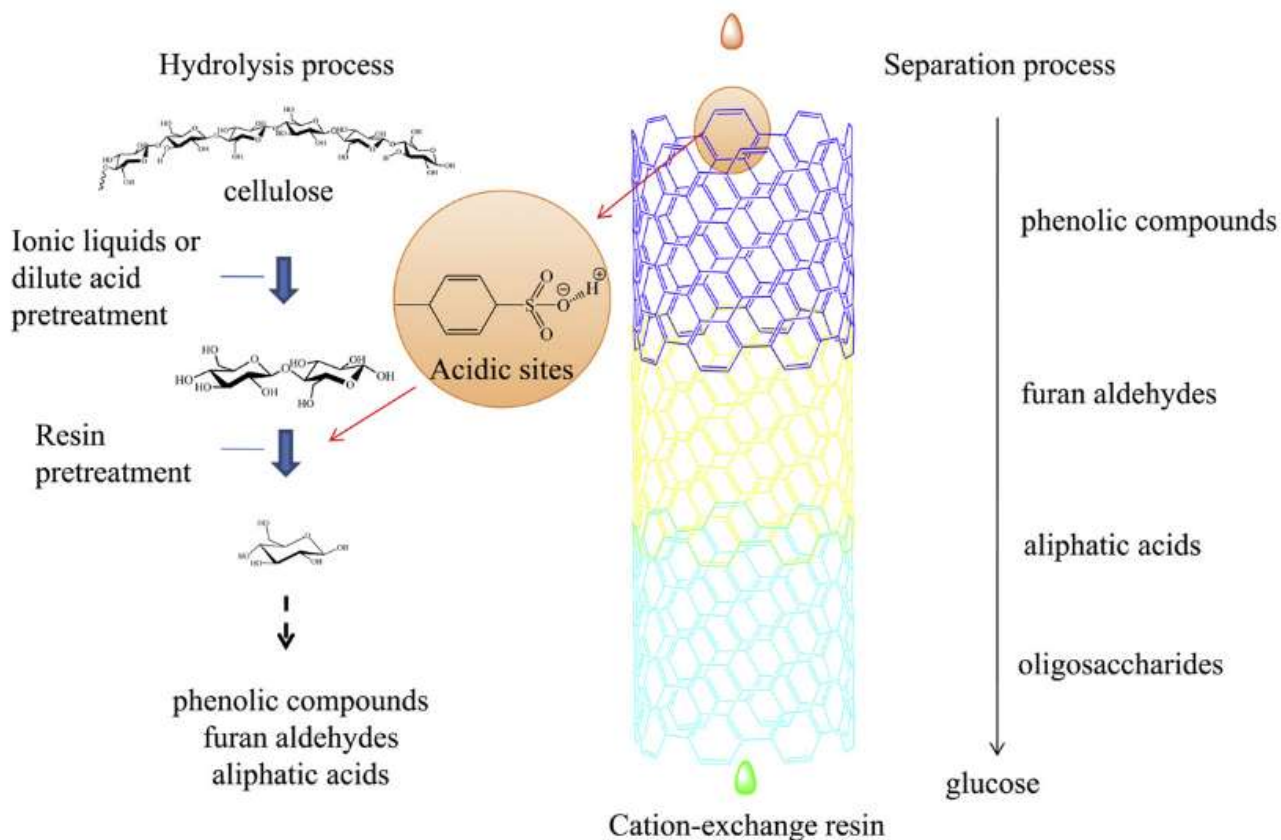


Figure 1.9. Combined cellulose conversion and product separation by IER. Reprinted with permission from [113].

The fouling and deactivation of packed resin could be due to the precipitation of oligosaccharides, phenolic compounds from lignin, and proteins by blocking catalytic sites [140]. IERs not only can be used for the hydrolysis of lignocellulosic material but also in other processes, such as the detoxification of hydrolysate to remove inhibitors [141,142] and conversion of monosaccharides to value-added products [143,144]

The efficacy of IERs is determined by their specific surface area, pore size, pore volume, active site concentration, and acidic type. To be highly effective in biomass pretreatment, IERs should have a high number of Bronsted acid sites, a good affinity for the reactant substrates, and good thermal stability. Furthermore, solid catalyst composition, porosity, presence of water to have ions in the liquid phase from IER, and reactor specifications could make it probable for hydrolysis of lignocellulosic biomass on a practical level [113]. Various functional groups, such as strong/weak acid groups, can modify the physiochemical stabilities of acidic IERs. The most important chemical and physical properties are

porosity, type of functionalisation, thermal stability, and capacity, which need to be considered before using IERs for any pretreatment process.

1.4.4.4. Porosity

The porosity and particle size of an IER can also be controlled through polymerisation conditions and uniform particle size manufacturing technology [139]. Typically, polymerisation IERs are spherical beads with polydisperse particle size distribution ranging from 0.3-1.2 mm, specific gravity 1.1-1.5 in a water-swollen state and bulk density 560-960 g L⁻¹ for a wet resinous product [88].

Porosity in an IER can be controlled by the cross-linking degree and the use of porogen during the manufacture. The more crosslinking degree, the more rigid the matrix. The polymeric matrix is hydrophobic, while the functional groups tend to be hydrophilic. This means that in the presence of polar liquids, the hydrophilic functional groups will form van der Waals bonds that will force the polymeric matrix to open (swelling) depending on the rigidity/flexibility of the matrix, therefore, the lever of cross-linkage. Apart from swelling, other properties of IERs, such as mechanical and chemical stabilities and capacity, are also linked to the cross-linkage level. As the cross-linkage increases in the polymer, the IER becomes more thermally and mechanically stable while the hydration and ion intake are reduced. [145].

Based on the crosslinking degree and the use of IERs can be divided into two categories:

- Gel-type: They are called like this because the low crosslinking degree (<10 wt.%) gives the polymeric resins a semi-transparent gel appearance. Due to their low crosslinking degree, they are less thermally and mechanically stable and have more swelling capacity. [146].
- Macroreticular: They are normally not transparent due to the larger cross-linking degree (9-50%). A high crosslinking degree generates more thermally and mechanically stable IERs, with limited swelling due to their rigidity, but with a certain fraction of permanent pores produced using the porogen during manufacture. [91]

Gel resins have higher initial exchange capacity and lower prices than macro-reticular resins of the same type. However, macro-reticular have a higher ability to elute foulants more effectively due to larger permanent pore structure and ability to work at harsher conditions in comparison to gel-type resins [147,148].

1.4.4.5. Type of Functionalisation

IERs typically have a cross-linked polymer matrix with a very homogeneous distribution of ion-active sites. Commercial acidic IERs can be categorised as strong acid resins or weak acid resins depending on the functional group attached to them, as shown in Figure 1.10.

- Strong acid resins are primarily sulfonic acid groups that act similarly to a sulfuric acid catalyst by removing hydrogen cations. Strong acid resins are known as sulfonated co-polymers, capable of exchanging cations or splitting neutral salts over the pH range.
- Weak acid cation exchange resins usually work similarly to weak acid and have available hydrogen from (R-COOH). One of the advantages of weak acid IERs is high regeneration efficiency using a small amount of acid, ultimately reducing waste from the regeneration process. Weak acid IERs are used for demineralisation, de-alkalization of water and water-softening processes [149].

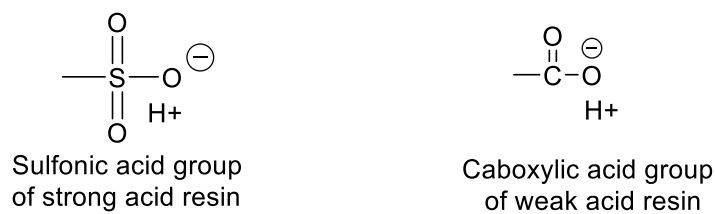


Figure 1.10. Functionality in ion exchange resins [138].

IER functional groups can be regenerated through different types of systems, such as co-flow and counter-flow block through backed bed processes with acid/bases depending on the functionality [139].

1.4.4.6. Thermal stability

The thermal stability of IERs depends on the type of functional group, the cross-linking degree, and the pH. Cationic resins, in comparison to anionic resins, are much more stable and can be operated up to 150 °C [139].

Thermal decomposition of an IER from 30-800 °C was tested in an oxidative environment and classified into three stages: the first step is the water evaporation and removal of physio-sorbed water (30-220 °C), the second step is the decomposition of active groups (220-400 °C) and crosslinking with the matrix and the third step is the combustion of polymer matrices (temp.>400 °C) [150,151]. The temperature ranges for all three steps may vary from one IER to another because of the change in the thermal stability of each IER.

1.4.4.7. Capacity

The number of exchange sites per unit weight for the dry resin (mmol/g) or units of volume for the wet resin (mmol L⁻¹) is a typical measure of IER capacity. At a high temperature (150-170 °C), cationic IERs lose their functional groups and activity. Furthermore, significant fouling of IER can occur, reducing its exchange activity by more than 80% [140].

Ion exchange has an interchange of ions between two phases, as shown in Figure 1.11. These resins are insoluble, and ions of the same charge exchange occur when contacted with a solution. The extent of the exchange will be determined by the ion concentration in the solution and the ion affinity for the insoluble phase compared to the solution phase. [152]. Furthermore, the exchange capacity is affected by the resin's intrinsic capacity, regeneration level, solution composition, flow rate through the column, temperature, particle size distribution, and swelling, which enhances the capacity [139].

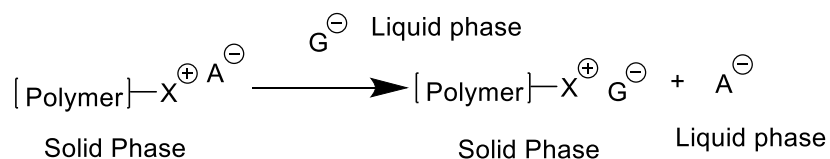


Figure 1.11. Ions exchange among the solid and solution phases of IERs [152] Legend: X⁺, fixed cation.

IERs are most commonly used in water softening, toxic metal removal, wastewater treatment, hydrometallurgy, sensors, chromatography, and biomolecular separations, as well as catalysts to replace homogeneous catalysts like sulfuric acid and immobilised metallic catalysts [152]. All these applications and capabilities (removing contaminants, ion exchange, and catalytic potential) make the IERs an interesting material for biomass pretreatment, such as hydrolysis. No literature was found where IERs alone had been used to hydrolyse any lignocellulosic materials due to IERs limited hydrolytic capacity, highly complex and resistant nature of the material as compared to cellulose and hemicellulose and inefficient in complete breakdown of lignocellulosic materials in fermentable sugars. IERs are always used with solvents like ionic liquids [153–158] to hydrolyse different herbaceous crops.

1.5. Advanced Pretreatment Methods using Ionic Liquids

Ionic liquids (ILs) are organic salts in liquid form at room temperature or close to it. ILs can replace volatile organic solvents in industrial applications because of special properties such as no vapour pressure, high thermal and chemical stability. However, when considering the use of ILs for biomass pretreatment applications, certain considerations should be made for recycling and regeneration requirements [159,160], as some ILs could be expensive. The high solvation capacity of ILs enables them to dissolve a wide range of materials with different polarities and structures, including biomass comprising hemicellulose, cellulose, lignin, silk, and chitin [161].

1.5.1. Some classifications of ILs

Room temperature ILs are salts that melt below 100 °C and can have tuneable properties (e.g. melting point, viscosity, polarity, opacity, and hydrogen bond basicity) depending on the choice of the cation and anion. However, the corrosivity and toxicity of room temperature ILs should be considered before using them in a chemical process [162].

ILs can be divided into Aprotic Ionic Liquids (AILs) and Protic Ionic Liquids (PILs). Ion generation is caused by covalent bond formation and breaking, which can result in AILs. On the other hand, PILs are formed by reversible proton transfer produced by ionic species. In Figure 1.12, the difference between the AILs and PILs forms of the IL made with imidazolium as a cation and acetate and chloride as the anion can be seen.

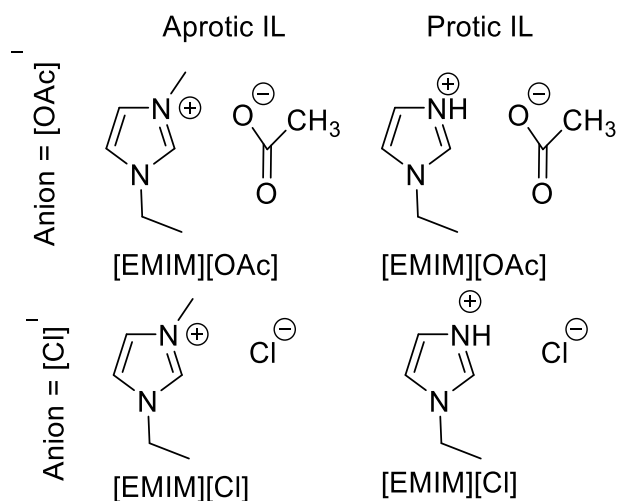


Figure 1.12. Structure of if imidazolium-based protic and aprotic IL adapted from [163].

The wide variety of ILs available provides high tunability of their properties, making them very interesting materials for many applications as solvents, catalysts, and extractive agents. ILs have also been studied for biomass pretreatment, so the next section summarises the main findings and work on ILs for biomass pretreatment.

1.5.2. ILs for Biomass Pretreatment

Lots of diverse ILs have been tested for lignocellulosic biomass pretreatment. The most typical cations used are: [BMIM]⁺, [EMIM]⁺, [Pyr]⁺, [TEA]⁺. The most common anions are [Cl]⁻, [HSO₄]⁻, [CH₃COO]⁻, [PF₆]⁻. The structures of the most common cations and anions along with their structures are presented in Appendix A1 Figure A1.5 and Figure A1.6, respectively.

For cellulose, the ideal IL should have a high dissolution capacity of cellulose while avoiding its decomposition [164]. However, IL pretreatment can be done to target other biomass components, such as lignin [165]. Appendix A1 Table A1.4 shows the different lignocellulose biomass and the ILs employed found in the literature and their impact on the cellulose, hemicellulose and lignin fractions. Most of the research for IL pretreatment for lignocellulose biomass in the past decade has been done to extract the maximum two components, cellulose and lignin, from raw material. The cellulose dissolution mechanism is shown in Figure 1.13 through intra and intermolecular hydrogen bonding in cellulose with IL ions.

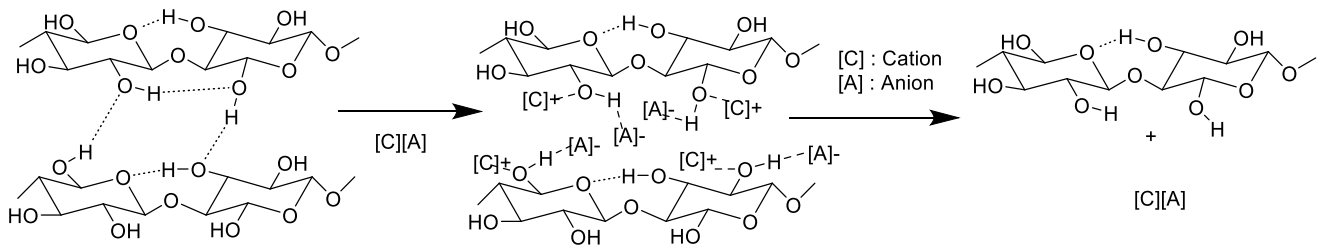


Figure 1.13. The dissolution mechanism of cellulose in ionic liquids adapted from [166]

In early research, the most common ILs for biomass pretreatment were imidazolium-based cations with various lengths of alkyl chains (C4, C6, C8) and anions, for instance, chloride and acetate [167–170]. For example, a [EMIM-OAc] could be used in lignocellulose biomass pretreatment such as hardwood Eucalyptus, after which there were significant changes in crystallinity of cellulose, ultimately increasing enzymatic sugars from treated biomass in comparison with untreated raw material. Pretreatment time of 4 h at 120 °C sugar yield maximised for pretreated Eucalyptus as compared to untreated material [171]. A general schematic of biomass fractionation using ILs is shown in Figure 1.14.

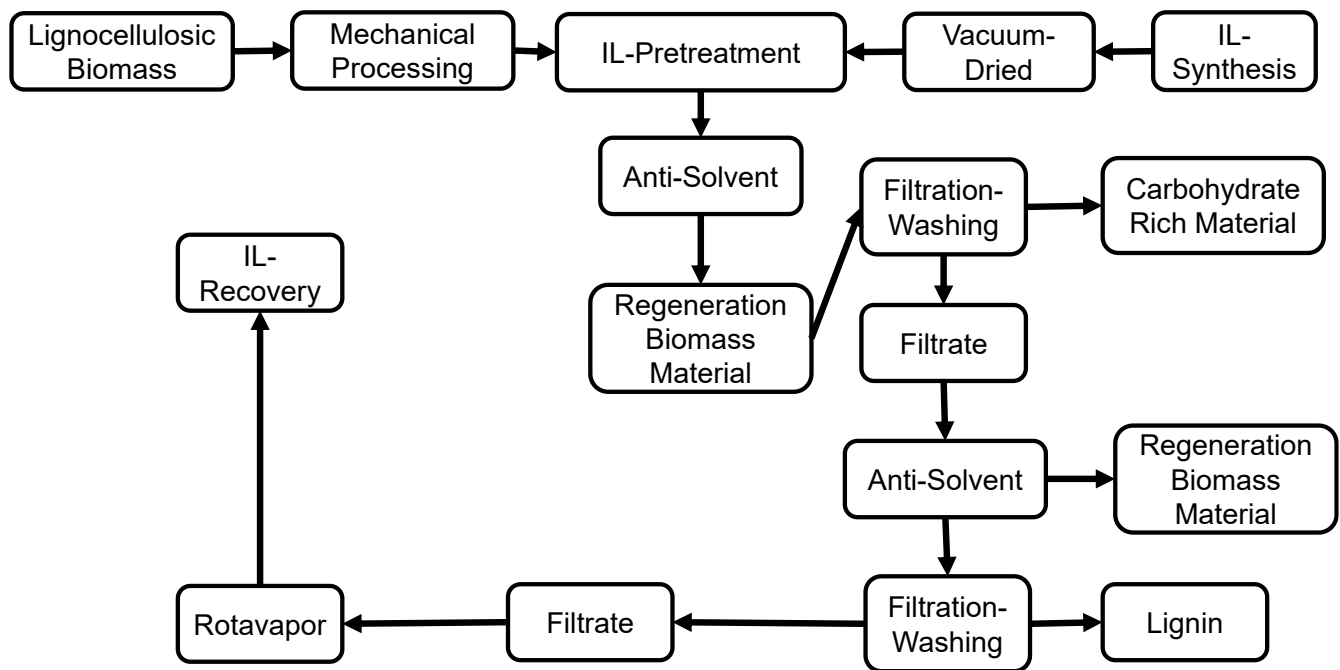


Figure 1.14. General schematic for lignocellulosic biomass fractionation with IL adapted from [172].

PILs offer a good selectivity for extracting lignin from the biomass with minimum impact on cellulose at around 100 °C [173–175]. On the other hand, AILs like imidazolium chloride-based ILs are more suitable for cellulose dissolution. However, with imidazolium cations, as alkyl chain length increases, the toxicity of IL increases and can be hazardous to the environment if released as a waste stream after an industrial process [176,177]. Using IL as a solvent for various lignocellulosic feedstocks makes it difficult to deduce the effects of the IL on the lignin, hemicellulose, and cellulose, as other important aspects influence the

pretreatment. Apart from the anion and cation, the solvent, antisolvent, particle size, biomass loading, temperature, and time are the main other parameters that highly influence the fractionation process. Therefore, parameters above mentioned and their effect on the pretreatment process are discussed in the next sections.

1.5.2.1. Effect of anion

The anion part of IL disrupts hydrogen bonding for biomass components [178], while the cationic part of IL interacts with biomass through covalent bonds [179]. Comparing both components, the anionic part plays a more significant role during biomass dissolution. The dissolution of any lignocellulosic components in an IL is significantly influenced by the length of the cation and anion, along with the presence of any solvent, such as water.

More specifically, small anions such as Cl⁻ ions have better dissolution of cellulose because it can better penetrate the structure and have strong electronegativity [180,181]. Their problem is the high melting temperature (50-300 °C) compared to other anions. For example, Ac⁻ anion makes lower melting points (-51-100 °C) IL, which is extensively studied and still has high cellulose dissolution [182]. Sulphonated anions have proven good for lignin dissolution from lignocellulosic biomass [183]. Anions such as [MeSO₄]⁻ and [HSO₄]⁻ can also be the most effective lignin/cellulose fractionation and enhancement of cellulose digestibility [184]. These anions can form strong hydrogen bonds with the hydroxyl groups in lignin, disrupting its structure and enhancing solubility. Furthermore, these anions can catalyse the breaking of particular links in lignin, such as the β-O-4 ether linkages, which are commonly seen in the structure of lignin [185]. This catalytic activity facilitates the decomposition of the lignin polymer into smaller, more soluble fragments.

ILs with anions: chloride, phosphate, and carboxylates have high hydrogen basicity to solubilise cellulose [186]. However, if hydrogen bond basicity in an IL is too high, it will start to compete/interact with hydrogen bond acidity, eventually reducing cellulose solubilisation [187,188].

1.5.2.2. Effect of cation

For the cation, the aromaticity seems to affect the lignocellulosic material dissolution [189]. It has been linked to the following: first structural effect, in which the p-electron delocalisation of the cation's unsaturated heterocyclic ring causes the IL to be more reactive with cellulose and allows more space for [Ac]⁻ anions to form H-bonds with cellulose. The second dynamic effect is that the cation's large saturated heterocyclic ring results in lower diffusion of both cations and anions [190]. The viscosity of IL is reduced by using a smaller cation with a shorter alkyl side chain, resulting in greater biomass

dissolving efficiency to some extent [191]. Because after a certain length, if the alkyl chain length with cation is increased, biomass solubility will decrease [181].

Furthermore, the melting point decreases its enhanced functionality, and biomass dissolution efficiency increases. Alkyl chains with cations can also influence the melting point of ionic liquids. For example, pyridinium cationic ionic liquids have a higher melting point than imidazolium-type ionic liquids [192]. Hydroxyl groups, on the other hand, have the opposite impact, most likely due to competition for H-bond formation with cellulose [188]. The melting point of ILs is generally reduced as the size of a cation with a low degree of symmetry and an increase in the size of anions with the same charge [193].

Cation has a secondary influence on fractionating lignin structure compared to anion in an IL. However, cations help in solubilising lignin by reducing the cohesive forces within the lignin structure, preventing reaggregation and promoting further interaction [194]. When a cation can effectively pair with anions with high hydrogen bond basicity, IL can disrupt lignin's structure and facilitate its dissolution.

Parameters Kamlet-Taft for an IL, which are temperature-dependent solvent polarity scales, can be used to predict the solubility of cellulose before experimentation [195,196]. IL with more hydrogen bond basicity is a very important factor in dissolving biomass material along with the structure of cation [197].

The overall ability of ionic liquids to dissolve biomass is mainly determined by the unique properties of the cation and anion and their interactions with the biomass's components. This comprehension enables the creation of task-specific ionic solutions customised to dissolve and process biomass effectively.

1.5.2.3. Effect of anti-solvent

Anti-solvent is also very important for the regeneration of cellulose, hemicellulose, and lignin because the yield and purity of each component change depending on which anti-solvent is used after the process. Conventionally, hot water, acetone/water mix is added to get Cellulose-Rich Material (CRM) and lignin obtained by evaporating acetone [198,199].

In comparison with alcohols such as methanol, ethanol, and others, water is a better choice as an anti-solvent because of its economic viability, environmentally friendly characteristics, and high yield of total reduceable sugars from cellulose [170]. However, when cellulose and lignin both are dissolved in IL from biomass dissolution, the two anti-solvents should be used, first ethanol to wash CRM and then water for lignin precipitation [200]. IL contamination is one of the pressing issues in regenerated material after the pretreatment process, which could denature enzymes during enzymatic hydrolysis. Furthermore, if there is lignin in CRM, it would significantly negatively impact post-process, like enzymatic hydrolysis. To minimise IL contamination, lignin could be regenerated separately [172]. To

have a high extraction yield of one biomass component, such as lignin from IL-treated biomass, extraction could be done in a sequential process [201].

In summary, antisolvents play a crucial role in the biomass pretreatment process with ionic liquids. They help effectively recover and separate biomass components while also improving the process's sustainability and cost-efficiency.

1.5.2.4. Effect of particle size and biomass loading

Particle size and biomass loading are very important factors in an IL pretreatment. To have maximum product yield after the process, the particle size of the raw material should be small (0.5-2 mm) because it produces maximum sugar yield [202,203]; however, in the case of regenerated biomass, yield increases with an increase in particle size [204,205]. The increase in yield is ascribed to multiple factors: less surface area for lignin re-precipitation, enhanced mass transfer, reduced fibre hornification, and decreased viscosity of the biomass-ionic liquid slurry [206]. Regarding biomass loading, at a lower Solid-to-Liquid ratio, each particle would receive a higher average value to heat, which could contribute to overcooking/burning the particle surface and reduction in cellulose digestibility [207]. On the contrary, high biomass loading of approximately 40-50 wt.% during IL pretreatment has drawbacks such as longer process time requirement, a partial transformation of cellulose crystallinity structure, increase in mixture viscosity, reduction in de-lignification and increase in hydrolysis kinetics [207–209]. Ideally, 10 wt.% of lignocellulosic raw material to an IL is considered to be optimum [210–212].

1.5.2.5. Effect of Temperature

Biomass pretreatment with an IL ranges for temperature and time 90-170 °C and 1-20 hrs, respectively [213–217]; however, for each lignocellulosic material having different physiochemical characteristics, optimum parameters will be different. During optimum temperature selection for the IL pretreatment process, the following considerations should be taken into account: IL lowest temperature for the liquid state, solubilisation efficiency for each biomass component, IL decomposition temperature, and temperature to maintain enzymatic activity if it is used during the pre-treatment process [177]. Similarly, longer pretreatment times facilitate lignin separation; however, carbohydrates would start to degrade. For example, for softwood such as eucalyptus to be treated with [EMIM-AC], the process temperature had to increase from 120 to 160 °C however, with IL [BMpy-Cl], process optimum conditions were time 10 min at 120 °C [218,219]. The product yield process time and temperature should be considered for optimum pretreatment results.

1.6. Mains findings, main research gaps and research objectives

Acid hydrolysis has been primarily studied using mineral acid. However, the literature on solid acid catalysts is scarce, as explained in the following paragraph.

Most solid catalysts, such as metal oxides, zeolites and carbonaceous materials, were tested with pure materials such as cellulose or hemicellulose. Among these catalysts, there are several significant challenges. A significant problem is the slow mass transfer between solid acid catalysts and cellulose, which might restrict the effectiveness of the hydrolysis process. The lack of optimal binding sites on the surfaces of solid acid catalysts impedes effective interaction with cellulose molecules [220]. Water, a solvent in acid-catalysed processes, can lead to the deactivation of catalytic sites or the hydrolysis of catalyst frameworks, hence necessitating the creation of hydrophobic solid acids [221]. The existence of possible catalyst poisons from biomass and biomass hydrolysates, including proteins and mineral ions, can adversely affect process performance [222]. The intricate and resistant characteristics of lignocellulosic biomass present obstacles to catalyst accessibility and efficacy. The diverse reaction characteristics between solid substrates (biomass) and solid catalysts hinder the comprehension and enhancement of the process [223]. Addressing these problems necessitates the creation of innovative catalysts featuring superior binding and catalytic domains, augmented hydrophobicity, and higher resistance to deactivation, alongside the advancement of more effective pretreatment techniques to augment biomass accessibility.

Using acidic ion-exchange resins to separate lignocellulosic material fractions in an aqueous system has not been studied extensively. An advantage of IERs is that they efficiently catalyse substrate decomposition into value-added products and remain stable in water and their mesoporous nature, which overcomes limitations related to other solid catalysts such as zeolite or carbonaceous solid acid [224].

Further, IERs with ionic liquids [153–158] such as [EMIM]OAc (1-ethyl-3-methylimidazolium acetate) [225], [BMIM]OAc (1-butyl-3-methylimidazolium acetate) [226], and [BMIM]Cl (1-butyl-3-methylimidazolium chloride) [153] utilised but not co-currently. The lignocellulosic biomass was first treated with IL to fractionate at a particular set of conditions, and then IERs were added to the system at a different set of conditions. Moreover, the ILs used were imidazolium-based, which has major drawbacks such as high cost, high viscosity, toxicity, recyclability problems, and moisture sensitivity [227,228]. Inexpensive protic ILs with IERs, such as triethyl ammonium acetate or triethylammonium hydrogen sulphate, had demonstrated better potential for scalability and feasibility.

Integrating IERs and ILs presents a promising yet underexplored research area in lignocellulosic biomass valorisation. To the best of our knowledge, systematic research on only IERs and comparison with the simultaneous use of IERs and inexpensive ILs for fractionation of different lignocellulosic biomass has not been done.

Therefore, this research aims to study the use of IERs in water and in inexpensive IL to assess their competitiveness and any symbiotic effect in the pretreatment of lignocellulosic biomass. Working with IERs-ILs for biomass fractionation systems, one of the challenges will be efficiently separating and recovering these components post-dissolution. This approach could lead to more sustainable and efficient biomass processing technologies, advancing the biorefinery field. Therefore, the main objectives of this thesis are the following:

- Investigate the influence of acidic IERs on the hydrolysis of lignocellulosic material in an aqueous system and compare it to mineral acid catalysts under similar operating conditions.
- Investigate the influence of different ILs in combination with different IERs on the fractionation process of a lignocellulosic material.
- Investigate how physiochemical characteristics of different lignocellulosic materials can influence the outcome of the pretreatment process using a combination of ILs and IERs.

Chapter 2. Materials and Methods

2.1. Chemicals

2.1.1. Biomass feedstock

Miscanthus x giganteus pellets, measured between 5 and 6 mm, were obtained from Aberystwyth University in 2016 (feedstock 1). The pellets came from the stem part of the energy crop. The biomass sample was harvested, milled (1 mm), and pelletised within three months of collection.

Pine Bark Wood (feedstock 2) was collected from a tree surgeon in the UK in 2023. Pine bark was chipped (10-40 mm), washed with water, and dried at ambient pressure and temperature.

Brewery-spent grains (feedstock 3) are produced from Barley malt by boiling it in hot water (~67 °C) for an hour; enzymes that exist naturally within the grain break down the starch into carbohydrates, which are fermented into alcohol.

2.1.2. Ion Exchange Resins (IERS)

Commercially available Ion Exchange resins (IERS) Amberlyst™ 15 (IER15), Amberlyst™ 35 (IER35), Amberlyst™ 45 (IER45), and Amberlyst™ 70 (IER70) were obtained from Dupont (France), while Purolite™ CT252 (IER252), Purolite™ CT275 (IER275), and Purolite™ CT482 (IER482) were procured from Purolite (UK).

2.1.3. Ionic Liquids (ILs)

ILs were synthesised using the following chemicals: trichloramine, acetic acid, Triethylamine hydrochloride, ethanol with (purity >99%), and sulfuric acid (purity ≥95%), procured from Acros Organics. For all the synthesis and experimental work, Milli-Q water with an electrical resistivity of 13.4 M cm and pH 6.998 at 25 °C and atmospheric pressure.

2.1.4. Synthesis of Fibre Detergent Solutions

Sodium dodecyl sulphate, ethylenediaminetetraacetic disodium salt (EDTA) (dehydrate), sodium borate, sodium phosphate dibasic (anhydrous), 2-ethoxyethanol, decahydronaphthalene, sodium sulphite, cetyl trimethyl ammonium bromide (CTAB) were procured from Acros Organics with purity >99% and used for compositional analysis.

2.1.5. Feedstock preparation

Lignocellulosic materials or any biowastes, such as wood, crops, seaweed, municipal solid waste, animal wastes, and other solids, need sample preparation to do any kind of pretreatment. Biomass usually needs drying and crushing to homogenise sample size. The standard ASTM (American Society for Testing and Materials) International E1757-01 [229] used for sample preparation with different modifications based on lignocellulosic material.

2.1.6. Miscanthus x giganteus grass (Feedstock 1)

The received pellets of *miscanthus x giganteus* were further ground into an average particle size of 1.0 mm using a heavy-duty cutting mill (Retsch SM 200). Raw material samples were prepared as per ASTM E1757-01 standard [229] however, prepared samples were kept at 20 °C after preparation. Further grinding and sieving into the different particle size ranges of the raw material were done using IKA Universal Mill M20 and Endecott's EFL 2000 Sieve Shaker, respectively. Samples with different particle size ranges were stored in sealed polyethene bags. Two particle size ranges: 425-800 µm and <106 µm were selected for analysis testing and labelled as MIS48 and MIS16, respectively.

2.1.7. Pine Bark Wood (Feedstock 2)

Pine Bark Wood (PB) was collected from the UK in 2023. Initial PB was dried in an oven at 105 °C for 48 hrs and was followed by the same steps presented for feedstock 1. Two main particle sizes, 425 to 800 µm and <106 µm, were selected for analysis testing and labelled as PB48 and PB16, respectively.

2.1.8. Brewery Spent Grains (Feedstock 3)

Brewery spent grains (BSG) were collected from the UK (Burning Soul Brewing) in 2023. BSG was initially dried in an oven at 105 °C for 48 hrs, and then the same preparation methodology as feedstock 1 was used. Two main particle sizes, 425 to 800 µm and <106 µm, were selected for analysis testing and labelled as BSG48 and BSG16, respectively.

2.2. Characterisation of IERs

2.2.1. Acid Capacity

The acid capacity in different IERs was measured through back titration. 0.04 M Sodium hydroxide (NaOH) and hydrogen chloride (HCl) solutions were prepared in 250 mL volumetric flasks. To dry the resins, approximately 2 g of IER were dried for 12 hrs in aluminium dishes at 105 °C. Around 1 g of each resin was transferred to 250 mL of NaOH solution stirred with a magnetic stirrer at 200 rpm at 25 °C for 8 hrs. Afterwards, the solution was filtered from mixed resin through vacuum filtration. Aliquots of 25 mL filtrate were titrated with an acid hydrogen chloride solution. Before titration, 2-3 drops of 1 mg mL⁻¹ of methyl red were added as an indicator (change from yellow to orange). The acid capacity of the IERs per gram of dried IER and other properties are summarised in Appendix 2 Table A2.1.

2.2.2. Swelling Degree

The swelling capacity as per Equation 2.1 shown below was measured to evaluate the change in the degree of swelling in the resin matrix of different IERs. Original resins were added separately in 150 mm disposable glass pipettes. The initial height of the packed resin was measured using a ruler. The pipette

was filled with deionised water, and after 1 hr, the new height of the resin was measured after swelling of the resin. The results are summarised in Appendix 2 Table A2.1.

$$\text{Swelling degree (\%)} = \frac{(\text{Height Wet IER} - \text{Height Dried IER})}{\text{Height Dried IER}} \times 100$$

Equation 2.1. Swelling Degree

2.3. Synthesis and Characterisation of Ionic Liquids (IL)

2.3.1. Synthesis of Triethylamine hydrogen sulphate [TEA][HSO₄] (TS)

Triethylammonium hydrogen sulphate IL, [TEA][HSO₄] (TS), was synthesised by adding drop-wise triethylamine from a burette into a beaker filled with sulfuric acid. The beaker with sulfuric acid was placed in an ice bath. The mixing of both solvents was done in equal amounts: 2.5 mols of triethylamine and 2.5 mols sulphuric acid [86,230]. After adding sulfuric acid, the reaction mixture was stirred for 3 hrs in an ice bath to achieve a colourless homogenous solution. Initial water content was measured by Karl Fischer titration with a V20 volumetric titrator (Mettler Toledo). The water content of the IL [TEA][HSO₄] was reduced using a Stuart Cold Finger Condenser RE402 rotary evaporator and a vacuum drying at 40 °C. Lastly, the water content of the ionic solution was adjusted to 20 wt.% [231]. The reaction mechanism is shown in Figure 2.1.

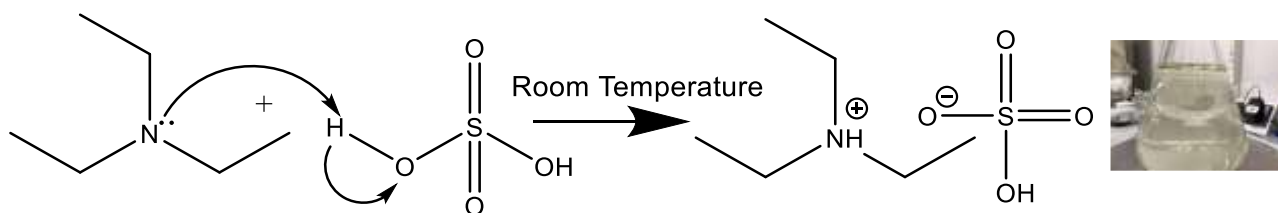


Figure 2.1. Triethylamine mixed with sulfuric acid in an ice bath.

2.3.2. Synthesis of Triethylamine acetate [TEA][OAc] (TA)

Triethylammonium acetate IL, [TEA][OAc] (TA), was synthesised by mixing drop-wise at 70 °C, 1.25 mol of triethylamine and 1.25 mol of acetic acid as [232]. Due to the low flash point of acetic acid at 39 °C, the mixing was carried out in a closed vessel using a two-neck round bottom flask. One neck was connected to a graham condenser with water used as condensing fluid, and the second was connected to a burette to add acetic acid. The round bottom flask was immersed in a water bath to heat at 70 °C. A magnetic stirrer was used to mix the reaction at 500 rpm. After completing the reaction, a black solution was formed and heated at 80 °C for 3 hrs in a conical flask to remove unreacted reactants. After completing the synthesis, the water content of the IL was measured and adjusted to 20 wt.%. The reaction mechanism is shown in Figure 2.2.

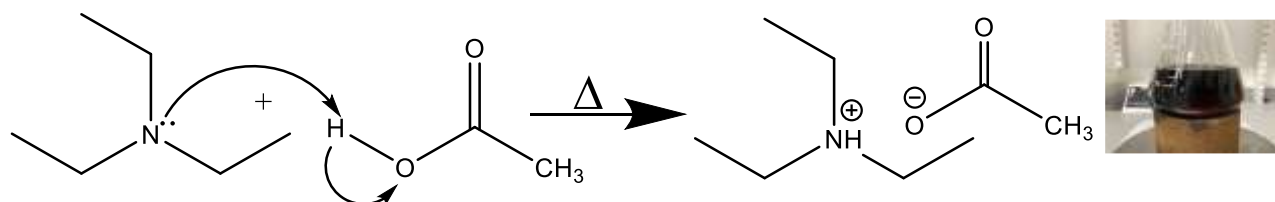
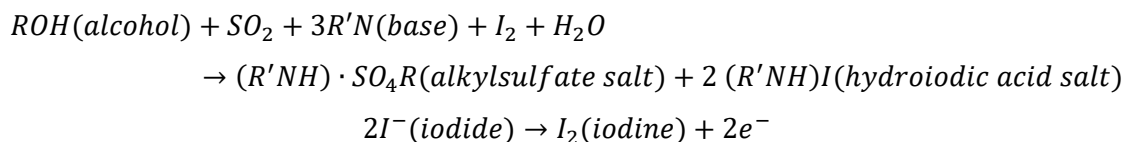


Figure 2.2. Triethylamine is mixed with acetic acid under a closed system.

2.3.3. Water Content

In ionic liquids (ILs), it is very important to know distilled water content because it influences their physiochemical properties and eventually influences lignocellulosic pretreatment results. Different ILs behave differently in the presence of water. For example, cation 1-ethyl-3-methylimidazolium with acetate anion produced better glucose yield with lower water content; however, hydrogen sulphate anion performed better at higher water content and additionally produced lignin fraction [233]. Water content in any liquid can be tested through the standard method ASTM International E203 using Karl Fisher (KF) Titration [234]. The working principle of KF titration is a simple redox reaction, as shown in Equation 2.2 [235].



Equation 2.2. Karl Fisher titration stoichiometry

Through redox reaction, intermediate alkyl sulphite salt is oxidised by iodine to produce alkyl sulphate salt. Eventually, during this oxidation, water in the solution is consumed. Once water is consumed, excess iodine is detected through the electrode. Even though iodine is generated electrochemically by anode oxidation at the generator electrode, it acts as a cathode containing catholyte. The anode is a double-pin platinum measuring electrode that monitors the current potential of the sample solution during titration [236]. Mettler Toledo V20 Volumetric KF Titrator was used for water content along with working medium Hydranal K and titrant Hydranal Composite 5K, both from Honeywell Research Chemicals. A sample of around ~0.5 mL was collected through a 1.0 mL syringe, weighed on a balance, and injected into the titration flask. A sample should be added when the potential in KF is stable and below the recommended value. The mass of the sample was obtained by measuring before and after injection. A change in current potential through a platinum electrode, along with the mass of the sample and time to reach the endpoint, was combined by the instrument to determine the water content of the sample under investigation.

2.4. Feedstock and Pulp Characterisation

Solid characterisation techniques were used to characterise and analyse the influence of different pretreatment factors on raw materials before and after the process.

2.4.1. Compositional analysis

The chemical composition of lignocellulosic materials was conducted through the fibre analysis method [237]. The procedure is below. First, a neutral detergent solution was made using 30 g of Sodium dodecyl sulphate, 18.61 g of EDTA (dehydrate), 6.81 g of Sodium borate, 4.56 g of Sodium phosphate dibasic (anhydrous), and 10.0 ml of 2-Ethoxy ethanol (ethylene glycol mono-ethyl ether) in a 500 ml beaker of pure water. The amalgamation was agitated via the beat and the magnetic stirrer. The volume was adjusted to 1L by the addition of distilled water. The pH was modified to a range of 6.9 to 7.1. Neutral detergent fibre (NDF) was determined by taking ~1.0 g of biomass in 100 mL of neutral detergent solution, 2.0 mL decahydronaphthalene, and 0.5 g sodium sulphite refluxed at 100 °C for 1 hr. After reflux, the residue was filtered and washed with hot water (100 mL) x 3 and acetone to remove any organic solvent. The residue was dried at 105 °C for 12 hrs, weighed and labelled NDF.

Acid detergent fibre (ADF) is determined using an acid detergent solution. The Solution was prepared using 1 L of 0.5 M sulfuric acid (H_2SO_4) and 20 g of CTAB. Biomass ~1.0 g in 100 mL of acid detergent solution and 2.0 mL decahydronaphthalene, refluxed at 100 °C for 1 hr. After reflux, the residue was filtered and washed with hot water (100 mL) x 3 and acetone to remove any organic solvent. The residue was dried at 105 °C for 12 hrs, weighed, and labelled ADF.

Acid detergent lignin (ADL) was estimated using 72% H_2SO_4 and ADF. Dried ADF was transferred to a Gooch crucible (grade 2), and the acid was added. The crucible was always filled with acid for 3 hrs. After 3 hrs, the residue was washed with excess hot water until the pH of the filtrate was ~7.0. The residue was dried at 105 °C for 12 hrs, weighed, and labelled ADL. Heating dried ADL at 500 °C for 5 hrs, the ash content was estimated.

2.4.2. Thermogravimetric Analysis (TGA) and Proximate Analysis

TGA is a thermal analytical technique where a sample's mass change is measured as a function of temperature or time under a controlled atmosphere. In a TGA, usually, precision balance is used to measure change in mass along with sample pan, reference pan and heating furnace [238]. The results of TGA analysis for a lignocellulosic material can vary and depend on the following factors: heating rate, type of sample, particle size, experimental atmosphere, and gas flow rate. Through TGA characterisation, the thermal degradation of biomass samples, the compositional analysis of lignocellulosic material, and the proximate analysis can be evaluated.

Proximate analysis is an important characterisation method used to determine moisture content (MC), volatile content (VC), ash content (AC), and fixed carbon (FC) in biomass raw materials and products. These parameters can influence the raw material's thermal behaviour and plant design. Proximate analysis can be used to assess the quality of biochar [239], biomass [240] and to calculate a higher heating value for a lignocellulosic material [241]. MC and AC can be measured according to standard ASTM E1756-08 [242] and ASTM E1755-01 [243]. However, due to the low amount of sample obtained for pulp and lignin, the proximate analysis was obtained from the thermogravimetric analysis (TGA) curves under an inert environment (N₂ gas) and an oxidative environment (air).

For the TGA analysis, 3-5 mg of the sample was weighed in a 70 µL alumina crucible using laboratory microbalance 2.1 g XP2U Mettler Toledo. The sample was placed in an autosampler for the Mettler Toledo TGA/DSC 3 STAR system. The schematic diagram of TGA/DSC is shown in Figure 2.3. The analyser has a precious micro balance within the furnace and is connected to the STARe Excellence Thermal Analysis software.

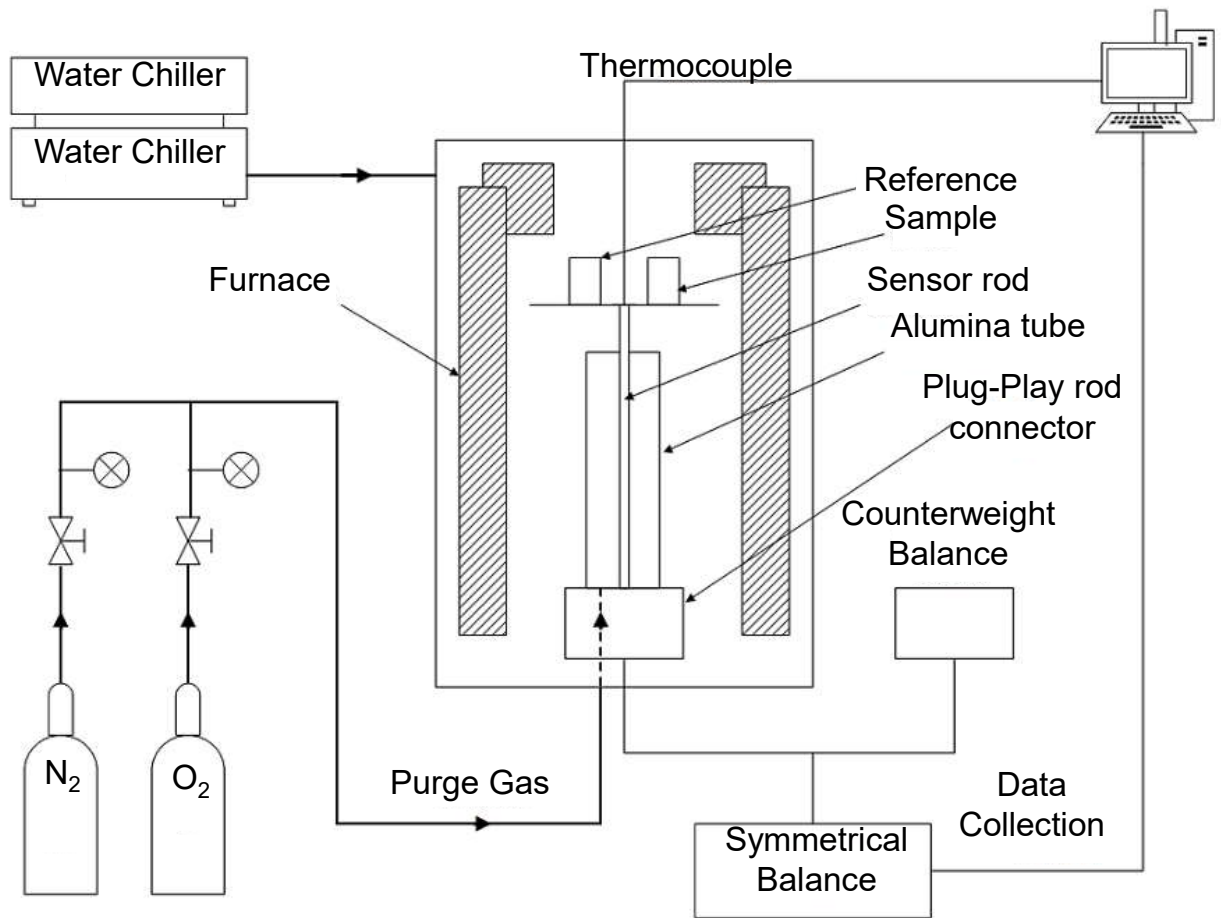


Figure 2.3. Schematic diagram of the TGA-DSC adapted from [244].

Under inert conditions, 50 mL min⁻¹ of nitrogen (N₂) was used as the carrier gas. The temperature was ramped from 25-900 °C with a heating rate of 10 °C min⁻¹, followed by an isotherm at 900 °C for 5 minutes. Under oxidative conditions, 50 mL min⁻¹ of air was used as the carrier gas. In this case, the temperature was ramped from 25-575 °C with a heating rate of 10 °C min⁻¹, followed by an isotherm at 575 °C for 5 minutes. The blank was conducted using an empty crucible, and the data were subtracted from the sample results to remove errors due to the buoyancy effect while heating. Each sample was analysed by triplicate. Through the TGA curve of the residual percentage of mass versus temperature, the differential thermogravimetric (DTG) curve was derived for all the samples to identify maximum decomposition temperatures (DTG_{max}). The second derivative was calculated to identify point changes in DTG curve temperature for different samples.

As mentioned, the proximate analysis was obtained from the TGA curves. Under inert conditions, the moisture content (MC) was calculated as the percentage of mass loss between 25-105 °C, and the volatile content (VC) was calculated as the mass loss in the temperature range of 105-900 °C. From the TGA curve under oxidative conditions, the ash content (AC) was obtained from the residual percentage mass at 575 °C [245]. Finally, the fixed carbon (FC) was calculated through difference as per Equation 2.3.

$$FC \text{ (wt. \%)} = 100 - MC - AC - VC$$

Equation 2.3. Fixed carbon calculation

where:

FC = Fixed carbon (wt.%)

MC = Moisture content (wt.%)

AC = Ash content (wt.%)

VC = Volatile content (wt.%)

2.4.3. Ultimate Analysis and Higher Heating Value (HHV)

The quantification of elements: carbon (C), hydrogen (H), nitrogen (N), and sulphur (S) for any biomass is known as ultimate analysis. Elemental analysis can be very useful in determining the quality of air required for combustion, as well as the volume and composition of combustion gases. For example, a fuel's higher carbon and hydrogen content results in a higher calorific value. Moreover, through elemental analysis, hydrogen to carbon effective ratio can be calculated, meaning how easily solid feedstock can be converted into hydrocarbons [246,247]. The elemental composition is usually calculated through the combustion of a sample at high temperatures, around ~1000 °C under static or dynamic conditions. In this process, high purity of oxygen is used to convert carbon into carbon dioxide, hydrogen into water, and nitrogen and sulphur into their respective oxides. The combustion products

are carried by a helium flow to a high-purity copper reactor to remove unreacted oxygen and convert nitrogen oxides to nitrogen gas. The concentration of each gas in the combusted gas mixture (CO_2 , N_2 , H_2O , SO_2) is determined through gas chromatography and thermal conductivity detector. Sometimes, individual gases can also be analysed through separate infrared (IR) detectors and thermal conductivity cells [248].

Ultimate analysis was conducted using CHNS-O Analyser Flash 2000 – Organic Elemental Analyser, Thermo-Scientific with operating parameter furnace at $900\text{ }^\circ\text{C}$, oven $50\text{ }^\circ\text{C}$, helium as carrier gas flow rate 140 mL min^{-1} with high purity oxygen grade N5.5 at pressure 3.5 bar, detector thermal conductivity detector (TCD) with filament level around $1000\text{ }\mu\text{V}$. TCD can detect gases such as hydrogen, oxides of carbon, nitrogen and sulphur, and inorganic gases. The working principle is a measurement of thermal conductivity, which is dependent on gas composition. TCD has two channels: the first for sample components with a carrier gas and the second for carrier gas acting as a reference. The difference in thermal conductivity between both cells results in voltage difference, ultimately proportional to the sample concentration of different gases [249,250]. Sulphanilamide (CE Instruments) was used as a calibration standard, and vanadium pentoxide (CE Instruments) was used as an oxidising agent. Three replicates were done for each sample, and the average was taken to minimise experimental error. Samples were analysed in triplicates on a dry basis by drying overnight in a furnace at $105\text{ }^\circ\text{C}$.

The heating value for any lignocellulosic material is an important characteristic to know the inherent energy released by a material upon combustion. This parameter is also used to compare conventional fossil fuels, and the type of fuel used as a power plant fuel. A higher heating value is also known as gross calorific value, considered as the enthalpy of complete combustion of a fuel when all the carbon and all hydrogen are converted to carbon dioxide and water, respectively. Furthermore, a higher heating value is defined at standard conditions of pressure 1 atmosphere and temperature $25\text{ }^\circ\text{C}$ for all products, including condensation enthalpy of water [251]. However, in the case of lignocellulosic material, other factors can influence HHV. For example, lignocellulosic material, which is a mixture of cellulose, hemicellulose, lignin and other compounds, depends on environmental factors: field location, rain, humidity, sunlight exposure, harvest time, etcetera. Elemental composition in a material can be related to its inherent energy content [241,252]. The higher heating value (HHV) for biomass and pulp can be estimated through Equation 2.4 [201,253].

$$HHV (MJ/kg) = 0.335[C] + 1.423[H] - 0.154[O] - 0.145[N]$$

Equation 2.4. HHV using elemental composition percentages.

where:

C = Carbon (wt.%)

H = Hydrogen (wt.%)

O = Oxygen (wt.%)

N = Nitrogen (wt.%)

2.4.4. Attenuated Total Reflectance-Fourier Transformation Infrared Spectroscopy (ATR-FTIR)

Electromagnetic radiation at the macroscopic level behaves as a wave, but at the atomic or molecular scale, it acts close to a photon particle, which is a discrete packet of energy that can be divided into different regions based on wavelength. When electromagnetic radiation in the form of middle infrared ($4000-400\text{ cm}^{-1}$) is absorbed by a molecule or an atom, it vibrates in multiple forms: asymmetric, symmetric, transverse, and rotation of a group of atoms around a node [254,255]. Based on the selection rule molecular vibrational mode through infrared (IR) can be activated that can be linked to changes in the permanent dipole. In conclusion, the vibrational frequency of a chemical functional group in a specific region is dependent on the types of atoms and chemical bonds involved [256]. IR spectra mostly represent percent transmission (% Transmittance) or absorbance.

Fourier Transformation Infrared (FTIR) is a technique where infrared radiation is passed through a sample where some of the radiation absorbed by the sample and some transmitted through it results in an infrared spectrum. The MIR scan is divided into two regions: the first functional group between 4000 to 1450 cm^{-1} and the second fingerprint region from 1450 to 500 cm^{-1} . The fingerprint region is unique to each chemical compound. Through FTIR, the quality of a material can be determined along with its functional groups. It has a certain advantage as compared to other techniques regarding analysis, such as speed, sensitivity, mechanical stability and internally calibrated [257]. Attenuated Total Reflection (ATR) is an additional accessory to the FTIR technique, in which total internal reflected infrared is measured after contact with the sample. In ATR-FTIR, the infrared passes through an optically dense material (crystal) placed in very close and firm contact with the sample. This enables the analysis of solid samples directly with high sensitivity without requiring the preparation of pellets. It is also more surface-sensitive.

An evanescent wave is created when the material is subjected to attenuated energy from passing the IR beam through the crystal and then to the detector in the IR spectrometer. For the ATR-FTIR technique, the following conditions must be fulfilled: the sample must have direct contact with the crystal,

the refractive index of the crystal should be higher than the sample to have total internal reflectance, and the MIR range should be applied [258].

Thermo-Scientific Nicolet iS50 FT-IR & iS50 ATR with diamond crystal along with OMNIC™ Spectra software used to analyse the feedstock, pulp, lignin and ILs. A mercury cadmium telluride-A detector was used because of its highest mid-infrared sensitivity, with a low throughput requirement at a faster scanning rate while maintaining constant IR response. The detector works under cryogenic conditions, usually with liquid nitrogen, and a quantum detector, meaning detecting photons while measuring [259]. The results were obtained between 400-4000 cm^{-1} after 64 scans with a resolution of 4 cm^{-1} . The detailed conditions of operation for the equipment are in Appendix 2 Table A2.2.

2.4.5. X-ray Diffraction (XRD)

X-rays are a kind of electromagnetic spectrum generated through metal when electrons produced by a heated cathode strike a metal surface. For a generation of X-rays, high voltage ranging from 20-50 kV is required, with an anode made up of metal and a cooling water system to avoid overheating [260]. When high-energy electrons interact with an anode it produces characteristic radiation depending on the type of anode material. The working principle of characteristic radiation is that an incident electron collides with an electron of some atomic shell in the anode and knocks it out. This gap produced is filled by an electron from a higher shell. This transferring of electrons to lower levels releases energy as X-ray fluorescence. This radiation is dependent on the electronic structure of each element. For example, $K\alpha$ radiation is produced when an electron transfers from the L shell to the K shell, and $K\beta$ radiation is produced when an electron transfers from the M shell to the K shell. To reduce $K\beta$ radiation, a nickel (Ni) $K\beta$ filter can be used, which consists of 0.02 mm thin Ni foil where its core electron absorbs copper (Cu) $K\beta$ radiation [261].

Through powder XRD crystallinity of any solid material can be analysed along with its allomorphs and crystallinity index. In this technique a beam of X-ray impinges on a solid sample which rotates in the plane with an angle (θ) relative to the X-ray beam which reflects when encounters a crystal plane in the sample causing constructive interference diffraction of the beam and this reflected radiation is counted by a detector forming an angle 2θ with the sample [256]. The constructive interference due to in phase of scattered waves produced due to the difference in path lengths of the waves is equal to an integer multiple of the wavelength. The distance between crystal lattice planes considered d with lower beam transverse an extra length of $2d \sin(\theta)$ [254]. The constructive interference at angle θ can be described by Bragg's law as shown in Equation 2.5.

$$2d \sin(\theta) = n\lambda$$

Equation 2.5. Bragg's law equation

where:

n = Positive integer order of reflection

θ = Angle of incidence (°)

λ = Wavelength of incident X-ray (nm)

d = Distance between crystal lattice planar (nm)

XRD analyses of dried raw material and pulp were conducted using the Bruker D8 advance instrument with Diffrac.EVA software will extract data with the LYNXEYE detector. The analyses were performed within the angle range $2\theta = 10-80^\circ$ with a step size of 0.0204° operated at voltage 40 kV and current 40 mA using Cu-K α 1 radiation with a wavelength of 0.1546 nm. The details of the equipment set parameters are summarised in Appendix 2 Table A2.3.

After the analysis, the background from the diffractogram was subtracted, and the degree of crystallinity index (CrI) was calculated through the Segal equation [262]. using the crystalline and amorphous phases of cellulose as shown in Equation 2.6.

$$CrI = \left(\frac{I_{002} - I_{am}}{I_{002}} \right) \times 100\%$$

Equation 2.6. Segal equation for the calculation of the crystallinity index

where:

I_{200} = Maximum intensity at $2\theta = \sim 22.0-22.5^\circ$ due to crystalline part of solid

I_{am} = Minimum intensity at $2\theta = \sim 18.0-18.5^\circ$ due to amorphous part of solid

Calculating crystallinity (X_d) based on areas of crystalline and amorphous peaks deconvolution was done using the Gaussian function, ranging from 2θ equal 5° to 40° (Equation 2.7). Peaks due to crystallographic planes were assigned at 101, $1\bar{0}\bar{1}$, 002 and 040 with an amorphous peak at a minimum diffraction profile between $1\bar{0}\bar{1}$ and 002 peak [263,264].

$$X_d = \left(1 - \frac{S_a}{S_a + S_{cr}} \right) \times 100\%$$

Equation 2.7. Crystallinity calculation using the Gaussian function.

where:

S_a = Amorphous integrated area

S_{cr} = Sum of integrated area of peaks: 101, $1\bar{0}\bar{1}$, 002, and 040.

The Crystallite size was calculated using the Scherrer equation (Equation 2.8) using the full width half maximum value (FWHM) at the position, $2\theta \sim 22.5^\circ$, with an instrument broadening correction factor.

$$\tau = \frac{\kappa \times \lambda}{\beta \times \cos(\theta)}$$

Equation 2.8. Scherrer equation for the calculation of the crystallite size

where:

τ = crystallite size

κ = constant shape factor as 0.94

λ = X-ray wavelength (0.154060 nm)

β = line broadening at FWHM in radians

θ = Bragg's angle in degrees.

2.4.6. Scanning Electron Microscopy-Energy Dispersive X-ray (SEM-EDX)

Scanning Electron Microscope (SEM) uses electrons instead of light for imaging. It has several advantages over traditional microscopes, for example, a large depth of field allowing more specimens at one time, higher resolution, magnified much higher levels and clear images. The schematic diagram of SEM [265]. There are major components in SEM: an electron gun as an electron source, electromagnetic lenses to focus the electron beam and demagnify the beam into a small electron scope, a deflection system to change the direction of the electron beam and detectors to collect signals emitted from a sample under investigation [266,267]. The whole equipment is under total vacuum to protect the electron source from oxidation, prevent scattering of electrons, and reduce water partial pressure and carbon around the sample. Even though SEM provide 3D images with high resolution and high magnification, the technique has some disadvantages: expensive, large, special training required to operate, sample preparation required, analysis is limited to solid samples and a small risk of radiation exposure due to electrons scatter passing through the sample surface [268]. SEM can be connected to energy dispersive X-ray (EDX), through which elements on the surface of a solid material under investigation can be determined. Through SEM-EDX, different solid material structures can be classified by examination of surface morphology, identification of particle contamination, structural analysis, identification of corrosion and oxidation problems [269]. The solid samples were dried and analysed using the SEM-EDX JEOL 7800 series equipment before the analysis.

2.5. Experimental setup for reaction and purification

2.5.1. Reaction set-up and procedure

Experimental reactions were carried out in Radley carousel hot plates using a 50 mL Ace round bottom pressure flask with a sealed screw cap (with a gas valve).

For the reaction, ~2.0 g of biomass sample and ~20.0 g of solvent (water, water + mineral acid, IL or IL + mineral acid) were loaded and added to the flask. Then, the desired amount of IER (from 0 to

1.5 g) was weighed and loaded into the flask using either mesh baskets of 0.25 g capacity each (up to 4 baskets) or directly loaded into the flask (up to 1.5 g). The flask was sealed, and the temperature was set on the hot plate. When the desired temperature was reached, the flask was pressurised with compressed air at 0.2 MPa. If stirring was used, the stirring was activated, and the reaction was left for 2 hrs. Afterwards, the flask was removed from the hotplate and cooled to room temperature.

2.5.2. Product Washing

2.5.2.1. Pulp washing for acid hydrolysis experiments

After the reaction, the mixture is filtrated using filter paper and vacuum. If the IERs were loaded inside the stainless-steel mesh baskets, the baskets were removed at this point. The solid is washed with deionised water at 90 °C until the pH is 7 (approx. 500 mL). The solid is transferred to a drying oven to dry overnight [270].

2.5.2.2. Pulp washing for experiments in which ILs are involved

2.5.2.2.1. Pulp-Washing

After the pretreatment reaction, the round bottom flasks were removed from the hotplate and cooled to room temperature. The pretreated mixture was transferred to 50 mL centrifuge tubes with 30 mL ethanol in each tube. If IERs were loaded inside the stainless-steel baskets, they were first removed, and the remaining mixture was centrifuged at 10,000 rpm for 15 min. The liquid was decanted from the tubes. This pulp washing and centrifugation were repeated 3 times. Subsequently, the washed pulp was transferred to a cellulose thimble and subjected to Soxhlet extraction for 10 hrs with 150 mL of ethanol to remove the residual solvent. The pulp was air-dried overnight under the fume hood and stored in a plastic bag at room temperature. If the IER was loaded directly into the flask, the IER was separated from the pulp after air-drying using a sieve.

2.5.2.2.2. Lignin-Washing

After all the pulp was washed and separated, the liquid solution contained the following: ethanol, dissolved lignin, original solvent, and soluble lignin. To recover lignin, ethanol was removed using a BUCHI R210 rotavapor at 75 °C under vacuum (289 mbar). After removing ethanol, 40 mL of deionised water was added to precipitate lignin. After 12 hrs, the mixture was transferred to 50 mL centrifuge tubes. The liquid was removed after centrifuging at 10,000 rpm for 15 min. To finish the washing, 30 mL (3 times) of deionised water was added, centrifuged at 10,000 rpm for 15 min, and decanted. Washed lignin was mixed with 15 mL of ethanol and transferred to a Petri dish. The Petri dish was placed under a fume hood overnight at room temperature to evaporate the ethanol. Lastly, lignin was scrapped off the petri dish and transferred to a glass vial for further analysis. The remaining solution, the water, was

removed through the rotavapor at 75 °C under a vacuum 120 mbar, and the solvent was stored in a glass bottle.

Chapter 3. Evaluation of Ionic Exchange Resins for Acid Hydrolysis

3.1. Introduction

Acid hydrolysis of lignocellulosic biomass is one of the pretreatment methods used to fractionate the lignocellulosic matrix into its three major components: cellulose, hemicellulose, and lignin. One of the main objectives of this process is to gain accessibility to the cellulosic fraction when processing downstream, such as in the production of bioethanol. Conventionally, concentrated or diluted mineral acids such as sulfuric acid (H_2SO_4) or hydrochloric acid (HCl) are used to fractionate lignocellulosic materials [271]. Due to the toxic, corrosive and hazardous nature of these acids, the equipment used for this process step requires to be corrosion resistant. There is also the need for neutralisation and recovery of the acid, and inhibitors for the downstream steps can be produced [271].

Dilute acid hydrolysis (DAH), using 0.3-2.5 wt.%, [272] is sometimes preferred to concentrated acid hydrolysis (72 wt.% sulfuric acid or 42 wt.% hydrochloric acid or 77-83 wt.% phosphoric acid). One example is when hydrolysis is the preliminary step to fermentation. This is because DAH can prevent the formation of fermentation inhibitors, such as furan and phenolic derivatives [273,274]. However, at high temperatures (110-240 °C), DAH can produce pseudo-lignin by dehydration and polymerization of inhibitory products such as furfural and 5-HMF to form an aromatic lignin-like structure. It can deposit on the cellulosic pulp and act as a barrier between the cellulosic polysaccharides and the enzymes. This hinders the fermentation process and decreases the biofuel/bioethanol production yield [275].

This chapter will explore the use of ion exchange resins (IERS), specifically sulfonated acid exchange resins, and how they compare to conventional methods. Therefore, this chapter is split into two main sections and objectives: first, acid hydrolysis with two ion exchange resins (Amberlyst 35 and Amberlyst 70) will be evaluated with different loadings to find out the effect of each IER to biomass ratio and select the most active resin. IER70 and IER35 are two distinct kinds of cation exchange resins. IER70 consists of a matrix composed of a copolymer of chlorinated styrene and divinylbenzene, which contains functional sulfonic acid groups. The material possesses a macro-porous configuration and is specifically engineered for high-temperature environments, capable of withstanding temperatures up to 190°C. The acid site concentration of IER70 is lower (2.55 mmol g⁻¹) than that of IER35 [276].

On the other hand, IER35 is derived from a styrene-divinylbenzene copolymer that does not contain chlorine, and it contains sulfonic acid groups. This IER has a greater concentration of acid sites (~5.2 mmol g⁻¹) and functions at temperatures below 150°C [277]. The main distinction is that IER70 exhibits superior thermal stability due to its chlorinated backbone, whereas IER35 exhibits higher acidity but is constrained to lower operational temperatures [278].

Second, it will compare the ion exchange resins with mineral acids solutions (H_2SO_4 and HCl) at equal proton concentration to evaluate the differences between mineral acids and solid acids. This concentration of acid has not been reported previously in literature, and there is no comparison of IER and mineral acids at the same equivalent concentration of protons.

Miscanthus x giganteus was used as lignocellulosic biomass feedstock to compare the IERs. This feedstock type was selected for hydrolysis due to its advantageous characteristics, including high biomass production (winter harvest yields range 11-14 tonnes of dry mass per hectare per year [279]), favourable composition (cellulose 43-55 wt.%, hemicellulose 18-23 wt.% and lignin 17-25 wt.%), strong responsiveness to pretreatment (due to high carbohydrate contents as compared to lignin), and greater product yields (ethanol 70% of theoretical yield after hot water pretreatment [280]). These qualities make it superior to normal woody biomass [281,282]. Stainless steel mesh baskets (with a maximum capacity of 0.250 g of dry IER each) were used to load the resins. Different IER loadings from zero baskets (0 g of IER) to four baskets (1 g of dry IER) were compared for the hydrolysis of 2 g of biomass feedstock. The solvent used in this chapter was distilled water. All the experiments presented in this section were performed at 0.2 MPa and 110 °C for 2 hrs. After each experiment, the pulp was washed as described in section 2.5.2.2. The nomenclature used in this chapter is introduced and presented in Table 3.1.

A blank experiment was conducted with empty baskets and water only to understand and isolate the effect of water at 110 °C. The resulting pulp for the blank was labelled as P-IER00-0B.

Table 3.1. Summary of nomenclature for the raw material and pulp samples in Chapter 3

Name	Nomenclature
Miscanthus x giganteus (425-800 μm)	MIS48
Pulp	P
Ionic Exchange Resin	IER
Cationic Exchange Resin Amberlyst 35	IER35
Cationic Exchange Resin Amberlyst 70	IER70
No ion exchange resin	IER00
Number of Baskets (# = 0, 1, 2, 3, 4)	0B, 1B, 2B, 3B, 4B
Pulp-resin-number of baskets	P-IERXX-#B
Pulp-equivalent protons of HCl to 2 baskets of Amberlyst XX	P-HCl (2B-IERXX)
Pulp-equivalent protons of H_2SO_4 to 2 baskets of Amberlyst XX	P- H_2SO_4 (2B-IERXX)

3.2. Effect of Ion Exchange Loading on Acid Hydrolysis

3.2.1. Compositional-Proximate-Ultimate analyses

The particle size 425-800 μm of the raw material *Miscanthus x giganteus* (MIS48) was prepared according to the section 2.1.5, was analysed for extractives, cellulose, hemicellulose, and acid detergent lignin, as shown in Table 3.2. This selection of this particle size range was made due to several factors: it required less energy compared to fine particle size ($< 75 \mu\text{m}$), and was suitable for various pretreatment methods [206].

Table 3.2. Chemical composition (wt.%) of raw material and pretreated pulp.

Material	Extractives	Cellulose	Hemicellulose	Acid Detergent Lignin
MIS48	5.84	52.51	23.15	12.23
P-IER00-0B	-	52.81	23.79	11.86
P-IER70-1B	-	53.69	18.10	11.95
P-IER70-2B	-	54.80	18.36	11.77
P-IER35-1B	-	55.97	20.65	12.38
P-IER35-2B	-	55.57	20.37	12.29

From Table 3.2, the chemical composition of the raw material was within the range cellulose 43-55 wt.%, hemicellulose 18-23 wt.% and acid detergent lignin 7-13 wt.% as shown in the literature [184,283,284]. The lack of changes in composition in the P-IER00-0B from blank and M48 is demonstrated when the biomass is subjected to mild operating conditions, hence concluding that it needs a catalyst to fractionate the material. This was expected, as water can only remove water-soluble compounds weakly bonded to the lignocellulosic matrix [285]. To fractionate the main components in the material through hot water, the temperature should be high, ranging from 170-200 $^{\circ}\text{C}$ [282,286]. When evaluating the changes in compositional analysis between the original biomass and the pulps obtained after adding IER, the main difference is the hydrolysis of the hemicellulose fraction, while cellulose and lignin seemed to be less affected. This is expected as IERs contain Brønsted acid sites, which easily dissolve the hemicellulose fraction of the material in liquid phase [158] [144]. Comparing the resins, IER70 decreased the hemicellulose content of the pulp by ~ 2 wt.% as compared with IER35. IER70 (2.55 mmol g^{-1}) has approximately 50% of the acid capacity of IER35 (5.20 mmol g^{-1}), but it has a similar acid strength (-117 kJ mol^{-1} as shown in Appendix 2, Table A2.1). This is because IER70 has chlorine atoms close to the sulfonic acid groups. The electronegativity of chlorine atoms increases the acid strength of the sulfonic groups in the IERs, increasing their average acid strength. This suggests that acid strength made the acid sites more effective, even at lower concentrations [278,287].

Table 3.3 presents the proximate analysis results for MIS48 and the pulps produced after hydrolysis. The values obtained for the raw material MIS48 were consistent with previous literature [288], except for the moisture content. This could be because the *Miscanthus x giganteus* used in this work was intentionally first dried and then pre-processed for milling and palletisation. Regarding pulp samples, they were dried at 105 °C overnight to remove the bulk moisture and stored in plastic bags, so Table 3.3 results showed moisture content through TGA, which has higher sensitivity and controlled conditions, revealing residual moisture that persists or is more tightly bound within the biomass structure.

Table 3.3. Proximate analysis (wt.%) of raw material and pretreated pulp.

Material	Moisture Content	Volatile Content	Ash Content	Fixed Carbon
MIS48	3.21 ± 0.05	81.76 ± 0.91	3.36 ± 0.34	11.67 ± 0.51
P-IER00-0B	4.39 ± 0.06	82.83 ± 0.12	3.66 ± 0.04	9.12 ± 0.10
P-IER70-1B	3.92 ± 0.08	83.52 ± 0.09	2.48 ± 1.02	10.08 ± 1.03
P-IER70-2B	3.83 ± 0.06	86.34 ± 0.55	2.28 ± 0.16	7.54 ± 0.65
P-IER70-3B	3.18 ± 0.36	85.70 ± 0.36	2.92 ± 0.24	8.19 ± 0.09
P-IER70-4B	4.38 ± 0.26	83.48 ± 1.06	2.57 ± 0.44	9.56 ± 1.75
P-IER35-1B	3.71 ± 0.05	86.25 ± 0.03	0.32 ± 0.08	9.72 ± 0.01
P-IER35-2B	3.82 ± 0.05	85.80 ± 0.13	0.52 ± 0.51	9.87 ± 0.69
P-IER35-3B	3.89 ± 0.10	85.76 ± 0.06	0.45 ± 0.14	9.90 ± 0.10
P-IER35-4B	4.08 ± 0.02	85.41 ± 0.40	0.64 ± 0.01	9.88 ± 0.41

Proximate analysis tends to show significant value differences when there are dramatic changes in cellulose, hemicellulose, and lignin contents when *Miscanthus x giganteus* is pretreated under harsh conditions (5 wt.% sulphuric acid at 175 °C for 1 h) decrease volatile content (from 73 to 43 wt.%) and increase fixed carbon (from 25 to 55 wt.%) significantly [289]. However, the proximate analysis values for the pulps obtained using different amounts of IERs showed slight variations. This could indicate that IERs only cause small changes or soft effects in the material's physiochemical chemical characteristics.

The moisture content for pulps produced showed no significant differences to the MIS48 sample. The presence of IERs increased the volatile content, showing a maximum increase of ~5 wt.% for 2 baskets of IER70 (86.3 wt.%) and 1 basket of IER35 (86.3 wt.%). For a higher number of baskets, there was observed to be no improvement. This could be related to inefficient mass transfer. A higher volatile content value (81.8 wt.%) in a lignocellulosic material means it is less thermally stable, making it more reactive and well-suited for energy production. However, it has been reported that an increase in the volatile matter normally lowers the fixed carbon, and as a result, the overall higher heating value is reduced of the pulp obtained [290].

The ash content decreased significantly when the resin IER35 was used. For example, it was reduced from 3.7 wt.% (P-IER00-0B) down to 0.3 wt.% (P-IER35-1B). This could indicate that this resin might have some effect on the most recalcitrant components or inorganic compounds in the raw material. As this resin has a higher acid concentration per gram, it might be better at favouring the leaching of inorganics into the liquid phase by ion exchange effects. This is a positive result as removing recalcitrant and inorganics can help make cellulose accessible for processes such as enzymatic hydrolysis [291]. Therefore, the use of IERs seems to have a positive effect on cellulose's reactivity and accessibility.

Table 3.4 presents the ultimate analysis of the raw material and the pulp after acid hydrolysis with IERs. The raw material showed some nitrogen but no sulphur content, which can be dependent on the conditions when the energy crop was cultivated and harvested [292,293]. The data did not reveal significant differences in carbon, hydrogen, and nitrogen content in the pulp for all the samples analysed. This aligns with the small changes observed in the proximate analysis.

Table 3.4. Ultimate analysis (wt.%) of raw material and hydrolysed pulp.

Material	C	H	S	N
MIS48	43.96 ± 0.09	6.02 ± 0.06	0.00 ± 0.00	0.23 ± 0.02
P-IER00-0B	44.21 ± 0.19	5.77 ± 0.05	0.00 ± 0.00	0.24 ± 0.02
P-IER70-1B	44.62 ± 0.20	5.85 ± 0.05	0.00 ± 0.00	0.25 ± 0.02
P-IER70-2B	45.46 ± 0.10	5.84 ± 0.02	0.00 ± 0.00	0.30 ± 0.03
P-IER70-3B	45.47 ± 0.48	6.10 ± 0.08	0.00 ± 0.00	0.29 ± 0.02
P-IER70-4B	44.57 ± 0.05	5.64 ± 0.05	0.08 ± 0.00	0.22 ± 0.01
P-IER35-1B	46.09 ± 0.19	5.84 ± 0.07	0.00 ± 0.00	0.23 ± 0.03
P-IER35-2B	45.99 ± 0.17	5.86 ± 0.02	0.00 ± 0.00	0.21 ± 0.01
P-IER35-3B	45.71 ± 0.63	5.86 ± 0.02	0.00 ± 0.00	0.23 ± 0.02
P-IER35-4B	46.16 ± 0.10	5.86 ± 0.11	0.00 ± 0.00	0.19 ± 0.02

No sulphur content increase after acid hydrolysis could indicate no leaching of sulphonic groups from the resin to the pulp [278]. To corroborate the sulphonic groups that remained in the ion exchange resin and that the hydrolysis was not conducted by sulphonic groups leached into the aqueous media, ultimate analysis for fresh and spent IER70 were done (Appendix 3 Table A3.1). The results showed no leaching of sulphonic groups for this resin, which confirms the acid hydrolysis is not performed by free sulphonic groups leached from the solid polymeric matrix. Finally, the higher heating value was calculated using Equation 2.4, which showed not much difference from the raw material (Appendix 3, Table A3.2). This was in agreement with previous literature [288,289,294].

3.2.2. Thermogravimetric analysis (TGA)

Thermogravimetric analysis (TGA) was performed to investigate the thermal stability of the raw material and hydrolysed pulp samples through thermal decomposition profiles. Appendix 3 Figure A3.1 represents the TGA and the derivative thermogravimetry (DTG) thermograms of the raw materials and treated pulp under an inert atmosphere. TGA thermograms in the appendix can be used to identify the following fractions by the temperature of degradation: the water evaporation (25-105 °C), hemicellulose degradation (220-315 °C) and cellulose degradation (315-400 °C) are narrow and distinctive; while the lignin is more spread over a temperature range of 100 to 900 °C [295]. This is because lignin has a three-dimensional structure full of aromatic rings and three major subunit monomers, P-4-hydroxyphenyl, G-4-hydroxy-3-methoxyphenyl, S-4-hydroxy-3,5-dimethoxy-phenyl, that makes its decomposition to become very broad [41]. The TGA and DTG peaks and their respective temperatures for all the samples are summarised in Appendix Table A3.4.

Figure 3.1 shows the DTG curves zoomed in the temperature range 200-600 °C (stage 2 and 3 degradation) for the raw material, the blank and the pulps after hydrolysis with IER70 (Figure 3.1.a) and IER35 (Figure 3.1.b).

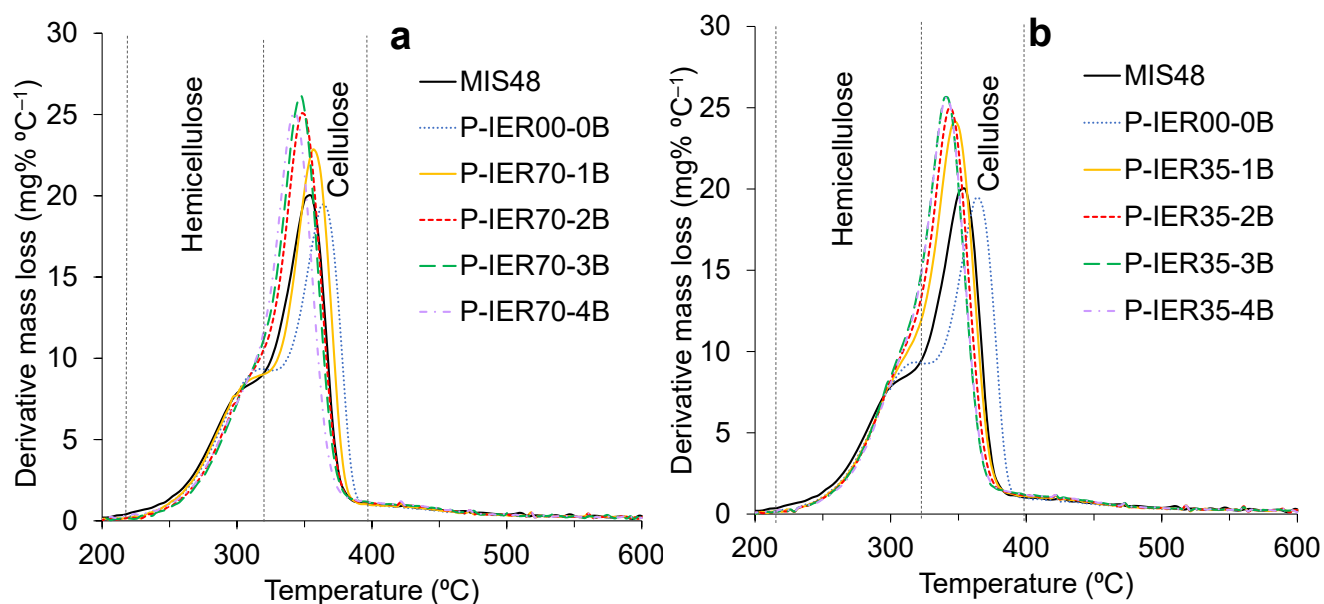


Figure 3.1. DTG curves for biomass and pulp obtained under N₂ conditions zoomed in 200-600 °C temperature range. Effect of IER loading from 0 to 4 baskets: (a) IER70; (b) IER35.

TGA and DTG profiles of raw material MIS48 are not very different from lignocellulosic materials observed in the literature. The first mass loss up to 105 °C occurred due to loss of water content in the sample and was followed by a thermally stable region. MIS48 major degradation temperature range was

approximately among 200-400 °C [296]. This major degradation temperature range was similar for all the pulp samples treated with both IER70 and IER35.

When assessing the blank in Figure 3.1a and Figure 3.1b, the first observation is that the blank is different from the raw material. This blank clearly shows a hemicellulose shoulder, with cellulose DTG_{max} temperature slightly shifting to higher temperatures. An increase in the DTG_{max} temperature for cellulose after pretreatment could be due to the removal of water-soluble compounds such as extractive, soluble oligomers, inorganic salts and polar molecules weakly bonded in the lignocellulosic matrix, making hemicellulose shoulder and cellulose peaks more visible [285]. As a result, the blank was selected as the reference point to assess the effect of the baskets.

When looking at the hemicellulose shoulder, the samples raw material MIS48, the blank and P-IER70-1B show more visibly this component in the DTG thermograms. However, for other IER70 and IER35, the cellulose peak overlaps with the hemicellulose shoulder, complicating the evaluation of the loading effect on the hemicellulose fraction. Considering the compositional analysis, the hemicellulose content was reduced by both IERs. Therefore, the lack of a clear hemicellulose peak in these samples was associated with the lower concentration of hemicellulose in the pulp.

With regards to cellulose, the cellulose DTG_{max} temperature for the blank P-IER00-0B was 364.6 °C (Appendix 3 Table A3.4). However, when IERs are used, the DTG_{max} temperature is shifted to lower temperatures mainly due to the partial removal of hemicellulose and inorganics and increasing the porosity of pulp, enhancing heat transfer and faster thermal decomposition. As a general trend, it can be observed that, for both IERs, the higher the number of baskets, the greater the shift towards lower temperature. Increasing the number of baskets for IER70 from 1 to 4 changes the cellulose DTG_{max} temperature from 356.5 °C to 342.0 °C. In the case of IER35, it changes from 347.8 °C to 342.3 °C, with no significant differences between 3 and 4 baskets. These results imply that the cellulose fraction is changed into a more degradable form by the IERs, making this fraction more thermally reactive [297]. The lack of improvement or plateau at high loadings could be related to mass transfer efficiency, or other reactions taking place, such as the decomposition of the cellulose peak.

The decrease in cellulose DGT_{max} temperature for IER35 was larger than for IER70 (except for 4 baskets). The main reason for the better performance of IER35 was associated with the higher concentration of sulphonic groups per gram of IER (5.20 meq g⁻¹ for IER35 compared to 2.55 meq g⁻¹ for IER70), which could favour the cellulose transformation towards amorphous cellulose [278].

The raw material and the treated pulp were also analysed under an oxidative environment. Figure 3.2 shows the TGA and DTG thermograms of the raw material and the pulp after hydrolysis with IER70 and

IER35, while Appendix 3 Table A3.5 summarises the peak temperatures, degradation rate, and mass lost under an oxidative environment. In the curves presented in Figure 3.2.c and Figure 3.2.d, there are also three distinctive degradation ranges in the DTG: the loss of water (25-105 °C), the devolatilisation of light molecules, and the generation of volatile compounds due to the decomposition of primarily hemicellulose and cellulose (220- 375 °C); and the combustion of the residual char (425-575 °C) [294].

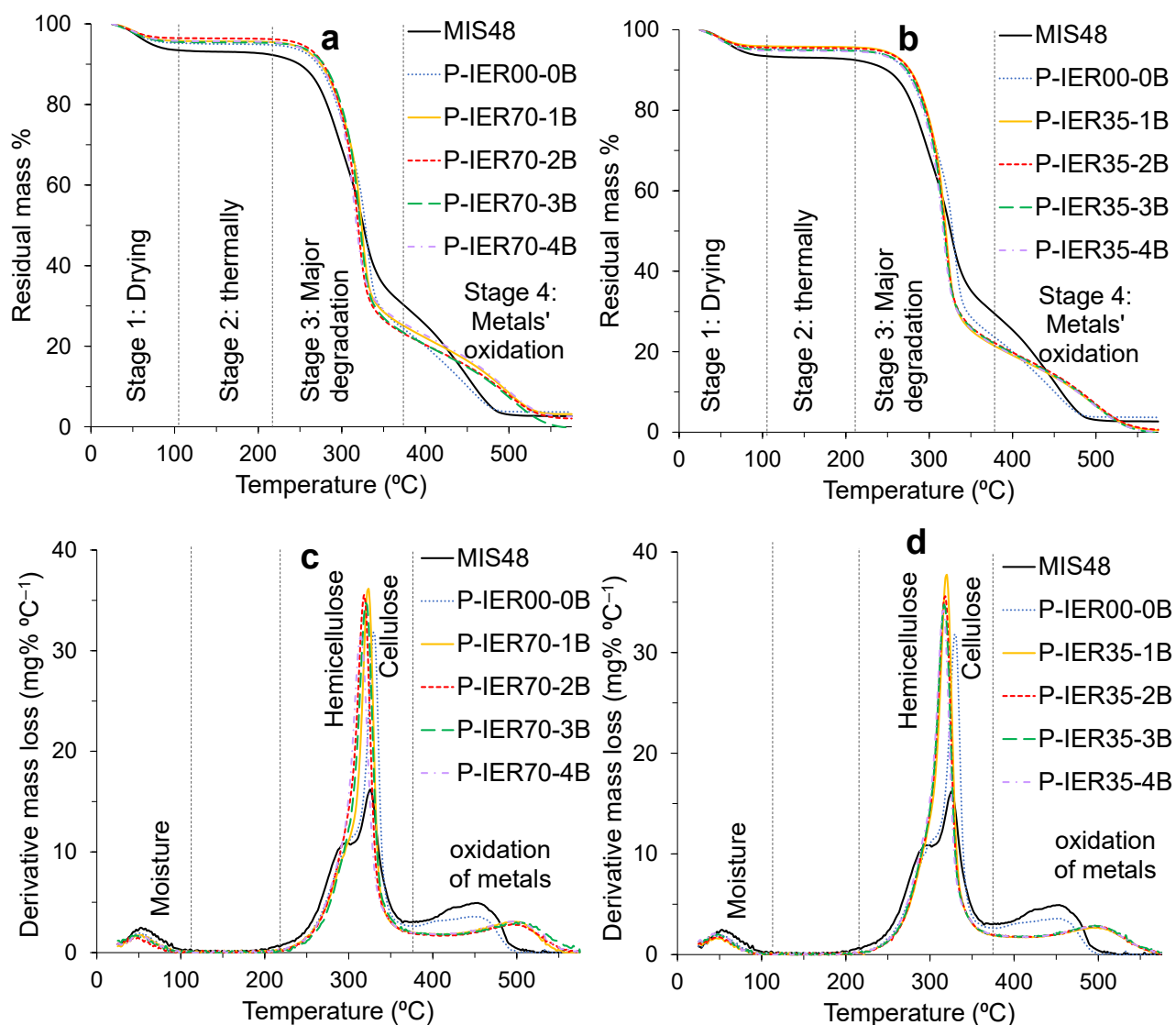


Figure 3.2. Thermogravimetric analysis (TGA) under air for MIS48 and Pulp pretreated pulp with different amounts of IER. (a) TGA for IER70; (b) TGA for IER35; (c) DTG for IER70; (d) DTG IER35.

Pulp treated with water showed the hemicellulose shoulder peak at 305.5 °C with a mass loss of 27.3 wt.%. The cellulose degradation peak temperature for the blank was observed at 329.3 °C with a mass loss of 52.0 wt.%. The third and last peak for char combustion was observed at 448.5 °C with mass loss at 89.6 wt.%. Although the DTG_{max} temperatures for these peaks shifted from the results obtained for the raw material, and the cellulose peak seemed to sharpen, the mass loss for these 3 peaks was similar

to the raw material (Appendix 3 Table A3.5). This could suggest no significant changes in composition and just the removal of weakly bonded fractions [294].

For the pulp treated with IER70, when the resin amount increased from 0.25 to 1.0 g (baskets 1 to 4), the hemicellulose peak temperature decreased from 292.6 °C to 278.0 °C with the mass loss decreased from 9 to 6 wt.% (Table A3.4). This agrees with the findings of the compositional analysis on the reduction of hemicellulose content. In the case of IER35, there was no change in hemicellulose peak degradation temperature regardless of IER35 loading (292.6 °C) with no significant changes in the mass loss either (around 11 wt.%) compared to the raw material or blank. This again agrees with the compositional analysis, where this IER showed less effect than IER70 in removing hemicellulose.

For cellulose, IER70 increased the cellulose mass loss from 31.8 wt.% in the blank to 36.1 wt.% for one basket. This indicates that the IER70 can expose and concentrate the cellulose fraction in the pulp. However, as the number of baskets increases from 1 to 4, the cellulose DTG_{max} temperature shifted from 323.8 °C to 314.6 °C with the mass loss percentage decreasing from 36.1 wt.% to 31.4 wt.% between 1 to 4 baskets. This could indicate that the lower content of IER70 exposes the cellulose by removing other easily soluble hemicellulose and cellulose fractions, but when higher amounts of IER are used, the cellulose is also hydrolysed. IER35 follows a similar trend, showing a higher mass loss of hemicellulose than IER70, so it has higher cellulose content, which agrees with the compositional analysis.

Both IERs showed char oxidation peak temperatures and mass loss changes compared to the raw material and the blank, as can be seen in Figure 3.2.c, Figure 3.2.d and Table A3.5. The temperature increased from 448.5 °C to around 494-500 °C. This might indicate some removal of lignin, which seems unlikely from the compositional analysis. Alternatively, it could indicate some removal through ion-exchange of alkali metals or other inorganics, which tend to catalyse the appearance of this peak at lower temperatures. Although there were differences with respect to the blank, neither IER70 nor IER35 showed a difference in this peak when comparing the different IER loadings and the different IERs. However, when looking at the TGA curves (Figure 3.2.a and b), it can be seen that the final residual mass at the end of the analysis (ash content) was lower for the IER35 than for the IER70, which could indicate higher capacity to remove inorganics.

In conclusion, both IERs show some effect in exposing the hemicellulose and degrading the cellulose at higher contents of IERs. Also, the IER70 seems to affect hemicellulose better than IER35, which allows the removal of cellulose at higher loadings of IER70 (4 baskets). This might be related to the lower pH, which can favour a more efficient hemicellulose hydrolysis. Finally, both IERs do not seem to

affect the lignin, but they might have some effect in removing alkali metals or inorganics, with IER35 being better at reducing the ash content.

3.2.3. X-ray Diffraction (XRD)

Figure 3.3 shows the XRD diffractograms after subtracting the background for the raw material, and all the samples showed the peaks at 16.2° , 22.3° , and 35.0° , which represent the crystallographic planes $101\text{-}10\bar{1}$, 002 and 040 of α -cellulose I, respectively [298].

Unfortunately, the XRD results do not show a clear trend in the increase or decrease of the crystalline peaks with the IER loading for IER35 or IER35.

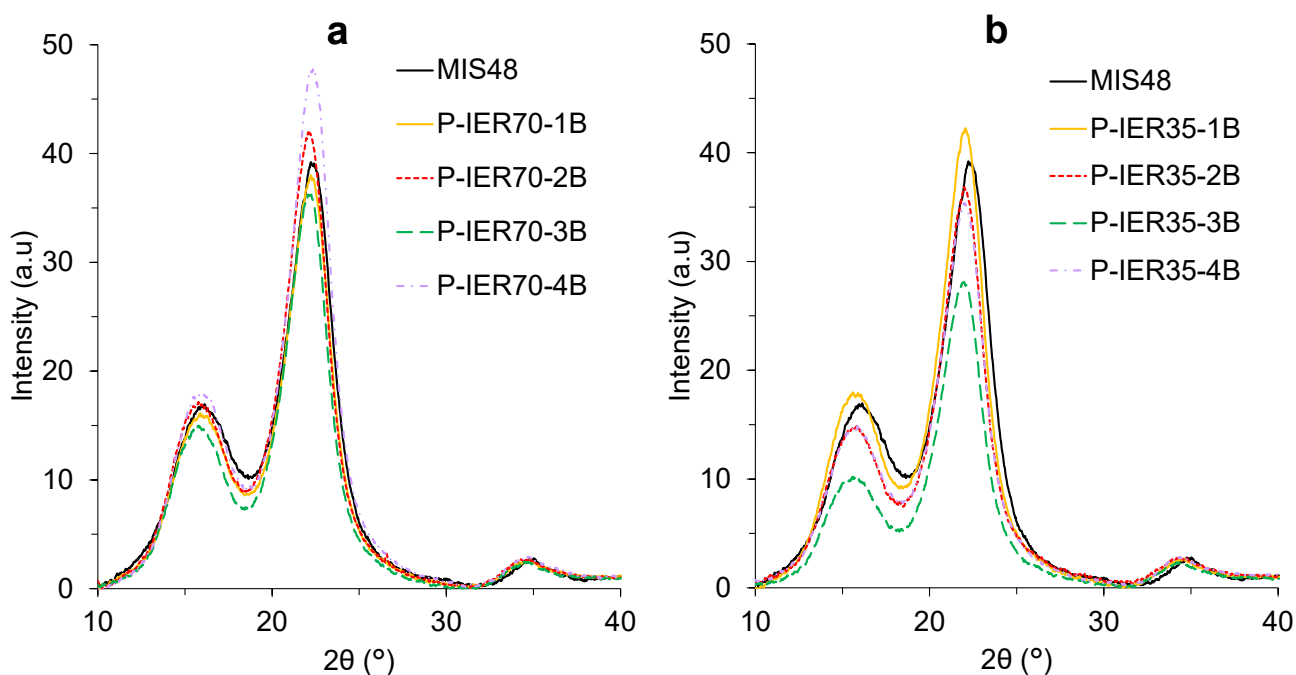


Figure 3.3. XRD diffractograms of untreated MIS 425-800 and cellulose pulp after hydrolysis.

From the XRD diffractogram, the crystallinity index (*CrI*) of cellulose can be calculated. Cellulose *CrI* using XRD is dependent on many factors, such as particle size [299,300], the measurement technique used [262] and the method applied to calculate it [264]. The proportions of lignin and hemicellulose in the pulp play a crucial role, as the cellulose crystallinity index is inversely proportional to their presence [207,301,302]. However, overall, the greater the removal of hemicellulose and lignin content from a lignocellulosic sample, the higher the increase in *CrI* [303]. The *CrI* calculation can be done using the Fit Peak Method (Segal equation) or the Area Deconvolution Method (see Chapter 2, section 2.4.5). Table 3.5 represents *CrI* values using both methods for comparison.

Table 3.5. Crystallinity Index (*Crl*) and crystallite size of untreated MIS48 and pretreated pulp.

Material	Peak Fit Method	Area Deconvolution Method
	<i>Crl</i> (%)	<i>Crl</i> (%)
MIS48	76.70 ± 0.84	54.58 ± 1.30
P-IER00-0B	82.22 ± 0.01	61.05 ± 0.64
P-IER70-1B	79.71 ± 1.78	58.32 ± 0.48
P-IER70-2B	80.98 ± 0.46	59.79 ± 0.75
P-IER70-3B	81.59 ± 0.09	61.10 ± 0.78
P-IER70-4B	81.88 ± 1.56	59.94 ± 1.84
P-IER35-1B	81.18 ± 0.63	59.58 ± 0.34
P-IER35-2B	82.51 ± 0.06	60.47 ± 0.31
P-IER35-3B	82.79 ± 0.16	58.50 ± 0.62
P-IER35-4B	80.10 ± 0.02	57.31 ± 0.58

Raw material MIS48 *Crl* was 76.60% for Fit Peak Method, which is in agreement with the literature using this method [304,305]. For all the pulp samples (including the blank) the *Crl* increased, probably due to the removal of hemicellulose and easy-to-hydrolyse or dissolve cellulose fractions. This is in agreement with results provided in the literature for dilute acid hydrolysis of lignocellulosic materials with mineral acids, where an increase in *Crl* is linked to the removal of amorphous xylan fractions [306] and subsequent access to crystalline cellulose regions [307]. When comparing the effects of IER loading, the differences are not significant enough to draw a conclusion.

The Area Deconvolution Method showed lower values of *Crl*, but it followed the same trends when compared to the area obtained by the Peak Fit Method. Appendix 3 (Figure A3.2) shows an example of XRD peak deconvolution for the raw material. Using the Gaussian function to deconvolute the planes (101), ($\bar{1}\bar{0}\bar{1}$) was not possible, so both were considered as a single peak for *Crl* estimation [308].

In conclusion, the XRD analysis seems to indicate an increase in the crystallinity of cellulose contained in the pulp but is not able to provide significant differences when IER loadings are compared. In addition, the Peak Fit Method using Segal equation is easier to apply and compare to the literature. Therefore, this method will be the one presented in future sections.

3.2.4. Attenuated Total Reflection Fourier Transformation Infrared (ATR-FTIR) Spectroscopy

ATR-FTIR analysis was conducted on the raw material MIS48 and the pretreated pulp to detect functional groups and understand structural changes, elucidating the possible effect of IER. For analysis of different functional groups of various compounds, the spectra were divided into the ranges summarised in Table 3.6.

Table 3.6. Functional groups of compounds identified in FTIR with corresponding absorption ranges [255].

Diagnostic	Absorption range cm^{-1}
Overall appearance	4000-400
Organics & hydrocarbons	3200-2700
Hydroxy or amino groups	3650-3250
Carbonyl compounds	1850-1650
Unsaturated weak/moderate	1670-1620
Aromatics	1615-1495
Multiple bonding (bond order 2/higher)	2300-1990

The full wavenumber range $400 - 4000 \text{ cm}^{-1}$ spectrums are shown in Appendix 3 Figure A3.3 and Figure A3.4. The ATR-FTIR spectral wavenumber and band assignments are presented in Appendix 3 Table A3.7. The main differences were observed in the range $<1800 \text{ cm}^{-1}$ with the fingerprint for OH and aliphatic C-H stretches showing at $>1800 \text{ cm}^{-1}$. For the spectra range $400 - 1800 \text{ cm}^{-1}$, the specific band assignments or ranges with spectral wave numbers were compared to the literature [305,309–312]. For the major components of lignocellulosic biomass, including lignin and carbohydrates (hemicellulose and cellulose), the representative peaks were:

- Peaks linked due to lignin are at different bands: $\sim 1230 \text{ cm}^{-1}$ are due to C-O stretching vibrations in lignin aryl alkyl ether linkages. The wavenumbers between $1500-1700 \text{ cm}^{-1}$, related to the stretching of the C=C in the aromatic rings of lignin [311].
- Peaks linked to cellulose are the strong peak at $\sim 990 \text{ cm}^{-1}$ due to C-C and C-O-C stretching characteristics of cellulose structure. The 900 cm^{-1} is linked to the β -glycosidic linkages between glucose units. Also, the crystallinity of the cellulose can be inspected by using the 1100 cm^{-1} peak. This peak is related to the asymmetric stretching vibration of the C-O-C β -1,4-glycosidic linkage in cellulose [305,312].
- Peaks linked to hemicellulose can be assessed at $\sim 1157 \text{ cm}^{-1}$, and $\sim 807 \text{ cm}^{-1}$, which are linked to carbohydrates mannose contained in hemicellulose, and the 1730 cm^{-1} for the C=O stretching related to hemicellulose [305,312].

The ATR-FTIR for IER70 and IER35 zoomed in the region $2000-400 \text{ cm}^{-1}$ are presented in Figure 3.4 and Figure 3.5, respectively. To compare the samples, the peaks at 1230 cm^{-1} , 1110 cm^{-1} and 807 cm^{-1} will be used as representative peaks for lignin, cellulose and hemicellulose, respectively.

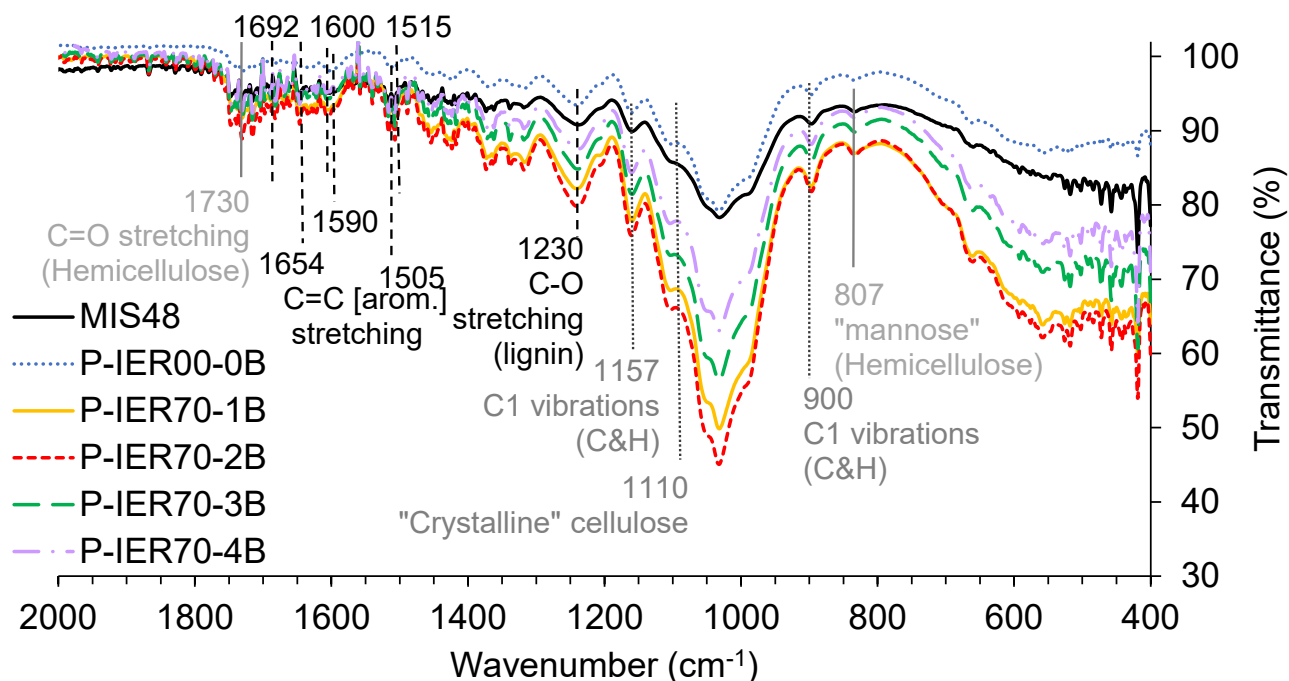


Figure 3.4. ATR-FTIR wavelength range 2000-400 cm^{-1} spectra MIS48, blank and pulps obtained after treatment with different amounts of IER70.

Comparing IER70 (Figure 3.4), when the number of baskets is increased to two, the intensity of these three peaks sharpens. This is an indication that none of these fractions drastically changed. However, the fact that the peaks of cellulose and hemicellulose sharpen is indicative of some removal of amorphous fractions (probably from hemicellulose and cellulose) that improve the signals for these two carbohydrates [313,314]. In the case of lignin, it has been shown in the literature that removing inorganics such as alkali metals can sharpen the lignin peaks [315,316]. Once the number of baskets is increased from two to four, the peaks decrease again. This could be the effect of transforming the crystalline cellulose into amorphous cellulose, which could affect the sharpness of the transmittance.

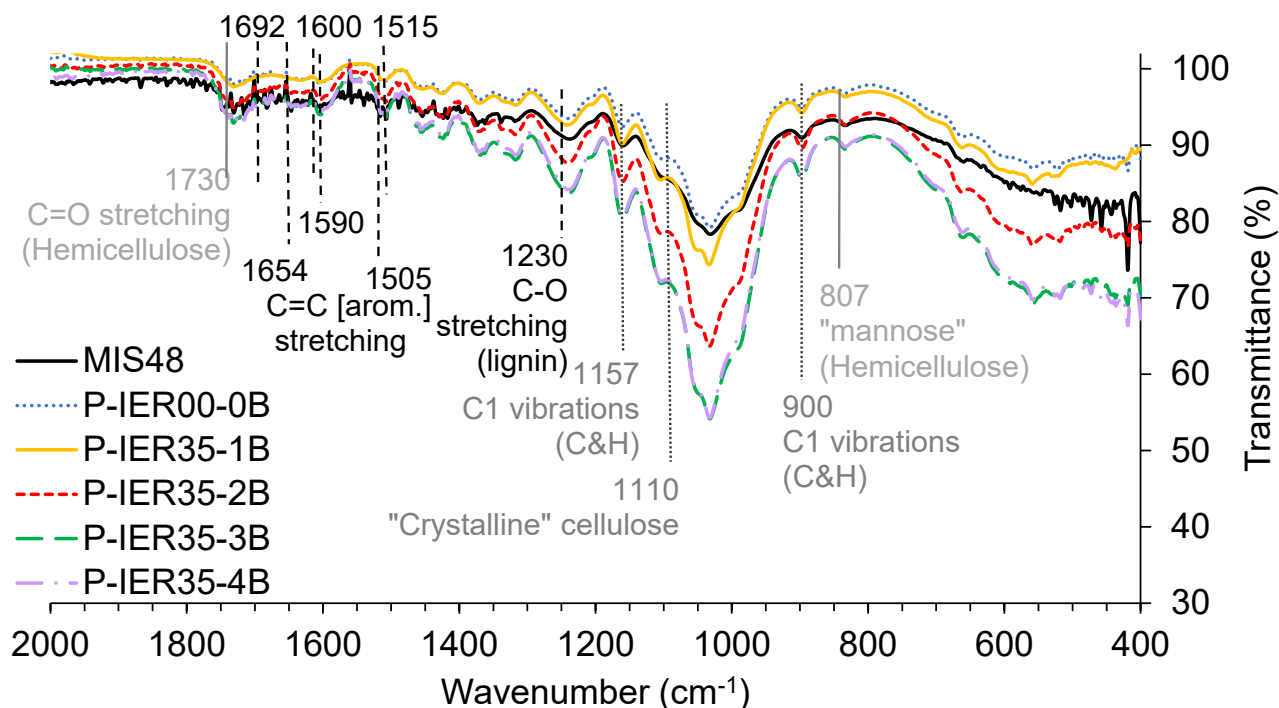


Figure 3.5. ATR-FTIR spectral wavelength range 2000-400 cm^{-1} for MIS48, blank and pulps treated with different amounts of IER35.

For IER35 (Figure 3.5), the peak intensities sharpen between one and four baskets. Also, 3 and 4 baskets overlap, showing no improvement beyond 3 baskets. This difference with IER35 and IER70 could be explained by the fact that hemicellulose is better removed with IER70, and then the cellulose could be accessed easier to undergo hydrolysis or transformation into amorphous cellulose, changing the ATR-FTIR for high loadings of IER70 to lower sharpness.

In conclusion, the different analyses show that IERs can perform the hydrolysis of MIS48, increase volatile content, and reduce ash content. They also decrease the thermal stability of cellulose and increase the cellulose crystallinity in the pulp. Comparing IER70 to IER35, although the former has around half the acid capacity of IER35, it seems to be better at removing hemicellulose and at transforming cellulose than IER35. When looking at the different characterisation techniques, it seems that 2 baskets is a good loading to compare IERs with conventional mineral acids hydrolysis, so 0.25 g of IER is optimal for 2 g of biomass. This is because for some of the analyses showed no improvement in the properties when going beyond this point, which could be linked to possible issues of mass transfer when too much IER is used. To assess if the solid acid is better than mineral acids, the next section will compare the pulp obtained using 2 baskets with the equivalent number of protons using HCl and H_2SO_4 .

3.3. Comparison of hydrolysis with solid IERs and mineral acids

3.3.1. Compositional-Proximate analyses

Table 3.7 shows the compositional analysis results for HCl and H₂SO₄ using an equivalent concentration of H⁺ as two baskets of IER.

Table 3.7. Chemical composition (wt.%) of biomass (MIS48) and pulp after acid hydrolysis IER35, IER70 and mineral acids.

Material	Cellulose	Hemicellulose	Acid Detergent Lignin
MIS48	52.51	23.15	12.23
P-IER00-0B	52.81	23.79	11.86
P-IER70-2B	54.80	18.36	11.77
P-HCl (IER70-2B)	58.67	15.61	14.61
P-H ₂ SO ₄ (IER70-2B)	54.78	22.14	12.81
P-IER35-2B	55.57	20.37	12.29
P-HCl (IER35-2B)	62.32	10.97	14.96
P-H ₂ SO ₄ (IER35-2B)	59.16	14.49	14.03

HCl had higher efficacy to remove hemicellulose and increase cellulose content compared to the corresponding IER and H₂SO₄ equivalent. However, the IER70 shows promise because it also reduced hemicellulose and increased cellulose (to a lesser extent), while keeping the acid detergent lignin unaffected.

For IER35, the content of acid detergent lignin was also the lowest, but the effect of concentrating the cellulose fraction and removing the hemicellulose fraction was not as good as for the mineral acids. These results could suggest that for IERs, the acid capacity is not the only factor affecting the performance and there might be other components, such as acid strength, that influence the efficiency to hydrolyse the biomass. Although they are not best at removing hemicellulose, their softer interaction with biomass could be beneficial to avoid acid hydrolysis inhibitors, such as pseudo-lignin [142,317–319]. It can also be concluded that at very low concentration of protons (like in the conditions equivalent to IER70), some acids such as H₂SO₄ lose dramatically their efficiency to remove hemicellulose.

Proximate analysis of the raw material and the pretreated pulp samples obtained from hydrolysis with IERs and equivalent mineral acids is shown in Table 3.8.

Table 3.8. Proximate analysis (wt.%) of MIS48 and pulps obtained from after acid hydrolysis using IERs and equivalent proton concentration of mineral acids.

Material	Moisture Content	Volatile Content	Ash Content (%)	Fixed Carbon (%)
MIS48	3.21 ± 0.05	81.76 ± 0.91	3.36 ± 0.34	11.67 ± 0.51
P-IER00-0B	4.39 ± 0.06	82.83 ± 0.12	3.66 ± 0.04	9.12 ± 0.10
P-IER70-2B	3.83 ± 0.06	86.34 ± 0.55	2.28 ± 0.16	7.54 ± 0.65
P-HCl (IER70-2B)	5.17 ± 0.95	84.64 ± 1.64	3.73 ± 0.53	6.47 ± 1.66
P-H ₂ SO ₄ (IER70-2B)	4.36 ± 0.03	83.50 ± 0.34	4.48 ± 0.18	7.66 ± 0.43
P-IER35-2B	3.82 ± 0.05	85.80 ± 0.13	1.52 ± 0.51	8.87 ± 0.69
P-HCl (IER35-2B)	4.37 ± 0.41	84.08 ± 0.28	4.85 ± 0.44	6.71 ± 0.28
P-H ₂ SO ₄ (IER35-2B)	4.07 ± 0.15	83.52 ± 0.21	4.59 ± 0.09	8.01 ± 0.07

All the pulp samples showed almost the same moisture content as the raw material. With regards to the volatile content, IERs are better at increasing this parameter, followed by the HCl, and then the H₂SO₄. Also, the IERs are better at reducing the ash content compared to the mineral acids. The results agree with some of the literature that states that ash content using dilute acid hydrolysis reduces the content of inorganics, such as calcium and magnesium [84]. However, the mineral acids seem to not affect or slightly increase the ash content. This behaviour has also been reported in literature, where the ash content may increase or decrease depending on the concentration and type of mineral acid [320]. Therefore, the results of proximate analysis indicate that there might be an element of ion-exchange, already discussed in Section 3.2, on how IERs could be beneficial to adsorb inorganic ions, and then favour higher leaching, that can result in lower ash content.

For the fixed carbon, the HCl is the best at decreasing this parameter. The fixed carbon is expected to increase when the volatile content decreases. The Fixed carbon and volatile matter have an inverse relationship with thermal treatment. As volatile matter is driven off, the relative percentage of fixed carbon naturally increases. However, this trend is not observed, and further analysis using other techniques such as TGA might be able to shed some light on this.

In conclusion, IERs are better at increasing volatile content and reducing ash content compared to the mineral acid counterparts, which is a positive outcome, as it is indicative of less recalcitrant composition of the pulps treated with IERs.

3.3.2. Thermogravimetric analysis (TGA)

The full thermal degradation TGA and DTG curves under inert conditions for biomass, blank and different acids (IER, HCl and H₂SO₄) is shown in Appendix 3 Figure A3.5. Figure 3.6 compares only the DTG curves for the range of temperature 200-600 °C. When comparing 2 baskets of IER70 and the

equivalent mineral acid concentration to the blank (Figure 3.6.a), it is noticeable that each acid had a distinct influence on the biomass. HCl has a strong effect on the hemicellulose shoulder by decreasing its presence. However, there are no significant differences between the blanks for the cellulose peak. This indicates that this acid can hydrolyse hemicellulose, which is the least thermochemically stable among the three major components of biomass [321] regardless of the type of lignocellulosic biomass [322].

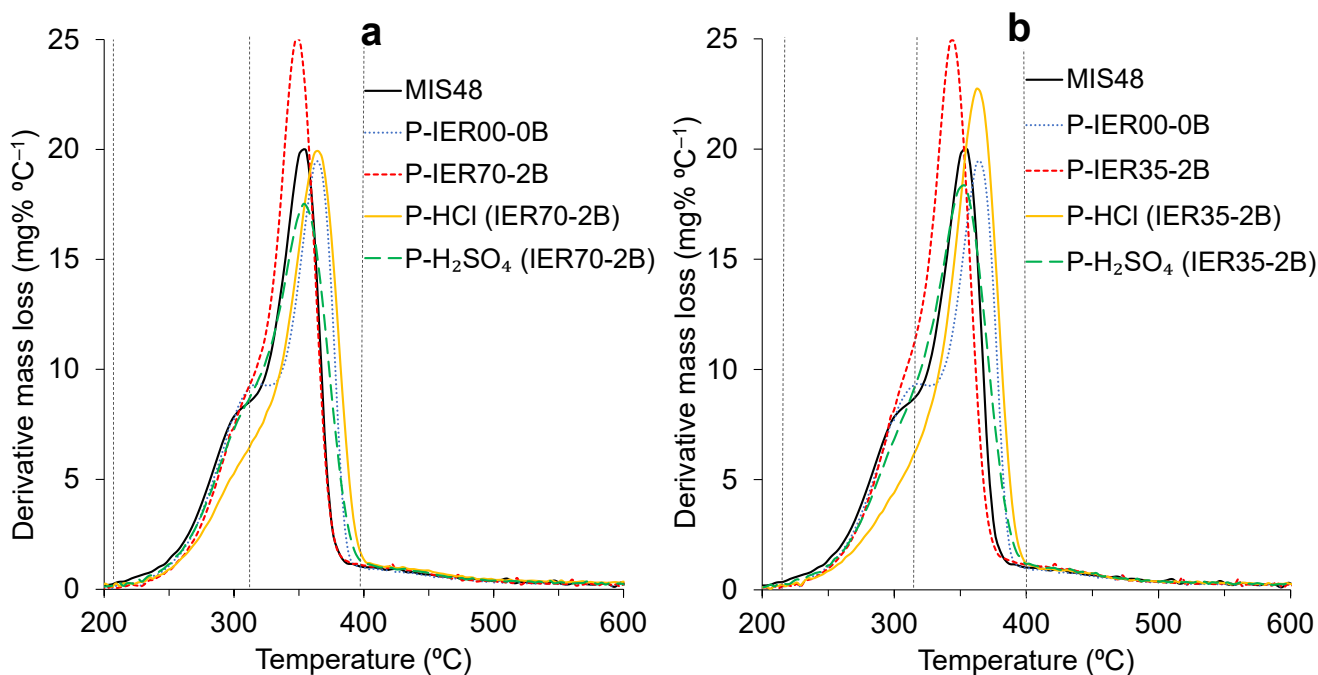


Figure 3.6. DTG curves under (N_2) inert conditions for biomass and pulp, comparing hydrolysis using two baskets of IER or mineral acids with equivalent proton concentration: (a) IER70 and equivalent mineral acids; (b) IER35 and equivalent mineral acids.

H_2SO_4 can shift the cellulose DTG_{max} to lower temperatures but the peak is not as sharp as for the IER70. When looking at the IER70, the major influence is on the cellulose peak. This means that IER70 is capable of having more influence on this fraction of the lignocellulosic material. The shift towards lower DTG_{max} , correlates with the results of VC observed in the proximate analysis. These results imply that IER70 has more capacity to affect cellulose structure by reducing its thermal stability – via transformation of the cellulose into amorphous cellulose or depolymerisation.

When comparing IER35 to its counterparts (Figure 3.6.b), similar trends to those observed by IER70 are noted. The major difference is that for HCl there is an increase in the sharpness of the cellulose peak, which could be related to the better exposure and higher content of cellulose in the pulp at that higher concentration of HCl, due to a more efficient removal of the hemicellulose.

These results show that even at dilute concentrations, IERs and mineral acids can access and change the biomass structural matrix. It also shows that different acid forms can act differently for the same lignocellulose material due to acid strength and reduction efficiency of inorganic content in it [84]. So, the hydrolysis is not only controlled by the number of protons present in the system. While all the acids tested affect the hemicellulose to less or higher degree, the cellulose fraction seems to be mainly affected by sulfonic groups and sulphuric acid.

Figure 3.7 shows a comparison of thermal stability and degradation behaviours of pulp samples under an oxidative environment.

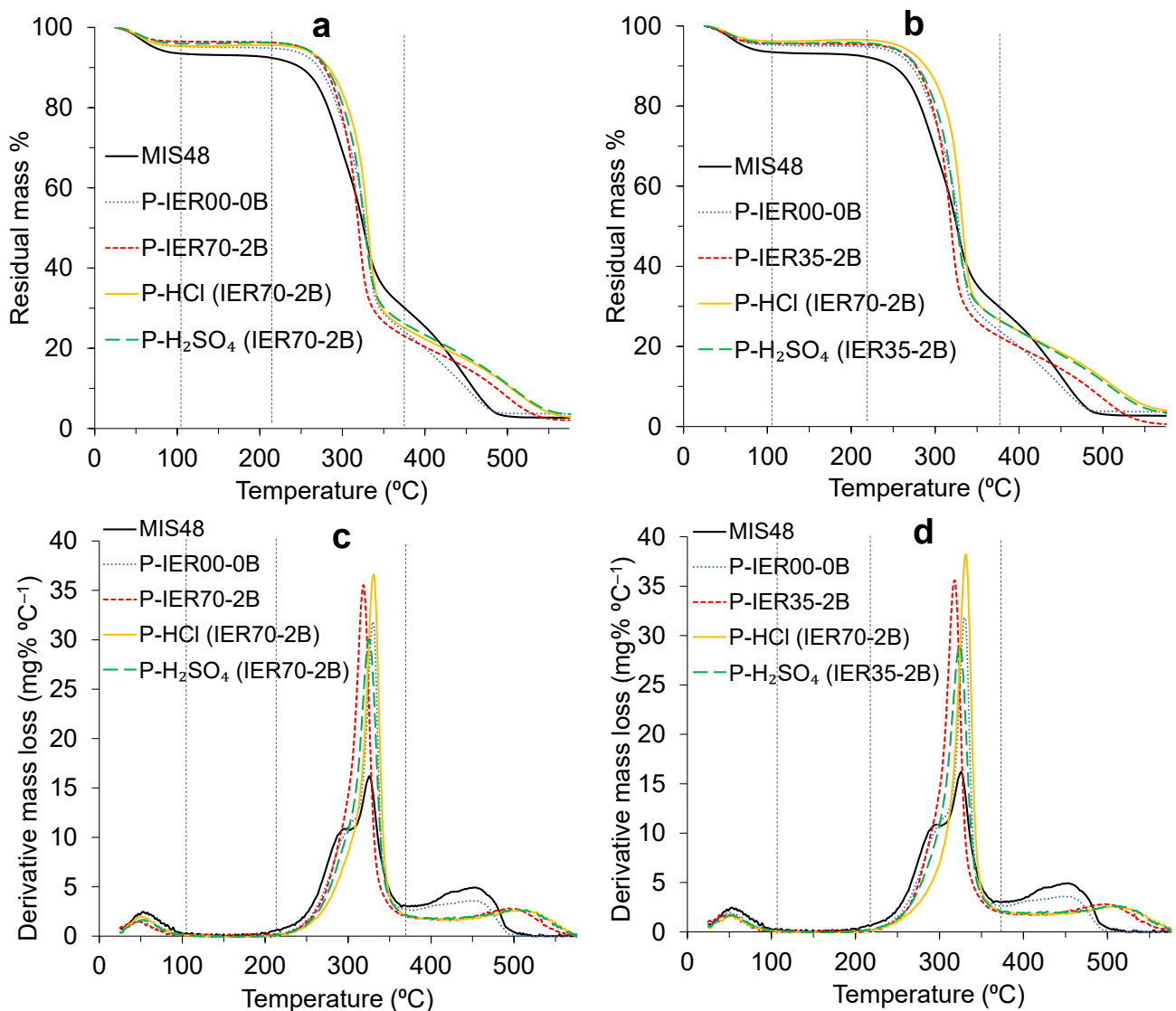


Figure 3.7. TGA-DTG curves under (air) oxidative conditions for biomass and pulp, comparing hydrolysis for two baskets of IER with an equivalent proton concentration of mineral acid.

Consistent with the experiment under N_2 , it shows that the IERs further reduced the thermal stability of the cellulose in the pulp compared to the mineral acid counterparts, as it shifted the DTG_{max} of cellulose to lower temperature, and the peak was sharper, regardless of the IER compared. It is also noticeable that the mineral acids show an increase in the temperature range of appearance for the third peak between 400-575 °C (oxidation of lignin). This can indicate that the removal of inorganics and alkali metals might occur for all the acids. The lack of these catalytic species elevates the activation energy necessary for thermal breakdown, hence moving the pyrolysis processes to higher temperatures. Furthermore, acid pre-treatment alters the biomass structure, making it more amorphous and porous, which facilitates thermal breakdown at lower temperatures but diminishes reactivity at higher temperatures [323,324]. However, the IERs show the DTG_{max} earlier than the mineral acids. This could indicate that the lignin fraction remaining in the pulp after hydrolysis could be easier to degrade thermally. Finally, it can be observed in the TGA curves (Figure 3.7.a and b) that the residual mass at the end of the analysis (ash content) is the lowest for the pulp treated with IERs.

3.3.3. X-ray Diffraction (XRD)

Figure 3.8 represents XRD diffractograms of the raw material (MIS48) and pulp samples obtained via MIS48 acid hydrolysis using IERs and mineral acids.

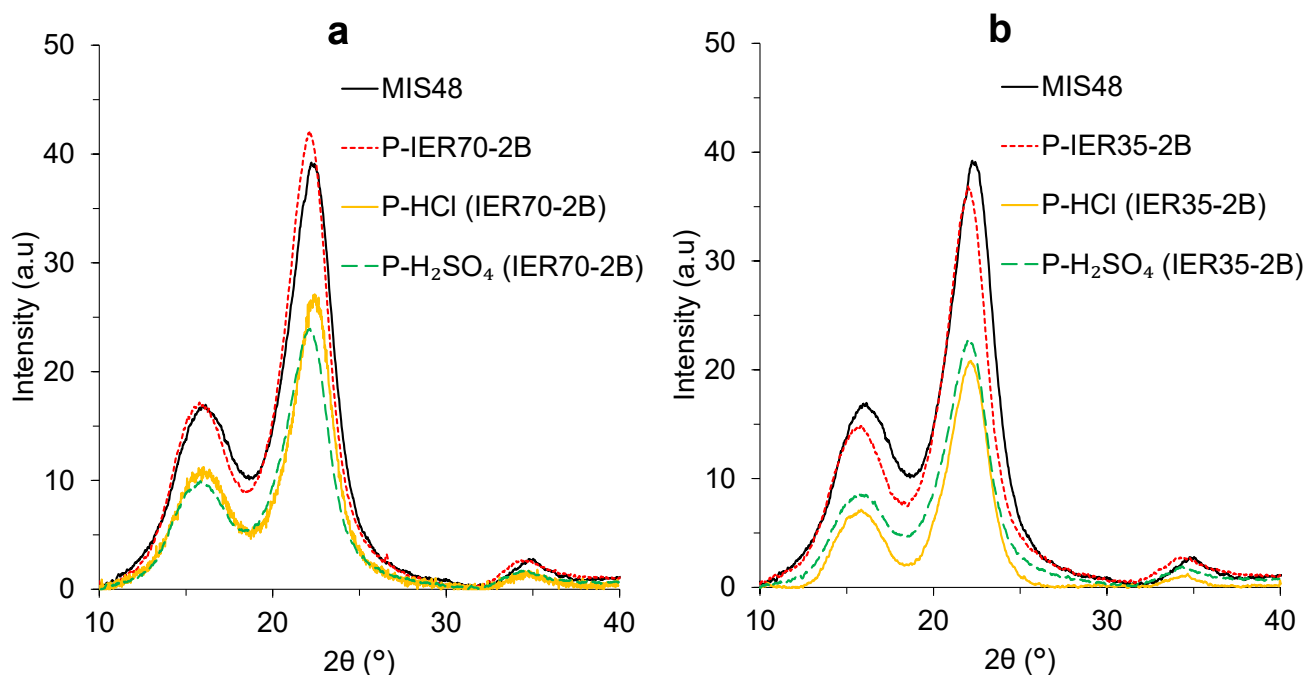


Figure 3.8. XRD diffractograms of MIS48 and pulp samples via hydrolysis using IER and mineral acids. (a) IER70 and equivalent mineral acids; (b) IER35 and equivalent mineral acids.

Looking at the Figure 3.8, the mineral acids seem to decrease significantly the intensity of the cellulose crystalline peaks. However, this is compensated by less intensity in the amorphous area (intensity at

around 18°). For this reason, the crystalline index (*CrI*) and crystallite size were calculated using the Peak Fit Method and are represented in Table 3.9.

Table 3.9. Crystallinity Index (*CrI*) and crystallite size of pulp.

Material	<i>CrI</i> (%)	Crystallite size (nm)
MIS48	76.70 ± 0.84	3.24 ± 0.00
P-IER70-2B	80.98 ± 0.46	3.40 ± 0.01
P-HCl (IER70-2B)	82.96 ± 0.01	3.52 ± 0.07
P-H ₂ SO ₄ (IER70-2B)	80.18 ± 0.19	3.54 ± 0.01
P-IER35-2B	82.51 ± 0.06	3.48 ± 0.01
P-HCl (IER35-2B)	82.67 ± 0.19	3.70 ± 0.03
P-H ₂ SO ₄ (IER35-2B)	81.88 ± 0.39	3.61 ± 0.03

All the acids increased the *CrI*. This was expected because the removal of the hemicellulose and amorphous part of the cellulose can enhance the crystallinity index [325–327]. This is expected, as the acid content is very diluted. Also, it is different to when concentrated acid is used, where the deconstruction of the cellulose crystalline structure is more predominant, and a lower *CrI* would be expected [303,328]. The differences between IERs and the mineral acids are insignificant, but HCl has a slightly higher crystallinity index. This might be because this acid can mainly attack hemicellulose and has no impact whatsoever on the cellulose under the conditions of operation tested.

Lastly, the crystallite size of pulp increases compared to MIS48, maximising for hydrochloric acid. The elimination of hemicellulose and the redistribution of lignin, occurring concurrently with the enlargement of crystallite size, might enhance the overall accessibility of cellulose to enzymes [329]. The alteration in crystallite size might indicate that the pre-treatment has successfully altered the biomass structure, often linked to enhanced digestibility [330]. The increase in crystallite size can be due to more effect of acid pretreatment on amorphous regions of the biomass as compared to crystalline regions [307]. Through the results of XRD, it can be concluded both IERs and dilute mineral acids increase the *CrI*, mainly because of the removal of hemicellulose, and that at these concentrations (2.55 mmol/g of IER70 and 5.20 mmol/g of IER35), the acids cannot significantly alter dramatically the crystalline structure of cellulose.

3.3.4. Attenuated Total Reflection Fourier Transformation Infrared (ATR-FTIR) Spectroscopy

FTIR-ATR on pulp samples after acid hydrolysis using IER70 and IER35, along with their comparison of dilute acid hydrolysis using hydrochloric and sulfuric acids are represented in Figure 3.9 and Figure

3.10, respectively. FTIR-ATR results of dilute acid hydrolysis using either mineral acids or IERs clearly show sharper and more visible peaks after the pretreatment as compared to the raw material, indicating that the hydrolysis increases the cellulose proportion of the raw material along with its purity [326,331].

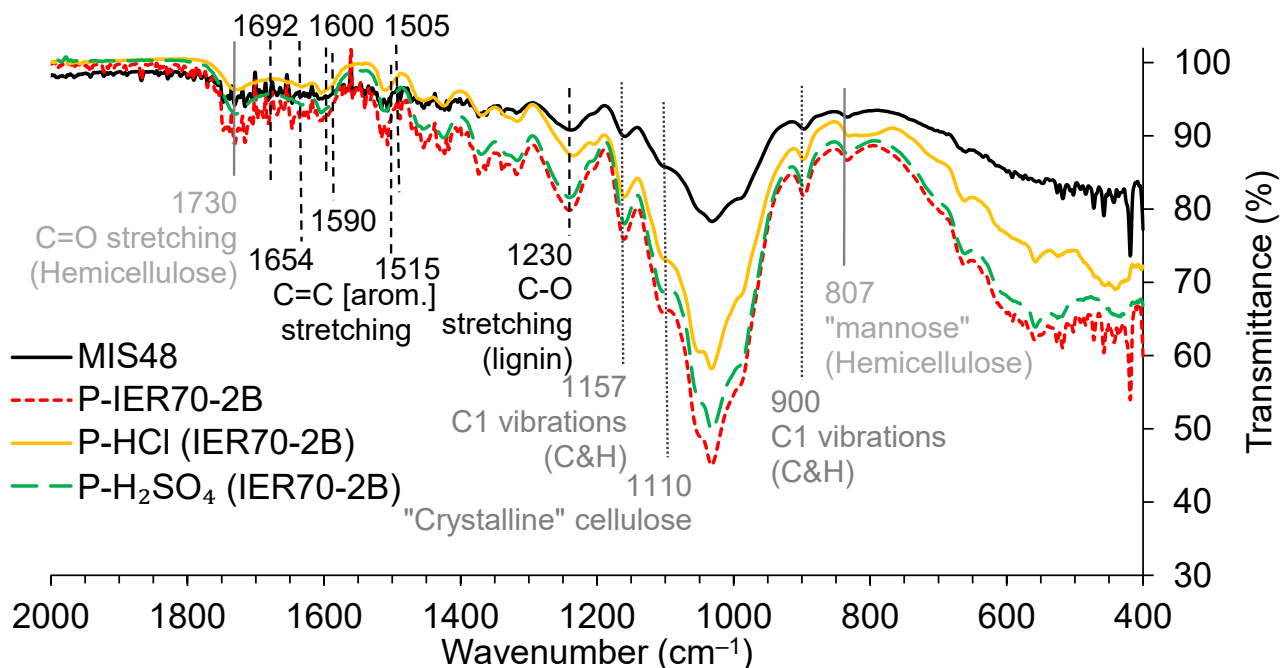


Figure 3.9. ATR-FTIR spectral wavelength range 2000-400 cm^{-1} for MIS48, Pulp treated with IER70, and dilute acid hydrolysis.

Comparing pulp sample of IER70 (Figure 3.9) to mineral acid hydrolysis, the pretreatment method that increases more the sharpness of the peaks is the one was using IER70. This could be related to the combined effect of IER in the removal of hemicellulose, transformation of the cellulose and removal of inorganics commented in Section 3.2.1.

In the case of IER35 (Figure 3.10) the pretreatment showing the lowest transmittance was the mineral acid HCl. This could be explained if we combine the results with the TGA, in which the IER35 showed in the largest transformation of hemicellulose towards amorphous and less thermally stable cellulose, and HCl showed the highest peak of cellulose. Again, this could impact the sharpness of the peaks, as it was discussed in Section 3.2.4.

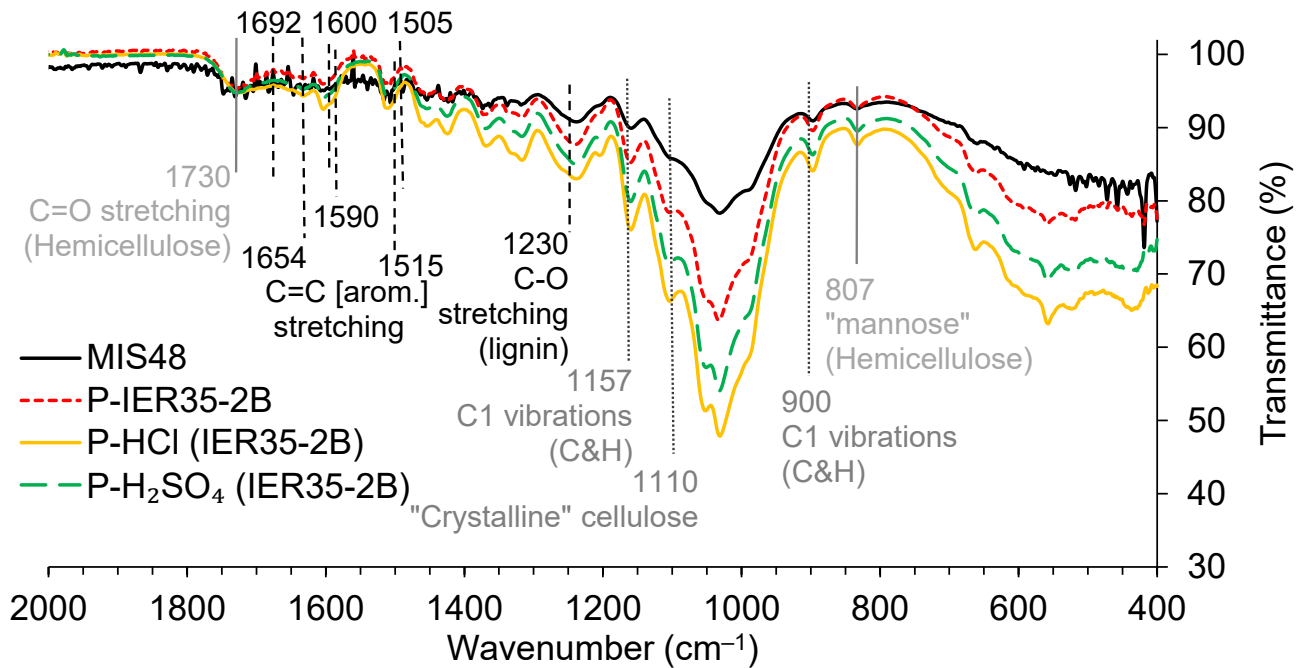


Figure 3.10. ATR-FTIR spectral wavelength range 2000-400 cm⁻¹ for MIS48, Pulp treated with IER35, and dilute acid hydrolysis.

In conclusion, the IERs have more of an effect on transforming the cellulose into amorphous cellulose. This increases the volatile content and decreases the ash content of the pulp. Therefore, they have additional benefits compared to mineral acids in reducing recalcitrance and thermal stability of miscanthus x giganteus.

3.4. Conclusions

This work has demonstrated that IERs are promising catalysts for hydrolysis lignocellulosic biomass. The comparison of IER70 and IER35 at different loadings showed that for IERs, the acid capacity is not the only parameter to consider when it comes to hydrolysis performance, as acid strength can have an important role in improving the removal of hemicellulose. Also, IERs showed they can increase the exposure of the cellulose structure and, at sufficiently 0.25 g of loading, can start transforming the cellulose into amorphous cellulose. This has the benefit of increasing the volatile content (81.8 wt.% to 85.8 wt.%) and reducing the ash content (3.4 wt.% to 1.5 wt.%). Comparing IER70 and IER35, the higher acid strength of the IER70 made it more apt for removing hemicellulose, making the cellulose more accessible and easier to undergo hydrolysis or transformation into amorphous cellulose. Along with the chemical properties of IERs, the physical properties are also important. After 2 hours under a magnetic stirrer, IER35 was ground by abrasion, while IER70 was better at maintaining its integrity. Therefore, if IERs were to be used without metal baskets in a larger-scale setting, then IER70 would be a better choice.

Due to their cation exchange capacity, IERs lower the inorganic content, lowering the ash content and increasing the volatile content. Therefore, IERs are better than mineral acids at reducing the recalcitrance and thermal stability of the pulp.

In addition, the TGA analysis showed that IERs were more efficient in transforming crystalline cellulose to amorphous cellulose than mineral acids, which facilitates downstream processes that require converting cellulose into sugars and its derivatives.

IERs do not seem to significantly affect the lignin at the conditions tested. Therefore, in Chapter 4, IERs will be combined with ionic liquids, a green solvent that can cause the delignification of the biomass. This will enable to explore the impact of the IERs when the lignin fraction is removed, and the hemicellulose and cellulose are more exposed to transformations.

Chapter 4. Evaluation of Ionic Exchange Resin and Ionic Liquid mixtures for lignocellulosic biomass fractionation

4.1. Introduction

Chapter 3 concluded that IERs provide a soft hydrolysis effect on the cellulose and hemicellulose fractions and are not strong enough to break lignin carbohydrate complexes.

This Chapter 4 will explore using acidic IERs combined with ionic liquids (ILs) to evaluate whether combining IERs and ILs can dissolve or remove the lignin and provide a better interaction to access the cellulose and hemicellulose. ILs are organic salts that maintain their liquid state at or near room temperature. ILs are renowned for their properties, as described in Chapter 1, Section 1.5. Their chemical characteristics can be modified by altering their cation or anion constituents [162], rendering them extremely adaptable for various applications. Some specialised ionic liquids (ILs) are utilised to dissolve lignin because they can penetrate its intricate structure and depolymerise it [161]. Lignin has a high thermochemical stability compared to the other lignocellulosic components and acts as a shell that hinders the hydrolysis of cellulose and hemicellulose. Two ILs have been selected for this chapter due to their simplicity of production and low cost. Triethylammonium Hydrogen Sulphate (TS) and Triethylammonium Acetate (TA). The first one is acidic, while the second one is neutral.

With this purpose in mind, this chapter has been split into three main sections, each with its objectives. The first section will compare the results obtained using two stainless steel mesh baskets with IER70 from Chapter 4 (with water as the solvent) to the same system using different concentrations of TS in water.

In the second and third sections, the IER will be added to the reaction system without using stainless steel mesh baskets. The biomass loading, time (t), temperature (T), and pressure (P) will be the same as the ones used in Chapter 4 (Introduction). Then, different concentrations of IL in distilled water will be used to pretreat *Miscanthus x giganteus* to see the synergic effect of the IER and IL on the raw material regarding its fractionation. The results from testing the neutral triethylammonium acetate IL will be presented in the second section. Subsequently, the results with the triethylammonium hydrogen sulphate IL will be presented in the third section.

After each experiment, the pulp was recovered and washed according to Section 2.5.2.2. This pulp was characterised to assess changes in comparison to the raw material under different pretreatment conditions. The nomenclature used in this chapter is presented in Table 4.1.

Table 4.1. Summary of nomenclature for samples in chapter 4.

Name	Nomenclature
<i>Miscanthus x giganteus</i> (425-800 μm)	MIS48
<i>Miscanthus x giganteus</i> (<106 μm)	MIS16
IL Triethylammonium hydrogen sulphate at ## wt.% in water	TS##
Triethylammonium acetate at ## wt.% in water	TA##
Ionic Exchange Resin Amberlyst 70	IER70
Pulp recovered after pretreatment with IL-TA only	P-TA##
Pulp recovered after pretreatment with IL-TA + Amberlyst 70	P-TA##-IER70
Pulp recovered after pretreatment with IL-TS only	P-TS##
Pulp recovered after pretreatment with IL-TS + Amberlyst 70	P-TS##-IER70

4.2. Preliminary experiments of IL (TS) + IER70 using mesh baskets

4.2.1. Scanning Electron Microscopy-Energy Dispersive X-Ray (SEM-EDX)

Lignocellulosic material M48 (*Miscanthus x giganteus* 425-800 μm) was used to test the effect of different concentrations of IL-TS and with IER70 in mesh baskets to fractionate the raw material into carbohydrate-rich fraction and lignin. However, when using the baskets, the colour of the solution changed from the typically observed dark brown to a green colour during the experiment, and the colour of the pulp also altered from the typically observed dark brown to green. This suggested that the IL solution was dissolving the mesh baskets. The mesh baskets were made of Stainless Steel (SS) grade 316L. Stainless is generally resistive to low (< 15 wt.%) and high (> 85 wt.%) concentrations of sulfuric acid, and it can be used for short-term contact with room-temperature sulfuric acid [332]. However, it becomes less resistant to intermediate concentrations of acidic solutions and at high temperatures [333]. The primary elements in Stainless Steel 316L are chromium (16-18 wt.%), nickel (10-14 wt.%) and molybdenum (2-3 wt.%) [334,335]. Due to their highly acidic nature, the IL-TS dissolved the mesh baskets during the reaction, and these elements were dissolved in solution. The subsequent incorporation of these transition metals into the pulp interfered with the technical analysis using either TGA or ultimate analysis, making it challenging to investigate the influence of IER70 in IL-TS on the lignocellulose material. To avoid this, metal mesh baskets should be made from a material such as Inconel alloys (601, 600, 625), which have excellent high-temperature strength and corrosion resistance, suitable for harsh acidic environments [336].

SEM-EDX analysis confirmed the presence of transition metals in the pulp after pretreatment. Table 4.2 shows the compositional analysis for the raw material and the pulp samples P-TS60 (no IER70 in mesh baskets involved) and P-TS60-IER70 (IER70 in mesh baskets involved). In addition, Figure A4.1 and

Figure A4.2 in Appendix 4 show the EDX colour mapping for P-TS60 and P-TS60-IER70, respectively. As shown in Table 4.2, the raw material sample (M48) revealed the presence of elements such as silicon (Si) (0.7 wt.%) and calcium (Ca) (1.2 wt.%), but no iron, (Fe) molybdenum (Mo) or chromium (Cr) was detected. In the pulp treated with only IL-TS60, the Si and Ca were also present at higher concentrations, 3.5 wt.% and 1.8 wt. % respectively, and sulphur (1.9 wt.%) was also detected. After an IL pretreatment of lignocellulosic material, the inorganic content is higher (5.6 - 10.9 wt.%) [86,156], because the relative amount of ash increases in the pulp as amorphous biomass components decompose or dissolve in a liquid phase. Moreover, the pulp has a high amount of sulphur (1.9-11.1 wt.%), mainly due to residual IL-TS, which cannot be entirely removed from the pulp even after washing with ethanol overnight [337].

As predicted, the results showed the presence of iron (12.2 wt.%), molybdenum (2.2 wt.%), and chromium (0.9 wt.%) in the pulp treated with IL-TS60 and the IER70 in the mesh baskets, confirming the transfer of these elements from the mesh basket to the pulp. Acidic conditions facilitate the protonation of functional groups in biomass, especially carboxyl and hydroxyl groups. This establishes binding sites for metal cations, enabling their substitution of protons and integration into the biomass structure [338]. Transition metals can form compounds with lignin and other biomass constituents. The acidic environment may facilitate this process by revealing more possible binding sites [339]. Although SEM-EDX provides information on elements present on the surface layer of the pulp rather than in the entire bulk composition [340]. These results proved that metals from the baskets were dissolved and incorporated into the pulp during the pretreatment, and washing could not remove these elements from the pulp samples. It is worth mentioning that due to the non-conducting nature of biomass and pulp samples, the accumulation of electrons on the surface was observed during the SEM analyses, which decreased image quality under magnification.

Table 4.2. SEM-EDX elemental analysis of M48 treated with IL-TS (60 wt.%) in the absence or presence of two baskets of IER70. ND = Not detected.

Material	S (wt.%)	Si (wt.%)	Ca (wt.%)	Fe (wt.%)	Mo (wt.%)	Cr (wt.%)
M48	ND	0.7 ± 0.2	1.2 ± 0.7	ND	ND	ND
P-TS60	1.9 ± 0.1	3.5 ± 0.7	1.8 ± 0.4	ND	ND	ND
P-TS60-IER70	11.1 ± 1.1	2.1 ± 0.1	2.0 ± 0.1	12.2 ± 0.4	2.2 ± 0.0	0.87 ± 0.0

Stainless Steel mesh baskets cannot be used to work with IL-TS. Also, it was noticed that the acid-to-base ratio of IL-TS is a critical parameter to be controlled when preparing the IL and using it to fractionate lignocellulosic biomass. The preliminary results showed that pulp treated with only IL-TS was charred regardless of its concentration, which was unexpected for solutions even with low concentrations (60 wt.%) of IL. This was linked to the high acid-to-base ratio of these solutions. Concentrated acid tends to char the biomass because it promotes significant dehydration of biomass constituents. The rapid

removal of water molecules from cellulose and hemicellulose results in carbon-dense structures [335,341]. An indirect way of measuring the acid-to-base ratio by measuring the density was used to check this. It is reported that the density of a specific IL-TS solution increases with an increase in the acid-to-base ratio. More protons are transferred from the acid to the base, leading to a higher concentration of ionic species. This increased ionicity results in stronger electrostatic interactions between the ions, which can lead to a more compact structure and higher density. For instance, an IL-TS80 should have a 1.19 g mL^{-1} density with an acid-to-base ratio of 1 [342]. However, the IL-TS80 density obtained was 1.40 g mL^{-1} , indicating a higher acid-to-base ratio.

In summary, two main conclusions were obtained from these preliminary experiments. The first one is that stainless steel baskets cannot be used when the liquid media is changed from water to a mixture of water and IL-TS. The second main conclusion is that during the synthesis of the IL-TS, the mixing of acid and base should be as slow as possible at a constant rate. While making the IL-TS with equimolar triethylamine and sulfuric acid, the acid-to-base ratio changed from one batch to another if the mixing rate of acid and base were inconsistent (not at the same rate). As a result, the IL was prepared by mixing the sulphuric acid with triethylamine as slowly as possible, at a constant rate, and in large batches. This had two advantages: it enabled the production of an IL with acid-to-base ratios as close to one as possible, and it produced a 2-litre batch of IL to assess different parameters such as IL concentrations and different IERs under the same controlled condition of acid-to-base ratio.

4.3. Ionic liquid system (TA) with and without IER70 for MIS16

Mesh baskets were used to facilitate the separation of the IERs from the biomass. However, the previous section demonstrated that the integrity of the stainless steel can be compromised when specific concentrations of certain ILs are used. To study the influence of IER70 combined with different ILs, a smaller particle size of *miscanthus x giganteus*, M16, and a large particle size of the IER70 ($>425 \mu\text{m}$) were used. IERs are polymers, so they can slightly reduce their size by attrition while mixing with a magnetic stirrer during the pretreatment. However, the particle size ranges for the biomass ($< 106 \mu\text{m}$) and IER ($> 425 \mu\text{m}$) were different to provide easier separation of the pulp and the IER through sieving, with negligible cross-contamination after each pretreatment process.

4.3.1. Proximate and Ultimate analyses

Proximate analysis of pretreated pulp samples was vital to determine fuel characteristics: volatile matter, moisture, ash and fixed carbon. These characteristics define combustion properties and provide a better understanding of energy properties and environmental impact [343]. For example, lignocellulosic materials with higher moisture and ash contents eventually decrease the available energy content for that material [344].

Proximate analysis through TGA analysis of MIS16 and the pulps from pretreatment with two different IL-TA concentrations and with and without IER70 is shown in Table 4.3.

Table 4.3. Proximate analysis (wt.%) of raw material (MIS16) and pulp treated with two concentrations of IL-TA (40 and 80 wt.%) and the absence or presence of 0.25 g of IER70.

Material	Moisture Content	Volatile Content	Ash Content	Fixed Carbon
MIS16	2.98 ± 0.19	81.83 ± 0.52	3.90 ± 0.35	11.29 ± 0.25
P-TA40	5.85 ± 0.49	81.22 ± 0.22	5.56 ± 0.10	7.36 ± 0.53
P-TA40-IER70	5.20 ± 0.08	81.15 ± 0.10	5.47 ± 0.26	8.18 ± 0.43
P-TA80	4.76 ± 0.63	82.44 ± 0.53	5.32 ± 0.26	7.48 ± 0.90
P-TA80-IER70	5.21 ± 0.08	82.03 ± 0.55	4.68 ± 0.16	7.89 ± 0.50

Proximate analysis results showed no significant differences among the pulp samples treated with the combination of IL-TA+IER compared to IL-TA only (1-2 wt.% increase in moisture content and ash content and 3-4 wt.% reduction in fixed carbon). There were also no noteworthy changes between the raw material and the different pulps regarding proximate analysis results. This could indicate that the thermal degradation of the pulp was very similar to the biomass. Therefore, this suggests no significant changes in the composition of the solid fraction obtained after pretreatment.

Ultimate analysis can provide insight into whether the solid pulp obtained has undergone significant elemental changes after the pretreated biomass. However, the ultimate analysis of pulp samples treated with IL-TA with and without IER70 at different concentrations also showed minute changes (Appendix 4 Table A4.1). The only discrepancy was the nitrogen content for P-TA40-IER70-0.25 with values of 0.86 wt.% (around twice the nitrogen content in other samples), but this could be associated with residual IL, which can easily disrupt the accuracy of nitrogen content measurements by interfering with analytical procedures, resulting in elevated nitrogen values [345].

As a result, these two techniques did not reveal any effect of the IL-TA with and without IER. Other characterisation techniques were explored to provide more insights into this system.

4.3.2. Thermogravimetric analysis (TGA)

A TGA analysis was conducted to determine the thermal characteristics of the pulp in comparison to the original material in inert and reactive environments. The DTG curves for the 200-600 °C range under N₂ (inert) and O₂ (oxidative) environments are presented in Figure 4.1. a and b, respectively.

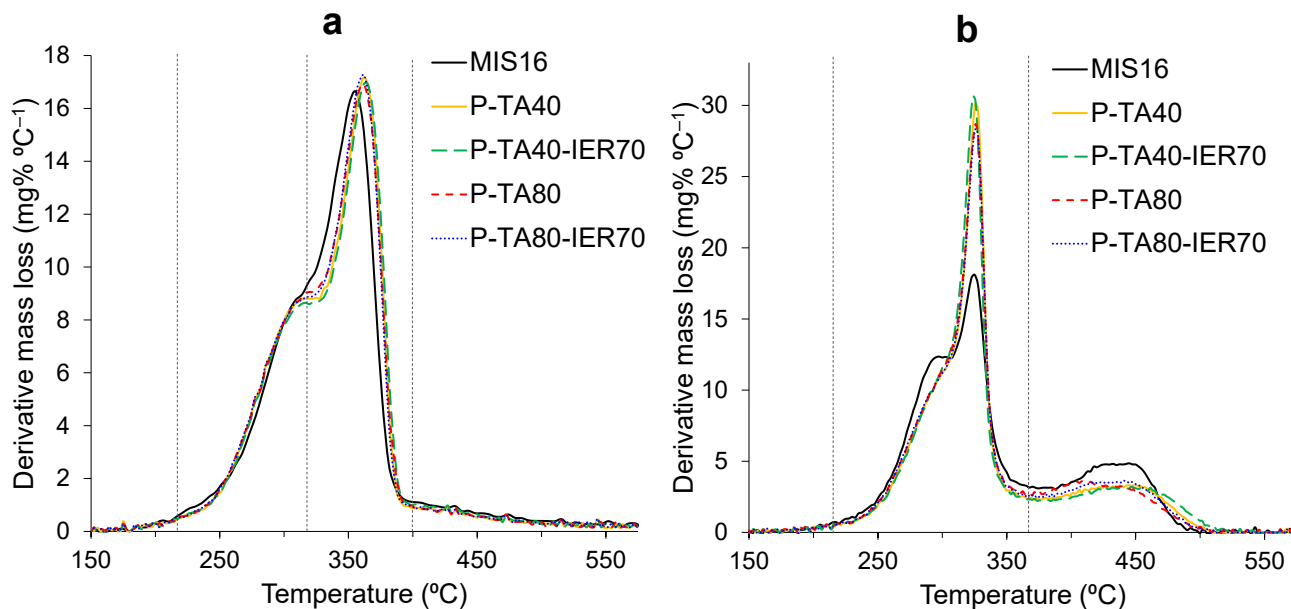


Figure 4.1. DTG curves of raw material and pulp treated with two concentrations of IL-TA (40 and 80 wt.%) and the absence or presence of 0.25 g of IER70. (a) under inert; (b) under air.

The TGA-DTG curves for the full range of temperatures and inert and oxidative conditions are given in Appendix 4 Figure A4.3. Furthermore, the DTG_{max} temperature peaks and their correlated TGA mass loss are presented in Appendix 4, Table A4.2 and Table A4.3 under inert and air atmospheres, respectively. When analysing the raw material under inert conditions (Figure 4.1.a), the typical DTG shoulder linked to hemicellulose (between 220-315 °C) was observed with a DTG_{max} temperature at 309 °C, a DTG_{max} value of 8.8 wt.% °C⁻¹ and a corresponding mass loss of 24.4 wt.% (Appendix 4, Table A4.2). Compared to the raw material, the hemicellulose shoulder in the pulp had a lower DTG_{max} value but overlapped less with the cellulose peak (dip in Figure 4.1.a for the pulp samples at ~325 °C). This can be caused by removing either the hemicellulose or the cellulose. Adding IER70 did not seem to make a difference in the thermal profiles of DTG.

The cellulose peak observed after the hemicellulose showed a DTG_{max} temperature at 356 °C for the raw material, with a DTG_{max} value of 16.6 wt.% °C⁻¹ and a corresponding mass loss of 59.0 wt.%, which agrees with the typical range for the cellulose peak (315-400 °C). For the pulp samples, the DTG_{max} temperature was slightly higher (362 °C) and sharper, which could indicate the better exposure of a uniform crystalline cellulose I or II structure [346,347].

Figure 4.1.b also showed the hemicellulose devolatilisation shoulder, typically seen at 220-320 °C, but with a high amount of hemicellulose in the raw material, the shoulder was more evident. The pulps showed a mass loss of 3-4 wt.% lower than the biomass for the hemicellulose region, confirming the pretreatment can solvate some hemicellulose from the biomass [348]. Under air, the cellulose peak temperature did not shift. However, the DTG_{max} increased significantly from 18 wt.% °C⁻¹ in the raw material to around 28-31 wt.% °C⁻¹ for the pulps, with IL-TA 40 wt.% system showing slightly higher DTG_{max} than IL-TA 80 wt.%. This sharpening of the peak indicates again changes in the cellulose structure to a uniform and crystalline structure or a better exposure to it [349–351]. Lastly, the third peak between 400 and 500 °C is due to the oxidation of lignin and inorganics in the biomass. The figure does not show significant shifts in the DTG_{max} temperature for this peak and shows a slight decrease in DTG_{max} value from 5 to 3 wt.% °C⁻¹, which could be indicative of some biomass delignification and the reason why the cellulose structure seems to be better exposed. It has been reported in the literature that ILs can effectively remove hemicellulose and lignin [345], so these results agree with the literature.

Finally, the TGA results show no significant differences when 0.25 g of IER70 was added in IL-TA to the pretreatment. Even though TA is a protic IL, it is a neutral IL. The IER70 could protonate the acetate anion in the IL. This could mean that when mixing the TA with IER70, the sulphonic groups of the IER70 might be neutralised by the cationic part of the IL, and the proton is used to form acetic acid, which is a weak acid with not sufficient capacity to hydrolyse cellulose [297]. Therefore, the main effect of the IER70 observed in Chapter 4 on the cellulose is not observed for the IL-TA-IER70 system. As a result, the main phenomenon that can be elucidated from the TGA analysis is that hemicellulose and lignin are removed to a small extent, exposing the cellulose crystalline structure slightly better. To confirm this, XRD analysis was performed to calculate the crystallinity index.

4.3.3. X-ray Diffraction (XRD)

XRD analysis was performed on pulp samples obtained from different concentrations of IL-TA pretreatment with and without IER70. Figure 4.2 shows the diffractograms for (a) IL-TA40 and (b) IL-TA80, compared to the raw material. MIS16 has three crystalline peaks at 16.2°, 22.3°, and 35.0°, representing 101-10 $\bar{1}$, 002 and 040 crystallographic planes of α -cellulose I, respectively [352]. The amorphous contribution can be measured by the intensity at 18.5°. For IL-TA40, either with or without IER70, there were no significant changes compared to the raw material (Figure 4.2.a). Both IL-TA and IER70 became ineffective in disturbing cellulose in the lignocellulosic matrix under these highly diluted conditions. Adding water to an IL helps to a certain extent in the dissolution of cellulose; however, a high percentage of water in the IL can become detrimental to the process. Water competes with IL for hydrogen bonding with cellulose, essential for disrupting the robust inter- and intra-molecular hydrogen bonds stabilising the cellulose structure. The competitive hydrogen bonding efficiently prevents the ionic

liquid from disturbing the crystalline areas of cellulose, hence limiting dissolution [353]. Water addition decreases the IL viscosity, enhancing the movement of molecules and promoting the interaction between cellulose and the IL [354]. Additionally, water can be a mediator in breaking the hydrogen bonds in the cellulose structure, accelerating cellulose dissolution by the IL [355]. Nevertheless, a significant amount of water can have adverse effects since an excessive amount competes with the IL for hydrogen bonding sites, diminishing the solvent power of the IL, and may result in the precipitation or aggregation of cellulose [356].

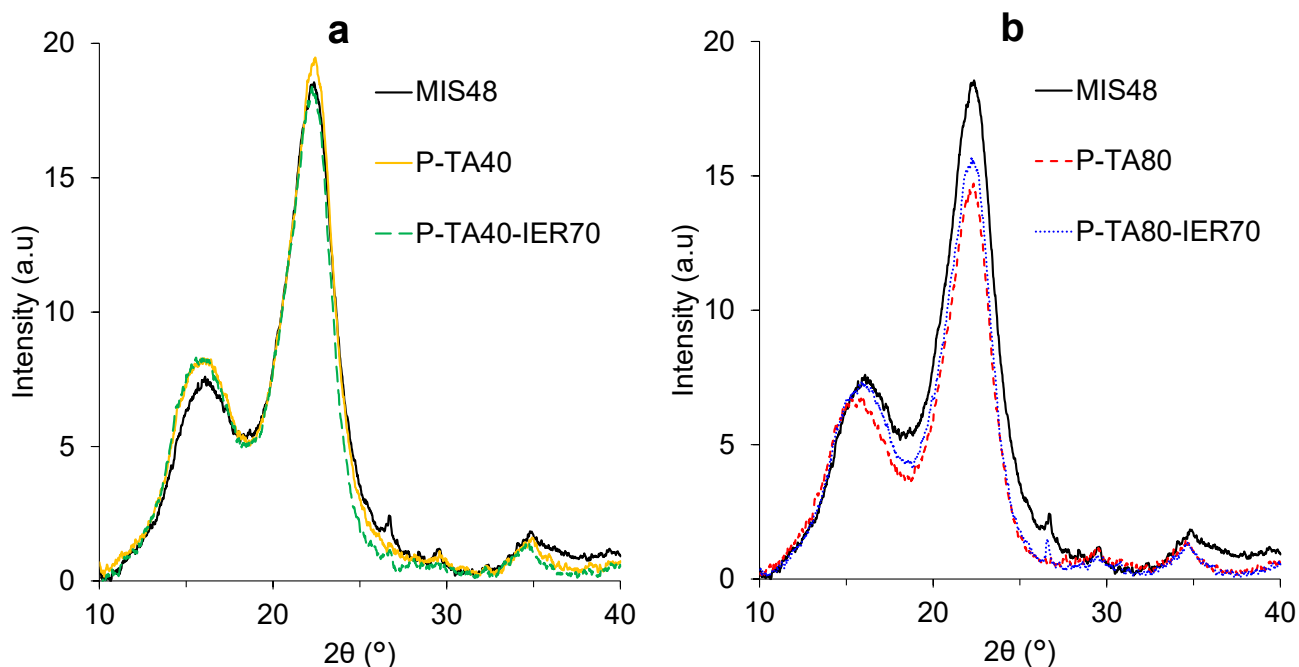


Figure 4.2. XRD diffractogram of raw material and pulp treated with IL-TA and the absence or presence of 0.25 g of IER70. (a) IL-TA 40 wt.%; (b) IL-TA 80 wt.%.

With higher IL-TA concentrations, the prominent crystalline peak narrowed at 22.3° , possibly due to the removal of amorphous components from the biomass, such as lignin and hemicellulose. Although the intensity decreases for the crystalline peaks at 22.3° (I_{002}), the intensity in the amorphous peak at 18.5° (I_{AM}) also decreases, so when the crystallinity index and the crystallite size are calculated (Table 4.4), the values showed no significant changes in the crystallinity of the pulp samples. Therefore, IL-TA with and without IER70 does not significantly affect the cellulose crystallinity.

Table 4.4. Crystallinity Index (*Crl*) and crystallite size of untreated MIS16 and pretreated pulp.

Material	<i>Crl</i> (%)	Crystallite size (nm)
MIS16	75.71 ± 0.16	3.13 ± 0.08
P-TA40	78.94 ± 1.36	3.33 ± 0.02
P-TA40-IER70	77.10 ± 1.93	3.24 ± 0.07
P-TA80	76.07 ± 0.12	3.20 ± 0.02
P-TA80-IER70	77.04 ± 1.73	3.20 ± 0.09

Considering both the TGA and XRD results, it seems that IL-TA40 with and without IER70 mainly has a slight effect on the hemicellulose and lignin, with a very minute effect on the cellulose structure. Beyond these minor influences, the combination of IER and IL did not seem to bring fruitful effects in terms of clearly removing lignin and hemicellulose or making changes in the cellulose structure. Finally, an ATR-FTIR analysis was conducted to determine if any chemical changes in the pulp occurred when using IL-TA and IER70 on MIS16.

4.3.4. Attenuated Total Reflection Fourier Transformation Infrared (ATR-FTIR) Spectroscopy

Figure 4.3 shows ATR-FTIR results for the biomass and the pulp samples treated with IL-TA with and without IER70 at different concentrations to assess if chemical changes occurred that cannot be evaluated with previous techniques. The results show no significant peak differences for pulp samples, regardless of the IL-TA concentration and the presence/absence of IER70.

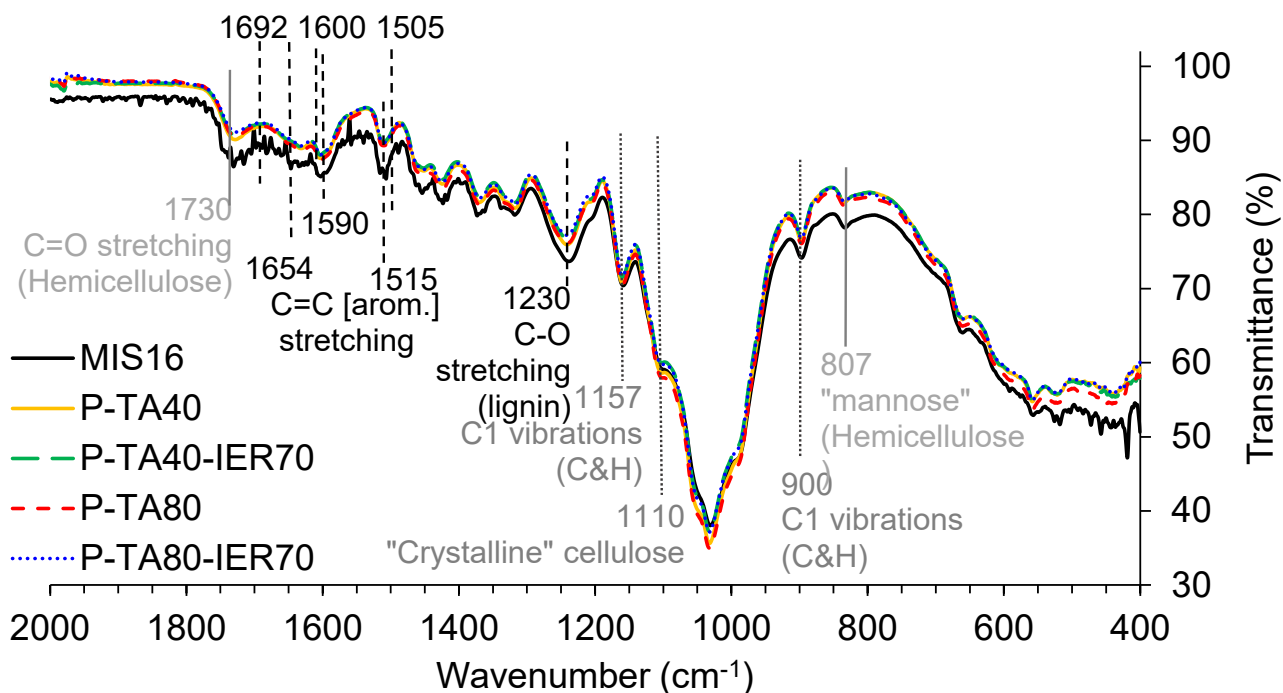


Figure 4.3. ATR-FTIR from 2000-400 cm^{-1} for raw material and pulp treated with two concentrations of IL-TA (40 and 80 wt.%) and the absence or presence of 0.25 g of IER70.

Hemicellulose changes between raw materials and pulps can be assessed using the absorption bands C1 vibrations 900 cm^{-1} , which corresponds to the C-H deformation in the furanose and pyranose rings present in hemicellulose [357,358]. The mannose contained in hemicellulose can also be evaluated with band 807 cm^{-1} , showing a lower presence of these peaks in the pulp samples.

Regarding lignin, peak intensities at 1654 , 1590 , and 1505 cm^{-1} due to carbon-carbon bond stretches in aromatic rings can be evaluated. Also, the 1230 cm^{-1} peak can be used, corresponding to the C-O stretching vibration in guaiacyl units, one of the building blocks of lignin. In this case, the pulp shows that all these bands have lower intensity of these bands, confirming the TGA discussion on the removal of lignin taking place in the process.

As a result, the FTIR analysis confirms the finding observed in TGA-DTG (4.2.2). IL-TA with IER70 is ineffective in fractionating lignocellulosic material into separate components due to IL-TA characteristics, only showing some slight effects on removing hemicellulose and lignin. In addition, there is no symbiotic effect with the IER70. Even though IL-TA is a protic ionic liquid (PIL), the acetate ion exhibits a notable propensity for establishing hydrogen bonds, which can interact with lignin. However, the efficacy of delignification also relies on the cationic capacity to break the intricate structure of lignin with acetate anion [359]. Therefore, the following section studies the combination of IER70, but this time using the Triethylammonium Hydrogen Sulphate (IL-TS), which has a strong acidic behaviour.

4.4. Ionic liquid system (TS) with and without IER70 for MIS16

IL-TS can dissolve a substantial amount of lignin from lignocellulosic biomass. Under harsh conditions, the IL preferentially dissolves lignin and hemicellulose while retaining a cellulose-rich pulp [360]. IL-TS exhibits a dual activity as a delignification agent and a catalyst for hydrolysis chemical bonds. This dual activity enables a more thorough breakdown of biomass, efficiently separating lignin and improving the extraction of carbohydrate-rich components at moderate operating conditions [361]. To test whether the acidic IL-TS can work symbiotically with IER, experiments were conducted with M16 and IER70 and two different concentrations of IL-TS in water (40% and 80% TS in water).

4.4.1. Proximate and ultimate analyses

Table 4.5 represents the proximate analysis of pulp samples upon IL-TS pretreatment with and without IER70 at different IL-TS concentrations (40 wt.%, 80 wt.%) in water. When IL-TS is used, the main changes observed are a decrease in the volatile content (10-12 wt.% lower) and an increase in the ash content (~7 wt.% higher) and fixed carbon percentage (4-5 wt.% higher). In addition, whenever IER70 is used with IL-TS, the proximate analysis values do not change much compared with only IL-TS. Finally, the proximate analysis does not reveal significant differences between the two IL-TS concentrations.

Table 4.5. Proximate analysis (wt.%) of raw material (MIS16) and pulp from IL-TS-IER70 treatment with two concentrations of TS (40 and 80wt.%) and the absence or presence of 0.25 g of IER70.

Material	Moisture Content	Volatile Content	Ash Content	Fixed Carbon
MIS16	2.98 ± 0.19	81.83 ± 0.52	3.90 ± 0.35	11.29 ± 0.25
P-TS40	2.63 ± 0.16	71.26 ± 0.16	10.60 ± 0.13	15.50 ± 0.20
P-TS40-IER70	2.92 ± 0.07	71.80 ± 0.65	10.57 ± 0.13	14.71 ± 0.53
P-TS80	3.19 ± 0.27	70.05 ± 0.29	10.89 ± 0.05	15.88 ± 0.45
P-TS80-IER70	2.46 ± 0.07	70.50 ± 0.49	10.12 ± 0.45	16.92 ± 0.96

The decrease from 81.8 to 70.1 wt.% in the volatile content for samples MIS16 and P-TS80 was expected due to the removal of lignin and hemicellulose from the pulp. This trend agrees with the literature [86,337]. Depending on the intensity of the operating parameters, the cellulose could also dissolve during the IL pretreatment. It would be unable to precipitate and recover as pulp after adding an antisolvent, which ultimately can also decrease the cellulose content or result in a pulp that only contains the most stable cellulose [207].

The fixed carbon is expected to increase when the volatile content decreases [362]. This is because the more recalcitrant and stable fractions of lignocellulosic material remain in the pulp, and therefore, more char will be obtained with better quality after the pyrolysis devolatilization [363,364].

The effect of IL pretreatment on the ash content depends on the biomass used. Biomass materials such as willow natural ability to absorb and accumulate heavy metals [365] and sewage sludge derives from wastewater treatment processes which collect contaminants from various sources, such as industrial effluents, urban runoffs and domestic waste [366] have high heavy metals, which can be removed through IL pretreatment, ultimately decreasing the ash content [367]. However, materials such as *miscanthus*, rice straw oil palm, and empty fruit bunches with either alkali or alkali earth metal have increased their ash content in the pulp after IL pretreatment [362,368]. ILs can form strong complexes with heavy metals, facilitating effective extraction via ion exchange and complexation mechanisms. Nonetheless, ILs are often less proficient at extracting alkali and alkaline earth metals (AAEMs) from biomass. AAEMs are often essential to the biomass architecture, creating crosslinks and reinforcing cell walls, hence complicating their extraction [369]. Although an increase in ash content does not make the pulp a suitable candidate for spontaneous combustion [370], it does not have a negative impact on any post-processing, such as enzymatic hydrolysis [86].

Regarding elementary analysis, Table 4.6 presents results for the ultimate analysis of the raw material and pulp upon IL-TS-IER70 pretreatment. Carbon content decreased from 44% to 39 wt.%, and there are traces of sulphur content (between 1-2 wt.%). As mentioned, IL-TS primarily disrupts the lignocellulosic matrix, leaving a pulp with the most stable and recalcitrant compounds, which can decrease the carbon content in the pulp [371,372]. The sudden appearance of sulphur traces could be linked to residual sulphur from IL-TS on the pulp [373]. However, George *et al.* [345] reported sulphur in the ash of switchgrass treated with IL-TS, and they hypothesised that this could be either incomplete removal of the IL or sulphur bound to the pulp chemically. They also reported a proportional correlation between the sulphur and ash contents, which could explain why the pulp samples have higher ash content. Regarding the use of IER70, the changes were not significantly different to IL-TS in the pulp samples.

Table 4.6. Ultimate analysis (wt.%) of raw material (MIS16) and the pretreated pulp for the IL-TS-IER70 system.

Sample	C	H	S	N
MIS16	43.87 ± 0.14	6.05 ± 0.06	0.00 ± 0.00	0.47 ± 0.01
P-TS40	40.67 ± 0.13	5.90 ± 0.08	0.84 ± 0.07	0.21 ± 0.01
P-TS40-IER70	40.81 ± 0.23	5.88 ± 0.05	0.84 ± 0.03	0.23 ± 0.00
P-TS80	38.66 ± 0.11	5.91 ± 0.02	1.09 ± 0.07	0.29 ± 0.01
P-TS80-IER70	39.08 ± 0.10	6.09 ± 0.04	1.52 ± 0.02	0.60 ± 0.02

In conclusion, the proximate and ultimate analyses showed the expected changes of ash, carbon and sulphur in the pulp resulting from IL-TS treatment, but analyses do not disclose any effect from the combination of IL-TS with the IER70 on the pulp samples.

4.4.2. Thermogravimetric analysis (TGA)

Figure 4.4 presents the DTG curves for pulp samples (a) under an (N_2) inert environment and (b) under an (air) oxidative environment for the temperature range 200-600 °C. The TGA-DTG profiles for the full temperature range are provided in Appendix 4 Figure A4.4. The main DTG temperature peaks and their correlated TGA mass loss are presented in Appendix 4, Table A4.4, and Table A4.5 under inert and air atmospheres, respectively.

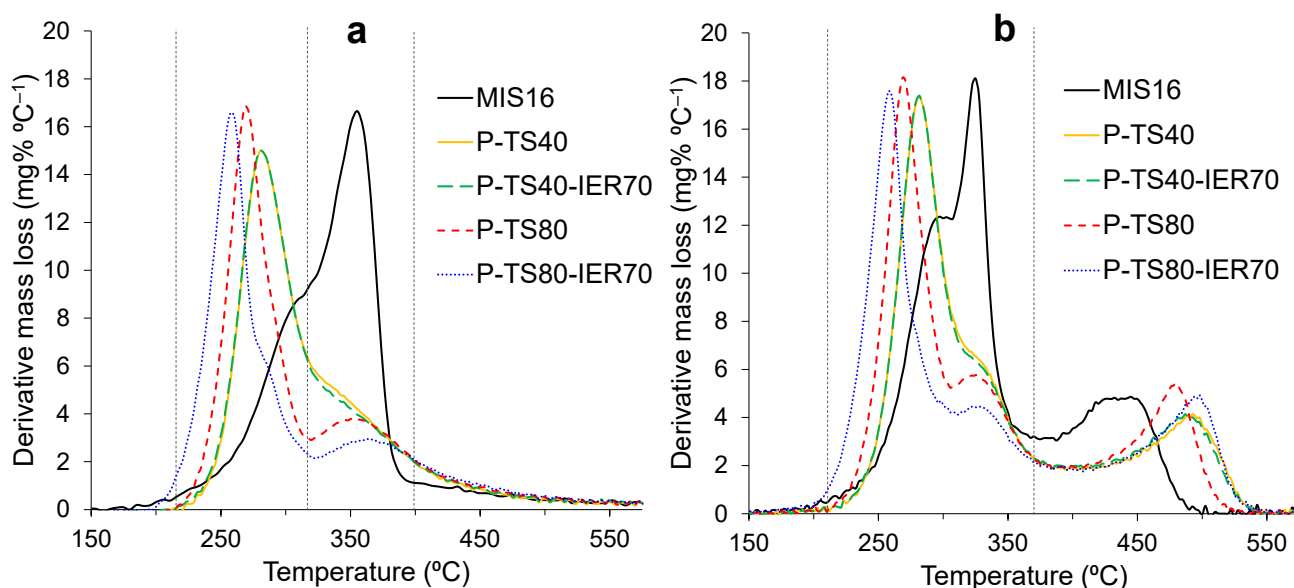


Figure 4.4. DTG curves for biomass, IL-TS-IER70, (a) under (N_2) inert and (b) under (air) oxidative treatment at different IL concentrations.

In this analysis, apparent differences in the pulp's thermal behaviour can be observed between the two IL-TS concentrations used, but the effect of adding IER70 to the IL-TS with 80 wt.% of TS and 20 wt.% water can also be observed.

Comparing the different concentrations of the IL, the more concentrated the IL-TS is, the less thermally stable the pulp becomes under both (N_2) inert and (air) oxidative conditions of TGA. The shapes of the DTG curves are also significantly different. The samples treated with IL-TS do not show the distinguishable hemicellulose peak/shoulder observed in the raw material between 220-315 °C. This is indicative of a substantial removal or depolymerisation of the hemicellulose in the pulp, which is expected, as previous studies show that under harsh conditions using acidic IL-TS, hemicellulose is the most susceptible to thermochemical degradation [352,374] and hydrolysis into the liquid phase [375].

The cellulose peak observed in the raw material between 300-400 °C with a DTG_{max} of ~17 wt.%/°C at 356 °C changes drastically into two peaks after being pretreated. After pretreatment, the 300-400 °C is still present but becomes the second most crucial peak (second peak) after a new main peak is observed between 200-330 °C (first peak). Yang et al., reported the first peak represents the amorphous fraction of cellulose and/or the depolymerisation of cellulose, hemicellulose and lignin caused by the disruption of the hydrogen bonding network and decomposition of polysaccharides to monosaccharides [376–378]. The DTG curves show that increasing the IL-TS concentration exacerbates the cellulose depolymerisation and the transformation of crystalline cellulose into amorphous cellulose. This is because the DTG_{max} temperature for the first peak is shifted to lower values (280.0 °C for IL-TS 40 wt.% and 268.7 °C for IL-TS 80 wt.%) and becomes sharper, and due to the less prominent presence of the second peak for higher concentration of IL-TS.

When evaluating the effect of the IER70 in combination with the IL-TS, IER70 with IL-TS40 shows no changes in thermal degradation under inert and oxidative conditions. This is similar to what was observed for the IL-TA-IER70 system. This could indicate that when the IL is neutral or the IL is too diluted, the IER70 has no symbiotic effect and could mainly interact with the IL rather than with the biomass. In contrast, when IER70 is added to IL-TS 80 wt.%, the IER70 influences the thermal stability of the pulp, which is further reduced (shifting the DTG_{max} temperature from 269 °C for IL-TS only to 257 °C for IL-TS with IER70). Furthermore, the IER70 also changes the second peak, increasing the DTG_{max} temperature from 356.5 to 362.2 °C. This could indicate the crystalline structure is converted or depolymerised further in the presence of IER70, leaving only the more thermally stable cellulose crystalline. In Chapter 4, it was observed that the IER70 could affect the crystalline structure of cellulose when used in water, and this chapter shows that this effect is still present in the IL-TS concentrated system.

After the devolatilisation peaks between 200-380 °C, the combustion of the pulp under oxidative conditions takes place, which is the third peak between 380 to 550 °C in Figure 4.4.b. This third peak is related to the oxidation of lignin and inorganics [379]. As expected, the raw material has a lower DTG_{max} temperature for this third peak than the pulps pretreated with IL-TS (445.0 °C for the raw material and between 480-500 °C for the pulps). The results of the DTG curves under oxidative environment showed no significant differences between IL-TS 40 wt.% with and without IER70 (DTG_{max} temperature around 498 °C). For IL-TS 80%, when IER70 is used, the DTG_{max} temperature is similar to IL-TS 40% (~497 °C), but when the IER70 is not present, the DTG_{max} temperature decreases to 480 °C.

The peak position, DTG_{max} temperature, and mass loss changes depend on the inorganic and lignin amounts. Generally, after an ILs pretreatment, the ash content in the pulp increases significantly relative

to the raw material as discussed in Section 4.4.1; however, when the same raw material is treated with dilute acid, it causes demineralisation removal of alkali metal [184,370]. Biomass containing alkali metals tends to ignite at lower temperatures, as they can facilitate the initial oxidation of carbon [380]. At temperatures above 400 °C, minerals are activated to play a catalytic role in the reaction process, which could reduce the initial temperature of char combustion [380]. Looking at the results, it is possible that the diluted IL-TS 40 wt.% causes some demineralisation of alkali metals, which does not occur with the IL-TS 80 wt.%. Therefore, the temperature is shifted to higher values for the diluted IL solution. In the case of the IL-TS 80 wt.% with IER70, the alkali metals could be removed through ion exchange with the IER70 such as sodium (Na) and potassium (K). However, this could not be demonstrated with the proximate analysis, as the ash content of the different pulps was very similar (Table 4.5). Another aspect to consider is the changes occurring in the lignin. If biomass is delignified, the combustion temperature is shifted towards lower temperatures [381]. Delignification can be facilitated in the presence of alkali metals. Therefore, the changes in the third stage of the oxidative curves could be a combination of the removal of alkali materials and the delignification of the biomass.

4.4.3. X-ray Diffraction (XRD)

During the analysis of the TGA curves, it was discussed that the crystalline structure of cellulose was transformed into amorphous cellulose through depolymerisation as amorphous cellulose is easily hydrolysed [264]. Therefore, XRD analysis was performed to assess the changes in the crystallinity index of the pulps obtained. On the contrary, cellulose chains are held securely together by intra- and intermolecular H-bonding due to the hydroxyl group presence, making cellulose more crystalline and more resistant to hydrolysis. Generally, IL treatment of lignocellulosic material decreases the crystallinity of cellulose in the material, ultimately accelerating hydrolysis [382]. This is because ILs can dissolve cellulose molecules by dissolving the network of intra- and intermolecular hydrogen bonds between them and creating a new network of IL-cellulose hydrogen bonds that will aid in their disintegration [383]. Also, after IL treatment, there is a decrease in CrI due to a change in crystalline cellulose to amorphous cellulose [384] because the crystalline cellulose is broken to amorphous, causing an increase in the chain spacing and reducing the cellulose polymerisation degree and crystallinity [385].

Figure 4.5 presents XRD results for IL-TS 40 wt.% (a) and IL-TS 80 wt.%. All the samples show the crystalline peaks for cellulose I at 16.0°, 22.2°, and 35.10°, representing 101-10 $\bar{1}$, 002, and 040 crystallographic planes of α -cellulose I, respectively.

For all the pulps, the peak at 22.2° shows a higher intensity (I_{002}) and is sharper. It can also be observed that the intensity in the amorphous area at 18.5° (I_{AM}) also decreases. This means that the crystallinity index will increase for the pulp samples. The crystallinity index (CrI) values are shown in Table 4.7,

showing that the CrI increased by 10% and the crystalline size increased to 3.7 nm. So, although the TGA analysis shows that the crystalline structure of cellulose is transformed to amorphous cellulose, the overall crystallinity of the pulp increased. To understand this characterisation technique, it is important to understand that the CrI is calculated using the Segal method to estimate the relative crystallinity of cellulose with intensities for amorphous (I_{AM}) and crystalline (I_{002}). This method indicates the extraction of amorphous parts from the lignocellulosic material under investigation [386] and how their removal improves crystallinity. The removal of amorphous lignin and hemicellulose enhances the available surface area of cellulose fibrils. The exposure of cellulose chains may result in a more organised structure, enhancing crystallinity. During IL pretreatment, the breakdown and regeneration process enables cellulose chains to reorganise into more ordered configurations, possibly enhancing crystallinity [387].

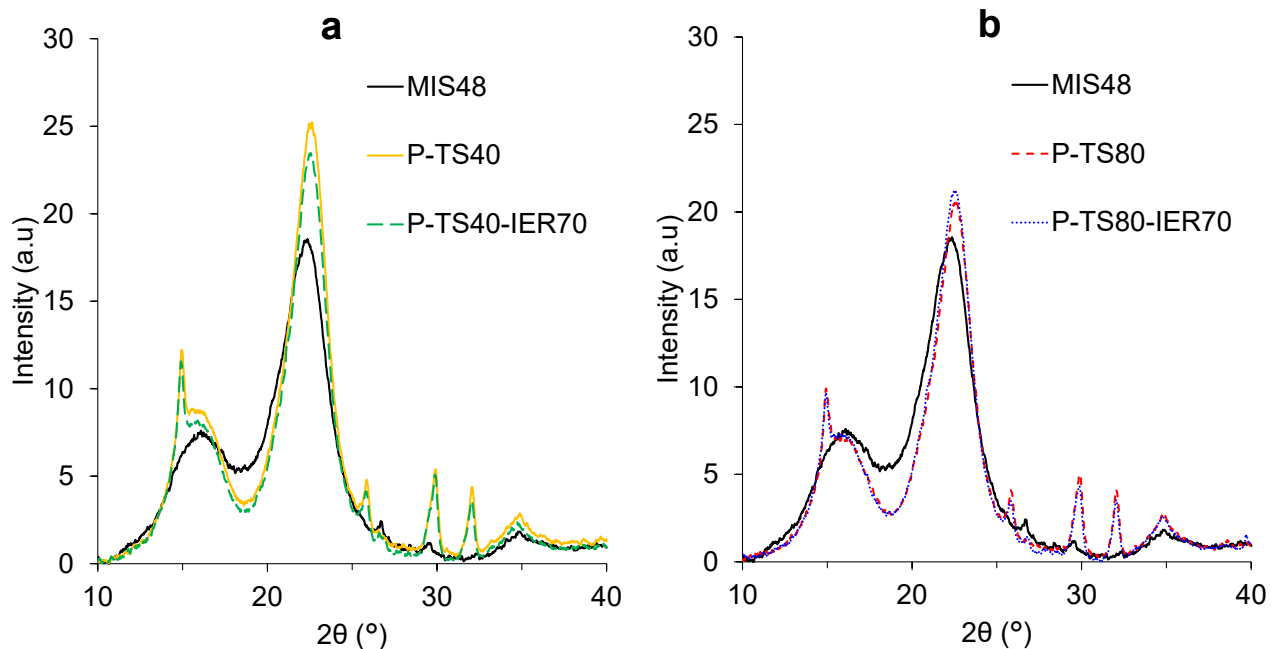


Figure 4.5. XRD diffractograms for the raw material and pulp treated with IL-TS-IER70 with and without IER70 for IL-TS (a) 40 wt.% and (b) IL-TS 80 wt.%.

The increase in CrI , therefore, is enhanced upon the removal of amorphous parts such as hemicellulose and lignin. Gundupalli *et al.* showed that pretreatments with ILs with hydrogen sulphate anion with different cations, such as Pyridinium or triethylamine, had more effect on xylan and lignin in biomass such as coconut pith compared to coconut coir and increased the CrI [388]. George *et al.* also reported that IL-TS can increase the CrI through the removal of the lignin and hemicellulose fractions [345].

Table 4.7. *Crl*, the crystallite size of untreated MIS16, and pulp with IL-TS-IER70 at different IL concentrations with and without IER70.

Material	<i>Crl</i> (%)	Crystallite size (nm)
MIS16	75.71 ± 0.16	3.13 ± 0.08
P-TS40	88.71 ± 1.54	3.99 ± 0.10
P-TS40-IER70	88.86 ± 0.71	4.00 ± 0.04
P-TS80	83.25 ± 0.00	3.81 ± 0.16
P-TS80-IER70	87.89 ± 0.00	3.80 ± 0.04

Furthermore, pretreated pulp samples show new peaks at 25.5°, possibly due to pseudo-lignin deposition on the pulp. Other reflections can also be observed at 29.7° and 32.0°, which were not feasible to determine and might be related to inorganic compounds.

To conclude, removing lignin and hemicellulose from the biomass significantly affected the crystallinity index value compared to transforming cellulose into amorphous cellulose which make it more readily available for downstream processing to produce biofuels.

4.4.4. Attenuated Total Reflection Fourier Transformation Infrared (ATR-FTIR)

Spectroscopy

FTIR analysis was done on the pulp samples treated with IL-TS and IER (Figure 4.6). The pulp samples show significant differences compared to the biomass sample. The particle size of the sample can influence ATR-FTIR results. However, the biomass and pulp samples analysed had the same particle size, eliminating the results' dependence on this parameter. FTIR was conducted to elucidate the chemical changes in the pulp after pretreatment by analysing the key wavelengths related to lignin, cellulose and hemicellulose (Appendix 3 Table A3.7).

As a general trend, the shifts from biomass FTIR to pulp follow the same pattern, with small differences depending on the concentration of IL-TS and the presence or absence of IER70.

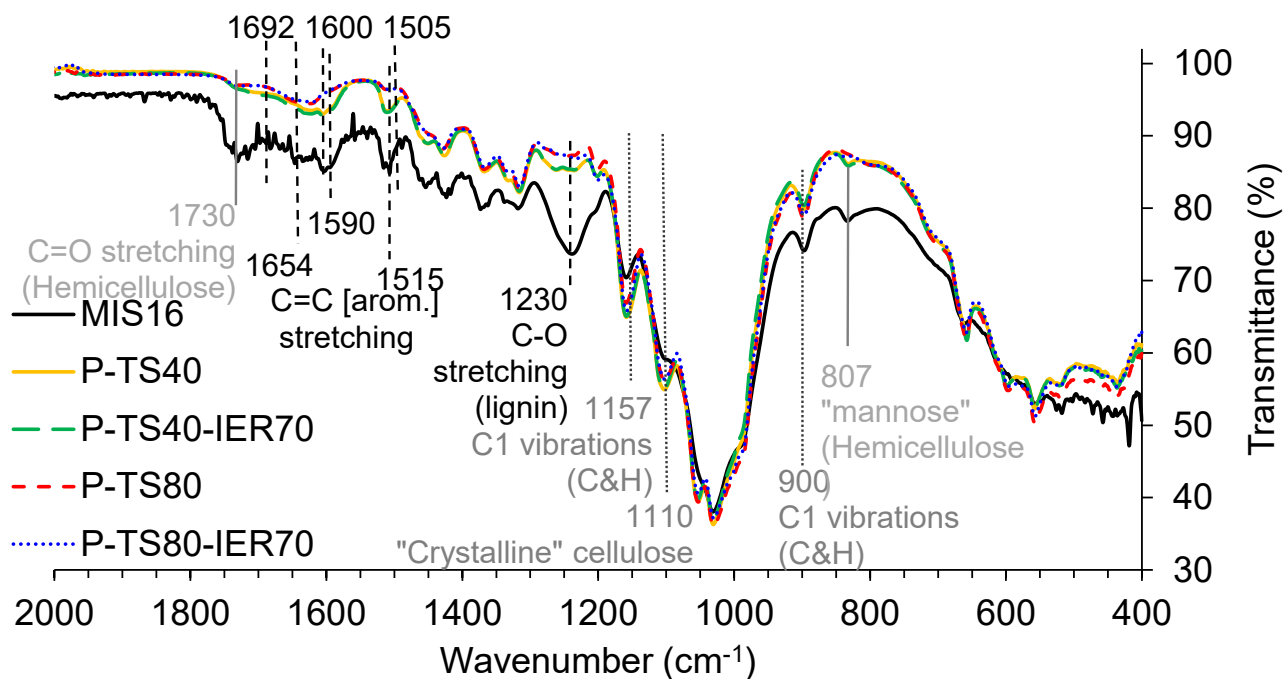


Figure 4.6. ATR-FTIR for the biomass and pulp samples treated with IL-TS-IER70 ranged from 2000 – 400 cm^{-1} at different IL concentrations.

The peak at 900 cm^{-1} is attributed to the C-H deformation in the furanose and pyranose rings present in hemicellulose to analyse the effect on hemicellulose. This band can indicate the presence of sugar units such as xylose, mannose, and arabinose. As can be observed, the pulp samples show less of this peak, confirming that hemicellulose was removed during the pretreatment.

The 1230 cm^{-1} peak can assess the lignin content. This peak is typically associated with the C-O stretching vibration in guaiacyl units, which is one of the building blocks of lignin. This band may also show the acetyl and uronic ester groups found in hemicellulose or can also overlap with the C-O stretching of polysaccharide chains in cellulose. However, the effect of the lignin is more pronounced, and therefore, this band is mainly associated with lignin [389]. In addition, the presence of functional groups in the lignin structure can also be evaluated for the wavelengths between 1500-1700 cm^{-1} , related to the stretching of the C=C in the aromatic rings of lignin [390]. As seen in the FTIR analysis, the pulps have higher transmittance in these bands, confirming there is less presence of lignin, with IL-TS 80 wt.% being the samples with less presence of these peaks. Additionally, the depolymerisation of lignin can also be observed by looking at the transmittance at 847 cm^{-1} , which signifies the change in the molecular weight of lignin is shifted if the transmittance value is higher [388].

The cellulose's crystallinity can be inspected using the 1100 cm^{-1} peak. This peak is related to the asymmetric stretching vibration of the C-O-C β -1,4-glycosidic linkage in cellulose [389]. This bond is crucial for linking glucose units in the cellulose polymer, and the intensity and sharpness of this peak

can also indicate the crystallinity [263,391]. Also, the peak at 1157 cm^{-1} is due to the asymmetric stretching of cellulose I and II [392]. The pulps obtained seem to have a higher presence of crystalline cellulose, which agrees with the XRD analysis.

FTIR-ATR spectral results can be used to calculate the Relative crystallinity index and lateral order index (LOI) [263,391]. Relative *CrI* indicates the conversion of cellulose I to cellulose II; the lateral order index (LOI) is related to the proportion of cellulose I to cellulose II. Table 4.8 shows the calculation of the Relative *CrI* and the LOI for the raw material and the pulps.

Table 4.8. Relative crystallinity index (Relative *CrI*) and lateral order index (LOI) of untreated MIS48 and pretreated pulp.

Sample	Relative <i>CrI</i>	Lateral order index
	A1370/A665	A1430/A898
MIS16	1.242 ± 0.001	1.110 ± 0.000
P-TS40	1.312 ± 0.000	1.097 ± 0.001
P-TS40-IER70	1.324 ± 0.001	1.092 ± 0.001
P-TS80	1.336 ± 0.000	1.122 ± 0.001
P-TS80-IER70	1.324 ± 0.001	1.118 ± 0.000

The result of Relative *CrI* indicates a specific change from cellulose I to cellulose II compared to the raw material. A maximum Relative *CrI* increase is higher (around 1.32) compared to MIS16 (1.24). The decrease in LOI (lateral order index proportion of cellulose I to cellulose II) values implies fewer hydrogen bonds of cellulose crystallinity with a weakly ordered cellulose structure [389]. However, in the case of LOI (lateral order index proportion of cellulose I to cellulose II), the changes are insignificant. A change from cellulose I to cellulose II after IL pretreatment is typically observed in literature [393].

After evaluating all the characterisation techniques and taking into consideration the literature, the following findings can be drawn for the IL-TS-IER70 system:

- Protic ionic liquids (PILs) such as IL-TS can effectively remove lignin from lignocellulosic material during pretreatment while maintaining, to a certain extent, the cellulose's structural integrity [394]. Lignin's three-dimensional network is connected by β -O-4 links, C-C, and ester bonds, which undergo solubilisation when interacting with IL-TS. During the π - π interactions between the cation and the aromatic carbon, the cation acts as a bridge for proton transfer, receiving protons from the β -ether bond and transferring them to the oxygen atom of the β -O bond, which causes the β -O-4 bonds to break [395] [396].
- The pH of IL plays a critical role in the fractionation of lignocellulosic material. IL-TS is highly acidic, with a density of 1.19 g/mL and a pH of 1.52 [342], whereas the density of IL-TA is

1.01 g mL⁻¹ with a pH of 6.95. For example, with acid, ILs such as IL-TS, hemicellulose and lignin are removed in the pretreated material [397], along with the cellulose transformation [398]. Acetate anion with triethylamine cation IL is not strong enough to fractionate the lignocellulosic material to remove lignin or modify cellulose structure. Additionally, IL-TA has less thermal stability than protic ILs like IL-TS because amines are incompletely protonated by acetic acid [345].

- The presence of hydrogen bonds between the anion and the oxygen atom in the ether bond of lignin facilitates the breaking of the ether bonds, as well as the glycosidic bonds that connect lignin with cellulose and hemicellulose [399]. These interactions cause the lignin to break into smaller aromatic fragments, disrupting the entanglement barrier that affects the polysaccharide chains. Consequently, the cellulose and hemicellulose become more chemically accessible. Under the acidic conditions of IL-TS, hemicellulose can be largely be hydrolysed [86,388].
- The anion part of the IL plays a crucial role in the depolymerisation of cellulose structure. The IL-TS can disrupt the hydrogen bonds between and between cellulose molecules, making it easier to dissolve cellulose. In particular, the anion receives hydrogen bonds in cellulose disintegration. When the lignocellulose component is dissolved in the ionic liquid, it disrupts the tissue within the cell wall, reducing its refractory character. Therefore, the pretreatment of regenerated cellulose results in a more disordered macrostructure [29,368].

4.5. Conclusions

This Chapter 4 examined the influence of IER70 on lignocellulosic material of herbaceous nature in the presence of protic ionic liquids TA and TS. This section summarises the main conclusion and findings in this chapter.

Use of stainless-steel mesh baskets with ionic liquids:

1. IERs can be enclosed in stainless steel mesh baskets during the reaction and provided similar method to separate and recover the IERs from the pretreated solid material biomass but it cannot be used to work with IL-TS that have a low pH (<2), because the stainless-steel metals are dissolved by the IL and interfere with biomass pretreatment.
2. The acid-to-base ratio of IL-TS is a critical parameter to control when preparing the IL and using it to fractionate lignocellulosic biomass. In preliminary tests of IL-TS with the mesh baskets, the acid-to-base ratio was not monitored, which created inconsistencies in some preliminary results and unexpected changes in the biomass (such as strong charring).

IL-TA-IER70 system:

1. Proximate analysis and ultimate analysis did not reveal any effect of the IL-TA with and without IER, and other characterisation techniques such as TGA, XRD and FTIR were needed to provide more insights into this system.
2. TGA results showed no symbiotic effect between IER70, and IL-TA and that the IL caused the main changes observed in the pulp. The hypothesis is that the cationic part of the IL might neutralise the sulphonic groups of the IER70, and the proton is used to form acetic acid, which is a weak acid with insufficient capacity to hydrolyse cellulose. Also, the acetate anions acted more as a buffer in the medium to stabilise the pH. Therefore, the main phenomena caused by the IL were a slight removal of the hemicellulose and the lignin and a minimal improvement in exposing the cellulose structure, which was confirmed by the small changes in the CrI obtained from the XRD analysis and by the small chemical changes observed in the FTIR-ATR analysis.

IL-TS-IER70 system:

1. IL-TS in the presence and absence of IER70 showed that the most recalcitrant and thermally stable lignocellulosic component crystalline cellulose remained in the pulp after pretreatment. This was elucidated from the proximate analysis, which showed lower volatile contents, higher fixed carbons and higher ash contents in the pulps. The proximate analysis could not reveal any difference between changing the IL-TS from diluted to concentrated or adding the IER70.

2. IT-LS disrupts the lignocellulosic matrix and decreases the volatile content. The fixed carbon percentage is expected to increase, as the fixed carbon is the solid carbon left in the char after devolatilization during pyrolysis.
3. TGA and FTIR results confirmed that IL-TS causes the removal of hemicellulose and delignification. At low concentrations of IL-TS, IER70 shows no enhancement in performance, while at high concentrations, it can assist with the cellulose transformation into amorphous cellulose.
4. The delay in the combustion peak in the TGA under air (380-550 °C) for diluted IL-TS and concentrated IL-TS with IER70 indicated the possibility of demineralisation of alkali metals. In the case of IER70, this could be promoted by its capacity to exchange ions.
5. XRD showed that removing lignin and hemicellulose from the biomass had a more significant effect than transforming cellulose into amorphous cellulose by changing the value of the crystallinity index obtained using the Segal method. As a result, the pulps showed a *CrI* 10% higher than the raw material instead of a reduced *CrI*.
6. The IL-TS can cause the delignification of lignin through the cleavage of the β -O-4 bonds in lignin. This helps to expose the hemicellulose and cellulose fractions better. The acid pH of the IL-TS can then hydrolyse the hemicellulose and transform the crystalline cellulose into amorphous cellulose. When the IER70 is involved in a concentrated system, it can also help remove alkali metals and assist with the depolymerisation of the hemicellulose and the cellulose.

As a result, the combination of concentrated IL-TS with IER70 was demonstrated to create a symbiotic effect. In the next chapter, the combination of TS80-IER will be further explored to assess whether the physicochemical properties of sulfonic exchange resins can play a role in improving this symbiotic effect. The effect of this combined pretreatment will also be tested for other biomasses with different hemicellulose compositions.

Chapter 5. Evaluation of Triethyl ammonium hydrogen sulphate with different Ionic Exchange Resins and Lignocellulosic Feedstocks

5.1. Introduction

Chapter 4 concluded that a macro-reticular strong acid resin such as Amberlyst 70 can be used as a catalyst with ionic liquids such as triethyl ammonium sulphate (IL-TS) to enhance the conversion of crystalline cellulose into amorphous and its subsequent depolymerisation and dissolution. The catalytic activity of any IERs during a chemical reaction can be influenced by their properties, such as total/operating cation exchange capacity, particle size, swelling capacity and thermomechanical stability [400,401]. For example, the effectiveness of sulfonated polystyrene ion exchange resins as a catalyst is influenced by the ability of acid sites to be accessed through diffusion within the polymer matrix. The outcome depends upon the degree to which the resins solvate and expand in the solvent and the presence or absence of any pore structure in the material [278].

This Chapter 5 will explore the use of different acidic IERs combined with TS80 to evaluate whether the various properties of IERs in the IL solution can influence and improve the lignocellulosic fractionation process to produce carbohydrate-rich material. Four ion exchange resins from Dupond are investigated: Amberlyst 15 (IER15), Amberlyst 35 (IER35), Amberlyst 45 (IER45) and Amberlyst 70 (IER70). Additionally, three Purolite resins will be also tested: Purolite CT-252 (IER252), Purolite CT-275 (IER275) and Purolite CT-485 (IER485). All these resins were selected because they are polyvinyl-divinylbenzene macroreticular resins and sulfonated. However, their variation in the crosslinking degree (low, medium and high crosslinking) affects their swelling capacity, as low crosslinking grants higher swelling and flexibility of the polymeric matrix to access the active sites. Also, there are differences in the sulphonation degree (conventionally sulphonated, over sulphonated), which confers higher or lower acid capacity. Finally, IER45, IER70 and IER485 are sulfonated and chlorinated resins, so they have chlorine incorporated into the polymeric matrix structure, providing higher acid strength and thermal stability. The properties of these resins are summarised in Table A2.1 in Appendix 2. Therefore, in the first section, these IERs will be tested with triethyl ammonium sulphate at 80 wt.% (TS80) to investigate any correlation between the IER properties and the performance in the system for fractionation of *Miscanthus x giganteus* (428-800 μm).

Although the combination of IL and IER was useful for lignocellulosic biomass with high cellulose content, such as *miscanthus x giganteus*, this might not be the case for other biomasses. Therefore, in the second section, the physiochemical properties of various lignocellulosic materials will be assessed to evaluate if there are significant differences in composition. The other selected materials are brewery spent grains (BSG) and pine bark (PB). This second section aims to confirm that the composition of these three biomasses is sufficiently distinctive so that the effectiveness of the selected IER in TS80 against composition can be evaluated (the aim of the third section).

Operating parameters, including biomass loading, pretreatment time (t), temperature (T), and pressure (p) and recovery of the biomass fractions, will be the same as the ones used in Chapter 3. Finally, the terminology used in this chapter is presented in Table 5.1.

Table 5.1. Summary of terminologies for samples used in Chapter 5.

Name	Nomenclature
<i>Miscanthus x giganteus</i> (425-800 µm)	MIS48
<i>Miscanthus x giganteus</i> (<106 µm)	MIS16
Brewery Spent Grain (425-800 µm)	BSG48
Pine Bark (425-800 µm)	PB48
Pulp	P
Ionic Liquid	IL
Triethylammonium hydrogen sulphate 80 wt. %	TS80
Ionic Exchange Resin	IER
Amberlyst 15	IER15
Amberlyst 35	IER35
Amberlyst 45	IER45
Amberlyst 70	IER70
Purolite Resin-CT 252	IER252
Purolite Resin-CT 275	IER275
Purolite Resin-CT 485	IER485
Treatment with TS80 and no IER	IER00
Pulp treated with TS80 and IERXX	P-IERXX
Pulp of BSG treated with TS80 and IER70	BSG48-P-IER70
Pulp of PB treated with TS80 and IER70	PB48-P-IER70

5.2. Ionic Liquid TS80 with different Ion Exchange Resins

Different IERs were tested with MIS48 in TS80 to determine their influence. This section's results will demonstrate the effect of IER properties on the recovered cellulose-rich pulp fraction using various analytical techniques.

5.2.1. Proximate and Ultimate analyses

Proximate analysis through TGA of the raw material (MIS48) and pulp after in TS80 with different IERs is shown in Table 5.2. To evaluate the effect of the IL only, a pulp using only TS80 was also compared (P-IER00). For the benchmark sample, volatile content decreased by ~6% compared to the raw material,

and ash content increased by ~2% due to removal of hemicellulose and lignin fractions from the pulp while leaving most inorganic materials (ash) largely unaffected. However, when comparing the IERs to the benchmark, no considerable further changes were observed. This indicated that the thermal degradation of pulp samples treated with different IERs had similar patterns and was not significantly different from only using TS80.

Table 5.2. Proximate analysis (wt.%) of raw material (MIS48) and pulp for TS80 with different IERs.

Material	Moisture Content (%)	Volatile Content (%)	Ash Content (%)	Fixed Carbon (%)
MIS48	3.21 ± 0.05	81.76 ± 0.91	3.36 ± 0.34	11.67 ± 0.51
P-IER00	4.70 ± 0.36	76.34 ± 0.14	5.54 ± 0.05	13.41 ± 0.30
P-IER70	3.86 ± 0.20	75.52 ± 0.23	6.84 ± 0.27	13.78 ± 0.33
P-IER45	3.43 ± 0.09	76.54 ± 0.41	6.46 ± 0.03	13.57 ± 0.34
P-IER35	3.23 ± 0.12	75.95 ± 0.13	7.02 ± 0.24	13.80 ± 0.23
P-IER15	3.42 ± 0.23	76.34 ± 0.71	6.75 ± 0.04	13.48 ± 0.89
P-IER482	3.19 ± 0.10	77.15 ± 0.21	5.31 ± 0.08	14.35 ± 0.16
P-IER252	3.66 ± 0.05	77.13 ± 0.25	5.24 ± 0.16	13.96 ± 0.11
P-IER275	3.73 ± 0.29	75.88 ± 0.04	6.61 ± 0.01	14.71 ± 0.14

The ultimate analysis was conducted to determine the influence of different IERs on the elemental composition of the pulp samples. The results presented in Table 5.3 showed no significant changes from the pulp for either benchmark or experiments with IER, except for samples treated with IER35 and IER70.

Table 5.3. Ultimate analysis (wt.%) of raw material (MIS48) and pulp for TS80 with different IERs.

Sample	C	H	S	N
MIS48	43.96 ± 0.09	6.02 ± 0.06	0.00 ± 0.00	0.23 ± 0.02
P-IER00	43.12 ± 0.16	6.09 ± 0.04	0.47 ± 0.01	0.24 ± 0.01
P-IER70	42.03 ± 0.06	6.16 ± 0.06	1.02 ± 0.02	0.50 ± 0.00
P-IER45	41.94 ± 0.13	6.08 ± 0.08	0.55 ± 0.01	0.25 ± 0.00
P-IER35	41.63 ± 0.11	5.68 ± 0.81	1.61 ± 0.40	0.64 ± 0.03
P-IER15	41.91 ± 0.08	6.24 ± 0.09	0.61 ± 0.01	0.33 ± 0.01
P-IER482	42.29 ± 0.04	6.38 ± 0.10	0.63 ± 0.01	0.34 ± 0.01
P-IER252	42.41 ± 0.02	6.24 ± 0.08	0.66 ± 0.05	0.41 ± 0.04
P-IER275	43.10 ± 0.17	6.07 ± 0.10	0.84 ± 0.17	0.69 ± 0.02

The nitrogen and sulphur contents of these two samples were higher compared to other pulp samples, especially in IER35, where sulphur increased to 1.61% and nitrogen increased to 0.64%. These could be due to incomplete pulp cleaning and residual IL in the samples.

Similar to Chapter 4, the ultimate and proximate analyses did not reveal significant differences between the IERs tested or between the IERs and the benchmark of only IL.

5.2.2. Thermogravimetric analysis (TGA)

Thermogravimetric analyses (TGA) of the pulp samples were conducted to determine their thermal characteristics compared to the original material in inert and oxidative environments. The DTG curves for the temperature range of 150-575 °C under an inert environment are presented in Figure 5.1. Additionally, Figure A5.1 and Figure A5.2 in Appendix 5 contain the thermogravimetric curves for the full range of temperatures for both inert and oxidative conditions. Moreover, DTG peak positions corresponding to mass loss are represented in Appendix 5, Table A5.1 and Table A5.2 under inert and air atmospheres, respectively.

In previous chapters, it has already been discussed the three major stages: dehydration stage, active stage, and passive stage [402]. The first stage involved the removal of moisture (25-110 °C) [238]. The second stage involved thermal degradation of hemicellulose (220-315 °C) and cellulose (315-400 °C), which resulted in substantial weight loss of the lignocellulosic material. The third stage is the thermal decomposition of lignin (400-900 °C), which was more challenging to degrade under this stage since it lost weight over a large temperature range (160-900 °C) and produced a solid residue [41].

TGA analysis clearly showed that TS80 caused significant changes in the thermal behaviour of the raw material, hence changing its chemical composition [337]. MIS48 had a clear hemicellulose shoulder at 303 °C (8.1 wt.% °C⁻¹), corresponding to a mass loss of ~ 20 wt.%. However, in the benchmark pulp P-IER00, a significant decrease of the hemicellulose (220-315 °C) is observed in the DTG profile due to the mild crosslinking nature of this carbohydrate, relative amorphousness, and easy to hydrolyse nature relative to cellulose. This has been reported in the literature for pulp fractions treated with acidic ionic liquids [403,404]. Acidic ionic liquids can cause partial and selective hydrolysis of hemicellulose, breaking down some of the more easily degraded linkages while leaving behind a more robust structure of hemicellulose [405,406].

The MIS48 DTG profile showed DTG_{max} (20 wt.% °C⁻¹) associated with cellulose at 355 °C, corresponding to a mass loss of 62 wt.%. However, the DTG_{max} for the benchmark increased to a value of 25 wt.% °C⁻¹ and shifted to a lower temperature of 268 °C, corresponding to a mass loss of 25 wt.%. The peak shift was caused by a decrease in the thermal stability of the cellulose present in the pulp

related to the lower crystallinity [378,407]. Moreover, particle size played a significant role in transforming crystalline cellulose into amorphous cellulose. The pulp produced from MIS48 with TS80 only (P-IER00) had higher DTG_{max} compared to the pulp from Chapter 4 obtained for MIS16 (P-TS80 in Figure 4.4).

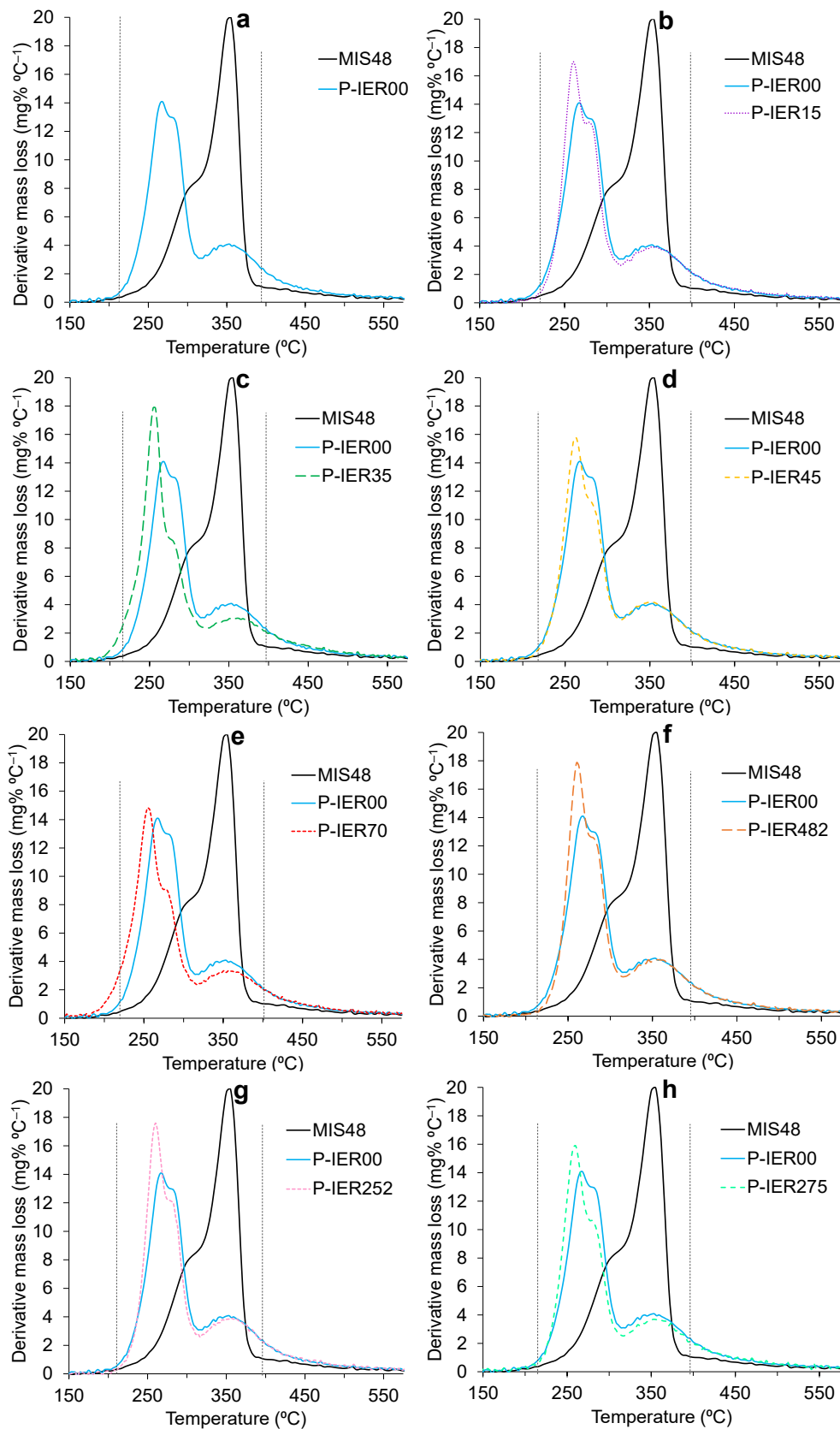


Figure 5.1. DTG curves under inert conditions for raw material and pulp treated with TS80 and different IERs: (a) IER00, (b) IER15, (c) IER35, (d) IER45, (e) IER70, (f) IER482, (g) IER252, and (h) IER275.

Mohosin *et al.* observed that cellulose with smaller particle sizes was more soluble and reactive in the solvent and that it was easier to convert crystalline cellulose into amorphous cellulose and then depolymerise it [408]. Reducing particle size significantly increases the surface area-to-volume ratio. This higher specific surface area allows ILs to penetrate more efficiently into the cellulose structure, facilitating better solvent–cellulose interactions [409]. Enhanced penetration increases the disruption of intermolecular and intramolecular hydrogen bonds within cellulose, promoting dissolution and amorphization [410]. This is more amenable to further processing steps like enzymatic hydrolysis.

When assessing the influence of different IERs on pulp fraction compared to the TS80 only sample, the main differences were observed in thermal stability and DTG_{max} of the amorphous cellulose peak. IER35 and IER70 were the only resins that clearly decreased the crystalline cellulose peak further and shifted more significantly the DTG_{max} max for an amorphous peak to a lower temperature of 257 °C. The acidic resins liberate hydrogen ions (H⁺) into the solution, thereby regulating the initial pace of cellulose depolymerisation. The size of the cellulose chains at the beginning is vital in determining the initial distribution of the product [297]. This difference can be seen in the crystalline cellulose peak positions at 280 °C in samples P-IER35 and P-IER70, where P-IER35 had lower DTG and higher mass loss than P-IER70 (Table A5.1). Hence, IER35 performs better than IER70 by providing a higher acid capacity (Table A2.1).

The IER15 did not show dramatic changes compared to IER35. This could be related to the low swelling capacity and the lower concentration of sulfonic groups. In addition, IER45 and IER482, which are supposed to be analogous to IER70, were not performing similarly, demonstrating that other textural or physicochemical properties might influence the behaviour of these resins.

Even though IER35 performed better than other resins, this IER suffered from a high attrition rate and low thermomechanical stability. Therefore, it was concluded that IER70 was the best-performing IER overall.

5.2.3. X-ray Diffraction (XRD)

XRD analysis was conducted to evaluate the changes in the crystallinity index of the obtained pulps. XRD results are presented in Figure 5.2 for TS80 and with different IERs.

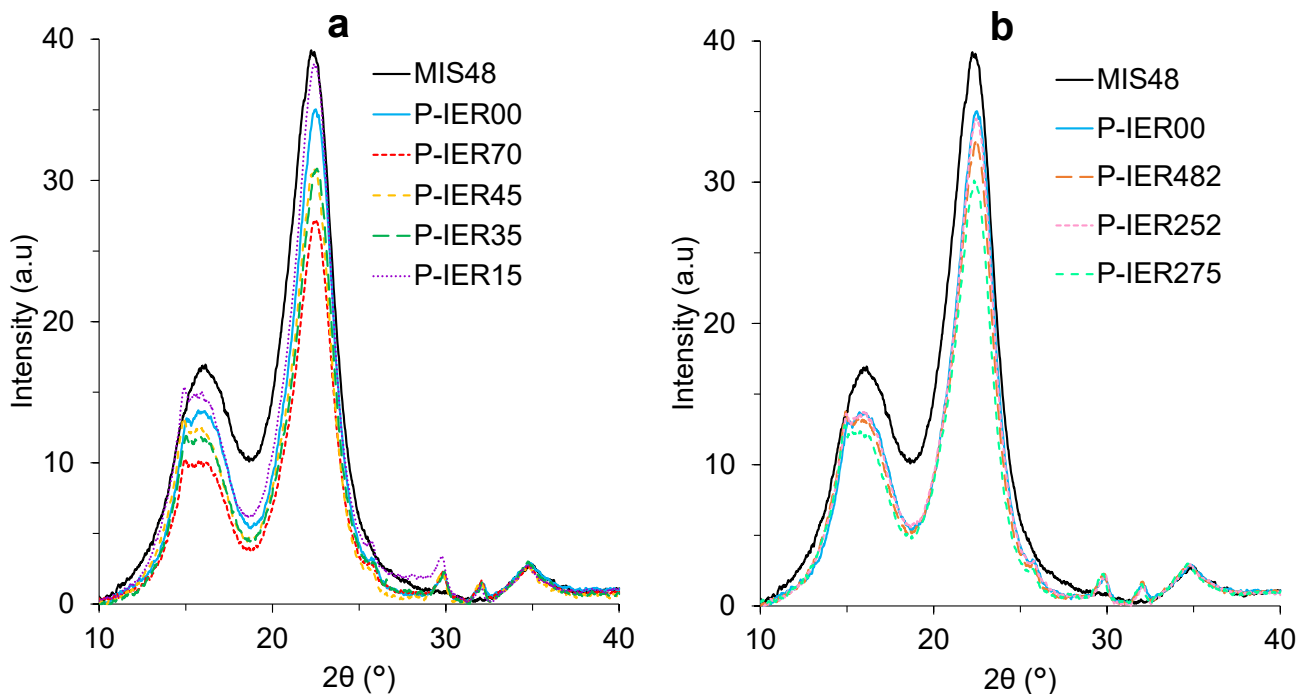


Figure 5.2. XRD diffractograms for raw material-pulp treated with TS80 and different IERs. (a) Amberlyst IERs and (b) Purolite IERs.

MIS48 and pulp samples showed the crystalline peaks for cellulose I at 16.0° , 22.2° , and 35.1° , representing $101\text{-}10\bar{1}$, 002 and 040 crystallographic planes of α -cellulose I, respectively. As TGA results, the raw material's particle size influenced the pulp sample's crystalline peaks. For all the pulps produced from MIS48, the peak at 22.2° showed a lower intensity (I_{002}), which was not the case for pulp samples from MIS16. The intensity in the amorphous area at 18.5° (I_{AM}) also decreased. There were no peaks at 15.8° , 29.7° , and 32.0° for inorganics, along with a peak at 25.5° for pseudo-lignin after IL-TS80 treated samples, which was different to what was seen in the previous chapter for MIS16 (Figure 4.5).

The results indicated that despite moderate operating conditions (110°C , 2 hrs, 10 w.%/v solid loading), the pretreatment severity on MIS16 was significantly higher than on MIS48. MIS16-treated pulp with TS80 had higher ash and pseudo-lignin contents than MIS48-treated pulp with TS80.

The crystallinity index (CrI) and crystallite size values are shown in Table 5.4. Overall, the crystallinity index increased for all the pulp samples. The CrI increased by $\sim 10\%$ compared to the raw material, and the crystalline size increased to ~ 3.7 nm. The increase in CrI , therefore, is enhanced upon the removal of amorphous parts such as hemicellulose and lignin, as discussed in Section 4.3.3. Hence, this removal from the biomass had a more pronounced influence on CrI than the transformation of cellulose into amorphous cellulose.

Table 5.4. Crystallinity index (*CrI*) and crystallite size of pulp treated with TS80 and different IERs.

Material	<i>CrI</i> (%)	Crystallite size (nm)
MIS48	76.70 ± 0.84	3.24 ± 0.00
P-IER00	85.85 ± 0.36	3.61 ± 0.02
P-IER70	85.80 ± 0.47	3.73 ± 0.07
P-IER45	86.76 ± 0.21	3.74 ± 0.02
P-IER35	87.60 ± 0.69	3.82 ± 0.04
P-IER15	85.82 ± 0.08	3.77 ± 0.07
P-IER482	87.40 ± 0.20	3.77 ± 0.14
P-IER252	85.26 ± 0.14	3.66 ± 0.06
P-IER275	85.56 ± 0.65	3.71 ± 0.06

Unfortunately, no significant differences were observed in terms of *CrI* and crystallite size after adding IERs to TS80. So, this technique did not reveal any correlation to the IER properties.

5.2.4. Attenuated Total Reflection Fourier Transformation Infrared (ATR-FTIR) Spectroscopy

ATR-FTIR analysis was conducted to confirm various IER influences in TS80 on pulp fractions. Figure 5.3 represents the raw material analysis, pulp treated with TS80 and different Amberlyst resins. Comparing the results of MIS48 with P-IER00, the peaks can be divided into two main categories: absorbed bands due to carbohydrates and absorbed bands due to lignin. Peak assignment was done according to the literature [303,411–413]. Full ATR-FTIR spectral wavelengths are presented in Appendix 5, Figure A5.3 and Figure A5.4.

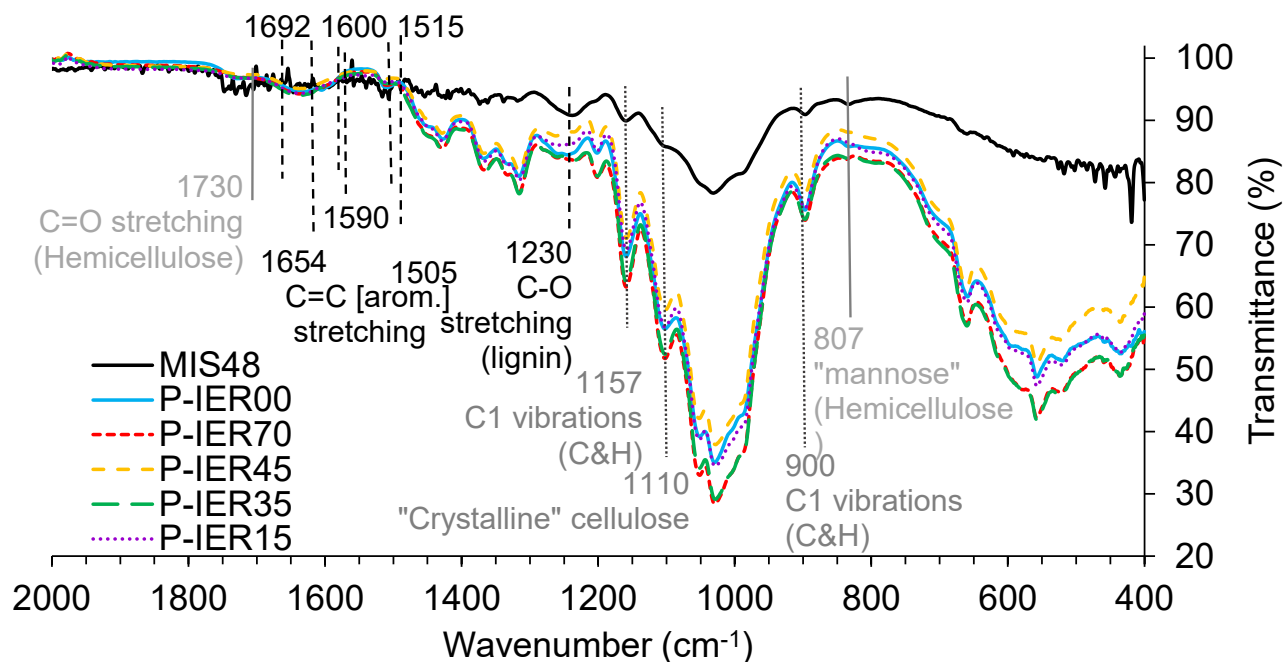


Figure 5.3. ATR spectra for raw material-pulp treated TS80 treatment with different Amberlyst IERs.

Cellulose peaks can be divided into two types: one for crystalline and the second for amorphous. Peaks became sharper for crystalline and amorphous structures, representing bands 1110 cm^{-1} and 900 cm^{-1} , respectively. The band at 1110 cm^{-1} represent symmetric bending $-\text{CH}_2$. The band at 900 cm^{-1} represent C-O-C stretching of β -(1,4) glycosidic linkages.

There are few distinguished peaks regarding hemicellulose other than 1730 cm^{-1} due to the absorption of acetyl group moieties in hemicellulose. Hemicellulose acts as a bridge between cellulose microfibrils and lignin. It is closely knitted to cellulose through hydrogen bonding and van der Waals forces while also interacting with lignin [414]. Moreover, hemicelluloses can form covalent connections with lignin moieties, creating lignin-carbohydrate complexes that are essential for the cellulose-hemicellulose-lignin framework [46].

Hemicellulose peaks always come in connection with lignin and cellulose. For example, a peak at 1230 cm^{-1} is typical for C-O single bond stretches in esters. Alkyl-aryl C-O single bond stretches also absorb at this number. Esters are found in the raw materials lignin (p-coumaric acid esters) and hemicellulose (ferulic acid and acetic acid esters). Alkyl-aryl C-O single bonds are present in lignin as methoxy groups connected to the aromatic rings [352]. Lastly, lignin peak intensities at 1515 cm^{-1} and 1505 cm^{-1} due to C = C guaiacyl aromatic skeletons vibrations and aromatic ring C = C stretching dropped in IL-TS80 pretreated pulp samples compared to the raw material.

Pulps with either IER70 or IER35 in TS80 made the peak sharper at 1057 cm^{-1} , assigned to the C-O-C stretching vibrations in the pyranose ring of cellulose (indicative of the glycosidic linkages). The increased intensity at 1057 cm^{-1} after adding IERs indicated that the resin addition had made the cellulosic part more accessible. This was due to the disruption of the crystalline structure of cellulose, leading to an increase in the amorphous content.

Figure 5.4 represents the raw material analysis, pulp treated with TS80 and different Purolite resins.

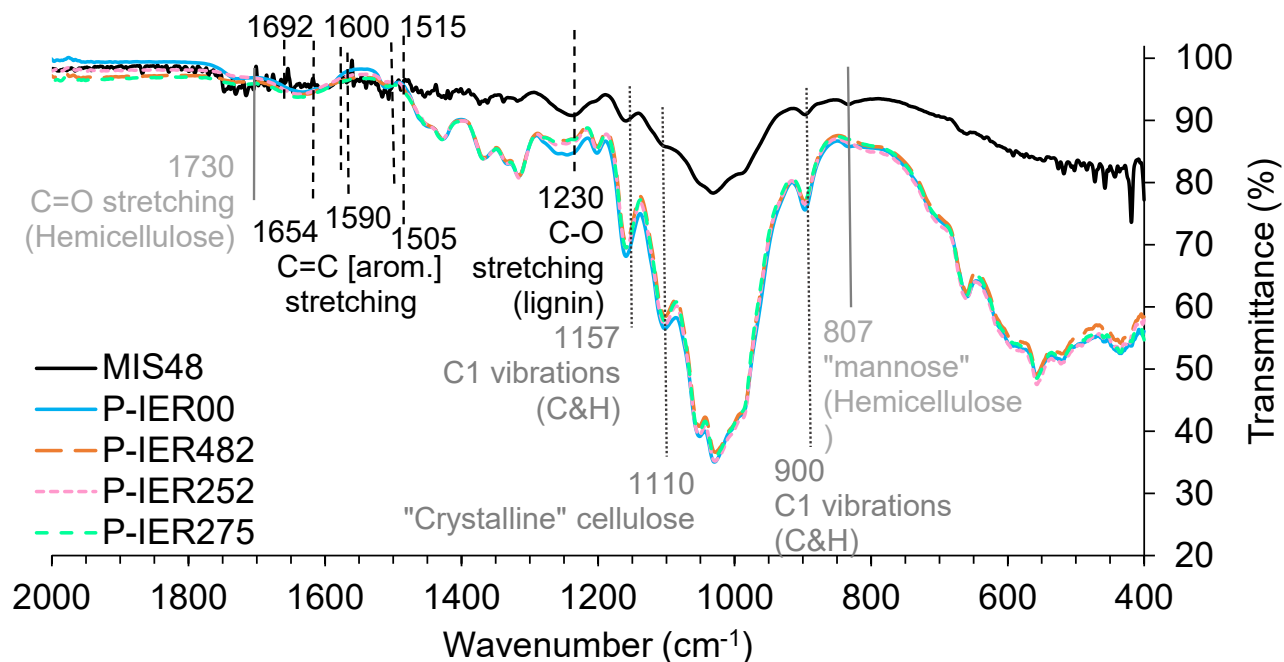


Figure 5.4. ATR spectra for raw material-pulp treated with TS80 and different Purolite IERs.

There were no significant differences in the ATR spectra for pulps produced with different Purolite IERs. However, all the Purolite resins in IL-TS80 lowered the band transmittance at 1230 cm^{-1} assigned to esters in lignin and hemicellulose. Overall, from ATR spectroscopy results, it can be concluded that Purolite resins were not very effective in TS80 compared to Amberlyst resins.

This section focused on how the properties of different micro-reticular IERs influence the pulp fraction after adding to TS80. For example, crosslinking degree, acid capacity, and solvent type influenced the swelling capacity of an IER [415]. The resin's molecular structure and cross-linking degree could significantly impact its ion exchange capabilities.

After testing all these IERs, it was found that IERs that were supposed to be similar (such as IER35 and IER275 or IER45, IER70 and IER482) did not perform similarly in TS80. This could be due to variations in the production process, such as the sulfonation method or post-treatment steps, that lead to differences in the distribution and accessibility of acid sites with the IER polymeric matrix or other

variations in the physicochemical properties that are not reported or could not be measured. So, there is still uncertainty on how these polymeric materials interact with the IL and the biomass.

From the resins tested, only IER70 and IER45 showed no signs of attrition after the process. This is because both resins contain chlorine in their polymeric matrix. Chlorine is crucial in enhancing the mechanical stability of ion exchange resins by increasing cross-linking, stabilising the polymer backbone, and improving rigidity and crush strength. These interactions help the resin withstand mechanical stress, oxidative degradation, and physical wear, ensuring long-term performance and durability [416–418].

After a comprehensive analysis of pulp and the properties of different IERs, it was evident that IER70 stands out. It consistently delivers optimal results for producing pulp with high amorphous fractions of cellulose while maintaining its integrity throughout the process. Therefore, the combination of TS80 and IER70 was selected for the subsequent tests.

5.3. Comparison of Lignocellulosic Materials

Before embarking on experiments involving different materials, it was imperative to understand their physiochemical properties thoroughly. The following section delves into a comparative analysis of the physiochemical properties of three selected materials (*miscanthus x giganteus*, brewery spent grains and pine bark), providing a comprehensive understanding of their unique characteristics. As mentioned in the material section (Chapter 3), these materials were selected based on their different physiochemical characteristics.

5.3.1. Proximate and Ultimate analyses

The proximate analysis of different raw materials is represented in Table 5.5. Pine bark (PB48) had high moisture and fixed carbon contents: 6.8 wt.% and 27.0 wt.%, respectively, while having the lowest volatile content at 62.5 wt.% compared to *Miscanthus x giganteus* (MIS48) and brewery spent grains (BSG48), having 81.8 wt.% and 74.9 wt.%, respectively. Brewery spent grains (BSG48) had the highest ash content (16.8 wt.%) and lowest fixed carbon (5.7 wt.%) among the raw materials.

PB48's high moisture content was attributed to water washing and left to dry at room temperature over a week. However, differences in volatile and fixed carbon contents were related to the raw materials intrinsic properties and structural composition. This higher fixed carbon and lower volatile content in PB48 were due to its higher lignin content, which provides structural rigidity and contributes to its higher calorific value than other raw materials [419,420].

Table 5.5. Proximate analysis (wt.%) of different raw materials.

Material	Moisture Content	Volatile Content	Ash Content	Fixed Carbon
MIS48	3.21 ± 0.05	81.76 ± 0.91	3.36 ± 0.34	11.67 ± 0.51
BSG48	2.62 ± 0.21	74.87 ± 0.15	16.81 ± 2.21	5.70 ± 2.40
PB48	6.77 ± 0.25	62.50 ± 1.03	3.76 ± 0.20	26.97 ± 0.76

BSG48 had a high ash content (16.8 wt.%), mainly due to its composition (70-85 wt.% fibre (cellulose and hemicellulose), around 20 wt.% protein, and varying amounts of lignin [421]. BSG48 consists primarily of the husks, pericarp, and seed coat layers of barley, which naturally contain significant amounts of inorganic minerals [422]. These components are left behind during brewing as the wort (a liquid solution of extracted grains with high sugar content) is extracted, concentrating the mineral content in the spent grains. Furthermore, steeping the grains in hot water during the brewing process can extract and concentrate minerals from the barley into the spent grains, resulting in a high ash content [423,424].

Table 5.6 represents the ultimate analysis of different raw materials. Differences observed: high carbon content in PB48 (50.2 wt.%) compared to MIS48 and high nitrogen content in BSG48 (4.9 wt.%) compared to the other two materials. One of the main reasons for the high carbon content in PB48 was its high lignin content, which contributes significantly to the material's overall carbon content as a softwood. [425,426].

Table 5.6. Ultimate analysis (wt.%) of different raw materials.

Sample	C	H	S	N
MIS48	44.98 ± 0.17	6.09 ± 0.08	0.00 ± 0.00	0.43 ± 0.05
BSG48	47.78 ± 1.10	6.68 ± 0.08	0.08 ± 0.00	4.87 ± 0.75
PB48	50.16 ± 0.16	5.61 ± 0.14	0.00 ± 0.00	0.52 ± 0.01

BSG48's high nitrogen content was related to high protein content in the form of amino acids [421], which was concentrated in the residue spent grain after the brewing process [427]. These factors collectively contribute to the elevated nitrogen levels observed in BSG48.

In conclusion, proximate and ultimate analyses of these lignocellulose materials depended on several factors: type of biomass, chemical composition, growth conditions, and pre-processing methods before the analysis, but it is evident that these three biomasses are significantly different.

5.3.2. Thermogravimetric analysis (TGA)

A TGA analysis of different raw materials was conducted to determine their thermal characteristics in inert and reactive environments. The DTG curves for the 150-575 °C range under inert and oxidative environments are presented in Figure 5.5.a and Figure 5.5.b, respectively. The TGA-DTG curves for the

full range of temperatures and inert and oxidative conditions are given in Appendix 5 Figure A5.5. The DTG_{max} temperature peaks and their correlated TGA mass loss are presented in Appendix 5, Table A5.6 and Table A5.7 under inert and air atmospheres, respectively.

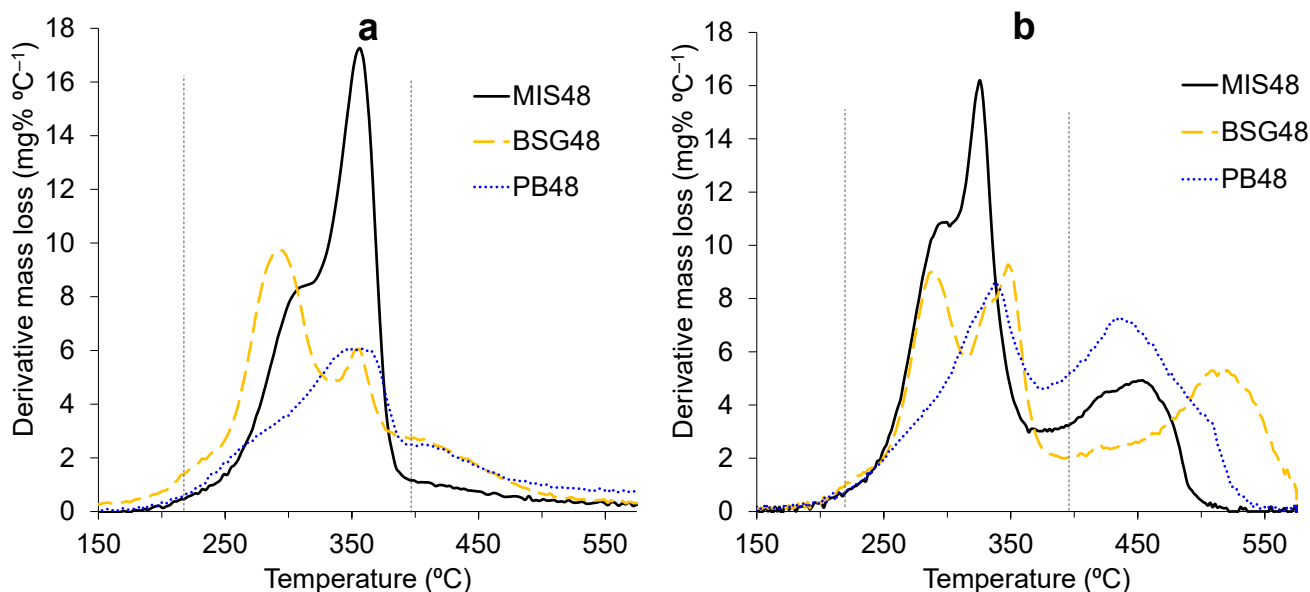


Figure 5.5. DTG curves under inert (a) and air (b) for different lignocellulosic materials.

All three raw materials had different thermal degradation profiles because each lignocellulosic material had a different chemical composition. Literature reports that MIS48 is composed of 43-56 wt.% cellulose, 17-25 wt.% lignin and 18- 23 wt.% hemicellulose [428]. Pine bark is composed of approximately 42-51 wt.% lignin, 17-24 wt.% cellulose, and 12-16 wt.% hemicellulose [429]. BSG mainly consists of 70-85 wt.% fibre (cellulose and hemicellulose), around 20% protein, and varying amounts of lignin [421].

Analysing DTG thermograms under nitrogen in Figure 5.5.a, only MIS48 had visible hemicellulose shoulder at 303 °C with a mass loss of ~20 wt.%. However, no hemicellulose shoulder was noticed in BSG48 and PB48. In the case of BSG48, hemicellulose was closely associated with cellulose and lignin in a complex matrix. This intimate association may cause the hemicellulose to degrade over a broader temperature range, overlapping with cellulose degradation, as shown in the DTG profile [430]. However, PB48 has a more rigid and complex structure due to its high lignin content, which encapsulates the hemicellulose, leading to its degradation simultaneously with cellulose or lignin, as shown in the DTG profile [431].

BSG48's first peak with DTG_{max} at 294 °C corresponds to a mass loss of 26 wt.%, presenting thermal degradation of amorphous cellulose and residual hemicellulose after enzymatic hydrolysis. This is due to the brewing process that can cause partial hydrolysis and depolymerisation of the hemicellulose chain

[432]. Additionally, the second peak is attributed to crystalline cellulose and lignin. As for PB48, there was one broad peak with DTG_{max} at 268 °C, corresponding to a mass loss of approximately 11 wt.%, linked to the high amount of lignin.

The MIS48 material contains high carbohydrate levels, leading to substantial weight loss from 200 °C to 380 °C as hemicellulose and cellulose decomposed. Due to its lower lignin content, this material exhibits a more specific and narrow temperature range for thermal degradation. On the other hand, PB48, with its high lignin content, undergoes thermal degradation in a broader temperature range of 200-500 °C. Finally, BSG48, known for its high fibre content (70-85 wt.%) [421], experienced significant weight loss within the 200-350 °C range, degrading cellulose and hemicellulose.

Under oxidative environmental conditions, each type of lignocellulosic material exhibited different DTG thermograms due to variations in chemical composition (Figure 5.5.b). PB48 contained the highest amount of lignin, so the second-peak DTG_{max} at 435 °C represents a mass loss of 70%. In the case of BSG48, the oxidation of inorganic matter occurred at 510 °C, with an 80% mass loss, which was because of higher ash content and lower lignin content, ultimately requiring a higher temperature for complete combustion compared to PB48 [433].

To sum up, the chemical composition of these biomass materials directly affects how they break down when heated. MIS48 had a distinct thermal degradation range because it had a lot of cellulose. PB48 experienced gradual weight loss because it had a high lignin content. BSG48 showed unique degradation characteristics due to its protein content. These differences are essential for optimising their use in bioenergy and industrial applications, making these three lignocellulosic feedstocks interesting for testing the combined IL-IER system selected in Section 5.2.

5.3.3. X-ray Diffraction (XRD)

XRD diffractograms of different raw materials are presented in Figure 5.6. Crystalline peak positions for cellulose I were at 16.0°, 22.2°, and 35.10°, representing 101-10 $\bar{1}$, 002 and 040 planes, respectively. The intensity for the amorphous peak was at 18.5° (I_{AM}). MIS48 had the highest peak intensities for both crystalline and amorphous peaks as compared to the other two materials, mainly due to high cellulose and hemicellulose contents in it [434]. Because of the high lignin content, cellulose peak intensities in PB48 were low [429]. The high amorphous content in PB48 made the peak 18.5° broad compared to MIS48, and there was no clear distinction between the amorphous intensity and the intensity of the crystalline cellulose peak at 16.0°.

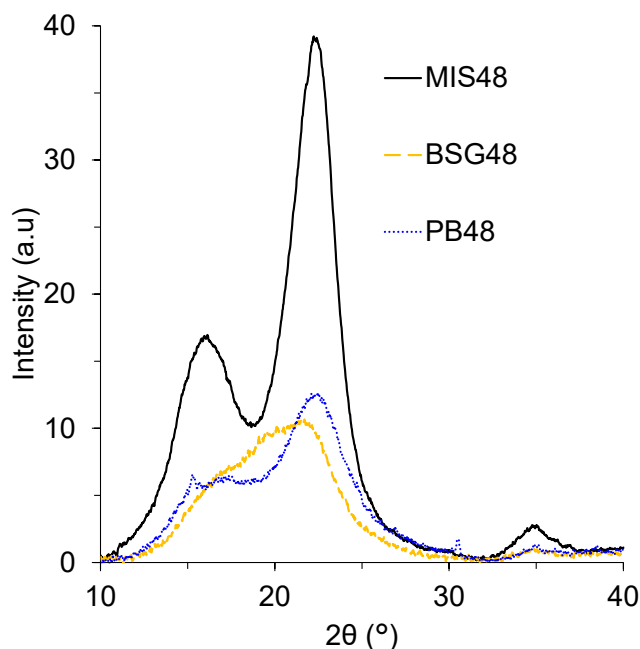


Figure 5.6. XRD diffractogram for different lignocellulosic materials.

BSG48 XRD analysis did not show an amorphous dip at 18° or a crystalline peak at 16° . Instead, BSG48 often exhibits a broad peak around 22° compared to the other two materials. The analysis confirmed that the brewery process made some structural changes in the raw material, making it more amorphous [435]. The lack of a distinctive peak at 16° indicates that the crystalline portion of cellulose in BSG48 was disturbed during the brewing process. The process, comprising mashing, boiling, and fermentation, can disintegrate the crystalline composition of cellulose, resulting in a less structured substance, ultimately lowering the crystallinity compared to other raw materials.

CrI and crystallite size are presented in Table 5.7. BSG48 had the lowest *CrI* (36.26°) as most of the material contains amorphous components and proteins [436] as compared to other materials [437]. MIS48 had a high cellulose content [438], which primarily contributes to its high *CrI* (76.70°) compared to low *CrI* (61.05°) in woody biomass. Regarding crystallite size, M48 had the largest crystallite size (3.2 nm) because it had the highest amount of crystalline cellulose compared to PB48 (2.6 nm). Cell wall composition significantly impacts crystallite size. For example, PB48 cellulose was often less ordered and more interspersed with amorphous regions due to the presence of other cell wall components. This leads to a less pronounced crystalline structure compared to MIS48 [37].

Table 5.7. Crystallinity Index (*Crl*) and crystallite size for different raw materials.

Material	<i>Crl</i> (%)	Crystallite size (nm)
MIS48	76.70 ± 0.84	3.24 ± 0.00
BSG48	36.36 ± 0.05	1.14 ± 0.03
PB48	61.05 ± 0.66	2.55 ± 0.12

The material's chemical composition affects the XRD diffraction pattern, *Crl*, and crystallite size of different lignocellulosic materials. MIS48 exhibited the highest *Crl* and crystallite size because it contained the most crystalline cellulose. On the other hand, BIS48 exhibited the lowest *Crl* and crystallite size because it contained the most amorphous components.

5.3.4. Attenuated Total Reflection Fourier Transformation Infrared (ATR-FTIR) Spectroscopy

ATR-FTIR analysis was done on the different raw materials (Figure 5.7). The spectra of all three materials showed significant differences due to differences in chemical compositions. In this section, only the main differences are discussed.

PB48 rich in lignin had strong peak intensities between 1505 and 1700 cm^{-1} , representing aromatic skeletal vibrations of benzene rings in lignin. Absorption bands at 1230 and 1264 cm^{-1} corresponding to syringyl ring C-O and guaiacyl-ring plus C=O stretching in lignin were high on PB48 compared to the other two raw materials. High lignin content in the PB48 spectrum has lower transmittance. Conversely, carbohydrate characteristics bands at 1157-1159 cm^{-1} and 1369-1373 cm^{-1} , representative of C-O-C symmetric stretching and C-H deformation vibration (cellulose and hemicellulose), respectively, were not as sharp as the other two raw materials [439,440].

BSG48 was a byproduct of the brewing industry, composed mainly of proteins, fibres, and residual starches. The strong amide I and amide II bands (1650 cm^{-1} and 1540 cm^{-1}) in BSG48 indicated a high protein content resulting from the brewing process [441]. These peaks were not present in the other two raw materials. The peaks at 1030 cm^{-1} and 1155 cm^{-1} in BSG48 were signs of cellulose and hemicellulose [442,443]. However, these peaks were often broader and less distinct due to the complex mixture of carbohydrates compared to M48. High amorphous content in BSG48 made β -glycosidic linkage peak at 895 cm^{-1} [444] less prominent than other raw materials, indicating a lower degree of crystallinity in its cellulose due to the processing effects of brewing.

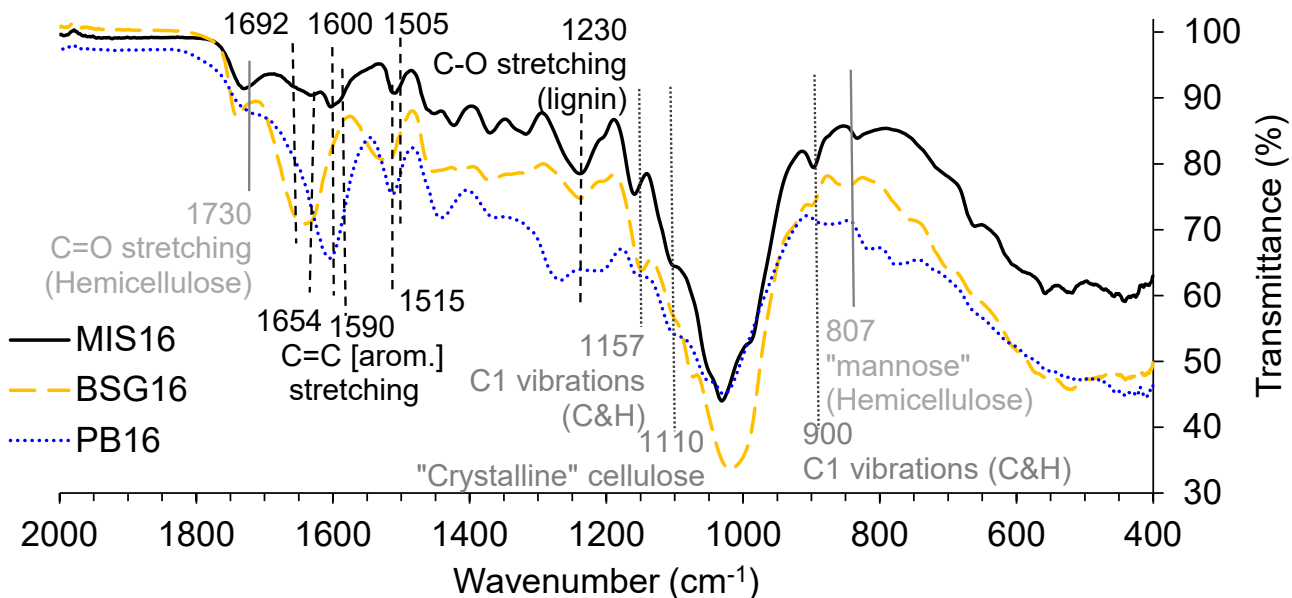


Figure 5.7. ATR spectra for different raw materials.

The FTIR-ATR spectra of PB48, BSG48, and M48 exhibited notable disparities in their chemical compositions and structural attributes. PB48 exhibited more noticeable lignin-related peaks and peaks corresponding to polyphenolic chemicals, attributable to its elevated lignin content. BSG48 exhibited a high protein content, as evidenced by the prominent Amide I and II bands and had a more intricate combination of carbohydrates with reduced crystallinity. Unlike the other materials, MIS48 had a high crystalline cellulose content, characterised by a unique β -glycosidic linkage peak.

In conclusion, the three materials have distinctive features that will help us better understand and uncover more information on how the ionic liquid TS80 and the IER70 work during the pretreatment of lignocellulosic materials.

5.4. Effect of TS80 and IER70 for different lignocellulosic materials (MIS48, BSG48 and PB48)

After selecting the best system in Section 5.2 and demonstrating the distinctive characteristics of the three selected feedstocks, the pretreatment of the biomasses using TS80 only and the combination of TS80 and IER70 were tested and compared.

5.4.1. Proximate and ultimate analyses

Proximate analysis through TGA for pulp after TS80 with and without IER70 pretreatment is presented in Table 5.8. Volatile content in the case of BSG48 did not change much. Still, ash content decreased by ~6 wt.%, whereas in the case of PB48, volatile content decreased by ~3 wt.%, and the ash content

increased by ~3 wt.% by comparing proximate analysis results of the raw material and pulp-treated samples with only TS80. The decrease in ash content in the case of BSG48 could be the removal of protein content favoured by the TS80 pretreatment. However, no considerable changes were observed in both materials for pulp samples when IER70 was added. Therefore, there are no significant variations in the proximate content of pulp samples with or without IER70 in TS80.

Table 5.8. Proximate analysis (wt.%) of raw materials after TS80-IER70 treatment.

Material	Moisture Content	Volatile Content	Ash Content	Fixed Carbon
MIS48	3.21 ± 0.05	81.76 ± 0.91	3.36 ± 0.34	11.67 ± 0.51
P-IER00	4.70 ± 0.36	76.34 ± 0.14	5.54 ± 0.05	13.41 ± 0.30
P-IER70	3.86 ± 0.20	75.52 ± 0.23	6.84 ± 0.27	13.78 ± 0.33
BSG48	2.62 ± 0.21	74.87 ± 0.15	16.81 ± 2.21	5.70 ± 2.40
BSG48-P-IER00	4.27 ± 0.30	73.78 ± 0.09	10.44 ± 0.18	11.51 ± 0.15
BSG48-P-IER70	4.26 ± 0.24	72.91 ± 1.11	10.71 ± 0.13	12.12 ± 1.35
PB48	6.77 ± 0.25	62.50 ± 1.03	3.76 ± 0.20	26.97 ± 0.76
PB48-P-IER00	5.78 ± 0.23	59.57 ± 0.21	6.28 ± 0.18	28.36 ± 0.24
PB48-P-IER70	5.76 ± 0.28	58.31 ± 0.73	6.89 ± 0.41	29.03 ± 0.91

The ultimate analysis of different raw materials and respective pulp samples upon TS80 pretreatment with and without IER70 is presented in Table 5.9. In the case of BSG48, there was a significant decrease in carbon content of ~6 wt.% compared to the raw material; however, in the case of PB48, there was a minor decrease in carbon content of ~2 wt.% when treated with TS80. This could be related to the cell wall structure of both materials, as discussed in Section 5.3. BSG48 was derived from barley. It has non-woody stems and is classified as an herbaceous plant [422]. On the other hand, PB48 is a softwood rich in lignin, polyphenolics and resilient materials [429]. Therefore, it was easy to remove lignin in BSG48 under moderate conditions compared to PB48, decreasing carbon content significantly. Moreover, TS80 decreased nitrogen content by ~3 wt.% in the case of BSG48 due to protein removal [445].

Table 5.9. Ultimate analysis (wt.%) of raw materials after TS80-IER70 treatment.

Sample	C	H	S	N
MIS48	43.96 ± 0.09	6.02 ± 0.06	0.00 ± 0.00	0.23 ± 0.02
P-IER00	43.12 ± 0.16	6.09 ± 0.04	0.47 ± 0.01	0.24 ± 0.01
P-IER70	42.03 ± 0.06	6.16 ± 0.06	1.02 ± 0.02	0.50 ± 0.00
BSG48	47.78 ± 1.10	6.68 ± 0.08	0.08 ± 0.00	4.87 ± 0.75
BSG48-P-IER00	41.40 ± 0.18	5.90 ± 0.12	1.16 ± 0.06	1.76 ± 0.02
BSG48-P- IER70	40.96 ± 0.14	6.18 ± 0.02	1.17 ± 0.01	1.46 ± 0.04
PB48	50.16 ± 0.16	5.61 ± 0.14	0.00 ± 0.00	0.52 ± 0.01
PB48-P-IER00	48.29 ± 0.20	5.26 ± 0.06	1.17 ± 0.06	0.73 ± 0.03
PB48-P-IER70	47.65 ± 0.23	5.41 ± 0.09	1.18 ± 0.03	0.79 ± 0.01

However, when IER70 was added to the system, the ultimate analysis was not significantly different from that when only TS80 was used.

Overall, TS80 significantly impacted BSG48 compared to other raw materials due to its cell wall composition. The IER70 addition did not considerably change the elemental analysis for pulp fractions.

5.4.2. Thermogravimetric analysis (TGA)

A TGA analysis of raw materials and pulp fractions with TS80 and IER70 was conducted to determine their thermal characteristics in inert and reactive environments. The DTG curves for the 150-575 °C range are presented in Figure 5.8. The TGA-DTG curves for the full range of temperatures under inert and oxidative conditions are in Appendix 5, Figure A5.5 and Figure A5.6. The DTG_{max} temperature peaks and their correlation with mass loss are presented in Appendix 5, Table A5.9 and Table A5.10 under inert (N₂) and air atmospheres, respectively.

The influence of TS80 and IER70 on MIS48 is discussed in Section 5.2.2. Therefore, this section will focus on the other two lignocellulosic samples. TGA-DTG under an inert environment for BSG48 and PB48 could be divided into three regions based on thermal degradation profile: 25-110 °C, 200-500 °C, and

400-900°C moisture removal, decomposition of carbohydrates, and lignin decomposition respectively. Both raw materials BSG48 and PB48, when treated with TS80, had reduced their thermal stability by lowering their DTG_{max} temperature. In the case of BSG48 DTG_{max} (~15 wt.% °C⁻¹), the temperature shifted to 283 °C with a mass loss of ~28 wt.%. Regarding PB48, DTG_{max} (~8 wt.% °C⁻¹), the temperature shifted to 277 °C with a mass loss of ~17 wt.%. After the pretreatment, a broad second peak representing residual crystalline cellulose and lignin fractions in both pulp fractions were the main fractions observed.

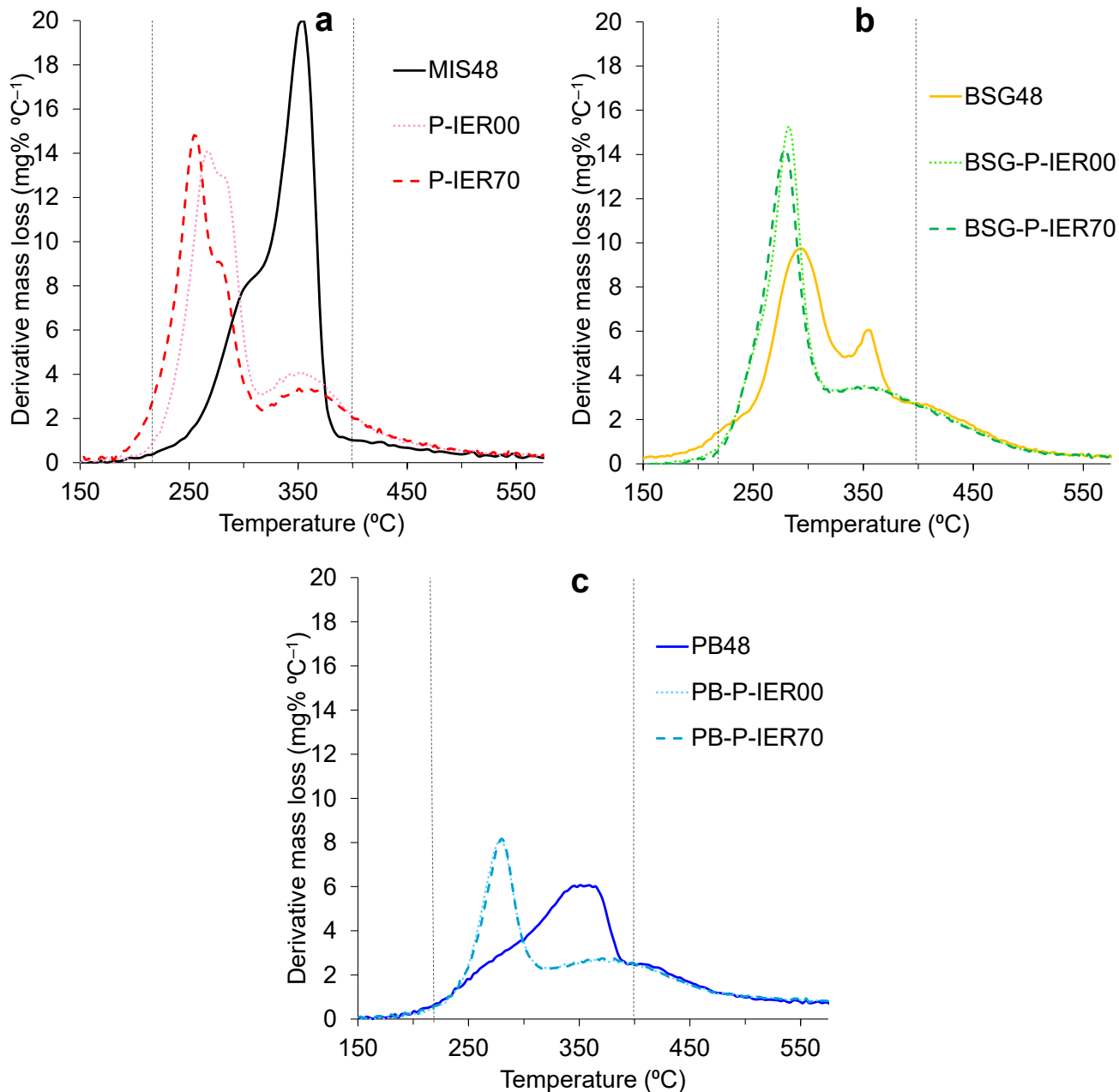


Figure 5.8. DTG curves for different raw materials under an inert environment for different raw materials and pulps treated with TS80-IER70. (a) MIS48, (b) BSG48 and (c) PB48.

Adding IER70 to TS80 for BSG48 and PB48 did not significantly improve the pulp's thermal characteristics compared to only TS80. For example, in the case of BSG48, when IER70 was added to TS80, DTG_{max} temperature increased by ~2.8 °C with a negligible increase in mass loss of around 0.6 wt.%. These minute changes could be due to hydrogen ions from IER70 as dilute acid pretreatment under moderate conditions able to extract protein from the BSG48 [432,446,447].

In the case of PB48, not even a shift in the DTG_{max} temperature was observed. PB48 is a softwood with the highest content of guaiacyl units [62] compared to other raw materials. For this reason, harsher conditions to fractionate the material might be needed [165]. Cox *et al.* explained that to achieve a cellulose-rich fraction from PB48, a longer pretreatment time (5 hrs) at 130 °C would be required [448]. Even though TS80 decreased the thermal stability of crystalline cellulose in PB48 by the low crystallinity of regenerated celluloses, IER70 did not have enough impact to produce any changes in the thermal characteristics of the pulp. For pretreatment with an ionic liquid (IL) to be effective, it should be able to simultaneously dissolve lignin and depolymerise polysaccharides, thereby resulting in cellulose that is free of lignin and hemicellulose upon regeneration [449].

In conclusion, the findings suggest that adding IER70 to TS80 for BSG48 and PB48 did not significantly change their respective pulp fraction thermal characteristics. However, this was not the case in MIS48. This highlights the importance of selecting an appropriate pretreatment for the right material and conditions to be effective.

5.4.3. X-ray Diffraction (XRD)

XRD diffractograms of different raw materials and their pulp fractions after TS80 with and without IER70 pretreatment are presented in Figure 5.9. *CrI* and crystallite size are presented in Table 5.10. Three raw materials' XRD results were analysed and discussed in section 5.3.3.

For MIS48, after using TS80 with IER70, crystalline peaks for cellulose I at 16.0° and 22.2°, decreased and became sharper. The intensity for the amorphous background at 18.5° (I_{AM}) was also reduced. This indicated the removal of amorphous components and partial conversion of crystalline to amorphous cellulose for MIS48. This removal increased the *CrI* and crystallite size to ~85% and ~3.6 nm, respectively. The addition of IER70 did not have a noticeable change in these values.

For BSG48, when pretreated with TS80, the crystallinity content increased along with the conversion of crystalline cellulose to amorphous cellulose. The pulp had clear peaks for crystalline cellulose and amorphous fractions, which were not in the case of BSG48. Adding IER70 to TS80 dropped the intensity of crystalline peaks at 16.0° and 22.2° significantly, along with the intensity of the amorphous peak at 18.5° decreased. This increased the *CrI* of the pulp fraction from 76% to 82% because of the removal of amorphous fraction fractions from the solid phase. The addition of IER70 caused no significant change in crystallite size.

Finally, the XRD diffractograms for PB48 showed that after TS80 pretreatment, the intensities for the amorphous peak (18.5°) decreased, and the crystalline peak (22.2°) increased. This indicated that under moderate conditions, there was a partial removal of amorphous fractions from PB48, increasing the *CrI*

(~75%) and crystallite size (~3.2 nm) compared to the original material. The addition of IER70 did not have a significant impact on these values due to the recalcitrant nature of PB48 as compared to other raw materials [450].

These results are not unexpected, as the previous chapter found that the effect of the IER70 is mainly on the cellulose, amorphous cellulose, and hemicellulose fraction. Therefore, the IER70 only produces benefits when biomass has a significant amount or minimum accessibility of the crystalline cellulose or when it can attack amorphous cellulose and hemicellulose.

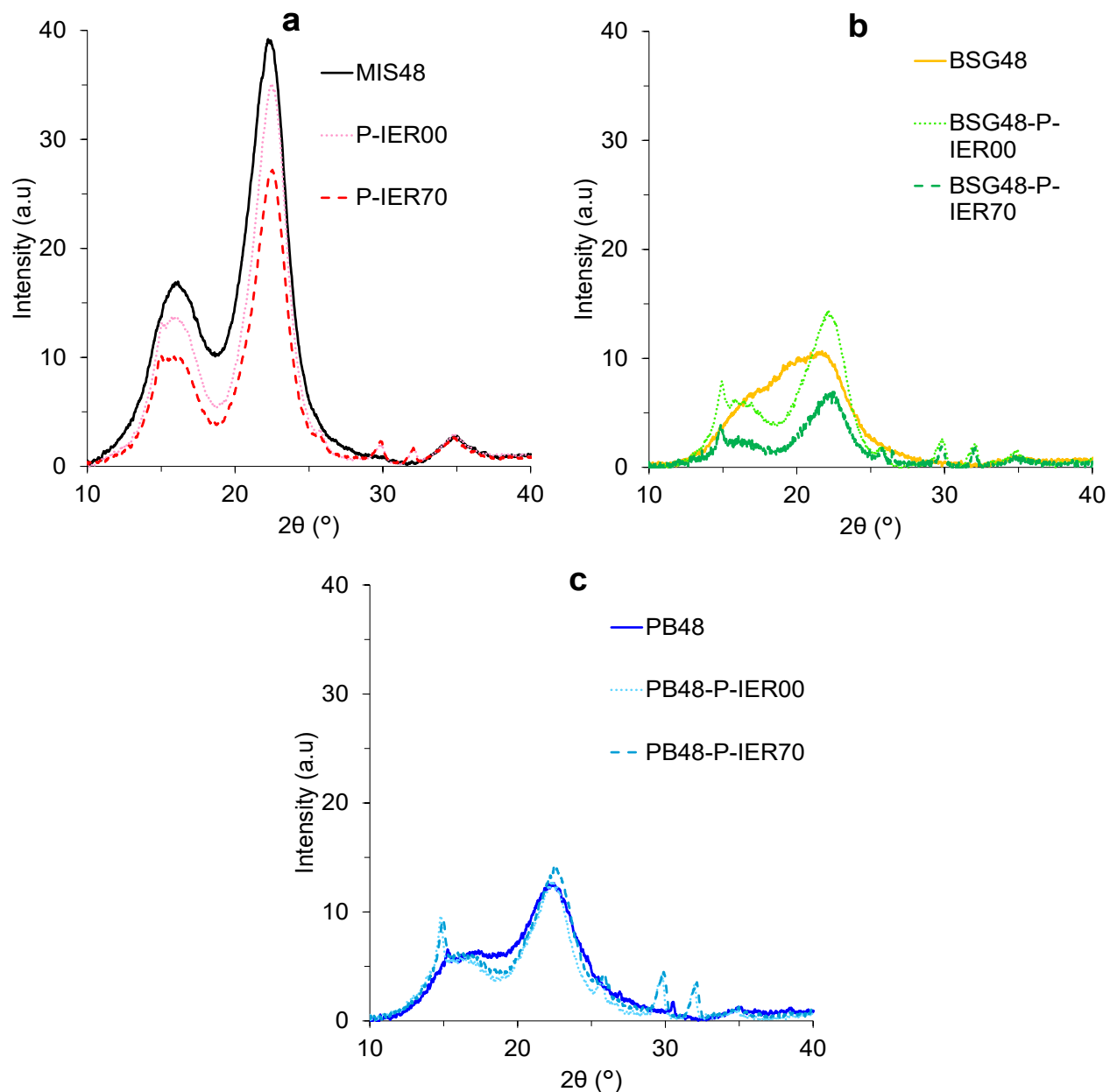


Figure 5.9. XRD diffractogram for different raw materials (MIS48, BSG48, PB48), pulp after TS80-IER70 treatment (a) MIS48, (b) BSG48 and (c) PB48.

Table 5.10. *CrI*, crystallite size for different raw materials (MIS48, BSG48, PB48), and pulp after TS80-IER70 treatment.

Material	<i>CrI</i> (%)	Crystallite size (nm)
MIS48	76.70 ± 0.84	3.24 ± 0.00
P-IER00	85.85 ± 0.36	3.61 ± 0.02
P-IER70	85.80 ± 0.47	3.73 ± 0.07
BSG48	36.36 ± 0.05	1.23 ± 0.03
BSG48-P-IER00	76.33 ± 0.08	3.12 ± 0.08
BSG48-P-IER70	82.27 ± 1.52	3.25 ± 0.07
PB48	61.05 ± 0.66	2.55 ± 0.12
PB48-P-IER00	75.45 ± 0.37	3.17 ± 0.14
PB48-P-IER70	74.18 ± 2.36	3.30 ± 0.18

IL pretreatment of different lignocellulosic materials could enhance the *CrI* and crystallite size. During the process, cellulose could dissolve partially. When it cools down, the cellulose chains that were previously mobile can reorganise and form larger and more organised structures. This led to an increase in both crystallinity index and crystallite size [451]. In addition, ionic liquid treatment can help convert cellulose I into cellulose II. This transformation is more likely to result in the development of well-organised cellulose II, leading to a high *CrI* [387]. Eliminating lignin and hemicellulose throughout the procedure exposes more cellulose surfaces for alignment and recrystallisation, which also affects the observed changes in crystallinity [451]. Overall, XRD results demonstrated that IER70's addition to TS80 substantially impacts biomasses with highly accessible cellulose, with BSG48's structure increasing its crystallinity more than the other two raw materials.

5.4.4. Attenuated Total Reflection Fourier Transformation Infrared (ATR-FTIR) Spectroscopy

ATR-FTIR analysis of different raw materials and pulp fractions is presented in Figure 5.10 to Figure 5.12. The detailed spectrum ranges from 3900-400 cm^{-1} for all the samples shown in Appendix 5, Figure A5.14 to Figure A5.16. In the case of MIS48, the addition of IER70 with TS80 made bands at 1034 cm^{-1} (C-O stretching), 1110 cm^{-1} (C-O stretching vibrations), 1157 cm^{-1} (C-O-C asymmetric stretching), and 1335 cm^{-1} (C-H bending vibrations) sharper because of cellulose structure became more exposed [452,453]. However, no differences were observed for the lignin adsorption bands.

In the case of BSG48, when treated with TS80, regardless of IER70, amide I and amide II bands (1650 cm^{-1} and 1540 cm^{-1}) were not observed, indicating the removal of high protein content created during the brewing process [441]. Critical peaks corresponding to functional groups such as cellulose, hemicellulose, and lignin showed alterations in intensity and position, indicating the effective disruption

of the lignocellulosic matrix and the removal of lignin, mainly caused by the TS80. IER70 addition to TS80 increased the band intensities at 1157 and 1130 cm^{-1} for C-O-C asymmetric stretching and C-O stretching vibrations in the cellulose structure, respectively, indicating an increase in the crystallinity of the pulp.

Finally, ATR-FTIR analysis of PB48 after TS80 pretreatment revealed no significant changes in the chemical composition and structure of the biomass compared to the other two raw materials. Peaks to observe include those around 1030-1060 cm^{-1} (C-O stretching in cellulose and hemicellulose), 1110 cm^{-1} (C-O-C asymmetric stretching in cellulose), and 1510-1600 cm^{-1} (aromatic ring vibrations in lignin). After TS80 pretreatment, the intensity of lignin-related peaks decreased, indicating partial delignification, while changes in the cellulose-related peaks may suggest alterations in cellulose crystallinity. The observed structural changes in PB48 were insignificant compared to those mentioned in the literature because of the moderate operating conditions used in this research [218,454]. Adding IER70 in TS80 did not change the ATR-FTIR spectra noticeably, reflecting minimal alterations in the PB48 chemical composition.

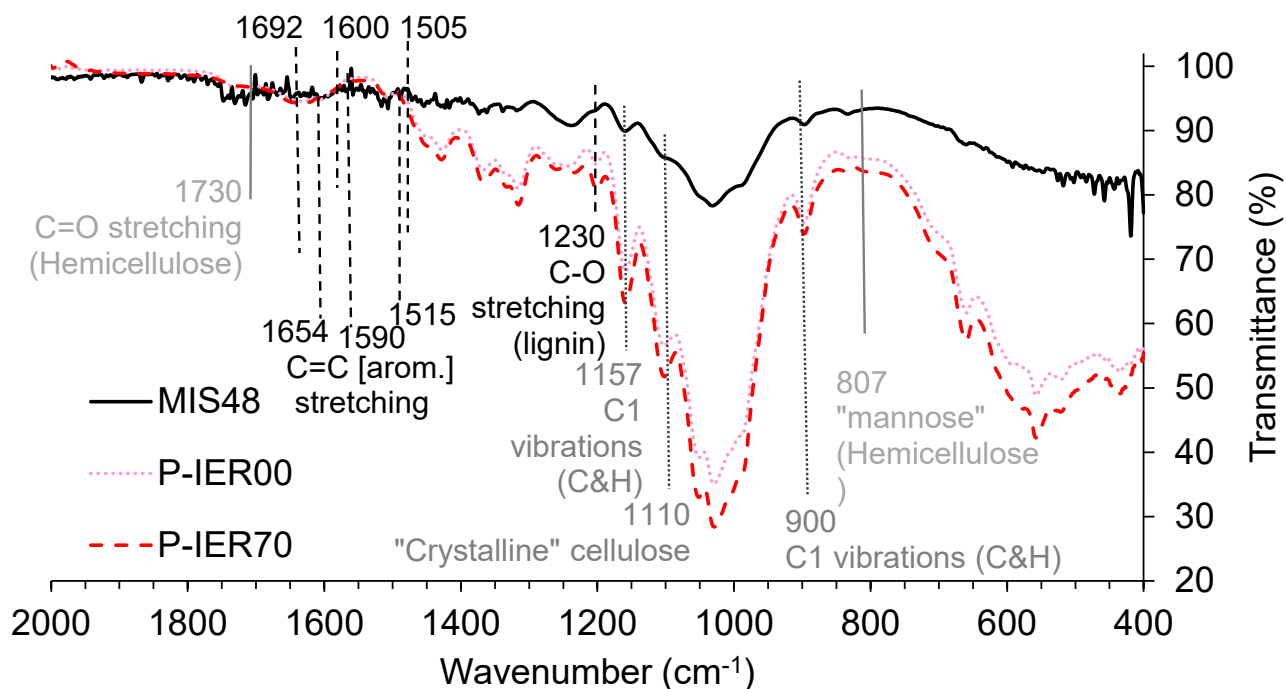


Figure 5.10. ATR-FTIR for MIS48, pulp after TS80-IER70 treatment.

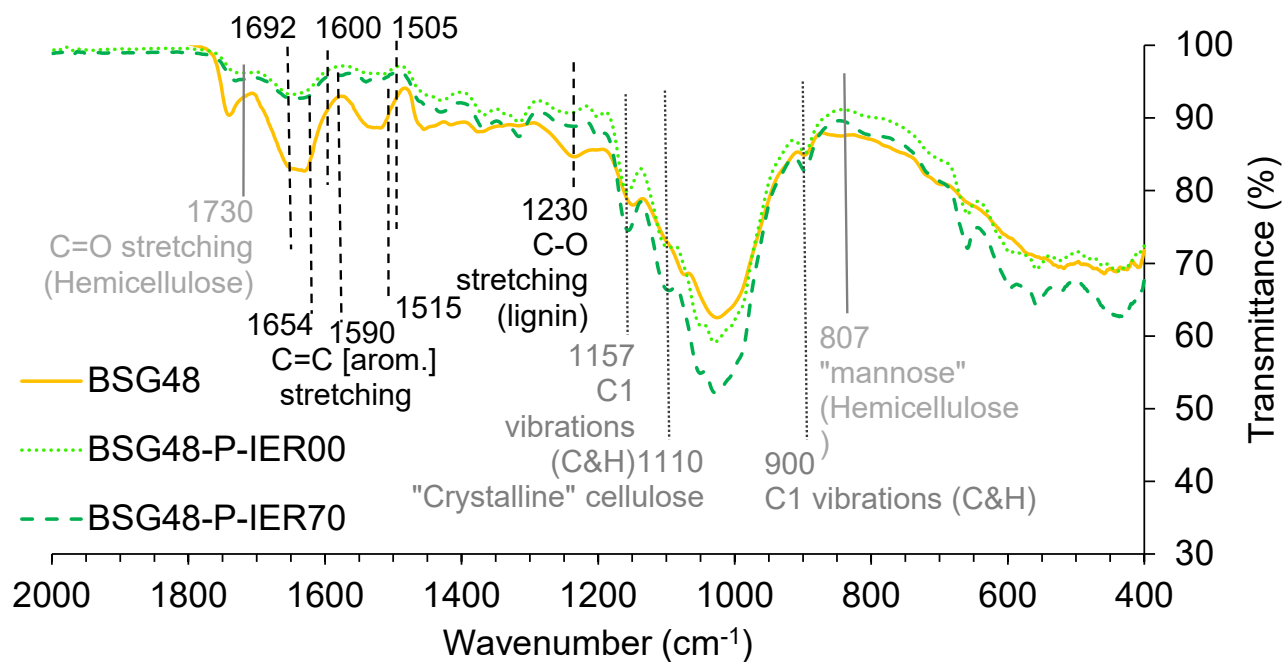


Figure 5.11. ATR-FTIR for BSG48, pulp after TS80-IER70 treatment.

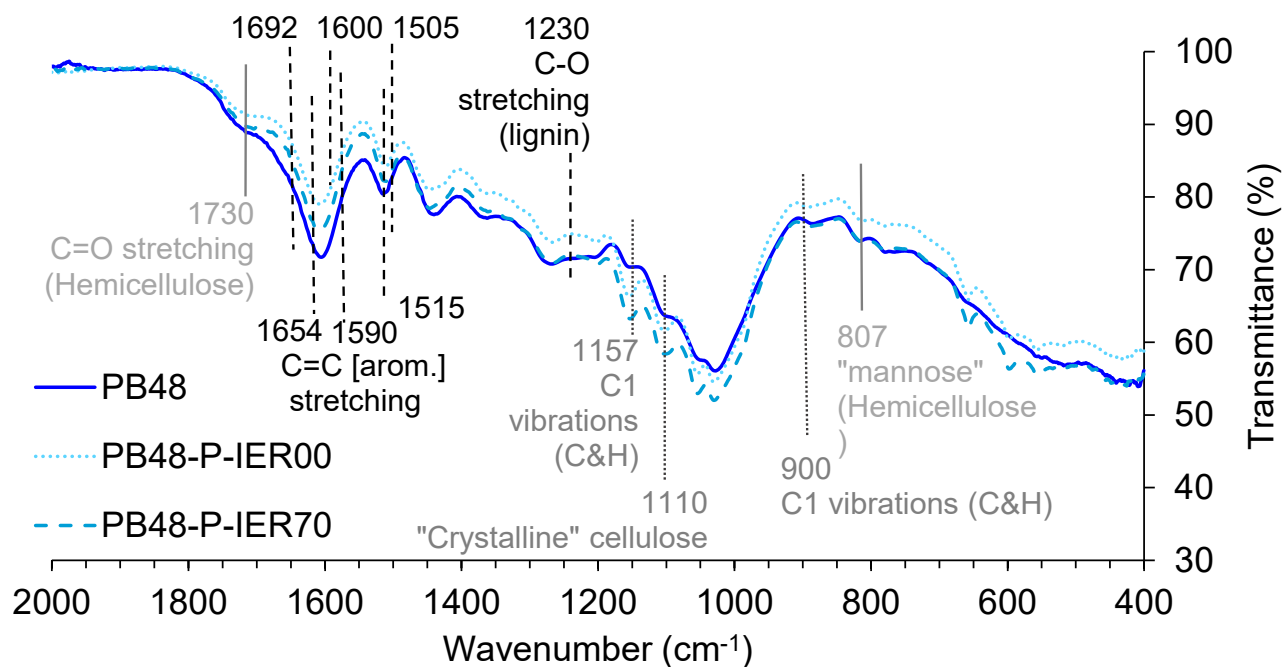


Figure 5.12. ATR-FTIR for PB48, pulp after TS80-IER70 treatment.

Overall, these spectral changes provide insights into the effectiveness of TS80 and IER70 pretreatment in modifying the structure under moderate conditions and agree with previous techniques that the effect of the IER70 is mainly noticeable when the cellulose fraction is accessible and/or highly present in the biomass.

5.5. Conclusions

This chapter examined the influence of various IERs on MIS48 in the presence of TS80. After selecting an IER, it was used to pretreat other raw materials in TS80. This section summarises the main conclusions and findings in this chapter.

Use of different IERs with ionic liquid TS80:

1. IER properties: although there is a general trend that thermomechanical stability, high acid strength, high ion exchange capacity, and swelling capacity were important in influencing the pulp fraction of MIS48 after the pretreatment, some properties of the IERs have yet to be unveiled, and that can affect their performance when combined with TS80.
2. IER70 showed the most promising results when used with TS80 to pretreat MIS48. The resin could convert crystalline cellulose to amorphous in highly acidic IL. The increase in the amorphous cellulose was confirmed through different analytical techniques: TGA-DTG, XRD, and ATR-FTIR.

Physicochemical characterisation of BSG48, PB48 and comparison with MIS48:

1. The cell wall composition of biomass significantly influenced proximate and ultimate analyses. Additionally, it depends on the preprocessing done to the material's moisture and ash contents. For example, PB48 was washed with water and dried in the open air, so it had a high moisture content of ~7% compared to other raw materials. Similarly, BSG48 had a very high ash content of ~16% as compared to the literature because of the source, in this case, barley malt, and brewery process [423].
2. TGA results showed that, depending on the chemical composition of lignocellulosic material, the thermal degradation profile changes in both inert and reactive environments. For instance, PB48, with high lignin content, degraded thermally over a wide range of temperatures with lower DTG_{max} than MIS48, which had the highest carbohydrate content. XRD analysis showed a similar trend as TGA; the material with the highest cellulose content had the highest crystalline peak intensities, in this case, MIS48. FTIR-ATR examination revealed that BSG48 had high protein content, which made the material highly amorphous compared to the other two raw materials.

TS80-IER70 system using different biomass compositions:

1. TS80 pretreatment under moderate conditions was the least effective on PB48 because of its recalcitrant nature (high lignin percentage) compared to the other two materials.
2. TGA analysis revealed that the IER70 addition to TS80 was the most influential in MIS48, lowering pulp thermal stability and increasing DTG_{max} compared to when only TS80 was used. Upon adding

IER70 to TS80, the thermal characteristics of pulp samples from BSG48 and PB48 showed no significant changes.

3. XRD results provided further insight into these pulp fractions. The results showed that *Crl* increased from 76% to 82% after adding IER70 to TS80, which mainly removed the amorphous fraction from the pulp.
4. All the analytical techniques revealed that pulp produced from TS80 pretreatment of pine bark did not show any physicochemical changes when IER70 was added to the process, mainly because of the nature of the material and the process's moderate operating conditions.

As a result, the combination of concentrated TS80 with IER70 can have a symbiotic effect on the produced pulp fraction of lignocellulosic material. However, the physicochemical properties of the raw material and operating conditions were essential to observe this influence. To see the maximum symbiotic effect, the lignocellulosic material should be high in carbohydrate fraction, as seen in this chapter and in the previous chapter for MIS48 and MIS16.

Chapter 6. Conclusions and Recommendations for Future Work

6.1. Conclusions

The present research work has provided extensive insight into ion exchange resins for hydrolysis and fractionation using water and ionic liquid solvents. The primary outcomes are:

Outcomes from Chapter 3. Hydrolysis of *Miscanthus x Giganteus* using IERs-water system

This study demonstrates that ion exchange resins can effectively catalyse the hydrolysis of lignocellulosic biomass in water, potentially replacing mineral acids in dilute conditions. The comparison of two ion exchange resins (IERs) at varying loadings demonstrated that acid capacity is not the sole factor influencing hydrolysis performance; acid strength significantly enhances hemicellulose removal, exposes the cellulose structure, and affects the proximate analysis of pretreated pulp. In comparison to IER35, IER70 had shown superior efficacy in biomass transformation. Furthermore, the mechanical stability of ion exchange resins is a crucial consideration when processing biomass in an aqueous solution with a magnetic stirrer. IER35 was compromised by abrasion, whereas IER70 maintained its structural integrity.

IERs were more influential than mineral acids in increasing volatile content and lowering the ash content in pulp. IERs could remove inorganics in the biomass through the cation exchange process and decrease the pulp's recalcitrance and thermal stability, ultimately improving its processability and conversion efficiency into valuable products. Despite this, the IERs did not significantly impact the lignin under the conditions of operation examined.

Outcomes from Chapter 4. Fractionation of *Miscanthus x Giganteus* using IERs-ILs system

Stainless steel mesh baskets provided a more straightforward method to separate and recover the IERs from the biomass aqueous systems in aqueous media. However, they cannot be used in IL-TS solutions for biomass pretreatment. An appropriate size of the raw material ($\epsilon < 106 \mu\text{m}$) was selected to efficiently separate the cellulosic-rich material from the IERs after IL pretreatment. There was no symbiotic effect between IER70 and IL-TA in the pulp. Inversely, the IL-TS with IER70 showed a symbiotic help to remove alkali metals and assist with the depolymerisation of the hemicellulose and the cellulose, resulting in pulp fraction rich in amorphous fraction.

Outcomes from Chapter 5. Fractionation of using IL-TS with different IERs and biomass feedstocks

IER properties such as high thermomechanical stability, high acid strength, high ion exchange capacity, and swelling capacity were influential in enhancing the fractionation of MIS48. IER70 showed the most promising results when used with TS80 to pretreat this type of lignocellulosic feedstock. However, when compared to other two feedstocks that had different composition (pine bark with high lignin content (42-

51 wt.% [429]) and brewery spent grains with high fibre content (70-85 wt.% [421]), it was made evident that the physicochemical properties (chemical composition) of the raw material and operating conditions (temperature, time, biomass loading, were essential to observe this influence. The lignocellulosic material should be high in carbohydrate fraction rather than lignin to see the maximum symbiotic effect.

Overall, this study has demonstrated that IERs can be used with water and ionic liquids for hydrolysis and fractionation of biomass, providing advantages such as better depolymerisation of cellulose and hemicellulose. A high IER acid capacity, acid strength and mechanical abrasion resistance are key to enhancing the benefits of IERs in the hydrolysis of biomass using water as a solvent and in the fractionation of biomass, assisting protonated ionic liquids, such as triethyl ammonium hydrogen sulphate.

From the systems studied, Amberlyst 70 proved to be the best ion exchange resin for cellulose transformation. Its acid strength and mechanical resistance were among the properties that made this IER optimal.

Amberlyst 70 exemplifies green chemistry principles (Table A1.1) by enabling efficient, low-waste biomass conversion with renewable feedstocks. Its reusability, non-toxic nature, and compatibility with aqueous systems align with catalysis, energy efficiency, and pollution prevention concepts. These resins promote safer chemical design by replacing hazardous acids and solvents, enhancing the sustainability and scalability of biorefineries

In summary, Amberlyst 70 in water or TS80 improved depolymerisation is crucial for biorefineries. It increases the accessibility and reactivity of biomass components, thereby enabling more efficient downstream conversion into renewable chemicals and fuels.

6.2. Recommendations for Future Work

The research was conducted to understand the hydrolytic capacity of acid IERs in an aqueous and acidic IL medium. Along with the chemical properties of selected IERs, their mechanical properties are fundamental in influencing biomass fractionation in water or IL-TS.

Acidic and macroreticular IERs in the water system can partially hydrolyse hemicellulose in the biomass; however, other IERs, such as basic IERs, and gel-type IERs must be investigated in water with different lignocellulosic materials.

The stainless mesh basket could not maintain its integrity in the presence of acidic IL. Other materials such as alloys should be investigated for mesh baskets that can withstand low pH solutions under severe operating conditions to better separate IERs from pretreated material in an acidic solution.

Magnetic IERs could be synthesised, analysed, and compared with the existing acidic IERs in both aqueous and IL systems. Magnetic resins could facilitate process operations during and after the pretreatment of lignocellulosic material, as they could be separated using a magnetic field.

Further, enzymatic hydrolysis should be done to see whether the symbiotic effect of IER70 and TS80 produces high sugar yields compared to pulp produced only from TS80. The process needs to be scaled up to see if the influence of acidic IER in IL-TS on the pulp fraction of biomass can be a viable option at the industrial level.

Finally, it would be recommended to perform a techno-economic analysis to assess whether a combination of IER and IL is economically viable and identify economic bottlenecks if the process needs to be scaled up.

References

- [1] A.A. Vertès, Biorefinery Roadmaps, in: *Biorefineries Integr. Biochem. Process. Liq. Biofuels*, 2014: pp. 59–71. <https://doi.org/10.1016/B978-0-444-59498-3.00003-8>.
- [2] J.H. Clark, V. Budarin, F.E.I. Deswarte, J.J.E. Hardy, F.M. Kerton, A.J. Hunt, R. Luque, D.J. Macquarrie, K. Milkowski, A. Rodriguez, O. Samuel, S.J. Tavener, R.J. White, A.J. Wilson, Green chemistry and the biorefinery: A partnership for a sustainable future, *Green Chem.* 8 (2006) 853–860. <https://doi.org/10.1039/b604483m>.
- [3] F.G. Calvo-Flores, F.J. Martin-Martinez, Biorefineries: Achievements and challenges for a bio-based economy, *Front. Chem.* 10 (2022). <https://doi.org/10.3389/FCHEM.2022.973417>.
- [4] A. Barragán-Ocaña, H. Merritt, O.E. Sánchez-Estrada, J.L. Méndez-Becerril, M. del Pilar Longar-Blanco, Biorefinery and sustainability for the production of biofuels and value-added products: A trends analysis based on network and patent analysis, *PLoS One* 18 (2023). <https://doi.org/10.1371/JOURNAL.PONE.0279659>.
- [5] M. Galbe, O. Wallberg, Pretreatment for biorefineries: A review of common methods for efficient utilisation of lignocellulosic materials, *Biotechnol. Biofuels* 12 (2019) 1–26. <https://doi.org/10.1186/s13068-019-1634-1>.
- [6] P.T. Anastas, J. Warner, *Green Chemistry: Theory and Practice*, (2000) 144. <https://doi.org/10.1093/OSO/9780198506980.001.0001>.
- [7] K. Wagemann, N. Tippkötter, Biorefineries: A short introduction, in: K. Wagemann, N. Tippkötter (Eds.), *Adv. Biochem. Eng. Biotechnol.*, Springer International Publishing, Cham, 2019: pp. 1–11. https://doi.org/10.1007/10_2017_4.
- [8] M. Hingsamer, G. Jungmeier, Chapter Five - Biorefineries, in: C. Lago, N. Caldés, Y.B.T.-T.R. of B. in the B. Lechón (Eds.), *Role Bioenergy Emerg. Bioeconomy Resour. Technol. Sustain. Policy*, Academic Press, 2019: pp. 179–222. <https://doi.org/https://doi.org/10.1016/B978-0-12-813056-8.00005-4>.
- [9] F.H. Isikgor, C.R. Becer, Lignocellulosic biomass: a sustainable platform for the production of bio-based chemicals and polymers, *Polym. Chem.* 6 (2015) 4497–4559. <https://doi.org/10.1039/c5py00263j>.
- [10] A. Corma Canos, S. Iborra, A. Velty, Chemical routes for the transformation of biomass into chemicals, *Chem. Rev.* 107 (2007) 2411–2502. <https://doi.org/10.1021/cr050989d>.
- [11] S. Joanna, CARBON FOR CHEMICALS, Birmingham, 2024. www.supergen-bioenergy.net (accessed August 15, 2024).
- [12] H. V. Lee, S.B.A. Hamid, S.K. Zain, Conversion of lignocellulosic biomass to nanocellulose: Structure and chemical process, *Sci. World J.* 2014 (2014). <https://doi.org/10.1155/2014/631013>.
- [13] T. Shahzadi, S. Mehmood, M. Irshad, Z. Anwar, A. Afroz, N. Zeeshan, U. Rashid, K. Sughra, Advances in lignocellulosic biotechnology: A brief review on lignocellulosic biomass and cellulases, *Adv. Biosci. Biotechnol.* 05 (2014) 246–251. <https://doi.org/10.4236/abb.2014.53031>.
- [14] D. Díez, A. Urueña, R. Piñero, A. Barrio, T. Tamminen, Determination of hemicellulose, cellulose, and lignin content in different types of biomasses by thermogravimetric analysis and pseudocomponent kinetic model (TGA-PKM Method), *Processes* 8 (2020).

<https://doi.org/10.3390/pr8091048>.

- [15] P. Phanthong, P. Reubroycharoen, X. Hao, G. Xu, A. Abudula, G. Guan, Nanocellulose: Extraction and application, *Carbon Resour. Convers.* 1 (2018) 32–43. <https://doi.org/10.1016/j.crcon.2018.05.004>.
- [16] C. Dong, Z. Zhang, Q. Lu, Y. Yang, Characteristics and mechanism study of analytical fast pyrolysis of poplar wood, *Energy Convers. Manag.* 57 (2012) 49–59. <https://doi.org/https://doi.org/10.1016/j.enconman.2011.12.012>.
- [17] E.M. Hodgson, D.J. Nowakowski, I. Shield, A. Riche, A. V Bridgwater, J.C. Clifton-Brown, I.S. Donnison, Variation in *Miscanthus* chemical composition and implications for conversion by pyrolysis and thermo-chemical bio-refining for fuels and chemicals, *Bioresour. Technol.* 102 (2011) 3411–3418. <https://doi.org/https://doi.org/10.1016/j.biortech.2010.10.017>.
- [18] A.S.N. Mahmood, J.G. Brammer, A. Hornung, A. Steele, S. Poulston, The intermediate pyrolysis and catalytic steam reforming of Brewers spent grain, *J. Anal. Appl. Pyrolysis* 103 (2013) 328–342. <https://doi.org/10.1016/j.jaap.2012.09.009>.
- [19] A. Liñán-Montes, S.M. De La Parra-Arciniega, M.T. Garza-González, R.B. García-Reyes, E. Soto-Regalado, F.J. Cerino-Córdova, Characterization and thermal analysis of agave bagasse and malt spent grain, *J. Therm. Anal. Calorim.* 115 (2014) 751–758. <https://doi.org/10.1007/s10973-013-3321-y>.
- [20] E.J.M. Joy, M.R. Broadley, S.D. Young, C.R. Black, A.D.C. Chilimba, E.L. Ander, T.S. Barlow, M.J. Watts, Soil type influences crop mineral composition in Malawi, *Sci. Total Environ.* 505 (2015) 587–595. <https://doi.org/10.1016/J.SCITOTENV.2014.10.038>.
- [21] M. Shabanpour, M. Daneshyar, M. Parhizkar, M.E. Lucas-Borja, D.A. Zema, Influence of crops on soil properties in agricultural lands of northern Iran, (n.d.). <https://doi.org/10.1016/j.scitotenv.2019.134694>.
- [22] B. Sun, X. Wang, F. Wang, Y. Jiang, X.-X. Zhang, Assessing the Relative Effects of Geographic Location and Soil Type on Microbial Communities Associated with Straw Decomposition, (2013). <https://doi.org/10.1128/AEM.00083-13>.
- [23] J. Eitzinger, M. Trnka, D. Semerádová, S. Thaler, E. Svobodová, P. Hlavinka, B. Šiška, J. Takáč, L. Malatinská, M. Nováková, M. Dubrovský, Z. Žalud, Regional climate change impacts on agricultural crop production in Central and Eastern Europe - Hotspots, regional differences and common trends, *J. Agric. Sci.* 151 (2013) 787–812. <https://doi.org/10.1017/S0021859612000767>.
- [24] J.L. Soong, I.A. Janssens, O. Grau, O. Margalef, C. Stahl, L. Van Langenhove, I. Urbina, J. Chave, A. Dourdain, B. Ferry, V. Freycon, B. Herault, J. Sardans, J. Peñuelas, E. Verbruggen, Soil properties explain tree growth and mortality, but not biomass, across phosphorus-depleted tropical forests, *Sci. Rep.* 10 (2020) 1–13. <https://doi.org/10.1038/s41598-020-58913-8>.
- [25] M. Pastuszczak, J. Stanek-Tarkowska, M. Kačániová, Impact of Soil Fertilized with Biomass Ash on Depth-Related Variability of Culturable Bacterial Diversity and Selected Physicochemical Parameters in Spring Barley Cultivation, *Int. J. Environ. Res. Public Health* 19 (2022) 13721. <https://doi.org/10.3390/ijerph192113721>.
- [26] Y. Yang, Improvement of rural soil properties and states by biomass carbon under the concept of sustainability: A research progress, *Front. Chem.* 10 (2022) 1078170. <https://doi.org/10.3389/fchem.2022.1078170>.

- [27] E.M. Hodgson, R. Fahmi, N. Yates, T. Barraclough, I. Shield, G. Allison, A. V. Bridgwater, I.S. Donnison, Miscanthus as a feedstock for fast-pyrolysis: Does agronomic treatment affect quality?, *Bioresour. Technol.* 101 (2010) 6185–6191. <https://doi.org/10.1016/j.biortech.2010.03.024>.
- [28] S. Pang, Advances in thermochemical conversion of woody biomass to energy, fuels and chemicals, *Biotechnol. Adv.* 37 (2019) 589–597. <https://doi.org/10.1016/j.biotechadv.2018.11.004>.
- [29] L. Ma, Y. Xu, J. Chen, C. Dong, Z. Pang, Preparation of Cellulose Nanocrystals by Synergistic Action of Ionic Liquid and Recyclable Solid Acid under Mild Conditions, *Molecules* 28 (2023). <https://doi.org/10.3390/molecules28073070>.
- [30] H. Kobayashi, T. Komanoya, S.K. Guha, K. Hara, A. Fukuoka, Conversion of cellulose into renewable chemicals by supported metal catalysis, *Appl. Catal. A Gen.* 409–410 (2011) 13–20. <https://doi.org/10.1016/j.apcata.2011.10.014>.
- [31] V. Pasangulapati, K.D. Ramachandriya, A. Kumar, M.R. Wilkins, C.L. Jones, R.L. Huhnke, Effects of cellulose, hemicellulose and lignin on thermochemical conversion characteristics of the selected biomass, *Bioresour. Technol.* 114 (2012) 663–669. <https://doi.org/10.1016/j.biortech.2012.03.036>.
- [32] K.C.C. De Carvalho, S.R. Montoro, M.O.H. Cioffi, H.J.C. Voorwald, Polyhydroxyalkanoates and Their Nanobiocomposites With Cellulose Nanocrystals, *Des. Appl. Nanostructured Polym. Blends Nanocomposite Syst.* (2016) 261–285. <https://doi.org/10.1016/B978-0-323-39408-6.00012-1>.
- [33] A. Zoghliami, G. Paës, Lignocellulosic Biomass: Understanding Recalcitrance and Predicting Hydrolysis, *Front. Chem.* 7 (2019) 874. <https://doi.org/10.3389/fchem.2019.00874>.
- [34] S.D. Stefanidis, K.G. Kalogiannis, E.F. Iliopoulou, C.M. Michailof, P.A. Pilavachi, A.A. Lappas, A study of lignocellulosic biomass pyrolysis via the pyrolysis of cellulose, hemicellulose and lignin, *J. Anal. Appl. Pyrolysis* 105 (2014) 143–150. <https://doi.org/https://doi.org/10.1016/j.jaap.2013.10.013>.
- [35] J.A. Rollin, Z. Zhu, N. Sathitsuksanoh, Y.H.P. Zhang, Increasing cellulose accessibility is more important than removing lignin: A comparison of cellulose solvent-based lignocellulose fractionation and soaking in aqueous ammonia, *Biotechnol. Bioeng.* 108 (2011) 22–30. <https://doi.org/10.1002/bit.22919>.
- [36] K. Karimi, M.J. Taherzadeh, A critical review of analytical methods in pretreatment of lignocelluloses: Composition, imaging, and crystallinity, *Bioresour. Technol.* 200 (2016) 1008–1018. <https://doi.org/10.1016/j.biortech.2015.11.022>.
- [37] R.S. Abolore, S. Jaiswal, A.K. Jaiswal, Green and sustainable pretreatment methods for cellulose extraction from lignocellulosic biomass and its applications: A review, *Carbohydr. Polym. Technol. Appl.* 7 (2024) 100396. <https://doi.org/10.1016/j.carpta.2023.100396>.
- [38] H. Kobayashi, A. Fukuoka, Current Catalytic Processes for Biomass Conversion, *New Futur. Dev. Catal. Catal. Biomass Convers.* (2013) 29–52. <https://doi.org/10.1016/B978-0-444-53878-9.00002-3>.
- [39] N.A.Z. Armir, A. Zulkifli, S. Gunaseelan, S.D. Palanivelu, K.M. Salleh, M.H.C. Othman, S. Zakaria, Regenerated cellulose products for agricultural and their potential: A review, *Polymers (Basel)*. 13 (2021) 3586. <https://doi.org/10.3390/polym13203586>.

- [40] Y. Pu, D. Zhang, P.M. Singh, A.J. Ragauskas, The new forestry biofuels sector, *Biofuels, Bioprod. Biorefining* 2 (2008) 58–73. <https://doi.org/10.1002/bbb.48>.
- [41] H. Yang, R. Yan, H. Chen, D.H. Lee, C. Zheng, Characteristics of hemicellulose, cellulose and lignin pyrolysis, *Fuel* 86 (2007) 1781–1788. <https://doi.org/10.1016/j.fuel.2006.12.013>.
- [42] P. Basu, Chapter 3 - Biomass Characteristics, in: P.B.T.-B.G. Basu *Pyrolysis and Torrefaction* (Third Edition) (Ed.), Academic Press, 2018: pp. 49–91. <https://doi.org/https://doi.org/10.1016/B978-0-12-812992-0.00003-0>.
- [43] L. Pereira Ramos, The chemistry involved in the steam treatment of lignocellulosic materials, *Quim. Nova* 26 (2003) 863–871. <https://doi.org/10.1590/s0100-40422003000600015>.
- [44] G. Dervilly-Pinel, V. Tran, L. Saulnier, Investigation of the distribution of arabinose residues on the xylan backbone of water-soluble arabinoxylans from wheat flour, *Carbohydr. Polym.* 55 (2004) 171–177. <https://doi.org/10.1016/j.carbpol.2003.09.004>.
- [45] W. Farhat, R.A. Venditti, M. Hubbe, M. Taha, F. Becquart, A. Ayoub, A Review of Water-Resistant Hemicellulose-Based Materials: Processing and Applications, *ChemSusChem* 10 (2017) 305–323. <https://doi.org/10.1002/cssc.201601047>.
- [46] J. Berglund, D. Mikkelsen, B.M. Flanagan, S. Dhital, S. Gaunitz, G. Henriksson, M.E. Lindström, G.E. Yakubov, M.J. Gidley, F. Vilaplana, Wood hemicelluloses exert distinct biomechanical contributions to cellulose fibrillar networks, *Nat. Commun.* 11 (2020). <https://doi.org/10.1038/s41467-020-18390-z>.
- [47] Y. Dou, Y. Yang, N.K. Mund, Y. Wei, Y. Liu, L. Wei, Y. Wang, P. Du, Y. Zhou, J. Liesche, L. Huang, H. Fang, C. Zhao, J. Li, Y. Wei, S. Chen, Comparative analysis of herbaceous and woody cell wall digestibility by pathogenic fungi, *Molecules* 26 (2021) 7220. <https://doi.org/10.3390/molecules26237220>.
- [48] E. Heinonen, G. Henriksson, M.E. Lindström, F. Vilaplana, J. Wohler, Xylan adsorption on cellulose: Preferred alignment and local surface immobilizing effect, *Carbohydr. Polym.* 285 (2022) 119221. <https://doi.org/10.1016/j.carbpol.2022.119221>.
- [49] J. Rao, Z. Lv, G. Chen, F. Peng, Hemicellulose: Structure, chemical modification, and application, *Prog. Polym. Sci.* 140 (2023) 101675. <https://doi.org/10.1016/j.progpolymsci.2023.101675>.
- [50] R.B. Santos, P.W. Hart, H. Jameel, H.M. Chang, Wood based lignin reactions important to the biorefinery and pulp and paper industries, *BioResources* 8 (2013) 1456–1477. <https://doi.org/10.15376/biores.8.1.1456-1477>.
- [51] T. Li, S. Takkellapati, The current and emerging sources of technical lignins and their applications, *Biofuels, Bioprod. Biorefining* 12 (2018) 756–787. <https://doi.org/10.1002/bbb.1913>.
- [52] S. Zhou, Y. Xue, A. Sharma, X. Bai, Lignin Valorization through Thermochemical Conversion: Comparison of Hardwood, Softwood and Herbaceous Lignin, *ACS Sustain. Chem. Eng.* 4 (2016) 6608–6617. <https://doi.org/10.1021/acssuschemeng.6b01488>.
- [53] Y. Zhao, U. Shakeel, M. Saif Ur Rehman, H. Li, X. Xu, J. Xu, Lignin-carbohydrate complexes (LCCs) and its role in biorefinery, *J. Clean. Prod.* 253 (2020) 120076. <https://doi.org/10.1016/j.jclepro.2020.120076>.
- [54] D. Tarasov, M. Leitch, P. Fatehi, Lignin-carbohydrate complexes: Properties, applications, analyses, and methods of extraction: A review, *Biotechnol. Biofuels* 11 (2018) 1–28.

<https://doi.org/10.1186/s13068-018-1262-1>.

- [55] U. Shakeel, S.U.R. Muhammad, Y. Zhao, H. Li, X. Xu, Y. Sun, J. Xu, Fundamentals of lignin-carbohydrate complexes and its effect on biomass utilization, *Emerg. Technol. Biorefineries, Biofuels, Value-Added Commod.* (2021) 133–155. https://doi.org/10.1007/978-3-030-65584-6_6.
- [56] X. Meng, Y. Pu, C.G. Yoo, M. Li, G. Bali, D.Y. Park, E. Gjersing, M.F. Davis, W. Muchero, G.A. Tuskan, T.J. Tschaplinski, A.J. Ragauskas, An In-Depth Understanding of Biomass Recalcitrance Using Natural Poplar Variants as the Feedstock, *ChemSusChem* 10 (2017) 139–150. <https://doi.org/10.1002/cssc.201601303>.
- [57] B.B. Hallac, A.J. Ragauskas, Analyzing cellulose degree of polymerization and its relevancy to cellulosic ethanol, *Biofuels, Bioprod. Biorefining* 5 (2011) 215–225. <https://doi.org/10.1002/bbb.269>.
- [58] P. Kumar, D.M. Barrett, M.J. Delwiche, P. Stroeve, Methods for Pretreatment of Lignocellulosic Biomass for Efficient Hydrolysis and Biofuel Production, *Ind. Eng. Chem. Res* (2009). <https://doi.org/10.1021/ie801542g>.
- [59] R. Sindhu, A. Pandey, P. Binod, Alkaline Treatment, in: *Pretreat. Biomass Process. Technol.*, Elsevier Inc., 2015: pp. 51–60. <https://doi.org/10.1016/B978-0-12-800080-9.00004-9>.
- [60] M.P. Garver, S. Liu, Development of Thermochemical and Biochemical Technologies for Biorefineries, in: *Bioenergy Res. Adv. Appl.*, 2014: pp. 457–488. <https://doi.org/10.1016/B978-0-444-59561-4.00027-9>.
- [61] R. Chen, S. Zhu, C. Chen, B. Cheng, J. Chen, Y. Wu, Reviving the acid hydrolysis process of lignocellulosic material in biorefinery, *BioResources* 9 (2014) 1824–1827. <https://doi.org/10.15376/biores.9.2.1824-1827>.
- [62] P. Alvira, E. Tomás-Pejó, M. Ballesteros, M.J. Negro, Pretreatment technologies for an efficient bioethanol production process based on enzymatic hydrolysis: A review, *Bioresour. Technol.* 101 (2010) 4851–4861. <https://doi.org/10.1016/j.biortech.2009.11.093>.
- [63] Y.H. Oh, I.Y. Eom, J.C. Joo, J.H. Yu, B.K. Song, S.H. Lee, S.H. Hong, S.J. Park, Recent advances in development of biomass pretreatment technologies used in biorefinery for the production of bio-based fuels, chemicals and polymers, *Korean J. Chem. Eng.* 32 (2015) 1945–1959. <https://doi.org/10.1007/s11814-015-0191-y>.
- [64] S.S. Hassan, G.A. Williams, A.K. Jaiswal, Emerging technologies for the pretreatment of lignocellulosic biomass, *Bioresour. Technol.* 262 (2018) 310–318. <https://doi.org/10.1016/j.biortech.2018.04.099>.
- [65] H. Chen, J. Liu, X. Chang, D. Chen, Y. Xue, P. Liu, H. Lin, S. Han, A review on the pretreatment of lignocellulose for high-value chemicals, *Fuel Process. Technol.* 160 (2017) 196–206. <https://doi.org/10.1016/j.fuproc.2016.12.007>.
- [66] S. Nanda, J. Mohammad, S.N. Reddy, J.A. Kozinski, A.K. Dalai, Pathways of lignocellulosic biomass conversion to renewable fuels, *Biomass Convers. Biorefinery* 4 (2014) 157–191. <https://doi.org/10.1007/s13399-013-0097-z>.
- [67] P.R. Seidl, A.K. Goulart, Pretreatment processes for lignocellulosic biomass conversion to biofuels and bioproducts, *Curr. Opin. Green Sustain. Chem.* 2 (2016) 48–53. <https://doi.org/10.1016/j.cogsc.2016.09.003>.
- [68] S.K. Bhatia, S.S. Jagtap, A.A. Bedekar, R.K. Bhatia, A.K. Patel, D. Pant, J. Rajesh Banu, C. V.

- Rao, Y.G. Kim, Y.H. Yang, Recent developments in pretreatment technologies on lignocellulosic biomass: Effect of key parameters, technological improvements, and challenges, *Bioresour. Technol.* 300 (2020). <https://doi.org/10.1016/j.biortech.2019.122724>.
- [69] D. Haldar, M.K. Purkait, A review on the environment-friendly emerging techniques for pretreatment of lignocellulosic biomass: Mechanistic insight and advancements, *Chemosphere* 264 (2021) 128523. <https://doi.org/10.1016/j.chemosphere.2020.128523>.
- [70] F. Bergius, Conversion of Wood To Carbohydrates and Problems in the Industrial Use of Concentrated Hydrochloric Acid, *Ind. Eng. Chem.* 29 (1937) 247–253. <https://doi.org/10.1021/ie50327a002>.
- [71] D. Steinbach, A. Kruse, J. Sauer, Pretreatment technologies of lignocellulosic biomass in water in view of furfural and 5-hydroxymethylfurfural production- A review, *Biomass Convers. Biorefinery* 7 (2017) 247–274. <https://doi.org/10.1007/s13399-017-0243-0>.
- [72] N.N. Nichols, R.E. Hector, B.C. Saha, S.E. Frazer, G.J. Kennedy, Biological abatement of inhibitors in rice hull hydrolyzate and fermentation to ethanol using conventional and engineered microbes, *Biomass and Bioenergy* 67 (2014) 79–88. <https://doi.org/10.1016/j.biombioe.2014.04.026>.
- [73] K. Świątek, S. Gaag, A. Klier, A. Kruse, J. Sauer, D. Steinbach, Acid hydrolysis of lignocellulosic biomass: Sugars and furfurals formation, *Catalysts* 10 (2020). <https://doi.org/10.3390/catal10040437>.
- [74] L.Q. Wang, L.Y. Cai, Y.L. Ma, Study on inhibitors from acid pretreatment of corn stalk on ethanol fermentation by alcohol yeast, *RSC Adv.* 10 (2020) 38409–38415. <https://doi.org/10.1039/d0ra04965d>.
- [75] Y.H. Jung, K.H. Kim, Acidic Pretreatment, in: A. Pandey, S. Negi, P. Binod, C.B.T.-P. of B. Larroche (Eds.), *Pretreat. Biomass Process. Technol.*, Elsevier, Amsterdam, 2015: pp. 27–50. <https://doi.org/10.1016/B978-0-12-800080-9.00003-7>.
- [76] B. Yang, C.E. Wyman, Dilute acid and autohydrolysis pretreatment., in: *Methods Mol. Biol.*, Humana Press, Totowa, NJ, 2009: pp. 103–114. https://doi.org/10.1007/978-1-60761-214-8_8.
- [77] R. Davis, L. Tao, E.C.D. Tan, M.J. Bidy, G.T. Beckham, C. Scarlata, J. Jacobson, K. Cafferty, J. Ross, J. Lukas, D. Knorr, P. Schoen, *Process Design and Economics for the Conversion of Lignocellulosic Biomass to Hydrocarbons: Dilute-Acid and Enzymatic Deconstruction of Biomass to Sugars and Biological Conversion of Sugars to Hydrocarbons*, 2013. <http://www.osti.gov/servlets/purl/1107470/> (accessed March 29, 2021).
- [78] D. Humbird, R. Davis, L. Tao, C. Kinchin, D. Hsu, A. Aden, P. Schoen, J. Lukas, B. Olthof, M. Worley, D. Sexton, D. Dudgeon, *Process design and economics for conversion of lignocellulosic biomass to ethanol*, 2011. <http://www.nrel.gov/docs/fy11osti/51400.pdf%5Cnpapers2://publication/uuid/49A5007E-9A58-4E2B-AB4E-4A4428F6EA66> (accessed July 10, 2021).
- [79] J.K.W. Chang, X. Duret, V. Berberi, H. Zahedi-Niaki, J.M. Lavoie, Two-step thermochemical cellulose hydrolysis with partial neutralization for glucose production, *Front. Chem.* 6 (2018) 117. <https://doi.org/10.3389/fchem.2018.00117>.
- [80] R. Timung, M. Mohan, B. Chilukoti, S. Sasmal, T. Banerjee, V. V Goud, Optimization of dilute acid and hot water pretreatment of different lignocellulosic biomass: A comparative study, *Biomass and Bioenergy* 81 (2015) 9–18. <https://doi.org/https://doi.org/10.1016/j.biombioe.2015.05.006>.

- [81] Y.P. Wijaya, R.D.D. Putra, V.T. Widyaya, J.M. Ha, D.J. Suh, C.S. Kim, Comparative study on two-step concentrated acid hydrolysis for the extraction of sugars from lignocellulosic biomass, *Bioresour. Technol.* 164 (2014) 221–231. <https://doi.org/10.1016/j.biortech.2014.04.084>.
- [82] D.Y. Kim, Y.S. Kim, T.H. Kim, K.K. Oh, Two-stage, acetic acid-aqueous ammonia, fractionation of empty fruit bunches for increased lignocellulosic biomass utilization, *Bioresour. Technol.* 199 (2016) 121–127. <https://doi.org/10.1016/j.biortech.2015.09.049>.
- [83] S.I. Mussatto, Biomass Pretreatment With Acids, in: S.I.B.T.-B.F.T. for a L.F.B.B. Mussatto (Ed.), *Biomass Fractionation Technol. a Lignocellul. Feed. Based Biorefinery*, Elsevier, Amsterdam, 2016: pp. 169–185. <https://doi.org/10.1016/B978-0-12-802323-5.00008-6>.
- [84] M. Asadieraghi, W.M.A. Wan Daud, Characterization of lignocellulosic biomass thermal degradation and physiochemical structure: Effects of demineralization by diverse acid solutions, *Energy Convers. Manag.* 82 (2014) 71–82. <https://doi.org/https://doi.org/10.1016/j.enconman.2014.03.007>.
- [85] Y. Sun, G. Yang, Z.H. Jia, C. Wen, L. Zhang, ACID HYDROLYSIS OF CORN STOVER USING HYDROCHLORIC ACID: KINETIC MODELING AND STATISTICAL OPTIMIZATION Article, *Chem. Ind. Chem. Eng. Q.* 20 (2014) 531–539. <https://doi.org/10.2298/CICEQ130911035S>.
- [86] C.L. Chambon, M. Chen, P.S. Fennell, J.P. Hallett, Efficient fractionation of lignin- and ash-rich agricultural residues following treatment with a low-cost protic ionic liquid, *Front. Chem.* 7 (2019) 246. <https://doi.org/10.3389/fchem.2019.00246>.
- [87] J.J. Wilson, L. Deschatelets, N.K. Nishikawa, Comparative fermentability of enzymatic and acid hydrolysates of steam-pretreated aspenwood hemicellulose by *Pichia stipitis* CBS 5776, *Appl. Microbiol. Biotechnol.* 31 (1989) 592–596. <https://doi.org/10.1007/BF00270801>.
- [88] S. Mateo, I.C. Roberto, S. Sánchez, A.J. Moya, Detoxification of hemicellulosic hydrolyzate from olive tree pruning residue, *Ind. Crops Prod.* 49 (2013) 196–203. <https://doi.org/10.1016/j.indcrop.2013.04.046>.
- [89] J.C. Parajó, H. Dominguez, J.M. Dominguez, Study of charcoal adsorption for improving the production of xylitol from wood hydrolysates, *Bioprocess Eng.* 16 (1996) 39–43. <https://doi.org/10.1007/s004490050285>.
- [90] F. Carvalheiro, L.C. Duarte, S. Lopes, J.C. Parajó, H. Pereira, F.M. Gírio, Evaluation of the detoxification of brewery's spent grain hydrolysate for xylitol production by *Debaryomyces hansenii* CCMI 941, *Process Biochem.* 40 (2005) 1215–1223. <https://doi.org/10.1016/j.procbio.2004.04.015>.
- [91] K.K. Cheng, B.Y. Cai, J.A. Zhang, H.Z. Ling, Y.J. Zhou, J.P. Ge, J.M. Xu, Sugarcane bagasse hemicellulose hydrolysate for ethanol production by acid recovery process, *Biochem. Eng. J.* 38 (2008) 105–109. <https://doi.org/10.1016/j.bej.2007.07.012>.
- [92] Z.Y. Sun, Y.Q. Tang, T. Iwanaga, T. Sho, K. Kida, Production of fuel ethanol from bamboo by concentrated sulfuric acid hydrolysis followed by continuous ethanol fermentation, *Bioresour. Technol.* 102 (2011) 10929–10935. <https://doi.org/10.1016/j.biortech.2011.09.071>.
- [93] N. Mosier, C. Wyman, B. Dale, R. Elander, Y.Y. Lee, M. Holtzapple, M. Ladisch, Features of promising technologies for pretreatment of lignocellulosic biomass, *Bioresour. Technol.* 96 (2005) 673–686. <https://doi.org/10.1016/j.biortech.2004.06.025>.
- [94] N. Akhtar, K. Gupta, D. Goyal, A. Goyal, Recent advances in pretreatment technologies for efficient hydrolysis of lignocellulosic biomass, *Environ. Prog. Sustain. Energy* 35 (2016) 489–

511. <https://doi.org/10.1002/ep.12257>.

- [95] F.M. Gírio, C. Fonseca, F. Carvalheiro, L.C. Duarte, S. Marques, R. Bogel-Lukasik, Hemicelluloses for fuel ethanol: A review, *Bioresour. Technol.* 101 (2010) 4775–4800. <https://doi.org/10.1016/j.biortech.2010.01.088>.
- [96] F. Carvalheiro, L.C. Duarte, F.M. Gírio, Hemicellulose biorefineries: A review on biomass pretreatments, *J. Sci. Ind. Res. (India)*. 67 (2008) 849–864.
- [97] R. Kumar, C.E. Wyman, Does change in accessibility with conversion depend on both the substrate and pretreatment technology?, *Bioresour. Technol.* 100 (2009) 4193–4202. <https://doi.org/10.1016/J.BIORTECH.2008.11.058>.
- [98] J.S. Kim, Y.Y. Lee, T.H. Kim, A review on alkaline pretreatment technology for bioconversion of lignocellulosic biomass, *Bioresour. Technol.* 199 (2016) 42–48. <https://doi.org/10.1016/j.biortech.2015.08.085>.
- [99] R. Sierra, C.B. Granda, M.T. Holtzaple, Lime pretreatment., *Methods Mol. Biol.* 581 (2009) 115–124. https://doi.org/10.1007/978-1-60761-214-8_9.
- [100] T.H. Kim, R. Gupta, Y.Y. Lee, Pretreatment of biomass by aqueous ammonia for bioethanol production., in: *Methods Mol. Biol.*, Humana Press, Totowa, NJ, 2009: pp. 79–91. https://doi.org/10.1007/978-1-60761-214-8_6.
- [101] D. Kumari, R. Singh, Pretreatment of lignocellulosic wastes for biofuel production: A critical review, *Renew. Sustain. Energy Rev.* 90 (2018) 877–891. <https://doi.org/10.1016/j.rser.2018.03.111>.
- [102] Y.C. Park, J.S. Kim, Comparison of various alkaline pretreatment methods of lignocellulosic biomass, *Energy* 47 (2012) 31–35. <https://doi.org/10.1016/j.energy.2012.08.010>.
- [103] Z. Zhang, M.D. Harrison, D.W. Rackemann, W.O.S. Doherty, I.M. O'Hara, Organosolv pretreatment of plant biomass for enhanced enzymatic saccharification, *Green Chem.* 18 (2016) 360–381. <https://doi.org/10.1039/c5gc02034d>.
- [104] X.L. Du, Q.Y. Bi, Y.M. Liu, Y. Cao, K.N. Fan, Conversion of biomass-derived levulinate and formate esters into γ -valerolactone over supported gold catalysts, *ChemSusChem* 4 (2011) 1838–1843. <https://doi.org/10.1002/CSSC.201100483>.
- [105] S.E. Hunter, C.E. Ehrenberger, P.E. Savage, Kinetics and Mechanism of Tetrahydrofuran Synthesis via 1,4-Butanediol Dehydration in High-Temperature Water, (2006). <https://doi.org/10.1021/jo061017o>.
- [106] M. Gelosia, A. Bertini, M. Barbanera, T. Giannoni, A. Nicolini, F. Cotana, G. Cavalaglio, Acid-assisted organosolv pre-treatment and enzymatic hydrolysis of cynara cardunculus L. For glucose production, *Energies* 13 (2020). <https://doi.org/10.3390/en13164195>.
- [107] Y.H.P. Zhang, S.Y. Ding, J.R. Mielenz, J.B. Cui, R.T. Elander, M. Laser, M.E. Himmel, J.R. McMillan, L.R. Lynd, Fractionating recalcitrant lignocellulose at modest reaction conditions, *Biotechnol. Bioeng.* 97 (2007) 214–223. <https://doi.org/10.1002/bit.21386>.
- [108] N. Sathitsuksanoh, Z. Zhu, Y.H.P. Zhang, Cellulose solvent- and organic solvent-based lignocellulose fractionation enabled efficient sugar release from a variety of lignocellulosic feedstocks, *Bioresour. Technol.* 117 (2012) 228–233. <https://doi.org/10.1016/j.biortech.2012.04.088>.
- [109] A. Demirbaş, Aqueous glycerol delignification of wood chips and ground wood, *Bioresour.*

Technol. 63 (1998) 179–185. [https://doi.org/10.1016/S0960-8524\(97\)00063-1](https://doi.org/10.1016/S0960-8524(97)00063-1).

- [110] F.G. Calvo-Flores, J.A. Dobado, Lignin as renewable raw material, *ChemSusChem* 3 (2010) 1227–1235. <https://doi.org/10.1002/cssc.201000157>.
- [111] H.Q. Lê, J.-P. Pokki, M. Borrega, P. Uusi-Kyyny, V. Alopaeus, H. Sixta, Chemical Recovery of γ -Valerolactone/Water Biorefinery, (2018). <https://doi.org/10.1021/acs.iecr.8b03723>.
- [112] K. Zhang, Z. Pei, D. Wang, Organic solvent pretreatment of lignocellulosic biomass for biofuels and biochemicals: A review, *Bioresour. Technol.* 199 (2016) 21–33. <https://doi.org/10.1016/j.biortech.2015.08.102>.
- [113] F. Guo, Z. Fang, C.C. Xu, R.L. Smith, Solid acid mediated hydrolysis of biomass for producing biofuels, *Prog. Energy Combust. Sci.* 38 (2012) 672–690. <https://doi.org/10.1016/j.pecs.2012.04.001>.
- [114] N.H. Chung, L.Q. Dien, T.D. Cuong, N. Van Lieu, P.H. Hoang, Influence of the acidity of solid catalyst HSO 3 -ZSM-5 on the hydrolysis of pretreated corncob, *RSC Adv.* 8 (2018) 41776–41781. <https://doi.org/10.1039/c8ra09190k>.
- [115] S. Li, Z. Gu, B.E. Bjornson, A. Muthukumarappan, Biochar based solid acid catalyst hydrolyze biomass, *J. Environ. Chem. Eng.* 1 (2013) 1174–1181. <https://doi.org/10.1016/j.jece.2013.09.004>.
- [116] I.S. Tan, M.K. Lam, K.T. Lee, Hydrolysis of macroalgae using heterogeneous catalyst for bioethanol production, *Carbohydr. Polym.* 94 (2013) 561–566. <https://doi.org/10.1016/j.carbpol.2013.01.042>.
- [117] W. Namchot, N. Panyacharay, W. Jonglertjunya, C. Sakdaronnarong, Hydrolysis of delignified sugarcane bagasse using hydrothermal technique catalyzed by carbonaceous acid catalysts, *Fuel* 116 (2014) 608–616. <https://doi.org/10.1016/j.fuel.2013.08.062>.
- [118] Q. Liu, H. Fan, J. Qi, S. Zhang, G. Li, Catalytic hydrolysis of corncob cellulosic polysaccharide into saccharides using SnO₂-Co₃O₄/C biochar catalyst, *Iran. Polym. J. (English Ed.)* 29 (2020) 383–392. <https://doi.org/10.1007/s13726-020-00805-9>.
- [119] S. Xu, Z. Tan, G. Cai, C. Xiong, W. Tan, Y. Zhang, Sulfonic acid catalyst based on silica foam supported copolymer for hydrolysis of cellulose, *Catal. Commun.* 71 (2015) 56–60. <https://doi.org/10.1016/j.catcom.2015.07.023>.
- [120] C. Bai, L. Zhu, F. Shen, X. Qi, Black liquor-derived carbonaceous solid acid catalyst for the hydrolysis of pretreated rice straw in ionic liquid, *Bioresour. Technol.* 220 (2016) 656–660. <https://doi.org/10.1016/j.biortech.2016.08.112>.
- [121] I. Kurnia, A. Yoshida, N. Chaihad, A. Bayu, Y. Kasai, A. Abudula, G. Guan, Hydrolysis of cellulose and woody biomass over sustainable weak-acid carbon catalysts from alkaline lignin, *Fuel Process. Technol.* 196 (2019) 106175. <https://doi.org/10.1016/j.fuproc.2019.106175>.
- [122] W. Qi, C. He, Q. Wang, S. Liu, Q. Yu, W. Wang, N. Leksawasdi, C. Wang, Z. Yuan, Carbon-Based Solid Acid Pretreatment in Corncob Saccharification: Specific Xylose Production and Efficient Enzymatic Hydrolysis, *ACS Sustain. Chem. Eng.* 6 (2018) 3640–3648. <https://doi.org/10.1021/acssuschemeng.7b03959>.
- [123] D.M. Lai, L. Deng, J. Li, B. Liao, Q.X. Guo, Y. Fu, Hydrolysis of cellulose into glucose by magnetic solid acid, *ChemSusChem* 4 (2011) 55–58. <https://doi.org/10.1002/cssc.201000300>.
- [124] H. Guo, Y. Lian, L. Yan, X. Qi, R.L. Smith, Cellulose-derived superparamagnetic carbonaceous

solid acid catalyst for cellulose hydrolysis in an ionic liquid or aqueous reaction system, *Green Chem.* 15 (2013) 2167–2174. <https://doi.org/10.1039/c3gc40433a>.

- [125] B. Rekha, R. Saravanathamizhan, Preparation and characterization of biomass-based nanocatalyst for hydrolysis and fermentation of catalytic hydrolysate to bioethanol, *Biomass Convers. Biorefinery* 13 (2023) 1601–1612. <https://doi.org/10.1007/s13399-020-01207-w>.
- [126] Y.B. Huang, Y. Fu, Hydrolysis of cellulose to glucose by solid acid catalysts, *Green Chem.* 15 (2013) 1095–1111. <https://doi.org/10.1039/c3gc40136g>.
- [127] S. Prodingler, M.A. Derewinski, Recent Progress to Understand and Improve Zeolite Stability in the Aqueous Medium, *Pet. Chem.* 60 (2020) 420–436. <https://doi.org/10.1134/S0965544120040143>.
- [128] T. Ennaert, J. Van Aelst, J. Dijkmans, R. De Clercq, W. Schutyser, M. Dusselier, D. Verboekend, B.F. Sels, Potential and challenges of zeolite chemistry in the catalytic conversion of biomass, *Chem. Soc. Rev.* 45 (2016) 584–611. <https://doi.org/10.1039/c5cs00859j>.
- [129] T. Chen, C. Xiong, Y. Tao, Enhanced hydrolysis of cellulose in ionic liquid using mesoporous ZSM-5, *Molecules* 23 (2018). <https://doi.org/10.3390/molecules23030529>.
- [130] M.F. Paiva, E.M. Albuquerque, P.M. de Souza, J.H. Bitter, G. Vanhove, R. Wojcieszak, F.B. Noronha, Cellulose depolymerization using zinc chloride hydrate and solid acid catalysts, *Cellulose* (2024) 1–20. <https://doi.org/10.1007/S10570-024-06107-0>.
- [131] A. Aho, N. Kumar, K. Eränen, T. Salmi, M. Hupa, D.Y. Murzin, Catalytic pyrolysis of biomass in a fluidized bed reactor: Influence of the acidity of h-beta zeolite, *Process Saf. Environ. Prot.* 85 (2007) 473–480. <https://doi.org/10.1205/psep07012>.
- [132] X. Xing, W. Liu, S. Xu, J. Hao, H-Beta Zeolite as Catalyst for the Conversion of Carbohydrates into 5-Hydroxymethylfurfural: The Role of Calcination Temperature, *Catalysts* 14 (2024) 248. <https://doi.org/10.3390/catal14040248>.
- [133] J. Pang, A. Wang, M. Zheng, T. Zhang, Hydrolysis of cellulose into glucose over carbons sulfonated at elevated temperatures, *Chem. Commun.* 46 (2010) 6935–6937. <https://doi.org/10.1039/c0cc02014a>.
- [134] I. Thushari, S. Babel, Preparation of solid acid catalysts from waste biomass and their application for microwave-assisted biodiesel production from waste palm oil, *Waste Manag. Res.* 36 (2018) 719–728. https://doi.org/10.1177/0734242X18789821/ASSET/IMAGES/LARGE/10.1177_0734242X18789821-FIG6.JPEG.
- [135] G.J. Moody, An Introduction to Ion Exchange, 1970. [https://doi.org/10.1016/s0021-9673\(01\)98496-1](https://doi.org/10.1016/s0021-9673(01)98496-1).
- [136] I.O.N. Exchange, FS-TER-006 ION EXCHANGE SERIES: TERTIARY TREATMENTS Title ION EXCHANGE (FS-TER-006), 2015. http://dardel.info/IX/processes/design_principles.html (accessed July 2, 2021).
- [137] C.F.C. Michaud, Ion Exchange Resin Synthesis and Reactions – WCP Online, *Water Cond. Purif. Int. Mag.* (2017) 1. <https://wcponline.com/2017/04/15/ion-exchange-resin-synthesis-reactions/> (accessed July 3, 2021).
- [138] V.M. Bhandari, L.G. Sorokhaibam, V. V. Ranade, Chapter 9 - Ion Exchange Resin Catalyzed Reactions—An Overview, in: *Ind. Catal. Process. Fine Spec. Chem.*, Elsevier Inc., 2016: pp. 393–426. <https://doi.org/10.1016/B978-0-12-801457-8.00009-4>.

- [139] Dow Chemical Company, *Dowex Ion Exchange Resins: Fundamentals of Ion Exchange*, 1999.
- [140] Y. Kim, R. Hendrickson, N. Mosier, M.R. Ladisch, Plug-flow reactor for continuous hydrolysis of glucans and xylans from pretreated corn fiber, *Energy and Fuels* 19 (2005) 2189–2200. <https://doi.org/10.1021/ef050106l>.
- [141] D.L.A. Fernandes, C.M. Silva, A.M.R.B. Xavier, D. V. Evtuguin, Fractionation of sulphite spent liquor for biochemical processing using ion exchange resins, *J. Biotechnol.* 162 (2012) 415–421. <https://doi.org/10.1016/j.jbiotec.2012.03.013>.
- [142] I.M. De Mancilha, M.N. Karim, Evaluation of Ion Exchange Resins for Removal of Inhibitory Compounds from Corn Stover Hydrolyzate for Xylitol Fermentation, *Biotechnol. Prog.* 19 (2003) 1837–1841. <https://doi.org/10.1021/bp034069x>.
- [143] R.A. Schraufnagel, H.F. Rase, Levulinic Acid from Sucrose Using Acidic Ion-Exchange Resins, *Ind. Eng. Chem. Prod. Res. Dev.* 14 (1975) 40–44. <https://doi.org/10.1021/i360053a009>.
- [144] I. Agirrezabal-Telleria, A. Larreategui, J. Requies, M.B. Güemez, P.L. Arias, Furfural production from xylose using sulfonic ion-exchange resins (Amberlyst) and simultaneous stripping with nitrogen, *Bioresour. Technol.* 102 (2011) 7478–7485. <https://doi.org/10.1016/j.biortech.2011.05.015>.
- [145] J.E. Powell, *Ion Exchange Resins*, 1959. <https://doi.org/10.1021/ja01510a069>.
- [146] Ion Exchangers: Information | Merck, (n.d.). https://www.merckmillipore.com/GB/en/analytics-and-sample-preparation/ion-exchanger/detailed-information-about-ion-exchangers/0Amb.qB.9hsAAAFCKxJ3_xE,nav?ReferrerURL=https%3A%2F%2Fwww.google.com%2F (accessed July 2, 2021).
- [147] Matten, Types of Resins, (n.d.). <http://www.mattenplant.com/ion-exchange-ix/overview/types-of-resins/> (accessed July 2, 2021).
- [148] TULSION. T-45 BD Macro. BIODIESEL PRODUCTION: MACRO vs. GEL Why do Macro resins work better than gels? - PDF Free Download, (n.d.). <https://docplayer.net/154622130-Tulsion-t-45-bd-macro-biodiesel-production-macro-vs-gel-why-do-macro-resins-work-better-than-gels.html> (accessed July 2, 2021).
- [149] Www.purolite.com, Weak Acid Cation Resin | Purolite | www.purolite.com, Wwww.Purolite.Com (2021) 1. <https://www.purolite.com/product-type/ion-exchange-weak-acid-cation-resin> (accessed July 22, 2021).
- [150] R.M.A. Saboya, J.A. Cecilia, C. García-Sancho, A. V. Sales, F.M.T. de Luna, E. Rodríguez-Castellón, C.L. Cavalcante, Synthesis of biolubricants by the esterification of free fatty acids from castor oil with branched alcohols using cationic exchange resins as catalysts, *Ind. Crops Prod.* 104 (2017) 52–61. <https://doi.org/10.1016/j.indcrop.2017.04.018>.
- [151] R.S. Juang, T.S. Lee, Oxidative pyrolysis of organic ion exchange resins in the presence of metal oxide catalysts, *J. Hazard. Mater.* 92 (2002) 301–314. [https://doi.org/10.1016/S0304-3894\(02\)00025-0](https://doi.org/10.1016/S0304-3894(02)00025-0).
- [152] S.D. Alexandratos, Ion-Exchange resins: A retrospective from industrial and engineering chemistry research, *Ind. Eng. Chem. Res.* 48 (2009) 388–398. <https://doi.org/10.1021/ie801242v>.
- [153] T. You, L. Zhang, S. Zhou, F. Xu, Protic acid resin enhanced 1-butyl-3-methylimidazolium chloride pretreatment of *Arundo donax* Linn., *Bioresour. Technol.* 167 (2014) 574–577. <https://doi.org/10.1016/j.biortech.2014.06.049>.

- [154] K.M. Lee, G.C. Ngoh, A.S.M. Chua, Ionic liquid-mediated solid acid saccharification of sago waste: Kinetic, ionic liquid recovery and solid acid catalyst reusability study, *Ind. Crops Prod.* 77 (2015) 415–423. <https://doi.org/10.1016/j.indcrop.2015.09.016>.
- [155] D. Groff, A. George, N. Sun, N. Sathitsuksanoh, G. Bokinsky, B.A. Simmons, B.M. Holmes, J.D. Keasling, Acid enhanced ionic liquid pretreatment of biomass, *Green Chem.* 15 (2013) 1264–1267. <https://doi.org/10.1039/c3gc37086k>.
- [156] T. You, L. Shao, R. Wang, L. Zhang, F. Xu, Facile isothermal solid acid catalyzed ionic liquid pretreatments to enhance the combined sugars production from *Arundo donax* Linn., *Biotechnol. Biofuels* 9 (2016) 177. <https://doi.org/10.1186/s13068-016-0589-8>.
- [157] T.T. You, L.M. Zhang, F. Xu, Progressive deconstruction of *Arundo donax* Linn. to fermentable sugars by acid catalyzed ionic liquid pretreatment, *Bioresour. Technol.* 199 (2016) 271–274. <https://doi.org/10.1016/j.biortech.2015.08.152>.
- [158] N. Di Fidio, A.M.R. Galletti, S. Fulignati, D. Licursi, F. Liuzzi, I. De Bari, C. Antonetti, Multi-step exploitation of raw *arundo donax* L. For the selective synthesis of second-generation sugars by chemical and biological route, *Catalysts* 10 (2020) 79. <https://doi.org/10.3390/catal10010079>.
- [159] R. Ballini, 4.1 Introduction, in: *Eco-Friendly Synth. Fine Chem.*, Royal Society of Chemistry, 2009: pp. 155–185. <https://app.knovel.com/hotlink/khtml/id:kt00C1TED3/eco-friendly-synthesis/task-speci-introduction>.
- [160] T. Vancov, A.S. Alston, T. Brown, S. McIntosh, Use of ionic liquids in converting lignocellulosic material to biofuels, *Renew. Energy* 45 (2012) 1–6. <https://doi.org/10.1016/j.renene.2012.02.033>.
- [161] K.C. Badgujar, B.M. Bhanage, Factors governing dissolution process of lignocellulosic biomass in ionic liquid: Current status, overview and challenges, *Bioresour. Technol.* 178 (2015) 2–18. <https://doi.org/10.1016/j.biortech.2014.09.138>.
- [162] P. Mäki-Arvela, I. Anugwom, P. Virtanen, R. Sjöholm, J.P. Mikkola, Dissolution of lignocellulosic materials and its constituents using ionic liquids—A review, *Ind. Crops Prod.* 32 (2010) 175–201. <https://doi.org/10.1016/j.indcrop.2010.04.005>.
- [163] M.M. Hossain, A. Rawal, L. Aldous, Aprotic vs protic ionic liquids for lignocellulosic biomass pretreatment: Anion effects, enzymatic hydrolysis, solid-state NMR, distillation, and recycle, *ACS Sustain. Chem. Eng.* 7 (2019) 11928–11936. <https://doi.org/10.1021/acssuschemeng.8b05987>.
- [164] H. Olivier-Bourbigou, L. Magna, D. Morvan, Ionic liquids and catalysis: Recent progress from knowledge to applications, *Appl. Catal. A Gen.* 373 (2010) 1–56. <https://doi.org/10.1016/j.apcata.2009.10.008>.
- [165] T.J. Szalaty, Ł. Klapiszewski, T. Jesionowski, Recent developments in modification of lignin using ionic liquids for the fabrication of advanced materials—A review, *J. Mol. Liq.* 301 (2020) 112417. <https://doi.org/10.1016/j.molliq.2019.112417>.
- [166] J. Baruah, B.K. Nath, R. Sharma, S. Kumar, R.C. Deka, D.C. Baruah, E. Kalita, Recent trends in the pretreatment of lignocellulosic biomass for value-added products, *Front. Energy Res.* 6 (2018) 141. <https://doi.org/10.3389/fenrg.2018.00141>.
- [167] F. Xu, Y.C. Shi, D. Wang, Enhanced production of glucose and xylose with partial dissolution of corn stover in ionic liquid, 1-Ethyl-3-methylimidazolium acetate, *Bioresour. Technol.* 114 (2012) 720–724. <https://doi.org/10.1016/j.biortech.2012.03.023>.

- [168] P. Varanasi, P. Singh, R. Arora, P.D. Adams, M. Auer, B.A. Simmons, S. Singh, Understanding changes in lignin of *Panicum virgatum* and *Eucalyptus globulus* as a function of ionic liquid pretreatment, *Bioresour. Technol.* 126 (2012) 156–161. <https://doi.org/10.1016/j.biortech.2012.08.070>.
- [169] Z. Qiu, G.M. Aita, M.S. Walker, Effect of ionic liquid pretreatment on the chemical composition, structure and enzymatic hydrolysis of energy cane bagasse, *Bioresour. Technol.* 117 (2012) 251–256. <https://doi.org/10.1016/j.biortech.2012.04.070>.
- [170] W. Xiao, W. Yin, S. Xia, P. Ma, The study of factors affecting the enzymatic hydrolysis of cellulose after ionic liquid pretreatment, *Carbohydr. Polym.* 87 (2012) 2019–2023. <https://doi.org/10.1016/j.carbpol.2011.10.012>.
- [171] Ö.P. Çetinkol, D.C. Dibble, G. Cheng, M.S. Kent, B. Knierim, M. Auer, D.E. Wemmer, J.G. Pelton, Y.B. Melnichenko, J. Ralph, B.A. Simmons, B.M. Holmes, Understanding the impact of ionic liquid pretreatment on eucalyptus, *Biofuels* 1 (2010) 33–46. <https://doi.org/10.4155/bfs.09.5>.
- [172] A.M. da Costa Lopes, K.G. João, D.F. Rubik, E. Bogel-Lukasik, L.C. Duarte, J. Andreaus, R. Bogel-Lukasik, Pre-treatment of lignocellulosic biomass using ionic liquids: Wheat straw fractionation, *Bioresour. Technol.* 142 (2013) 198–208. <https://doi.org/10.1016/j.biortech.2013.05.032>.
- [173] E.C. Achinivu, R.M. Howard, G. Li, H. Gracz, W.A. Henderson, Lignin extraction from biomass with protic ionic liquids, *Green Chem.* 16 (2014) 1114–1119. <https://doi.org/10.1039/c3gc42306a>.
- [174] E.G.A. Rocha, T.C. Pin, S.C. Rabelo, A.C. Costa, Evaluation of the use of protic ionic liquids on biomass fractionation, *Fuel* 206 (2017) 145–154. <https://doi.org/10.1016/j.fuel.2017.06.014>.
- [175] A.M. Asim, M. Uroos, S. Naz, N. Muhammad, Pyridinium protic ionic liquids: Effective solvents for delignification of wheat straw, *J. Mol. Liq.* 325 (2021) 115013. <https://doi.org/10.1016/j.molliq.2020.115013>.
- [176] R.J. Bernot, M.A. Brueseke, M.A. Evans-White, G.A. Lamberti, Acute and chronic toxicity of imidazolium-based ionic liquids on *Daphnia magna*, 2005. <https://doi.org/10.1897/03-635.1>.
- [177] M.M. and M.G. A. Vijaya Bhaskar Reddy, *Comprehensive Biotechnology*, in: M. Moo-Young (Ed.), *Compr. Biotechnol.*, 3rd ed., Elsevier Science & Technology, Amsterdam, Netherlands, 2019: pp. 190–198. <https://doi.org/10.1016/B978-0-444-64046-8.00121-X>.
- [178] R.C. Remsing, G. Hernandez, R.P. Swatloski, W.W. Masefski, R.D. Rogers, G. Moyna, Solvation of carbohydrates in N,N'-dialkylimidazolium ionic liquids: A multinuclear NMR spectroscopy study, *J. Phys. Chem. B* 112 (2008) 11071–11078. <https://doi.org/10.1021/jp8042895>.
- [179] G. Ebner, S. Schiehser, A. Potthast, T. Rosenau, Side reaction of cellulose with common 1-alkyl-3-methylimidazolium-based ionic liquids, *Tetrahedron Lett.* 49 (2008) 7322–7324. <https://doi.org/10.1016/j.tetlet.2008.10.052>.
- [180] J. Vitz, T. Erdmenger, C. Haensch, U.S. Schubert, Extended dissolution studies of cellulose in imidazolium based ionic liquids, *Green Chem.* 11 (2009) 417–42. <https://doi.org/10.1039/b818061j>.
- [181] R.P. Swatloski, S.K. Spear, J.D. Holbrey, R.D. Rogers, Dissolution of Cellose with Ionic Liquids, *J. AM. CHEM. SOC* 124 (2002) 4974–4975. <https://doi.org/10.1021/ja025790m>.

- [182] L. Feng, Z. Ian Chen, Research progress on dissolution and functional modification of cellulose in ionic liquids, *J. Mol. Liq.* 142 (2008) 1–5. <https://doi.org/10.1016/j.molliq.2008.06.007>.
- [183] W.E.S. Hart, J.B. Harper, L. Aldous, The effect of changing the components of an ionic liquid upon the solubility of lignin, *Green Chem.* 17 (2015) 214–218. <https://doi.org/10.1039/c4gc01888e>.
- [184] A. Brandt, M.J. Ray, T.Q. To, D.J. Leak, R.J. Murphy, T. Welton, Ionic liquid pretreatment of lignocellulosic biomass with ionic liquid–water mixtures, *Green Chem.* 13 (2011) 2489–2499. <https://doi.org/10.1039/c1gc15374a>.
- [185] R.M. Dias, L.C. G Petrin, F.H. B Sosa, M. da Costa Lopes, A.P. Coutinho, M.C. da Costa, Investigation of Kraft Lignin Solubility in Protic Ionic Liquids and Their Aqueous Solutions, *Cite This Ind. Eng. Chem. Res* 59 (2020) 18193–18202. <https://doi.org/10.1021/acs.iecr.0c02605>.
- [186] A. Pinkert, K.N. Marsh, S. Pang, M.P. Staiger, Ionic liquids and their interaction with cellulose, *Chem. Rev.* 109 (2009) 6712–6728. <https://doi.org/10.1021/cr9001947>.
- [187] A. Pinkert, K.N. Marsh, S. Pang, Reflections on the solubility of cellulose, *Ind. Eng. Chem. Res.* 49 (2010) 11121–11130. <https://doi.org/10.1021/ie1006596>.
- [188] H. Zhao, G.A. Baker, Z. Song, O. Olubajo, T. Crittle, D. Peters, Designing enzyme-compatible ionic liquids that can dissolve carbohydrates, *Green Chem.* 10 (2008) 696–70. <https://doi.org/10.1039/b801489b>.
- [189] B. Lu, A. Xu, J. Wang, Cation does matter: How cationic structure affects the dissolution of cellulose in ionic liquids, *Green Chem.* 16 (2014) 1326–1335. <https://doi.org/10.1039/c3gc41733f>.
- [190] M. Zavrel, D. Bross, M. Funke, J. Büchs, A.C. Spiess, High-throughput screening for ionic liquids dissolving (ligno-)cellulose, *Bioresour. Technol.* 100 (2009) 2580–2587. <https://doi.org/10.1016/j.biortech.2008.11.052>.
- [191] H. Wang, G. Gurau, R. Rogers, Dissolution of Biomass Using Ionic Liquids, in: *Struct. Interact. Ion. Liq.*, 2013: pp. 79–105. <https://doi.org/10.1007/978-3-642-38619-0-3>.
- [192] Uju, A. Nakamoto, Y. Shoda, M. Goto, W. Tokuhara, Y. Noritake, S. Katahira, N. Ishida, C. Ogino, N. Kamiya, Low melting point pyridinium ionic liquid pretreatment for enhancing enzymatic saccharification of cellulosic biomass, *Bioresour. Technol.* 135 (2013) 103–108. <https://doi.org/10.1016/j.biortech.2012.06.096>.
- [193] P. Wasserscheid, W. Keim, Ionic liquids - New “solutions” for transition metal catalysis, *Angew. Chemie - Int. Ed.* 39 (2000) 3772–3789. [https://doi.org/10.1002/1521-3773\(20001103\)39:21<3772::aid-anie3772>3.0.co;2-5](https://doi.org/10.1002/1521-3773(20001103)39:21<3772::aid-anie3772>3.0.co;2-5).
- [194] J. Zubeltzu, E. Formoso, E. Rezabal, Lignin solvation by ionic liquids: The role of cation, *J. Mol. Liq.* 303 (2020) 112588. <https://doi.org/10.1016/j.molliq.2020.112588>.
- [195] S. Trivedi, N.I. Malek, K. Behera, S. Pandey, Temperature-dependent solvatochromic probe behavior within ionic liquids and (ionic liquid + water) mixtures, *J. Phys. Chem. B* 114 (2010) 8118–8125. <https://doi.org/10.1021/jp102217u>.
- [196] J.M. Lee, J.M. Prausnitz, Polarity and hydrogen-bond-donor strength for some ionic liquids: Effect of alkyl chain length on the pyrrolidinium cation, *Chem. Phys. Lett.* 492 (2010) 55–59. <https://doi.org/10.1016/j.cplett.2010.03.086>.
- [197] N. Muhammad, Z. Man, M.A. Bustam, M.I.A. Mutalib, C.D. Wilfred, S. Rafiq, Dissolution and

delignification of bamboo biomass using amino acid-based ionic liquid, *Appl. Biochem. Biotechnol.* 165 (2011) 998–1009. <https://doi.org/10.1007/s12010-011-9315-y>.

- [198] D.A.B. Sidik, N. Ngadi, N.A.S. Amin, Optimization of lignin production from empty fruit bunch via liquefaction with ionic liquid, *Bioresour. Technol.* 135 (2013) 690–696. <https://doi.org/10.1016/j.biortech.2012.09.041>.
- [199] N. Sun, M. Rahman, Y. Qin, M.L. Maxim, H. Rodríguez, R.D. Rogers, Complete dissolution and partial delignification of wood in the ionic liquid 1-ethyl-3-methylimidazolium acetate, *Green Chem.* 11 (2009) 646–65. <https://doi.org/10.1039/b822702k>.
- [200] H. Lateef, S. Grimes, P. Kewcharoenwong, B. Feinberg, Separation and recovery of cellulose and lignin using ionic liquids: A process for recovery from paper-based waste, *J. Chem. Technol. Biotechnol.* 84 (2009) 1818–1827. <https://doi.org/10.1002/jctb.2251>.
- [201] C.L. Chambon, V. Fitriyanti, P. Verdía, S.M. Yang, S. Hérou, M.M. Titirici, A. Brandt-Talbot, P.S. Fennell, J.P. Hallett, Fractionation by Sequential Antisolvent Precipitation of Grass, Softwood, and Hardwood Lignins Isolated Using Low-Cost Ionic Liquids and Water, *ACS Sustain. Chem. Eng.* 8 (2020) 3751–3761. <https://doi.org/10.1021/acssuschemeng.9b06939>.
- [202] Y. Yang, M. Zhang, D. Wang, A Comprehensive Investigation on the Effects of Biomass Particle Size in Cellulosic Biofuel Production, *J. Energy Resour. Technol. Trans. ASME* 140 (2018). <https://doi.org/10.1115/1.4039602/367378>.
- [203] Y. Yang, M. Zhang, J. Zhao, D. Wang, Effects of particle size on biomass pretreatment and hydrolysis performances in bioethanol conversion, *Biomass Convers. Biorefinery* 13 (2023) 13023–13036. <https://doi.org/10.1007/S13399-021-02169-3/FIGURES/7>.
- [204] P. Weerachanchai, S.S.J. Leong, M.W. Chang, C.B. Ching, J.M. Lee, Improvement of biomass properties by pretreatment with ionic liquids for bioconversion process, *Bioresour. Technol.* 111 (2012) 453–459. <https://doi.org/10.1016/j.biortech.2012.02.023>.
- [205] D. Fu, G. Mazza, Optimization of processing conditions for the pretreatment of wheat straw using aqueous ionic liquid, *Bioresour. Technol.* 102 (2011) 8003–8010. <https://doi.org/10.1016/j.biortech.2011.06.023>.
- [206] C.L. Chambon, P. Verdía, P.S. Fennell, J.P. Hallett, Process intensification of the ionic liquid pretreatment: effects of biomass loading, particle size and scale-up from 10 mL to 1 L, *Sci. Rep.* 11 (2021) 15383. <https://doi.org/10.1038/s41598-021-94629-z>.
- [207] H.T. Tan, K.T. Lee, Understanding the impact of ionic liquid pretreatment on biomass and enzymatic hydrolysis, *Chem. Eng. J.* 183 (2012) 448–458. <https://doi.org/10.1016/j.cej.2011.12.086>.
- [208] S. Negi, A.K. Pandey, Ionic Liquid Pretreatment, in: *Pretreat. Biomass Process. Technol.*, Elsevier Inc., 2015: pp. 137–155. <https://doi.org/10.1016/B978-0-12-800080-9.00008-6>.
- [209] A.G. Cruz, C. Scullin, C. Mu, G. Cheng, V. Stavila, P. Varanasi, D. Xu, J. Mentel, Y. De Chuang, B.A. Simmons, S. Singh, Impact of high biomass loading on ionic liquid pretreatment, *Biotechnol. Biofuels* 6 (2013) 52. <https://doi.org/10.1186/1754-6834-6-52>.
- [210] K. Ninomiya, K. Inoue, Y. Aomori, A. Ohnishi, C. Ogino, N. Shimizu, K. Takahashi, Characterization of fractionated biomass component and recovered ionic liquid during repeated process of cholinium ionic liquid-assisted pretreatment and fractionation, *Chem. Eng. J.* 259 (2015) 323–329. <https://doi.org/10.1016/j.cej.2014.07.122>.
- [211] R. Financie, M. Moniruzzaman, Y. Uemura, Enhanced enzymatic delignification of oil palm

biomass with ionic liquid pretreatment, *Biochem. Eng. J.* 110 (2016) 1–7.
<https://doi.org/10.1016/j.bej.2016.02.008>.

- [212] P. Weerachanchai, K.H. Lim, J.M. Lee, Influence of organic solvent on the separation of an ionic liquid from a lignin-ionic liquid mixture, *Bioresour. Technol.* 156 (2014) 404–407.
<https://doi.org/10.1016/j.biortech.2014.01.077>.
- [213] J.Y. Kim, E.J. Shin, I.Y. Eom, K. Won, Y.H. Kim, D. Choi, I.G. Choi, J.W. Choi, Structural features of lignin macromolecules extracted with ionic liquid from poplar wood, *Bioresour. Technol.* 102 (2011) 9020–9025. <https://doi.org/10.1016/j.biortech.2011.07.081>.
- [214] J.A. Perez-Pimienta, M.G. Lopez-Ortega, P. Varanasi, V. Stavila, G. Cheng, S. Singh, B.A. Simmons, Comparison of the impact of ionic liquid pretreatment on recalcitrance of agave bagasse and switchgrass, *Bioresour. Technol.* 127 (2013) 18–24.
<https://doi.org/10.1016/j.biortech.2012.09.124>.
- [215] J.G. Lynam, M. Toufiq Reza, V.R. Vasquez, C.J. Coronella, Pretreatment of rice hulls by ionic liquid dissolution, *Bioresour. Technol.* 114 (2012) 629–636.
<https://doi.org/10.1016/j.biortech.2012.03.004>.
- [216] N. Labbé, L.M. Kline, L. Moens, K. Kim, P.C. Kim, D.G. Hayes, Activation of lignocellulosic biomass by ionic liquid for biorefinery fractionation, *Bioresour. Technol.* 104 (2012) 701–707.
<https://doi.org/10.1016/j.biortech.2011.10.062>.
- [217] L.T.P. Trinh, Y.J. Lee, J.W. Lee, H.J. Lee, Characterization of ionic liquid pretreatment and the bioconversion of pretreated mixed softwood biomass, *Biomass and Bioenergy* 81 (2015) 1–8.
<https://doi.org/10.1016/j.biombioe.2015.05.005>.
- [218] C. Li, L. Sun, B.A. Simmons, S. Singh, Comparing the Recalcitrance of Eucalyptus, Pine, and Switchgrass Using Ionic Liquid and Dilute Acid Pretreatments, *Bioenergy Res.* 6 (2013) 14–23.
<https://doi.org/10.1007/s12155-012-9220-4>.
- [219] Uju, Y. Shoda, A. Nakamoto, M. Goto, W. Tokuhara, Y. Noritake, S. Katahira, N. Ishida, K. Nakashima, C. Ogino, N. Kamiya, Short time ionic liquids pretreatment on lignocellulosic biomass to enhance enzymatic saccharification, *Bioresour. Technol.* 103 (2012) 446–452.
<https://doi.org/10.1016/j.biortech.2011.10.003>.
- [220] G. Yang, X. Luo, L. Shuai, Bioinspired Cellulase-Mimetic Solid Acid Catalysts for Cellulose Hydrolysis, *Front. Bioeng. Biotechnol.* 9 (2021). <https://doi.org/10.3389/FBIOE.2021.770027>.
- [221] F. Liu, K. Huang, A. Zheng, F.S. Xiao, S. Dai, Hydrophobic Solid Acids and Their Catalytic Applications in Green and Sustainable Chemistry, *ACS Catal.* 8 (2018) 372–391.
https://doi.org/10.1021/ACSCATAL.7B03369/ASSET/IMAGES/LARGE/CS-2017-03369E_0028.JPEG.
- [222] L. Vilcocq, P.C. Castilho, F. Carneiro, L.C. Duarte, Hydrolysis of Oligosaccharides Over Solid Acid Catalysts: A Review, *ChemSusChem* 7 (2014) 1010–1019.
<https://doi.org/10.1002/CSSC.201300720>.
- [223] A. Shrotri, H. Kobayashi, A. Fukuoka, Cellulose Depolymerization over Heterogeneous Catalysts, *Acc. Chem. Res.* 51 (2018) 761–768.
<https://doi.org/10.1021/ACS.ACCOUNTS.7B00614>.
- [224] Y. Patiño, L. Faba, R. Peláez, J. Cueto, P. Marín, E. Díaz, S. Ordóñez, The Role of Ion Exchange Resins for Solving Biorefinery Catalytic Processes Challenges, *Multidisciplinary Digital Publishing Institute*, 2023. <https://doi.org/10.3390/catal13060999>.

- [225] A.M. Da Costa Lopes, M. Brenner, P. Falé, L.B. Roseiro, R. Bogel-Lukasik, Extraction and Purification of Phenolic Compounds from Lignocellulosic Biomass Assisted by Ionic Liquid, Polymeric Resins, and Supercritical CO₂, *ACS Sustain. Chem. Eng.* 4 (2016) 3357–3367. <https://doi.org/10.1021/acssuschemeng.6b00429>.
- [226] C.H. Ma, Y.G. Zu, L. Yang, J. Li, Two solid-phase recycling method for basic ionic liquid [C4mim]Ac by macroporous resin and ion exchange resin from *Schisandra chinensis* fruits extract, *J. Chromatogr. B Anal. Technol. Biomed. Life Sci.* 976–977 (2015) 1–5. <https://doi.org/10.1016/j.jchromb.2014.11.003>.
- [227] S. Singh, B.A. Simmons, Ionic Liquid Pretreatment: Mechanism, Performance, and Challenges, in: *Aqueous Pretreat. Plant Biomass Biol. Chem. Convers. to Fuels Chem.*, John Wiley & Sons, Ltd, 2013: pp. 223–238. <https://doi.org/10.1002/9780470975831.ch11>.
- [228] Y. Cao, R. Zhang, T. Cheng, J. Guo, M. Xian, H. Liu, Imidazolium-based ionic liquids for cellulose pretreatment: recent progresses and future perspectives, *Appl. Microbiol. Biotechnol.* 101 (2017) 521–532. <https://doi.org/10.1007/s00253-016-8057-8>.
- [229] ASTM International, ASTM E1757-01 Standard Preparation of Biomass for Compositional Analysis, *ASTM Int.* 01 (2015) 1–4. <https://www.astm.org/DATABASE.CART/HISTORICAL/E1757-01R15.htm> (accessed March 15, 2021).
- [230] S.M.S.N.S. Zahari, H. Azman, L. Karim, Triethylammonium hydrogen sulfate ionic liquid as a low-cost solvent: A short review of synthesis, analysis and applications, *MATEC Web Conf.* 204 (2018). <https://doi.org/10.1051/mateconf/201820400006>.
- [231] F.J.V. Gschwend, A. Brandt, C.L. Chambon, W.C. Tu, L. Weigand, J.P. Hallett, Pretreatment of lignocellulosic biomass with low-cost ionic liquids, *J. Vis. Exp.* 2016 (2016) 54246. <https://doi.org/10.3791/54246>.
- [232] P. Attri, R. Bhatia, J. Gaur, B. Arora, A. Gupta, N. Kumar, E.H. Choi, Triethylammonium acetate ionic liquid assisted one-pot synthesis of dihydropyrimidinones and evaluation of their antioxidant and antibacterial activities, *Arab. J. Chem.* 10 (2017) 206–214. <https://doi.org/10.1016/j.arabjc.2014.05.007>.
- [233] F.J.V. Gschwend, J.P. Hallett, A. Brandt-Talbot, Exploring the effect of water content and anion on the pretreatment of poplar with three 1-Ethyl-3-methylimidazolium ionic liquids, *Molecules* 25 (2020). <https://doi.org/10.3390/molecules25102318>.
- [234] ASTM International, Standard Test Method for Water Using Volumetric Karl Fischer Titration, *ASTM Int.* (2016) 1–9. <https://www.astm.org/e0203-16.html> (accessed May 10, 2023).
- [235] METTLER TOLEDO, Good Titration Practice™ in Karl Fischer Titration, Columbus, 2011. https://www.mt.com/dam/MT-NA/KarlFischerHelpPage/GTP_KarlFischer.pdf (accessed May 12, 2023).
- [236] A. Lucio, How It Works: The Karl Fischer Titration, Iowa, 2013. http://www.emdmillipore.com/chemicals/aquastar-karl-fischer-faqs-and-tech-notes/c_yPab.s1OEMgAAAEiPkg7mMef (accessed May 12, 2023).
- [237] Y.D. Singh, Determination of Carbohydrate Composition in Lignocellulosic Biomass for Biofuel Production, *Preprints* (2018) 1–6. <https://doi.org/10.20944/PREPRINTS201809.0419.V1>.
- [238] J. Cai, D. Xu, Z. Dong, X. Yu, Y. Yang, S.W. Banks, A. V. Bridgwater, Processing thermogravimetric analysis data for isoconversional kinetic analysis of lignocellulosic biomass

pyrolysis: Case study of corn stalk, *Renew. Sustain. Energy Rev.* 82 (2018) 2705–2715. <https://doi.org/10.1016/j.rser.2017.09.113>.

- [239] K.T. Klasson, Biochar characterization and a method for estimating biochar quality from proximate analysis results, *Biomass and Bioenergy* 96 (2017) 50–58. <https://doi.org/10.1016/j.biombioe.2016.10.011>.
- [240] J. Parikh, S.A. Channiwala, G.K. Ghosal, A correlation for calculating elemental composition from proximate analysis of biomass materials, *Fuel* 86 (2007) 1710–1719. <https://doi.org/10.1016/j.fuel.2006.12.029>.
- [241] J. Parikh, S.A. Channiwala, G.K. Ghosal, A correlation for calculating HHV from proximate analysis of solid fuels, *Fuel* 84 (2005) 487–494. <https://doi.org/https://doi.org/10.1016/j.fuel.2004.10.010>.
- [242] ASTM International, ASTM E1756-08 Standard Test Method for Determination of Total Solids in Biomass, *ASTM Int.* (2015) 1–3. <https://www.astm.org/DATABASE.CART/HISTORICAL/E1756-08R15.htm> (accessed March 15, 2021).
- [243] ASTM, Standard test method for ash in biomass E1755 - 01, *Astm* 44 (2015) 153–161. <http://dx.doi.org/10.1016/j.biortech.2014.03.009> <http://dx.doi.org/10.1016/j.biortech.2014.08.121> <http://www.scrip.org/journal/PaperDownload.aspx?DOI=10.4236/ajac.2011.27095> <http://dx.doi.org/10.1016/j.foodres.2011.04.040> <http://dx.doi.org/10.1016/j.foodres.2011.04.040> (accessed March 15, 2021).
- [244] N. Aniza, S. Hassan, M. Inayat, Thermogravimetric kinetic analysis of Malaysian poultry processing waste material under inert and oxidative atmospheres, *J. Mech. Eng. Sci.* 10 (2016) 2289–4659. <https://doi.org/10.15282/jmes.10.2.2016.1.0185>.
- [245] R. García, C. Pizarro, A.G. Lavín, J.L. Bueno, Biomass proximate analysis using thermogravimetry, *Bioresour. Technol.* 139 (2013) 1–4. <https://doi.org/10.1016/j.biortech.2013.03.197>.
- [246] M. Zhang, F.L.P. Resende, A. Moutsoglou, D.E. Raynie, Pyrolysis of lignin extracted from prairie cordgrass, aspen, and Kraft lignin by Py-GC/MS and TGA/FTIR, *J. Anal. Appl. Pyrolysis* 98 (2012) 65–71. <https://doi.org/10.1016/j.jaap.2012.05.009>.
- [247] N. Chen, T. Degnan, L.R. Koenig, Liquid fuel from carbohydrates, *Chemtech* 16 (1986) 506–511.
- [248] A. Nzihou, *Handbook on characterization of biomass, biowaste and related by-products*, 1st Editio, Springer Nature Switzerland AG, Cham, Switzerland, 2020. <https://doi.org/10.1007/978-3-030-35020-8>.
- [249] TRACES Centre, Thermal Conductivity Detector, TRACES Cent. (2020) 1–2. https://www.utsc.utoronto.ca/~traceslab/PDFs/GC_TCD.pdf (accessed May 3, 2023).
- [250] H. Laajimi, F. Galli, G.S. Patience, D. Schieppati, Experimental methods in chemical engineering: Gas chromatography—GC, *Can. J. Chem. Eng.* 100 (2022) 3123–3144. <https://doi.org/10.1002/cjce.24395>.
- [251] A. Friedl, E. Padouvas, H. Rotter, K. Varmuza, Prediction of heating values of biomass fuel from elemental composition, *Anal. Chim. Acta* 544 (2005) 191–198. <https://doi.org/10.1016/J.ACA.2005.01.041>.
- [252] S.A. Channiwala, P.P. Parikh, A unified correlation for estimating HHV of solid, liquid and gaseous fuels, *Fuel* 81 (2002) 1051–1063. [https://doi.org/10.1016/S0016-2361\(01\)00131-4](https://doi.org/10.1016/S0016-2361(01)00131-4).

- [253] S. Nanda, P. Mohanty, K.K. Pant, S. Naik, J.A. Kozinski, A.K. Dalai, Characterization of North American Lignocellulosic Biomass and Biochars in Terms of their Candidacy for Alternate Renewable Fuels, *Bioenergy Res.* 6 (2013) 663–677. <https://doi.org/10.1007/s12155-012-9281-4>.
- [254] G.S.P. D.C. Boffito, C. Neagoe, G. Cerrato, C. Boffito, G.L. Chiarello, C.L. Bianchi, M.G. Rigamonti, A. Benamer, Chapter 11 Spectroscopy, in: G.S. Patience (Ed.), *Exp. Methods Instrum. Chem. Eng., Second Edi*, Elsevier, 2018: pp. 339–383. <https://www.sciencedirect.com/science/article/abs/pii/B9780444637826000112>.
- [255] J. Coates, Interpretation of Infrared Spectra, A Practical Approach, in: *Encycl. Anal. Chem.*, 2006: pp. 10815–10837. <https://doi.org/10.1002/9780470027318.a5606>.
- [256] A. Ferrer, C. Alciaturi, A. Faneite, J. Ríos, Analyses of biomass fibers by XRD, FT-IR, and NIR, in: *Anal. Tech. Methods Biomass*, Springer International Publishing, 2016: pp. 45–83. <https://doi.org/973385>.
- [257] N. Thermo, *Introduction to Fourier Transform Infrared Spectrometry*. Thermo Nicolet Corporation, 2001.
- [258] www.perkinelmer.com, FTIR Spectroscopy: Attenuated Total Reflectance (ATR), [Www.Perkinelmer.Com](http://www.perkinelmer.com) (n.d.). https://cmdis.rpi.edu/sites/default/files/ATR_FTIR.pdf (accessed May 4, 2023).
- [259] Thermo Fisher Scientific Inc, High Speed, High-Sensitivity Detectors for Use in the Mid-Infrared Spectral Range, 2007. [https://mmrc.caltech.edu/FTIR/Nicolet/Nicolet Tech Notes/MCT detector Thermo.pdf](https://mmrc.caltech.edu/FTIR/Nicolet/Nicolet%20Tech%20Notes/MCT%20detector%20Thermo.pdf) (accessed March 13, 2021).
- [260] Bruker, *Innovation with Integrity D8 Series User Manual D8 ADVANCE / D8 DISCOVER Original Instructions*, Kalsruhe, 2010. http://nanoqam.ca/wiki/lib/exe/fetch.php?media=d8_advance_discover_user_manual_vol._1_do_c-m88-exx153_v6.pdf (accessed May 8, 2023).
- [261] V.K. Pecharsky, P.Y. Zavalij, *Fundamentals of powder diffraction and structural characterization of materials*, 1st ed., Springer New York, NY, New York, 2005. <https://doi.org/10.1007/b106242>.
- [262] A. Thygesen, J. Oddershede, H. Lilholt, A.B. Thomsen, K. Ståhl, On the determination of crystallinity and cellulose content in plant fibres, *Cellulose* 12 (2005) 563–576. <https://doi.org/10.1007/s10570-005-9001-8>.
- [263] J. He, S. Cui, S.Y. Wang, Preparation and crystalline analysis of high-grade bamboo dissolving pulp for cellulose acetate, *J. Appl. Polym. Sci.* 107 (2008) 1029–1038. <https://doi.org/10.1002/app.27061>.
- [264] S. Park, J.O. Baker, M.E. Himmel, P.A. Parilla, D.K. Johnson, *Cellulose crystallinity index: Measurement techniques and their impact on interpreting cellulase performance*, 2010. <https://doi.org/10.1186/1754-6834-3-10>.
- [265] P. University, *Scanning Electron Microscope - Radiological and Environmental Management - Purdue University*, Purdue Univ. (2023) 1. [https://www.purdue.edu/ehps/rem/laboratory/equipment safety/Research Equipment/sem.html](https://www.purdue.edu/ehps/rem/laboratory/equipment%20safety/Research%20Equipment/sem.html) (accessed May 8, 2023).
- [266] C. Scheu, W.D. Kaplan, *Introduction to Scanning Electron Microscopy*, San Jose, 2012. <https://doi.org/10.1002/9783527652167.ch1>.
- [267] D.C. Joy, *Introduction to the scanning electron microscope*, Davis, 2003.

<https://doi.org/10.1017/s1431927603447788>.

- [268] M. Kannan, Scanning Electron Microscopy: Principle, Components and Applications, in: Phys. Princ. Electron Microsc., 2018: pp. 81–92.
- [269] Gossman Forensics, How Does Scanning Electron Microscope / Energy Dispersive X-ray (SEM / EDX) Work ?, 2012. <https://www.gossmanforensics.com/pdf-library/pdf-analytical-methods/sem-edx.pdf> (accessed May 8, 2023).
- [270] K. Rajan, D.J. Carrier, Effect of dilute acid pretreatment conditions and washing on the production of inhibitors and on recovery of sugars during wheat straw enzymatic hydrolysis, Biomass and Bioenergy 62 (2014) 222–227. <https://doi.org/10.1016/j.biombioe.2014.01.013>.
- [271] J. Singh, M. Suhag, A. Dhaka, Augmented digestion of lignocellulose by steam explosion, acid and alkaline pretreatment methods: A review, Carbohydr. Polym. 117 (2015) 624–631. <https://doi.org/10.1016/j.carbpol.2014.10.012>.
- [272] U. Dziekońska-Kubczak, J. Berłowska, P. Dziugan, P. Patelski, M. Balcerek, K. Pielech-Przybylska, A. Czyzowska, J. Domański, Comparison of steam explosion, dilute acid, and alkali pretreatments on enzymatic saccharification and fermentation of hardwood sawdust, BioResources 13 (2018) 6970–6984. <https://doi.org/10.15376/biores.13.3.6970-6984>.
- [273] P. Sannigrahi, A.J. Ragauskas, S.J. Miller, Effects of Two-Stage Dilute Acid Pretreatment on the Structure and Composition of Lignin and Cellulose in Loblolly Pine, BioEnergy Res. 2008 13 1 (2008) 205–214. <https://doi.org/10.1007/S12155-008-9021-Y>.
- [274] D. Watkins, M. Nuruddin, M. Hosur, A. Tcherbi-Narteh, S. Jeelani, Extraction and characterization of lignin from different biomass resources, J. Mater. Res. Technol. 4 (2015) 26–32. <https://doi.org/10.1016/J.JMRT.2014.10.009>.
- [275] F. Hu, A. Ragauskas, Suppression of pseudo-lignin formation under dilute acid pretreatment conditions, RSC Adv. 4 (2014) 4317–4323. <https://doi.org/10.1039/c3ra42841a>.
- [276] Dow-Lenntech, Dow-Rohm-Haas-Amberlyst-70-Strongly-Acidic-Catalyst-Lenntech, 2006. www.lenntech.com Fax. +31-152-616-289 info@lenntech.com Tel. +31-152-610-900 www.lenntech.com Fax. (accessed September 8, 2022).
- [277] Dow-Lenntech, AMBERLYST™ 35WET Industrial Grade Strongly Acidic Catalyst, 2006. www.lenntech.com Fax. +31-152-616-289 info@lenntech.com Tel. +31-152-610-900 www.lenntech.com Fax. (accessed September 8, 2022).
- [278] P.F. Siril, H.E. Cross, D.R. Brown, New polystyrene sulfonic acid resin catalysts with enhanced acidic and catalytic properties, J. Mol. Catal. A Chem. 279 (2008) 63–68. <https://doi.org/10.1016/j.molcata.2007.10.001>.
- [279] N.E. Yates, A.B. Riche, I. Shield, M. Zapater, F. Ferchaud, G. Ragalini, N. Roncucci, Investigating the Longterm Biomass Yield of Miscanthus Giganteus and Switchgrass When Harvested As a Green Energy Feedstock, in: Pap. 23Rd Eur. Biomass Conf. Setting Course a Biobased Econ., 2015: pp. 61–67.
- [280] E. Khullar, Miscanthus conversion to ethanol: effect of particle size and pretreatment conditions for hot water (Thesis), University of Illinois, 2012. <https://core.ac.uk/download/pdf/10200916.pdf> (accessed October 12, 2021).
- [281] C. Wang, Y. Kong, R. Hu, G. Zhou, Miscanthus: A fast-growing crop for environmental remediation and biofuel production, GCB Bioenergy 13 (2021) 58–69. <https://doi.org/10.1111/gcbb.12761>.

- [282] N.A. Boakye-Boaten, S. Xiu, G. Shahbazi, J. Fabish, Liquid Hot Water Pretreatment of *Miscanthus X giganteus* for the Sustainable Production of Bioethanol, *BioResources* 10 (2015). <https://doi.org/10.15376/biores.10.3.5890-5905>.
- [283] T. van der Weijde, A.F. Torres, O. Dolstra, A. Dechesne, R.G.F. Visser, L.M. Trindade, Impact of Different Lignin Fractions on Saccharification Efficiency in Diverse Species of the Bioenergy Crop *Miscanthus*, *Bioenergy Res.* 9 (2016) 146–156. <https://doi.org/10.1007/s12155-015-9669-z>.
- [284] B. Godin Richard Agneessens Patrick Gerin Jérôme Delcarte, P. Gerin, Lignin in plant biomasses: comparative metrological assessment of the detergent fiber and the insoluble dietary fiber methods, *Cellulose* 22 (2015) 2325–2340. <https://doi.org/10.1007/s10570-015-0656-5>.
- [285] S. Collura, B. Azambre, J.V. Weber, Thermal behavior of *Miscanthus* grasses, an alternative biological fuel, *Environ. Chem. Lett.* 3 (2005) 95–99. <https://doi.org/10.1007/s10311-005-0007-0>.
- [286] H.Q. Li, C.L. Li, T. Sang, J. Xu, Pretreatment on *Miscanthus lutarioriparius* by liquid hot water for efficient ethanol production, *Biotechnol. Biofuels* 6 (2013) 1–10. <https://doi.org/10.1186/1754-6834-6-76>.
- [287] C. Antonetti, A.M. Raspolli Galletti, S. Fulignati, D. Licursi, Amberlyst A-70: A surprisingly active catalyst for the MW-assisted dehydration of fructose and inulin to HMF in water, *Catal. Commun.* 97 (2017) 146–150. <https://doi.org/10.1016/j.catcom.2017.04.032>.
- [288] S. Collura, B. Azambre, G. Finqueneisel, T. Zimny, J.V. Weber, *Miscanthus × Giganteus* straw and pellets as sustainable fuels: Combustion and emission tests, *Environ. Chem. Lett.* 4 (2006) 75–78. <https://doi.org/10.1007/s10311-006-0036-3>.
- [289] A.M. Cortés, A. V. Bridgwater, Kinetic study of the pyrolysis of *miscanthus* and its acid hydrolysis residue by thermogravimetric analysis, *Fuel Process. Technol.* 138 (2015) 184–193. <https://doi.org/10.1016/j.fuproc.2015.05.013>.
- [290] R.C. Brown, Thermochemical processing of biomass : conversion into fuels, chemicals and power, 1st Editio, John Wiley and Sons, Limited, 2011., Chichester, West Sussex, 2011. <https://eds.a.ebscohost.com/eds/detail/detail?vid=2&sid=86b3fb50-74d2-435d-ad1a-336dd4fbcfa1%40sessionmgr4006&bdata=JnNpdGU9ZWRzLWxpdmU%3D#db=cat00594a&AN=aston.b1535772> (accessed November 13, 2020).
- [291] A.A. Awoyale, D. Lokhat, P. Okete, Investigation of the effects of pretreatment on the elemental composition of ash derived from selected Nigerian lignocellulosic biomass, *Sci. Rep.* 11 (2021) 21313. <https://doi.org/10.1038/s41598-021-00672-1>.
- [292] V.D. Zheljaskov, C.L. Cantrell, T. Astatkie, J.B. Cannon, Lemongrass productivity, oil content, and composition as a function of nitrogen, sulfur, and harvest time, *Agron. J.* 103 (2011) 805–812. <https://doi.org/10.2134/agronj2010.0446>.
- [293] L. Talukdar, J. Hussain, S. Dutta, P. Dutta, Nitrogen and Sulphur interaction on nutrient use efficiency in field crops: A review, ~ 1372 ~ *Pharma Innov. J.* 11 (2022) 1372–1376. <http://www.thepharmajournal.com> (accessed August 20, 2024).
- [294] M. Jeguirim, S. Dorge, G. Trouvé, Thermogravimetric analysis and emission characteristics of two energy crops in air atmosphere: *Arundo donax* and *Miscanthus giganthus*, *Bioresour. Technol.* 101 (2010) 788–793. <https://doi.org/https://doi.org/10.1016/j.biortech.2009.05.063>.
- [295] L. Sanchez-Silva, D. López-González, J. Villaseñor, P. Sánchez, J.L. Valverde,

Thermogravimetric–mass spectrometric analysis of lignocellulosic and marine biomass pyrolysis, *Bioresour. Technol.* 109 (2012) 163–172.
<https://doi.org/https://doi.org/10.1016/j.biortech.2012.01.001>.

- [296] M. Jeguirim, S. Dorge, A. Loth, G. Trouvé, Devolatilization kinetics of miscanthus straw from thermogravimetric analysis, *Int. J. Green Energy* 7 (2010) 164–173.
<https://doi.org/10.1080/15435071003673641>.
- [297] R. Rinaldi, N. Meine, J. vom Stein, R. Palkovits, F. Schüth, Which controls the depolymerization of cellulose in ionic liquids: The solid acid catalyst or cellulose?, *ChemSusChem* 3 (2010) 266–276. <https://doi.org/10.1002/cssc.200900281>.
- [298] B.H. Davison, J. Parks, M.F. Davis, B.S. Donohoe, Plant Cell Walls: Basics of Structure, Chemistry, Accessibility and the Influence on Conversion, Aqueous Pretreat. *Plant Biomass Biol. Chem. Convers. to Fuels Chem.* (2013) 23–38.
<https://doi.org/https://doi.org/10.1002/9780470975831.ch3>.
- [299] O.O. Babich, O. V. Krieger, E.G. Chupakhin, O. V. Kozlova, Miscanthus plants processing in fuel, energy, chemical and microbiological industries, *Foods Raw Mater.* 7 (2019).
<https://doi.org/10.21603/2308-4057-2019-2-403-411>.
- [300] M. Yoshida, Y. Liu, S. Uchida, K. Kawarada, Y. Ukagami, H. Ichinose, S. Kaneko, K. Fukuda, Effects of cellulose crystallinity, hemicellulose, and lignin on the enzymatic hydrolysis of *Miscanthus sinensis* to monosaccharides, *Biosci. Biotechnol. Biochem.* 72 (2008) 805–810.
<https://doi.org/10.1271/bbb.70689>.
- [301] M. Dash, K. Mohanty, Effect of different ionic liquids and anti-solvents on dissolution and regeneration of *Miscanthus* towards bioethanol, *Biomass and Bioenergy* 124 (2019) 33–42.
<https://doi.org/10.1016/j.biombioe.2019.03.006>.
- [302] N. Xu, W. Zhang, S. Ren, F. Liu, C. Zhao, H. Liao, Z. Xu, J. Huang, Q. Li, Y. Tu, B. Yu, Y. Wang, J. Jiang, J. Qin, L. Peng, Hemicelluloses negatively affect lignocellulose crystallinity for high biomass digestibility under NaOH and H₂SO₄ pretreatments in *Miscanthus*, *Biotechnol. Biofuels* 5 (2012) 1–12. <https://doi.org/10.1186/1754-6834-5-58>.
- [303] M.A. Haque, D.N. Barman, T.H. Kang, M.K. Kim, J. Kim, H. Kim, H.D. Yun, Effect of dilute alkali pretreatment on structural features and enhanced enzymatic hydrolysis of *Miscanthus sinensis* at boiling temperature with low residence time, *Biosyst. Eng.* 114 (2013) 294–305.
<https://doi.org/10.1016/j.biosystemseng.2013.01.006>.
- [304] A.I. Osman, A.T. Ahmed, C.R. Johnston, D.W. Rooney, Physicochemical characterization of miscanthus and its application in heavy metals removal from wastewaters, *Environ. Prog. Sustain. Energy* 37 (2018) 1058–1067. <https://doi.org/10.1002/ep.12783>.
- [305] M. Dash, V. Venkata Dasu, K. Mohanty, Physico-chemical characterization of *Miscanthus*, *Castor*, and *Jatropha* towards biofuel production, *J. Renew. Sustain. Energy* 7 (2015).
<https://doi.org/10.1063/1.4926577>.
- [306] C. Kundu, S.P. Samudrala, M.A. Kibria, S. Bhattacharya, One-step peracetic acid pretreatment of hardwood and softwood biomass for platform chemicals production, *Sci. Rep.* 11 (2021) 11183. <https://doi.org/10.1038/s41598-021-90667-9>.
- [307] S.D. Kshirsagar, P.R. Waghmare, P. Chandrakant Loni, S.A. Patil, S.P. Govindwar, Dilute acid pretreatment of rice straw, structural characterization and optimization of enzymatic hydrolysis conditions by response surface methodology, *RSC Adv.* 5 (2015) 46525–46533.
<https://doi.org/10.1039/c5ra04430h>.

- [308] B.P. Rocky, A.J. Thompson, Characterization of the crystallographic properties of bamboo plants, natural and viscose fibers by X-ray diffraction method, *J. Text. Inst.* 112 (2021) 1295–1303. <https://doi.org/10.1080/00405000.2020.1813407>.
- [309] P.Y. Bruice, *Beauchamp Spectroscopy Tables 1*, 2011. http://www.cpp.edu/~psbeauchamp/pdf/spec_ir_nmr_spectra_tables.pdf (accessed March 12, 2021).
- [310] Sigma Aldrich, IR Spectrum Table & Chart | Sigma-Aldrich, IR Spectr. Table Chart (2018) 1. <https://www.sigmaaldrich.com/technical-documents/articles/biology/ir-spectrum-table.html> (accessed March 13, 2021).
- [311] J. Grams, M. Kwapińska, M. Jędrzejczyk, I. Rzeźnicka, J.J. Leahy, A.M. Ruppert, Surface characterization of *Miscanthus × giganteus* and Willow subjected to torrefaction, *J. Anal. Appl. Pyrolysis* 138 (2019) 231–241. <https://doi.org/10.1016/j.jaap.2018.12.028>.
- [312] T. Mimmo, P. Panzacchi, M. Baratieri, C.A. Davies, G. Tonon, Effect of pyrolysis temperature on *Miscanthus × giganteus* biochar physical, chemical and functional properties, *Biomass and Bioenergy* 62 (2014) 149–157. <https://doi.org/10.1016/j.biombioe.2014.01.004>.
- [313] S. Nuramirah, R.M. Zaki, I. Buniyamin, M.R. Mahmood, M.N. Zakaria, Characterization of Microcrystalline Cellulose Isolated from Paper Sludge, *Environ. Proc. J.* 9 (2024) 455–460. <https://doi.org/10.21834/E-BPJ.V9ISI17.5449>.
- [314] N. Montoya-Escobar, D. Ospina-Acero, J.A. Velásquez-Cock, C. Gómez-Hoyos, A. Serpa Guerra, P.F. Gañan Rojo, L.M. Vélez Acosta, J.P. Escobar, N. Correa-Hincapié, O. Triana-Chávez, R. Zuluaga Gallego, P.M. Stefani, Use of Fourier Series in X-ray Diffraction (XRD) Analysis and Fourier-Transform Infrared Spectroscopy (FTIR) for Estimation of Crystallinity in Cellulose from Different Sources, *Polymers (Basel)*. 14 (2022) 5199. <https://doi.org/10.3390/POLYM14235199/S1>.
- [315] J. Qi, Y. Hou, J. Liu, Z. Yuan, J. Fang, Z. Fang, H. Li, Alkali lignin as a pH response bifunctional material with both adsorption and flocculation for wastewater treatment, *Holzforschung* 76 (2022) 1032–1043. https://doi.org/10.1515/HF-2022-0117/DOWNLOADASSET/SUPPL/J_HF-2022-0117_SUPPL.DOCX.
- [316] T. Nejat, R. Naghdi, E. Nadali, P. Asgharzadeh Avajeghi, R. Jafari, Effects of nanoclay cloisite 20A and alkali treatments on structure-property relationships of bagasse/recycled polypropylene nanocomposites, *J. Thermoplast. Compos. Mater.* 37 (2024) 310–335. https://doi.org/10.1177/08927057231170802/ASSET/IMAGES/LARGE/10.1177_08927057231170802-FIG7.JPEG.
- [317] J.E. Lee, Y.N. Guragain, K.P. Bastola, P. V. Vadlani, Innovative methods to generate clean sugar stream from biomass feedstocks for efficient fermentation, *Bioprocess Biosyst. Eng.* 40 (2017) 633–641. <https://doi.org/10.1007/s00449-016-1727-1>.
- [318] W. de Carvalho, L. Canilha, S.I. Mussatto, G. Dragone, M.L.V. Morales, A.I.N. Solenzal, Detoxification of sugarcane bagasse hemicellulosic hydrolysate with ion-exchange resins for xylitol production by calcium alginate-entrapped cells, *J. Chem. Technol. Biotechnol.* 79 (2004) 863–868. <https://doi.org/10.1002/jctb.1061>.
- [319] G.T. Jeong, S.K. Kim, B.R. Oh, Production of fermentable sugars from *Chlorella* sp. by solid-acid catalyst, *Algal Res.* 51 (2020) 102044. <https://doi.org/10.1016/j.algal.2020.102044>.
- [320] G.L. Guo, D.C. Hsu, W.H. Chen, W.H. Chen, W.S. Hwang, Characterization of enzymatic saccharification for acid-pretreated lignocellulosic materials with different lignin composition,

- Enzyme Microb. Technol. 45 (2009) 80–87. <https://doi.org/10.1016/j.enzmictec.2009.05.012>.
- [321] P. Lenihan, A. Orozco, E. O'Neill, M.N.M. Ahmad, D.W. Rooney, G.M. Walker, Dilute acid hydrolysis of lignocellulosic biomass, *Chem. Eng. J.* 156 (2010) 395–403. <https://doi.org/10.1016/j.cej.2009.10.061>.
- [322] Y. Huang, Z. Wei, X. Yin, C. Wu, Pyrolytic characteristics of biomass acid hydrolysis residue rich in lignin, *Bioresour. Technol.* 103 (2012) 470–476. <https://doi.org/10.1016/j.biortech.2011.10.027>.
- [323] D. Chen, Y. Wang, Y. Liu, K. Cen, X. Cao, Z. Ma, Y. Li, Comparative study on the pyrolysis behaviors of rice straw under different washing pretreatments of water, acid solution, and aqueous phase bio-oil by using TG-FTIR and Py-GC/MS, *Fuel* 252 (2019) 1–9. <https://doi.org/10.1016/j.fuel.2019.04.086>.
- [324] C. Branca, C. Di Blasi, Demineralization Pretreatments for Reducing Biomass Variability in Pyrolysis, *ACS Omega* 9 (2024) 9536–9546. https://doi.org/10.1021/ACSOMEGA.3C09321/SUPPL_FILE/AO3C09321_SI_001.PDF.
- [325] A.A. Tesfaw, B.Z. Tizazu, Reducing sugar production from teff straw biomass using dilute sulfuric acid hydrolysis: Characterization and optimization using response surface methodology, *Int. J. Biomater.* 2021 (2021). <https://doi.org/10.1155/2021/2857764>.
- [326] D. Sahoo, S.B. Ummalyma, A.K. Okram, A. Pandey, M. Sankar, R.K. Sukumaran, Effect of dilute acid pretreatment of wild rice grass (*Zizania latifolia*) from Loktak Lake for enzymatic hydrolysis, *Bioresour. Technol.* 253 (2018) 252–255. <https://doi.org/10.1016/j.biortech.2018.01.048>.
- [327] Z. Ji, X. Zhang, Z. Ling, R.C. Sun, F. Xu, Tissue specific response of *Miscanthus × giganteus* to dilute acid pretreatment for enhancing cellulose digestibility, *Carbohydr. Polym.* 154 (2016) 247–256. <https://doi.org/10.1016/j.carbpol.2016.06.086>.
- [328] A. Kristiani, H. Abimanyu, A.H. Setiawan, Sudiyarmanto, F. Aulia, Effect of pretreatment process by using diluted acid to characteristic of oil palm's frond, *Energy Procedia* 32 (2013) 183–189. <https://doi.org/10.1016/j.egypro.2013.05.024>.
- [329] S.V. Pingali, V.S. Urban, W.T. Heller, J. McGaughey, H. O'Neill, M. Foston, D.A. Myles, A. Ragauskas, B.R. Evans, Breakdown of cell wall nanostructure in dilute acid pretreated biomass, *Biomacromolecules* 11 (2010) 2329–2335. <https://doi.org/10.1021/BM100455H>.
- [330] Q. Sun, M. Foston, X. Meng, D. Sawada, S.V. Pingali, H.M. O'Neill, H. Li, C.E. Wyman, P. Langan, A.J. Ragauskas, R. Kumar, Effect of lignin content on changes occurring in poplar cellulose ultrastructure during dilute acid pretreatment, *Biotechnol. Biofuels* 7 (2014) 150. <https://doi.org/10.1186/S13068-014-0150-6>.
- [331] S.B. Kim, S.J. Lee, E.J. Jang, S.O. Han, C. Park, S.W. Kim, Sugar recovery from rice straw by dilute acid pretreatment, *J. Ind. Eng. Chem.* 18 (2012) 183–187. <https://doi.org/10.1016/j.jiec.2011.11.016>.
- [332] The British Stainless Steel Association, Selection of stainless steels for handling sulphuric acid (H₂SO₄) – British Stainless Steel Association, *Br. Stainl. Steel Assoc.* (2024) 1. https://bssa.org.uk/bssa_articles/selection-of-stainless-steels-for-handling-sulphuric-acid-h2so4/ (accessed May 6, 2024).
- [333] J. Wang, J. Wang, H. Ming, Z. Zhang, E.H. Han, Effect of pH on corrosion behavior of 316L stainless steel in hydrogenated high temperature water, *Mater. Corros.* 69 (2018) 580–589.

<https://doi.org/10.1002/maco.201709761>.

- [334] Industrial Quick Search, Stainless Steel 316: What Is It? How Is It Made? Grades, IQS Dir. (2023). <https://www.iqsdirectory.com/articles/stainless-steel/stainless-steel-316.html> (accessed June 26, 2024).
- [335] V. Oriez, J. Peydecastaing, P.Y. Pontalier, Lignocellulosic biomass fractionation by mineral acids and resulting extract purification processes: Conditions, yields, and purities, *Molecules* 24 (2019). <https://doi.org/10.3390/molecules24234273>.
- [336] Hongli Metal Products, What Are Heat Treat Baskets Made Of? - Hongli Metal Mesh, *Www.Honglimetalmesh.Com* (2024) 1. <https://www.honglimetalmesh.com/what-are-heat-treat-baskets-made-of/> (accessed February 26, 2025).
- [337] F.J.V. Gschwend, F. Malaret, S. Shinde, A. Brandt-Talbot, J.P. Hallett, Rapid pretreatment of: *Miscanthus* using the low-cost ionic liquid triethylammonium hydrogen sulfate at elevated temperatures, *Green Chem.* 20 (2018) 3486–3498. <https://doi.org/10.1039/c8gc00837j>.
- [338] H. Zhang, S. Wu, J. Zhang, B. Li, Production of furans from pulp sheet over sulfated solid acid catalysts, *BioResources* 7 (2012) 4531–4544. <https://doi.org/10.15376/biores.7.4.4531-4544>.
- [339] H. Wei, W. Wang, P.N. Ciesielski, B.S. Donohoe, M. Zhang, M.E. Himmel, X. Chen, M.P. Tucker, Ferrous and ferric ion-facilitated dilute acid pretreatment of lignocellulosic biomass under anaerobic or aerobic conditions: Observations of Fe valence interchange and the role of Fenton reaction, *Molecules* 25 (2020) 1427. <https://doi.org/10.3390/molecules25061427>.
- [340] I. Michalak, K. Chojnacka, K. Marycz, Using ICP-OES and SEM-EDX in biosorption studies, *Microchim. Acta* 172 (2011) 65–74. <https://doi.org/10.1007/s00604-010-0468-0>.
- [341] D.O. Usino, T. Sar, P. Ylittervo, T. Richards, Effect of Acid Pretreatment on the Primary Products of Biomass Fast Pyrolysis, *Energies* 16 (2023) 2377. <https://doi.org/10.3390/en16052377>.
- [342] L. Weigand, S. Mostame, A. Brandt-Talbot, T. Welton, J.P. Hallett, Effect of pretreatment severity on the cellulose and lignin isolated from: *Salix* using ionic liquid pretreatment, *Faraday Discuss.* 202 (2017) 331–349. <https://doi.org/10.1039/c7fd00059f>.
- [343] B. Patel, Biomass Characterization and its Use as Solid Fuel for Combustion, *Iran. J. Energy Environ.* 3 (2012) 123–128. <https://doi.org/10.5829/idosi.ijee.2012.03.02.0071>.
- [344] M.K.D. Rambo, F.L. Schmidt, M.M.C. Ferreira, Analysis of the lignocellulosic components of biomass residues for biorefinery opportunities, *Talanta* 144 (2015) 696–703. <https://doi.org/10.1016/j.talanta.2015.06.045>.
- [345] A. George, A. Brandt, K. Tran, S.M.S.N.S. Zahari, D. Klein-Marcuschamer, N. Sun, N. Sathitsuksanoh, J. Shi, V. Stavila, R. Parthasarathi, S. Singh, B.M. Holmes, T. Welton, B.A. Simmons, J.P. Hallett, Design of low-cost ionic liquids for lignocellulosic biomass pretreatment, *Green Chem.* 17 (2015) 1728–1734. <https://doi.org/10.1039/c4gc01208a>.
- [346] A. Hiden, Comparison of the Thermal Degradation Properties of Crystalline and Amorphous Cellulose, as well as Treated Lignocellulosic Biomass, *BioResources* 11 (2016). <https://doi.org/10.15376/biores.11.3.6309-6319>.
- [347] N.M. Nurazzi, M.R.M. Asyraf, M. Rayung, M.N.F. Norraahim, S.S. Shazleen, M.S.A. Rani, A.R. Shafi, H.A. Aisyah, M.H.M. Radzi, F.A. Sabaruddin, R.A. Ilyas, E.S. Zainudin, K. Abdan, Thermogravimetric analysis properties of cellulosic natural fiber polymer composites: A review on influence of chemical treatments, *Polymers (Basel)*. 13 (2021) 2710.

<https://doi.org/10.3390/polym13162710>.

- [348] P. Halder, S. Kundu, S. Patel, M.H. Marzbali, R. Parthasarathy, K. Shah, Furfural and levoglucosenone production from the pyrolysis of ionic liquid pre-treated sugarcane straw, *Cellulose* 28 (2021) 133–151. <https://doi.org/10.1007/s10570-020-03547-2>.
- [349] T. Funazukuri, S. Ozawa, Effects of pretreatment with ionic liquids on cellulose hydrolysis under hydrothermal conditions, *Molecules* 24 (2019). <https://doi.org/10.3390/molecules24193572>.
- [350] Q. Hou, M. Ju, W. Li, L. Liu, Y. Chen, Q. Yang, H. Zhao, Pretreatment of lignocellulosic biomass with ionic liquids and ionic liquid-based solvent systems, *Molecules* 22 (2017). <https://doi.org/10.3390/molecules22030490>.
- [351] G. Cheng, P. Varanasi, R. Arora, V. Stavila, B.A. Simmons, M.S. Kent, S. Singh, Impact of ionic liquid pretreatment conditions on cellulose crystalline structure using 1-ethyl-3-methylimidazolium acetate, *J. Phys. Chem. B* 116 (2012) 10049–10054. <https://doi.org/10.1021/jp304538v>.
- [352] W.-C.T. Lisa, W. Michael, H. Herbert, S. Agnieszka, B.-T. Jason, P. Hallett, W.C.W.-C. Tu, Á.L. Weigand, Á.A. Brandt-Talbot, J.P. Hallett, L. Weigand, M. Hummel, Á.H. Sixta, H. Sixta, A. Brandt-Talbot, J.P. Hallett, Characterisation of cellulose pulps isolated from *Miscanthus* using a low-cost acidic ionic liquid, *Cellulose* 27 (2020) 4745–4761. <https://doi.org/10.1007/s10570-020-03073-1>.
- [353] H. Tadesse, R. Luque, Advances on biomass pretreatment using ionic liquids: An overview, *Energy Environ. Sci.* 4 (2011) 3913–3929. <https://doi.org/10.1039/c0ee00667j>.
- [354] M. Mazza, D.A. Catana, C. Vaca-Garcia, C. Cecutti, Influence of water on the dissolution of cellulose in selected ionic liquids, *Cellulose* 16 (2009) 207–215. <https://doi.org/10.1007/S10570-008-9257-X/FIGURES/8>.
- [355] C. Verma, A. Mishra, S. Chauhan, P. Verma, V. Srivastava, M.A. Quraishi, E.E. Ebenso, Dissolution of cellulose in ionic liquids and their mixed cosolvents: A review, *Sustain. Chem. Pharm.* 13 (2019) 100162. <https://doi.org/10.1016/J.SCP.2019.100162>.
- [356] J. Shi, K. Balamurugan, R. Parthasarathi, N. Sathitsuksanoh, S. Zhang, V. Stavila, V. Subramanian, B.A. Simmons, S. Singh, Understanding the role of water during ionic liquid pretreatment of lignocellulose: Co-solvent or anti-solvent?, *Green Chem.* 16 (2014) 3830–3840. <https://doi.org/10.1039/c4gc00373j>.
- [357] C. Li, G. Cheng, V. Balan, M.S. Kent, M. Ong, S.P.S. Chundawat, L. da C. Sousa, Y.B. Melnichenko, B.E. Dale, B.A. Simmons, S. Singh, Influence of physico-chemical changes on enzymatic digestibility of ionic liquid and AFEX pretreated corn stover, *Bioresour. Technol.* 102 (2011) 6928–6936. <https://doi.org/10.1016/j.biortech.2011.04.005>.
- [358] V.S. Borovkova, Y.N. Malyar, I.G. Sudakova, A.I. Chudina, D. V. Zimonin, A.M. Skripnikov, A. V. Miroshnikova, V.A. Ionin, A.S. Kazachenko, V. V. Sychev, I.S. Ponomarev, N. Issaoui, Composition and Structure of Aspen (*Pópulus trémula*) Hemicelluloses Obtained by Oxidative Delignification, *Polymers (Basel)*. 14 (2022) 4521. <https://doi.org/10.3390/polym14214521>.
- [359] N. Labbé, A. Annamraju, K. Rajan, X. Zuo, B.K. Long, S.V. Pingali, T.J. Elder, Atomic Level Interactions and Suprastructural Configuration of Plant Cell Wall Polymers in Dialkylimidazolium Ionic Liquids, *Biomacromolecules* 24 (2023) 2164–2172. <https://doi.org/10.1021/acs.biomac.3c00047>.
- [360] A. Brandt-Talbot, F.J.V. Gschwend, P.S. Fennell, T.M. Lammens, B. Tan, J. Weale, J.P. Hallett,

An economically viable ionic liquid for the fractionation of lignocellulosic biomass, *Green Chem.* 19 (2017) 3078–3102. <https://doi.org/10.1039/c7gc00705a>.

- [361] S.M.S.N.S. Zahari, A.T.M. Amin, N.M. Halim, F.A. Rosli, W.I.T.A. Halim, N.A. Samsukamal, B. Sasithran, N.Z. Ariffin, H.H. Azman, N.H. Hassan, Z.S. Othman, Deconstruction of Malaysian agro-wastes with inexpensive and bifunctional triethylammonium hydrogen sulfate ionic liquid, *AIP Conf. Proc.* 1972 (2018) 30024. <https://doi.org/10.1063/1.5041245/771249>.
- [362] N. Muhammad, W.N. Omar, Z. Man, M.A. Bustam, S. Rafiq, Y. Uemura, Effect of ionic liquid treatment on pyrolysis products from bamboo, *Ind. Eng. Chem. Res.* 51 (2012) 2280–2289. <https://doi.org/10.1021/ie2014313>.
- [363] F. Yang, X. Zuo, H. Yang, Q. Ke, Y. Huang, X. Cao, L. Zhao, Ionic liquid-assisted production of high-porosity biochar with more surface functional groups: Taking cellulose as attacking target, *Chem. Eng. J.* 433 (2022) 133811. <https://doi.org/10.1016/J.CEJ.2021.133811>.
- [364] Y. Yu, Z. Ren, Q. Shang, J. Han, L. Li, J. Chen, S. Fakudze, Z. Tian, C. Liu, Ionic liquid-induced low temperature graphitization of cellulose-derived biochar for high performance sodium storage, *Surf. Coatings Technol.* 412 (2021) 127034. <https://doi.org/10.1016/J.SURFCOAT.2021.127034>.
- [365] W. Dastyar, M. Zhao, W. Yuan, H. Li, Z.J. Ting, H. Ghaedi, H. Yuan, X. Li, W. Wang, Effective Pretreatment of Heavy Metal-Contaminated Biomass Using a Low-Cost Ionic Liquid (Triethylammonium Hydrogen Sulfate): Optimization by Response Surface Methodology-Box Behnken Design, *ACS Sustain. Chem. Eng.* 7 (2019) 11571–11581. <https://doi.org/10.1021/acssuschemeng.9b01457>.
- [366] J.G. Yao, S.Y. Tan, P.I. Metcalfe, P.S. Fennell, G.H. Kelsall, J.P. Hallett, Demetallization of Sewage Sludge Using Low-Cost Ionic Liquids, *Environ. Sci. Technol.* 55 (2021) 5291–5300. <https://doi.org/10.1021/acs.est.0c03724>.
- [367] P. Halder, S. Kundu, S. Patel, A. Setiawan, R. Atkin, R. Parthasarthy, J. Paz-Ferreiro, A. Surapaneni, K. Shah, Progress on the pre-treatment of lignocellulosic biomass employing ionic liquids, *Renew. Sustain. Energy Rev.* 105 (2019) 268–292. <https://doi.org/10.1016/j.rser.2019.01.052>.
- [368] M. Nurdin, H. Abimanyu, H. Putriani, L.O.M.I. Setiawan, M. Maulidiyah, D. Wibowo, A. Ansharullah, M. Natsir, L.O.A. Salim, Z. Arham, F. Mustapa, Optimization of OPEFB lignocellulose transformation process through ionic liquid [TEA][HSO₄] based pretreatment, *Sci. Rep.* 11 (2021) 11338. <https://doi.org/10.1038/s41598-021-90891-3>.
- [369] P.A. Yudaev, E.M. Chistyakov, Ionic Liquids as Components of Systems for Metal Extraction, *ChemEngineering* 6 (2022) 6. <https://doi.org/10.3390/CHEMENGINEERING6010006/S1>.
- [370] E.T. Matsobane, S. Bada, B. Genc, M. Onifade, Inhibition of Spontaneous Combustion Characteristic of Biomass Treated with Imidazolium-Based Ionic Liquids Using Thermogravimetric Analysis, *ACS Omega* 8 (2023) 33466–33480. https://doi.org/10.1021/ACSOMEGA.3C03265/ASSET/IMAGES/LARGE/AO3C03265_0024.JPG.
- [371] Z. Usmani, M. Sharma, P. Gupta, Y. Karpichev, N. Gathergood, R. Bhat, V.K. Gupta, Ionic liquid based pretreatment of lignocellulosic biomass for enhanced bioconversion, *Bioresour. Technol.* 304 (2020) 123003. <https://doi.org/10.1016/j.biortech.2020.123003>.
- [372] L.W. Yoon, T.N. Ang, G.C. Ngoh, A.S.M. Chua, Regression analysis on ionic liquid pretreatment of sugarcane bagasse and assessment of structural changes, *Biomass and*

Bioenergy 36 (2012) 160–169. <https://doi.org/10.1016/j.biombioe.2011.10.033>.

- [373] S. Mohd, S. Nizan, S. Zahari, Deconstruction of Biomass in Ionic Liquids: Reactivity of Cellulose, Imperial College London, 2015. <https://spiral.imperial.ac.uk/handle/10044/1/44539> (accessed December 17, 2023).
- [374] P.Y.S. Nakasu, T.C. Pin, J.P. Hallett, S.C. Rabelo, A.C. Costa, In-depth process parameter investigation into a protic ionic liquid pretreatment for 2G ethanol production, *Renew. Energy* 172 (2021) 816–828. <https://doi.org/10.1016/j.renene.2021.03.004>.
- [375] L. Testova, Isolation of birch xylan as a part of pulping-based biorefiner, Alto University, 2014. <https://aaltdoc.aalto.fi/bitstream/handle/123456789/14959/isbn9789526060163.pdf?sequence=1&isAllowed=y> (accessed November 18, 2021).
- [376] H. Yang, J. Jiang, B. Zhang, W. Zhang, W. Xie, J. Li, Experimental study on pretreatment effects of [BMIM]HSO₄/ethanol on the thermal behavior of cellulose, *RSC Adv.* 12 (2022) 10366–10373. <https://doi.org/10.1039/d2ra00876a>.
- [377] S. Singh, P. Varanasi, P. Singh, P.D. Adams, M. Auer, B.A. Simmons, Understanding the impact of ionic liquid pretreatment on cellulose and lignin via thermochemical analysis, *Biomass and Bioenergy* 54 (2013) 276–283. <https://doi.org/10.1016/j.biombioe.2013.02.035>.
- [378] M. Mohan, N.N. Deshavath, T. Banerjee, V. V. Goud, V.V. Dasu, Ionic Liquid and Sulfuric Acid-Based Pretreatment of Bamboo: Biomass Delignification and Enzymatic Hydrolysis for the Production of Reducing Sugars, *Ind. Eng. Chem. Res.* 57 (2018) 10105–10117. <https://doi.org/10.1021/acs.iecr.8b00914>.
- [379] Q. Yi, F. Qi, G. Cheng, Y. Zhang, B. Xiao, Z. Hu, S. Liu, H. Cai, S. Xu, Thermogravimetric analysis of co-combustion of biomass and biochar, *J. Therm. Anal. Calorim.* 112 (2013) 1475–1479. <https://doi.org/10.1007/s10973-012-2744-1>.
- [380] Z. Liu, Y. Zhang, L. Zhong, W. Orndroff, H. Zhao, Y. Cao, K. Zhang, W.P. Pan, Synergistic effects of mineral matter on the combustion of coal blended with biomass, *J. Therm. Anal. Calorim.* 113 (2013) 489–496. <https://doi.org/10.1007/s10973-013-3162-8>.
- [381] A. Bychkov, E. Podgorbunskikh, T. Skripkina, A. Burdukov, O. Lomovsky, Mechanochemical modification of the composition and structure of plant raw materials to control the combustion of alternative fuel, in: *MATEC Web Conf.*, 2017: pp. 1–4. <https://doi.org/10.1051/matecconf/201711506003>.
- [382] A. Brandt, Ionic Liquid Pretreatment of Lignocellulosic Biomass, Imperial College London, 2011. <https://doi.org/https://doi.org/10.25560/9166>.
- [383] E.-S.R.E. Hassan, F. Mutelet, Use of Ionic Liquids for the Treatment of Biomass Materials and Biofuel Production, in: *Carbohydrate, InTech*, 2017. <https://doi.org/10.5772/67026>.
- [384] J. Zhang, D. Zou, S. Zhai, Y. Yan, H. Yang, C. He, Y. Ke, S. Singh, G. Cheng, Enhancing the interaction between cellulose and dilute aqueous ionic liquid solutions and its implication to ionic liquid recycling and reuse, *Carbohydr. Polym.* 277 (2022) 118848. <https://doi.org/10.1016/j.carbpol.2021.118848>.
- [385] L. Ma, J.L. Goldfarb, Q. Ma, Enabling lower temperature pyrolysis with aqueous ionic liquid pretreatment as a sustainable approach to rice husk conversion to biofuels, *Renew. Energy* 198 (2022) 712–722. <https://doi.org/10.1016/j.renene.2022.08.077>.
- [386] A. Azizan, I.S. Azmi, R.A. Darim, N.A.A. Jusri, R. Jalil, M.F. Abdul Rahman, R.M. Salleh, N. Ibrahim, J. Salihon, Lignocellulosic ionic liquid pretreated biomaterial/biomass, *Mater. Today*

Proc. 46 (2020) 1688–1692. <https://doi.org/10.1016/j.matpr.2020.07.368>.

- [387] Z. Ling, S. Chen, X. Zhang, K. Takabe, F. Xu, Unraveling variations of crystalline cellulose induced by ionic liquid and their effects on enzymatic hydrolysis, *Sci. Rep.* 7 (2017) 1–11. <https://doi.org/10.1038/s41598-017-09885-9>.
- [388] M.P. Gundupalli, K. Bano, T.K. Panda, M. Sriariyanun, D. Bhattacharyya, Understanding the effect of low-concentrated protic ionic liquids (PILs) on coconut (*Cocos nucifera*) residues, *Biomass Convers. Biorefinery* 14 (2024) 3275–3291. <https://doi.org/10.1007/s13399-022-02572-4>.
- [389] V. Sorn, K.L. Chang, P. Phitsuwan, K. Ratanakhanokchai, C. Di Dong, Effect of microwave-assisted ionic liquid/acidic ionic liquid pretreatment on the morphology, structure, and enhanced delignification of rice straw, *Bioresour. Technol.* 293 (2019) 121929. <https://doi.org/10.1016/j.biortech.2019.121929>.
- [390] H.J. Jiang, S. Imberti, B.A. Simmons, R. Atkin, G.G. Warr, Structural Design of Ionic Liquids for Optimizing Aromatic Dissolution, *ChemSusChem* 12 (2019) 270–274. <https://doi.org/10.1002/cssc.201802016>.
- [391] Y.C. Sun, J.K. Xu, F. Xu, R.C. Sun, Structural comparison and enhanced enzymatic hydrolysis of eucalyptus cellulose via pretreatment with different ionic liquids and catalysts, *Process Biochem.* 48 (2013) 844–852. <https://doi.org/10.1016/j.procbio.2013.03.023>.
- [392] J.G. Lynam, Biomass Pretreatment using Ionic Liquid and Glycerol Mixtures, University of Nevada, 2015. http://scholarworks.unr.edu:8080/bitstream/handle/11714/2553/Lynam_unr_0139D_11841.pdf?sequence=1&isAllowed=y (accessed August 16, 2022).
- [393] N. Muhammad, Z. Man, M.I.A. Mutalib, M.A. Bustam, C.D. Wilfred, A.S. Khan, Z. Ullah, G. Gonfa, A. Nasrullah, Dissolution and Separation of Wood Biopolymers Using Ionic Liquids, *ChemBioEng Rev.* 2 (2015) 257–278. <https://doi.org/10.1002/cben.201500003>.
- [394] A. Brandt, J. Gräsvik, J.P. Hallett, T. Welton, Deconstruction of lignocellulosic biomass with ionic liquids, *Green Chem.* 15 (2013) 550–583. <https://doi.org/10.1039/c2gc36364j>.
- [395] I.P. Samayam, C.A. Schall, Saccharification of ionic liquid pretreated biomass with commercial enzyme mixtures, *Bioresour. Technol.* 101 (2010) 3561–3566. <https://doi.org/10.1016/j.biortech.2009.12.066>.
- [396] Y. Zhu, Z. Han, L. Fu, C. Liu, D. Zhang, Cleavage of the β -O-4 bond in a lignin model compound using the acidic ionic liquid 1-H-3-methylimidazolium chloride as catalyst: a DFT mechanistic study, *J. Mol. Model.* 24 (2018) 1–8. <https://doi.org/10.1007/s00894-018-3854-x>.
- [397] Z. Zhang, I.M. O'Hara, W.O.S. Doherty, Effects of pH on pretreatment of sugarcane bagasse using aqueous imidazolium ionic liquids, *Green Chem.* 15 (2013) 431–438. <https://doi.org/10.1039/c2gc36084e>.
- [398] I. Semerci, F. Güler, G. Ersan, K. Soysal, O. Ozturk, H. Altinisik, S. Tirpan, F. Ozcelik, Assessment of a protic ionic liquid with respect to fractionation and changes in the structural features of hardwood and softwood, *Bioresour. Technol. Reports* 8 (2019) 100334. <https://doi.org/10.1016/j.biteb.2019.100334>.
- [399] R.C. Remsing, R.P. Swatloski, R.D. Rogers, G. Moyna, Mechanism of cellulose dissolution in the ionic liquid 1-n-butyl-3-methylimidazolium chloride: A ^{13}C and $^{35/37}\text{Cl}$ NMR relaxation study on model systems, *Chem. Commun.* (2006) 1271–1273.

<https://doi.org/10.1039/b600586c>.

- [400] N. Jalilnejad Falizi, T. Güngören Madenoğlu, N. Kabay, M. Yüksel, 110th Anniversary: Transesterification of Corn Oil to Biodiesel by Ion Exchange Resins with Macroporous Structure, *Ind. Eng. Chem. Res.* 58 (2019) 18097–18106. <https://doi.org/10.1021/acs.iecr.9b02968>.
- [401] DOSHION POLYSCIENCE PVT. LTD., Ion Exchange Resin Properties: Key Features for Efficient Industrial Processes — Doshion Polyscience, DOSHION POLYSCIENCE PVT. LTD. (2024) 1. <https://www.doshionpoly.com/blog/important-properties-of-ion-exchange-resin> (accessed July 12, 2024).
- [402] O.O. Olatunji, S.A. Akinlabi, M.P. Mashinini, S.O. Fatoba, O.O. Ajayi, Thermo-gravimetric characterization of biomass properties: A review, in: *IOP Conf. Ser. Mater. Sci. Eng. Pap.*, IOP Conf. Series: Materials Science and Engineering, Nanchang, 2018: pp. 1–16. <https://doi.org/10.1088/1757-899X/423/1/012175>.
- [403] D. Fu, G. Mazza, Y. Tamaki, Lignin extraction from straw by ionic liquids and enzymatic hydrolysis of the cellulosic residues, *J. Agric. Food Chem.* 58 (2010) 2915–2922. <https://doi.org/10.1021/jf903616y>.
- [404] J. Zhang, L. Feng, D. Wang, R. Zhang, G. Liu, G. Cheng, Thermogravimetric analysis of lignocellulosic biomass with ionic liquid pretreatment, *Bioresour. Technol.* 153 (2014) 379–382. <https://doi.org/10.1016/j.biortech.2013.12.004>.
- [405] J.R. Bernardo, F.M. Gírio, R.M. Łukasik, The effect of the chemical character of ionic liquids on biomass pre-treatment and posterior enzymatic hydrolysis, *Molecules* 24 (2019). <https://doi.org/10.3390/molecules24040808>.
- [406] S.N. Sun, M.F. Li, T.Q. Yuan, F. Xu, R.C. Sun, Effect of ionic liquid pretreatment on the structure of hemicelluloses from corncob, *J. Agric. Food Chem.* 60 (2012) 11120–11127. <https://doi.org/10.1021/jf3021464>.
- [407] M. Moniruzzaman, T. Ono, Separation and characterization of cellulose fibers from cypress wood treated with ionic liquid prior to laccase treatment, *Bioresour. Technol.* 127 (2013) 132–137. <https://doi.org/10.1016/J.BIORTECH.2012.09.113>.
- [408] M.M. Rana, H. De la Hoz Siegler, Influence of ionic liquid (IL) treatment conditions in the regeneration of cellulose with different crystallinity, *J. Mater. Res.* 38 (2023) 328–336. <https://doi.org/10.1557/s43578-022-00797-7>.
- [409] T. Herawan, F.R. Panjaitan, S. Yamanaka, Morphological and Structural Changes in Microcrystalline Cellulose from OPEFB by Mechanical Grinding, *IOP Conf. Ser. Earth Environ. Sci.* 166 (2018) 12001. <https://doi.org/10.1088/1755-1315/166/1/012001>.
- [410] D.L. Minnick, A.M. Scurto, Reversible and non-reactive cellulose separations from ionic liquid mixtures with compressed carbon dioxide, *Chem. Commun.* 51 (2015) 12649–12652. <https://doi.org/10.1039/c5cc03519h>.
- [411] A. Azizan, N.A.A. Jusri, I.S. Azmi, M.F. Abd Rahman, N. Ibrahim, R. Jalil, Emerging lignocellulosic ionic liquid biomass pretreatment criteria/strategy of optimization and recycling short review with infrared spectroscopy analytical know-how, *Mater. Today Proc.* 63 (2022) S359–S367. <https://doi.org/10.1016/j.matpr.2022.03.548>.
- [412] I. Spiridon, C.-A. Teacă, R. Bodîrlău, Structural changes evidenced by FTIR spectroscopy in cellulosic materials after pre-treatment with ionic liquid and enzymatic hydrolysis, *BioResources*

6 (2011) 400–413. <https://doi.org/10.15376/biores.6.1.400-413>.

- [413] T.N. Ang, G.C. Ngoh, A.S.M. Chua, M.G. Lee, Elucidation of the effect of ionic liquid pretreatment on rice husk via structural analyses, *Biotechnol. Biofuels* 5 (2012). <https://doi.org/10.1186/1754-6834-5-67>.
- [414] R. Kaur, M. Sharma, Cereal polysaccharides as sources of functional ingredient for reformulation of meat products: A review, *J. Funct. Foods* 62 (2019) 103527. <https://doi.org/10.1016/J.JFF.2019.103527>.
- [415] R. Soto, C. Fité, E. Ramírez, M. Iborra, J. Tejero, Catalytic activity dependence on morphological properties of acidic ion-exchange resins for the simultaneous ETBE and TAAE liquid-phase synthesis, *React. Chem. Eng.* 3 (2018) 195–205. <https://doi.org/10.1039/c7re00177k>.
- [416] D. Reichenberg, Properties of Ion-Exchange Resins in Relation to their Structure. III. Kinetics of Exchange, *J. Am. Chem. Soc.* 75 (1953) 589–597. <https://doi.org/10.1021/ja01099a022>.
- [417] J. Guilera, E. Ramírez, C. Fité, M. Iborra, J. Tejero, Thermal stability and water effect on ion-exchange resins in ethyl octyl ether production at high temperature, *Appl. Catal. A Gen.* 467 (2013) 301–309. <https://doi.org/10.1016/J.APCATA.2013.07.024>.
- [418] D.M. Alonso, J.Q. Bond, D. Wang, J.A. Dumesic, Activation of amberlyst-70 for alkene oligomerization in hydrophobic media, *Top. Catal.* 54 (2011) 447–457. <https://doi.org/10.1007/S11244-011-9674-1/FIGURES/10>.
- [419] N. Nwokolo, S. Mamphweli, G. Makaka, Analytical and thermal evaluation of carbon particles recovered at the cyclone of a downdraft biomass gasification system, *Sustain.* 9 (2017) 645. <https://doi.org/10.3390/su9040645>.
- [420] X.H. Pham, B. Piriou, S. Salvador, J. Valette, L. Van de Steene, Oxidative pyrolysis of pine wood, wheat straw and miscanthus pellets in a fixed bed, *Fuel Process. Technol.* 178 (2018) 226–235. <https://doi.org/10.1016/j.fuproc.2018.05.029>.
- [421] S. Ikram, L.Y. Huang, H. Zhang, J. Wang, M. Yin, Composition and Nutrient Value Proposition of Brewers Spent Grain, *J. Food Sci.* 82 (2017) 2232–2242. <https://doi.org/10.1111/1750-3841.13794>.
- [422] K.M. Lynch, E.J. Steffen, E.K. Arendt, Brewers' spent grain: a review with an emphasis on food and health, *J. Inst. Brew.* 122 (2016) 553–568. <https://doi.org/10.1002/jib.363>.
- [423] S. Głowacki, A. Salamon, M. Sojak, W. Tulej, A. Bryś, T. Hutsol, M. Salamon, S. Kukharets, M. Janaszek-Mańkowska, The Use of Brewer's Spent Grain after Beer Production for Energy Purposes, *Materials (Basel)*. 15 (2022) 3703. <https://doi.org/10.3390/ma15103703>.
- [424] J. Naibaho, M. Korzeniowska, The variability of physico-chemical properties of brewery spent grain from 8 different breweries, *Heliyon* 7 (2021) e06583. <https://doi.org/10.1016/J.HELIYON.2021.E06583>.
- [425] S.H. Lamtom, R.A. Savidge, A reassessment of carbon content in wood: variation within and between 41 North American species, *Biomass and Bioenergy* 25 (2003) 381–388. [https://doi.org/10.1016/S0961-9534\(03\)00033-3](https://doi.org/10.1016/S0961-9534(03)00033-3).
- [426] I. Sable, U. Grinfelds, A. Jansons, L. Vikele, I. Irbe, A. Verovkins, A. Treimanis, Comparison of the properties of wood and pulp fibers from lodgepole pine (*Pinus contorta*) and scots pine (*Pinus sylvestris*), *BioResources* 7 (2012) 1771–1783.

- [427] C. Cacace, C. Cocozza, A. Traversa, R. Coda, C.G. Rizzello, E. Pontonio, F. De Mastro, G. Brunetti, M. Verni, Potential of native and bioprocessed brewers' spent grains as organic soil amendments, *Front. Sustain. Food Syst.* 6 (2022) 1010890. <https://doi.org/10.3389/fsufs.2022.1010890>.
- [428] Y.A. Gismatulina, V. V. Budaeva, A.N. Kortusov, E.I. Kashcheyeva, E.K. Gladysheva, G.F. Mironova, E.A. Skiba, N.A. Shavyrkina, A.A. Korchagina, V.N. Zolotukhin, G. V. Sakovich, Evaluation of Chemical Composition of *Miscanthus × giganteus* Raised in Different Climate Regions in Russia, *Plants* 11 (2022). <https://doi.org/10.3390/plants11202791>.
- [429] D.M. Fradinho, C.P. Neto, D. Evtuguin, F.C. Jorge, M.A. Irle, M.H. Gil, J. Pedrosa de Jesus, Chemical characterisation of bark and of alkaline bark extracts from maritime pine grown in Portugal, *Ind. Crops Prod.* 16 (2002) 23–32. [https://doi.org/10.1016/S0926-6690\(02\)00004-3](https://doi.org/10.1016/S0926-6690(02)00004-3).
- [430] S.I. Mussatto, G. Dragone, I.C. Roberto, Brewers' spent grain: generation, characteristics and potential applications, *J. Cereal Sci.* 43 (2006) 1–14. <https://doi.org/10.1016/J.JCS.2005.06.001>.
- [431] I. Miranda, J. Gominho, I. Mirra, H. Pereira, Chemical characterization of barks from *Picea abies* and *Pinus sylvestris* after fractioning into different particle sizes, *Ind. Crops Prod.* 36 (2012) 395–400. <https://doi.org/10.1016/j.indcrop.2011.10.035>.
- [432] J. Castilla-Archilla, M. Cermeño, M.G. Tuohy, R.J. FitzGerald, P.N.L. Lens, Brewers' spent grain pretreatment optimisation to enhance enzymatic hydrolysis of whole slurry and resuspended pellet, *Front. Chem. Eng.* 5 (2023) 1272988. <https://doi.org/10.3389/fceng.2023.1272988>.
- [433] O. Gil-Castell, N. Mascia, C. Primaz, F. Vásquez-Garay, M.G. Baschetti, A. Ribes-Greus, Brewer's spent grains as biofuels in combustion-based energy recovery processes: Evaluation of thermo-oxidative decomposition, *Fuel* 312 (2022) 122955. <https://doi.org/10.1016/j.fuel.2021.122955>.
- [434] E.-S. Hassan, F. Mutelet, J.-C. Moïse, The pretreatment of miscanthus using ionic liquids; a way for biofuel production, in: *MATEC Web Conf.*, 39th Edition of the Joint European Days on Equilibrium Between Phases, 2013: p. 3. <https://doi.org/10.1051/matecconf/20130301049>.
- [435] O.P. Gbenebor, O.A. Olanrewaju, M.A. Usman, S.O. Adeosun, Lignin from Brewers' Spent Grain: Structural and Thermal Evaluations, *Polymers (Basel)*. 15 (2023) 2346. <https://doi.org/10.3390/polym15102346>.
- [436] P. Alonso-Riaño, R. Melgosa, E. Trigueros, A.E. Illera, S. Beltrán, M.T. Sanz, Valorization of brewer's spent grain by consecutive supercritical carbon dioxide extraction and enzymatic hydrolysis, *Food Chem.* 396 (2022) 133493. <https://doi.org/10.1016/j.foodchem.2022.133493>.
- [437] M. Michelin, J.A. Teixeira, Liquid hot water pretreatment of multi feedstocks and enzymatic hydrolysis of solids obtained thereof, *Bioresour. Technol.* 216 (2016) 862–869. <http://dx.doi.org/10.1016/j.biortech.2016.06.018> (accessed July 12, 2021).
- [438] D. Danielewicz, B. Surma-Ślusarska, *Miscanthus × giganteus* stalks as a potential non-wood raw material for the pulp and paper industry. Influence of pulping and beating conditions on the fibre and paper properties, *Ind. Crops Prod.* 141 (2019) 111744. <https://doi.org/10.1016/J.INDCROP.2019.111744>.
- [439] Ö. Özgenç Keleş, S. Durmaz, S. Kuştaş, Chemical Analysis of Tree Barks using ATR-FTIR Spectroscopy and Conventional Techniques, *Bioresources* 12 (2017) 9143–9151. <https://doi.org/10.15376/biores.12.4.9143-9151>.

- [440] R. Feria-Reyes, S.O. Ramírez-Cruz, F. Ruiz-Aquino, L.H. Robledo-Taboada, M.A. Sánchez-Medina, O.F. Mijangos-Ricárdez, R. Gabriel-Parra, M.E. Suárez-Mota, R. Puc-Kauil, J. Porcallo-Vargas, Pine Bark as a Potential Source of Condensed Tannin: Analysis through Fourier Transform Infrared Spectroscopy (FTIR), Scanning Electron Microscopy (SEM), and Energy Dispersive X-ray (EDX), *Forests* 14 (2023) 1433. <https://doi.org/10.3390/f14071433>.
- [441] A.O. Balogun, F. Sotoudehniakarani, A.G. McDonald, Thermo-kinetic, spectroscopic study of brewer's spent grains and characterisation of their pyrolysis products, *J. Anal. Appl. Pyrolysis* 127 (2017) 8–16. <https://doi.org/10.1016/j.jaap.2017.09.009>.
- [442] L.D.M.S. Borel, A.M. Reis Filho, T.P. Xavier, T.S. Lira, M.A.S. Barrozo, An investigation on the pyrolysis of the main residue of the brewing industry, *Biomass and Bioenergy* 140 (2020) 105698. <https://doi.org/10.1016/j.biombioe.2020.105698>.
- [443] D. Outeiriño, I. Costa-Trigo, A. Paz, F.J. Deive, A. Rodríguez, J.M. Domínguez, Biorefining brewery spent grain polysaccharides through biotuning of ionic liquids, *Carbohydr. Polym.* 203 (2019) 265–274. <https://doi.org/10.1016/j.carbpol.2018.09.042>.
- [444] R. Ravindran, S. Jaiswal, N. Abu-Ghannam, A.K. Jaiswal, A comparative analysis of pretreatment strategies on the properties and hydrolysis of brewers' spent grain, *Bioresour. Technol.* 248 (2018) 272–279. <https://doi.org/10.1016/j.biortech.2017.06.039>.
- [445] A.E.J. Firth, P.Y.S. Nakasu, P.S. Fennell, J.P. Hallett, An Ionic Liquid-Based Biorefinery Approach for Duckweed Utilization, *ACS Sustain. Resour. Manag.* 1 (2024) 842–856. <https://doi.org/10.1021/acssusresmgmt.3c00008>.
- [446] F. Qin, A.Z. Johansen, S.I. Mussatto, Evaluation of different pretreatment strategies for protein extraction from brewer's spent grains, *Ind. Crops Prod.* 125 (2018) 443–453. <https://doi.org/10.1016/j.indcrop.2018.09.017>.
- [447] J.A. Rojas-Chamorro, I. Romero, J.C. López-Linares, E. Castro, Brewer's spent grain as a source of renewable fuel through optimized dilute acid pretreatment, *Renew. Energy* 148 (2020) 81–90. <https://doi.org/10.1016/j.renene.2019.12.030>.
- [448] B.J. Cox, J.G. Ekerdt, Pretreatment of yellow pine in an acidic ionic liquid: Extraction of hemicellulose and lignin to facilitate enzymatic digestion, *Bioresour. Technol.* 134 (2013) 59–65. <https://doi.org/10.1016/j.biortech.2013.01.081>.
- [449] D.A. Fort, R.C. Remsing, R.P. Swatloski, P. Moyna, G. Moyna, R.D. Rogers, Can ionic liquids dissolve wood? Processing and analysis of lignocellulosic materials with 1-n-butyl-3-methylimidazolium chloride, *Green Chem.* 9 (2007) 63–69. <https://doi.org/10.1039/b607614a>.
- [450] X. Yuan, L. He, S. Singh, B.A. Simmons, G. Cheng, Effect of Ionic Liquid Pretreatment on the Porosity of Pine: Insights from Small-Angle Neutron Scattering, Nitrogen Adsorption Analysis, and X-ray Diffraction, *Energy and Fuels* 31 (2017) 10874–10879. <https://doi.org/10.1021/acs.energyfuels.7b01567>.
- [451] J. Zhang, Y. Wang, L. Zhang, R. Zhang, G. Liu, G. Cheng, Understanding changes in cellulose crystalline structure of lignocellulosic biomass during ionic liquid pretreatment by XRD, *Bioresour. Technol.* 151 (2014) 402–405. <https://doi.org/10.1016/j.biortech.2013.10.009>.
- [452] M. Schwanninger, J.C. Rodrigues, H. Pereira, B. Hinterstoisser, Effects of short-time vibratory ball milling on the shape of FT-IR spectra of wood and cellulose, *Vib. Spectrosc.* 36 (2004) 23–40. <https://doi.org/10.1016/j.vibspec.2004.02.003>.
- [453] M. Kacuráková, P. Capek, V. Sasinková, N. Wellner, A. Ebringerová, FT-IR study of plant cell

wall model compounds: pectic polysaccharides and hemicelluloses, *Carbohydr. Polym.* 43 (2000) 195–203. [https://doi.org/10.1016/S0144-8617\(00\)00151-X](https://doi.org/10.1016/S0144-8617(00)00151-X).

- [454] N.K. Brar, W.J. Grigsby, S.J. Hill, L. Raymond, C.C. Weber, Understanding the effects of ionic liquids and antisolvent addition on the extraction and recovery of *Pinus radiata* bark components, *J. Wood Chem. Technol.* 42 (2022) 305–317. <https://doi.org/10.1080/02773813.2022.2088793>.
- [455] L. Li, J.S. Rowbotham, H. Christopher Greenwell, P.W. Dyer, An Introduction to Pyrolysis and Catalytic Pyrolysis: Versatile Techniques for Biomass Conversion, *New Futur. Dev. Catal. Biomass Convers.* (2013) 173–208. <https://doi.org/10.1016/B978-0-444-53878-9.00009-6>.
- [456] M. Witzler, A. Alzagameem, M. Bergs, B. El Khaldi-Hansen, S.E. Klein, D. Hielscher, B. Kamm, J. Kreyenschmidt, E. Tobiasch, M. Schulze, Lignin-derived biomaterials for drug release and tissue engineering, *Molecules* 23 (2018) 1885. <https://doi.org/10.3390/molecules23081885>.
- [457] W. Suliman, J.B. Harsh, N.I. Abu-Lail, A.M. Fortuna, I. Dallmeyer, M. Garcia-Perez, Influence of feedstock source and pyrolysis temperature on biochar bulk and surface properties, *Biomass and Bioenergy* 84 (2016) 37–48. <https://doi.org/10.1016/j.biombioe.2015.11.010>.
- [458] S. Dorge, M. Jeguirim, G. Trouvé, Thermal degradation of *Miscanthus* pellets: Kinetics and aerosols characterization, *Waste and Biomass Valorization* 2 (2011) 149–155. <https://doi.org/10.1007/s12649-010-9060-4>.
- [459] M.V. Kok, E. Özgür, Thermal analysis and kinetics of biomass samples, *Fuel Process. Technol.* 106 (2013) 739–743. <https://doi.org/10.1016/j.fuproc.2012.10.010>.
- [460] C.E. Greenhalf, D.J. Nowakowski, N. Yates, I. Shield, A. V. Bridgwater, The influence of harvest and storage on the properties of and fast pyrolysis products from *Miscanthus x giganteus*, *Biomass and Bioenergy* 56 (2013) 247–259. <https://doi.org/10.1016/j.biombioe.2013.05.007>.
- [461] A. Sanna, S. Li, R. Linforth, K.A. Smart, J.M. Andrésen, Bio-oil and bio-char from low temperature pyrolysis of spent grains using activated alumina, *Bioresour. Technol.* 102 (2011) 10695–10703. <https://doi.org/10.1016/j.biortech.2011.08.092>.
- [462] J. Shankar Tumuluru, R.D. Boardman, C.T. Wright, J.R. Hess, Some Chemical Compositional Changes in *Miscanthus* and White Oak Sawdust Samples during Torrefaction, 5 (2012) 3928–3947. <https://doi.org/10.3390/en5103928>.
- [463] A.M. da Costa Lopes, K.G. João, A.R.C. Morais, E. Bogel-Łukasik, R. Bogel-Łukasik, Ionic liquids as a tool for lignocellulosic biomass fractionation, *Sustain. Chem. Process.* 1 (2013) 1–31. <https://doi.org/10.1186/2043-7129-1-3>.
- [464] Z. Yinghuai, A. Oh, X. Siwei, N. S, J. A., Ionic Liquids in Catalytic Biomass Transformation, in: *Appl. Ion. Liq. Sci. Technol., InTech*, 2011: pp. 1–26. <https://doi.org/10.5772/20451>.
- [465] L. Wu, S.H. Lee, T. Endo, Effect of dimethyl sulfoxide on ionic liquid 1-ethyl-3-methylimidazolium acetate pretreatment of eucalyptus wood for enzymatic hydrolysis, *Bioresour. Technol.* 140 (2013) 90–96. <https://doi.org/10.1016/j.biortech.2013.04.072>.
- [466] J. Xu, B. Liu, H. Hou, J. Hu, Pretreatment of eucalyptus with recycled ionic liquids for low-cost biorefinery, *Bioresour. Technol.* 234 (2017) 406–414. <https://doi.org/10.1016/j.biortech.2017.03.081>.
- [467] F. Malaret, F.J.V. Gschwend, J.M. Lopes, W.C. Tu, J.P. Hallett, *Eucalyptus red grandis* pretreatment with protic ionic liquids: Effect of severity and influence of sub/super-critical CO₂

atmosphere on pretreatment performance, *RSC Adv.* 10 (2020) 16050–16060.
<https://doi.org/10.1039/d0ra02040k>.

- [468] C. Zhang, W. Xu, P. Yan, X. Liu, Z.C. Zhang, Overcome the recalcitrance of eucalyptus bark to enzymatic hydrolysis by concerted ionic liquid pretreatment, *Process Biochem.* 50 (2015) 2208–2214. <https://doi.org/10.1016/j.procbio.2015.09.009>.
- [469] M. Chen, F. Malaret, A.E.J. Firth, P. Verdía, A.R. Abouelela, Y. Chen, J.P. Hallett, Design of a combined ionosolv-organosolv biomass fractionation process for biofuel production and high value-added lignin valorisation, *Green Chem.* 22 (2020) 5161–5178.
<https://doi.org/10.1039/d0gc01143f>.
- [470] L.T.P. Trinh, Y.J. Lee, J.W. Lee, W.H. Lee, Optimization of Ionic Liquid Pretreatment of Mixed Softwood by Response Surface Methodology and Reutilization of Ionic Liquid from Hydrolysate, *Biotechnol. Bioprocess Eng.* 23 (2018) 228–237. <https://doi.org/10.1007/s12257-017-0209-x>.
- [471] M. Normark, L. Pommer, J. Gräsvik, M. Hedenström, A. Gorzsás, S. Winstrand, L.J. Jönsson, Biochemical Conversion of Torrefied Norway Spruce After Pretreatment with Acid or Ionic Liquid, *Bioenergy Res.* 9 (2016) 355–368. <https://doi.org/10.1007/s12155-015-9698-7>.
- [472] D. Fu, G. Mazza, Aqueous ionic liquid pretreatment of straw, *Bioresour. Technol.* 102 (2011) 7008–7011. <https://doi.org/10.1016/j.biortech.2011.04.049>.
- [473] X.D. Hou, N. Li, M.H. Zong, Significantly enhancing enzymatic hydrolysis of rice straw after pretreatment using renewable ionic liquid-water mixtures, *Bioresour. Technol.* 136 (2013) 469–474. <https://doi.org/10.1016/j.biortech.2013.02.118>.
- [474] N.L. Mai, S.H. Ha, Y.M. Koo, Efficient pretreatment of lignocellulose in ionic liquids/co-solvent for enzymatic hydrolysis enhancement into fermentable sugars, *Process Biochem.* 49 (2014) 1144–1151. <https://doi.org/10.1016/j.procbio.2014.03.024>.
- [475] Y.C. He, F. Liu, L. Gong, Z.Z. Zhu, Y. Ding, C. Wang, Y.F. Xue, H. Rui, Z.C. Tao, D.P. Zhang, C.L. Ma, Significantly improving enzymatic saccharification of high crystallinity index's corn stover by combining ionic liquid [Bmim]Cl-HCl-water media with dilute NaOH pretreatment, *Bioresour. Technol.* 189 (2015) 421–425. <https://doi.org/10.1016/j.biortech.2015.04.047>.
- [476] J.C. Ding, G.C. Xu, R.Z. Han, Y. Ni, Biobutanol production from corn stover hydrolysate pretreated with recycled ionic liquid by *Clostridium saccharobutylicum* DSM 13864, *Bioresour. Technol.* 199 (2016) 228–234. <https://doi.org/10.1016/j.biortech.2015.07.119>.
- [477] Z. Zhang, I.M. O'Hara, W.O.S. Doherty, Pretreatment of sugarcane bagasse by acid-catalysed process in aqueous ionic liquid solutions, *Bioresour. Technol.* 120 (2012) 149–156.
<https://doi.org/10.1016/j.biortech.2012.06.035>.
- [478] T.C. Pin, V.M. Nascimento, A.C. Costa, Y. Pu, A.J. Ragauskas, S.C. Rabelo, Structural characterization of sugarcane lignins extracted from different protic ionic liquid pretreatments, *Renew. Energy* 161 (2020) 579–592. <https://doi.org/10.1016/j.renene.2020.07.078>.
- [479] N. Nasirpour, S.M. Mousavi, S.A. Shojaosadati, A novel surfactant-assisted ionic liquid pretreatment of sugarcane bagasse for enhanced enzymatic hydrolysis, *Bioresour. Technol.* 169 (2014) 33–37. <https://doi.org/10.1016/j.biortech.2014.06.023>.
- [480] R. Prado, A. Brandt, X. Erdocia, J. Hallet, T. Welton, J. Labidi, Lignin oxidation and depolymerisation in ionic liquids, *Green Chem.* 18 (2016) 834–841.
<https://doi.org/10.1039/c5gc01950h>.
- [481] L.D. Tolesa, B.S. Gupta, M.J. Lee, Treatment of Coffee Husk with Ammonium-Based Ionic

Liquids: Lignin Extraction, Degradation, and Characterization, ACS Omega 3 (2018) 10866–10876. <https://doi.org/10.1021/acsomega.8b01447>.

- [482] Dupont, DuPont, Dupont (2024) 1. <https://www.dupont.com/solution-finder/results.html?BU=water-solutions> (accessed February 11, 2024).
- [483] M. Granollers, J.F. Izquierdo, F. Cunill, Effect of macroreticular acidic ion-exchange resins on 2-methyl-1-butene and 2-methyl-2-butene mixture oligomerization, Appl. Catal. A Gen. 435–436 (2012) 163–171. <https://doi.org/10.1016/j.apcata.2012.05.051>.
- [484] P. Company, A.R. Reserved, Purolite Product Guide Characteristics and Applications, 2011. <https://www.lenntech.com/Data-sheets/Purolite-Product-Summary-Guide-L.pdf> (accessed July 18, 2024).

Appendices

Appendix 1 (Literature Review)

Table A1.1. Principles of Green Chemistry and their application relevant to the research [6].

1.	Prevention	Prevent waste and treat or clean it after it has been created.	IERs minimize waste generation by enabling catalyst reusability and avoiding single-use corrosive acids ultimately reducing downstream waste.
2.	Atomic Economy	Methods should be designed to maximise the incorporation of all materials into the final product.	Not relevant
3.	Less Hazardous Chemical Waste	Methods should be designed to use and generate substances that possess little or no toxicity to human health and the environment.	Replacing mineral acids with IERs eliminates toxic acid waste streams.
4.	Design Safer chemicals	Chemical products should be designed to affect their desired function while minimising toxicity.	IERs are non-leaching, stable polymers designed for catalytic activity without releasing harmful substances.
5.	Safer Solvents and Auxiliaries	Auxiliary substances use (e.g., solvents, separation agents, etc.) should be made unnecessary wherever possible and innocuous when used.	Water-based hydrolysis with IERs avoids organic solvents. Ionic liquids like triethyl ammonium hydrogen sulphate (TS80) are recoverable and less toxic than traditional solvents.
6.	Design for Energy Efficiency	Energy requirements of chemical processes should be recognised for their environmental and economic impacts and should be minimised	IERs operate under mild conditions (80-150 °C) compared to conventional acid hydrolysis, reducing energy demands
7.	Use of Renewable Feedstocks	A raw material or feedstock should be renewable rather than depleting whenever technically and economically practicable.	IERs enable efficient conversion of renewable lignocellulosic biomass (e.g., Miscanthus × giganteus) into fuels/chemicals, reducing dependence on fossil resources.
8.	Reduce Derivatives	Unnecessary derivatisation (use of blocking groups, protection/ deprotection, temporary modification of physical/chemical processes) should be minimised or avoided because such steps require additional reagents and can generate waste.	Direct depolymerization of biomass into fermentable sugars or platform chemicals avoids unnecessary derivatization steps (e.g., protection/deprotection).
9.	Catalysis	Catalytic reagents (as selective as possible) are superior to stoichiometric reagents.	IERs act as reusable catalysts, replacing stoichiometric acids. Their selectivity enhances reaction efficiency while minimizing reagent consumption.
10.	Design for Degradation	Chemical products should be designed so that at the end of their function, they break down into innocuous	The resins themselves are chemically stable but do not persist in ecosystems.

		degradation products and do not persist in the environment.	
11.	Real-time analysis for Pollution Prevention	Analytical methodologies need to be further developed to allow for real-time, in-process monitoring and control before hazardous substances form.	Not Applicable.
12.	Inherently Safer Chemistry for Accident Prevention	Substances and the form of a substance used in a chemical process should be chosen to minimise the potential for chemical accidents, including releases, explosions, and fires.	IERs eliminate risks of handling concentrated acids (e.g., explosions, leaks). Their solid-phase nature minimizes exposure to hazardous substances

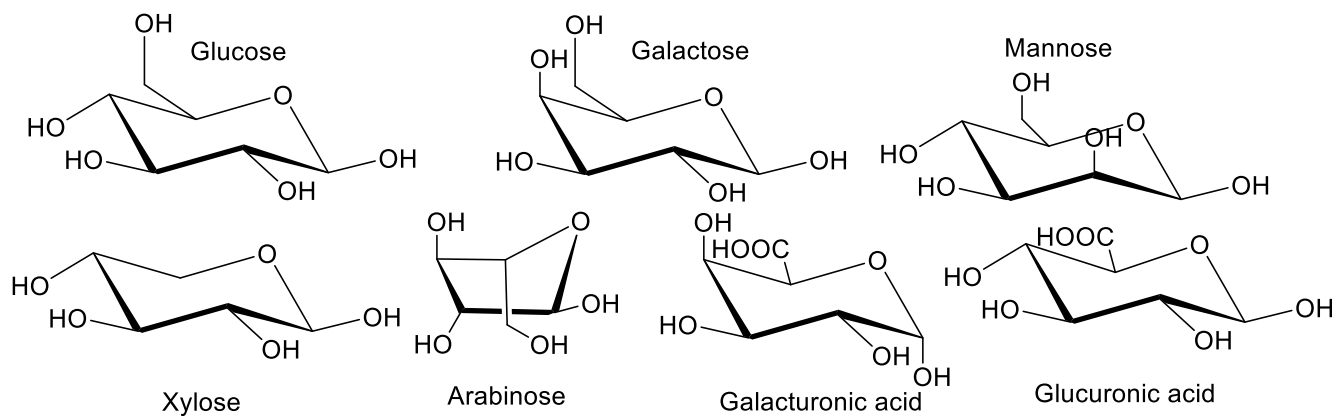


Figure A1.1. Main monomers of hemicellulose adapted from [455].

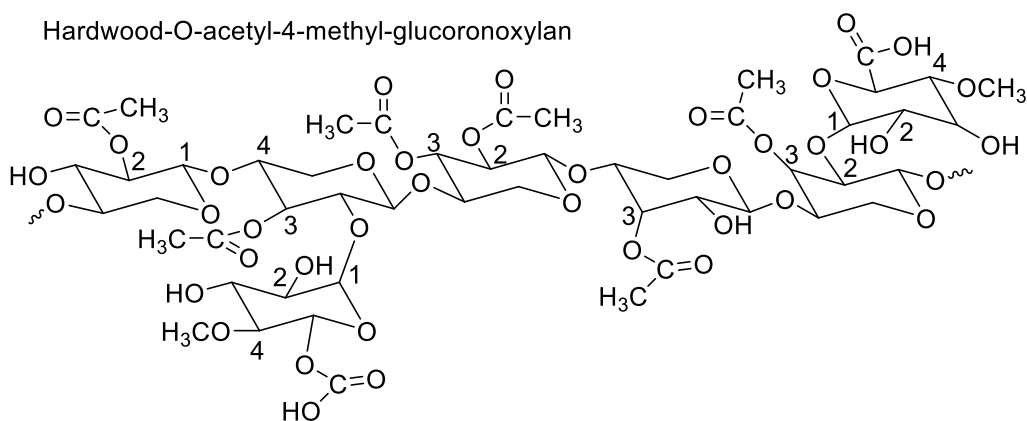


Figure A1.2. The major hemicellulose component in hardwoods adapted from [45].

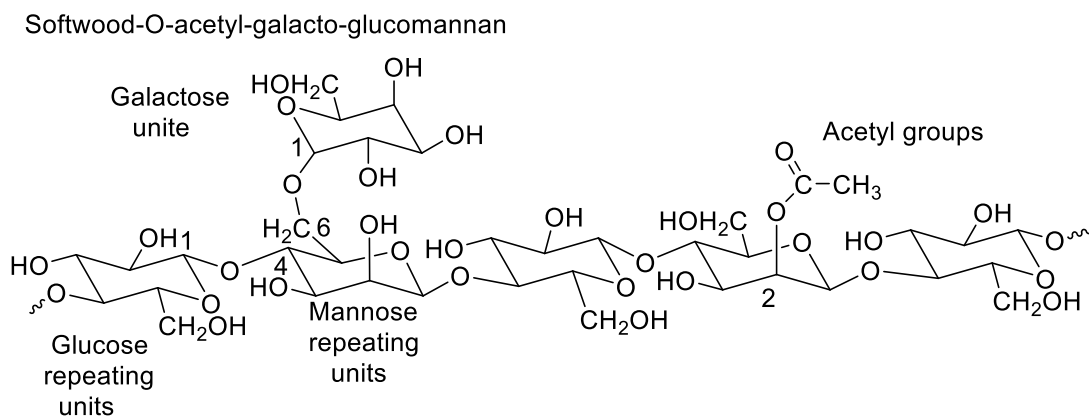


Figure A1.3. The major hemicellulose component in softwoods adapted from [45].

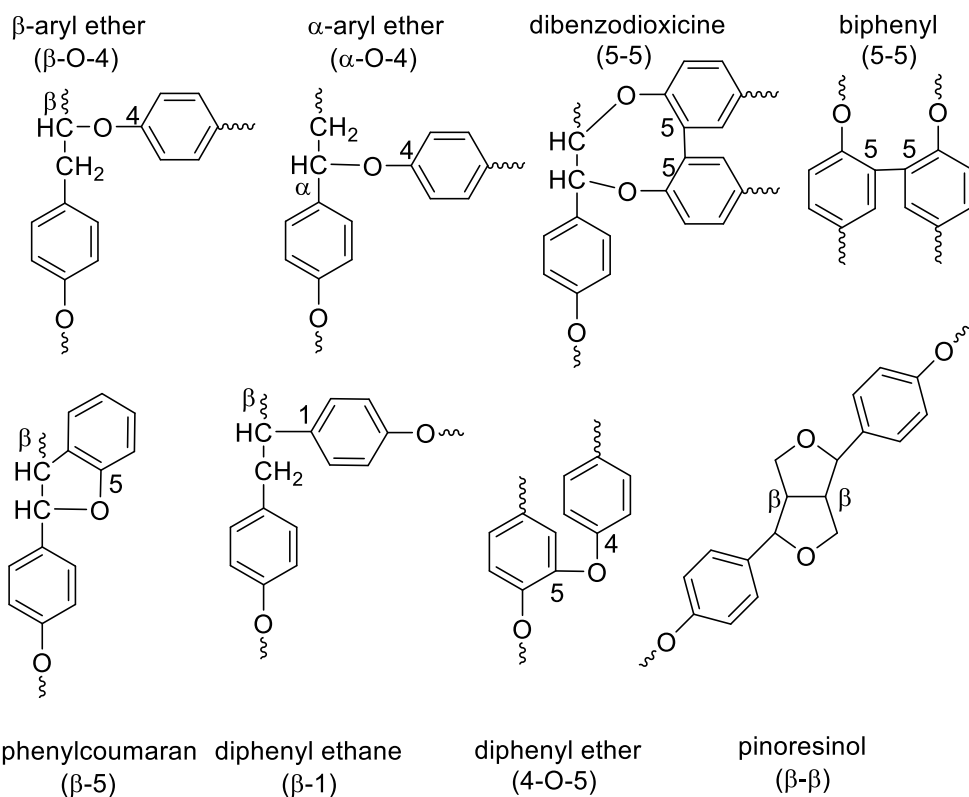


Figure A1.4. Lignin linkages: ether bonds, carbon-carbon bonds and other linkages [456].

Table A1.2. Proximate analysis (wt.%) as received for Miscanthus and Spent Grains [17–19,288,294,457–461].

Raw Material	Moisture Content (wt.%)	Volatile Content (wt.%)	Fixed Carbon (wt.%)	Ash Content (wt.%)
<i>Miscanthus</i> (Spain)	7.5	79.0	11.4	9.8
<i>Miscanthus giganteus</i>	10.0	78.8	9.5	2.7
MxG (Germany)	9.6	80.0	8.1	2.3
Miscanthus straw (France)	12.1	78.8	6.6	2.5
MxG (UK) (Nov)	4.2	73.9	19.3	2.7
MxG (UK) (Feb)	4.9	72.6	19.8	2.7
Miscanthus Pellets (France)	10.0	78.8	8.5	2.7
Miscanthus	2.0	80.5	16.0	1.5
MxG (UK) Sep	6.1	76.7	19.1	4.3
MxG (UK) June	5.3	90.9	7.2	1.9
Wheat spent grain (WSG) (UK)	6.6	75.2	16.0	2.2
Brewer spent grain (BSG) (UK)	4.6	61.4	17.0	6.5
BSG (UK)	8.0	78.0	9.5	4.5
Malt spent grain (MSG) (Mexico)	7.1	79.9	13.8	6.4

Table A1.3. Elemental analysis for miscanthus and Spent Grain [18,19,288,294,296,458–462].

Raw Material	C (wt.%)	H (wt.%)	N (wt.%)	S (wt.%)	O* (wt.%)
<i>Miscanthus x giganteus</i>	43.7	5.7	1.1	0.2	44.8
MxG (Germany)	47.1	5.4	0.4	0.1	46.8
Miscanthus straw (France)	43.7	5.7	1.1	<0.2	44.8
Miscanthus Pellets (France)	44.6	5.9	0.2	<0.2	43.2
MxG (Illinois, US)	43.5	5.9	0.3	-	50.4
Miscanthus	45.5	5.9	0.1	0.1	48.3
MxG (UK) Sep	44.9	5.6	0.9	-	48.7
MxG (UK) June	47.5	5.9	0.3	-	46.4
Wheat spent grain (WSG) (UK)	43.2	6.5	4.5	0.1	45.8
Brewer spent grain (BSG) (UK)	49.8	6.4	4.1	0.1	49.4
BSG (UK)	46.6	6.9	3.5	0.7	42.3
Malt spent grain (MSG) (Mexico)	46.8	7.0	0.7	0.3	38.7

*by difference

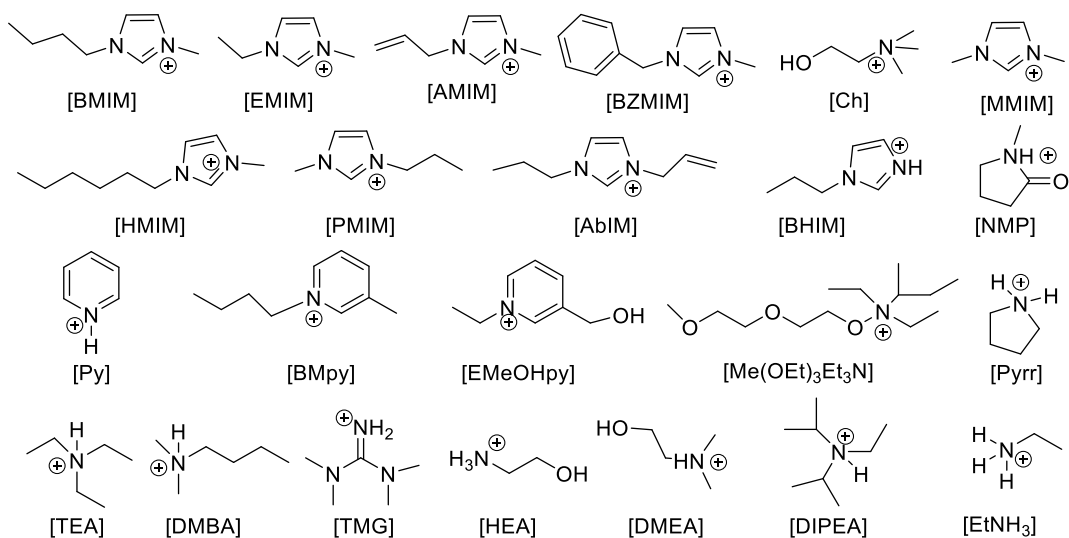


Figure A1.5. Common cations used ILs along with their structures adapted from [360,463,464].

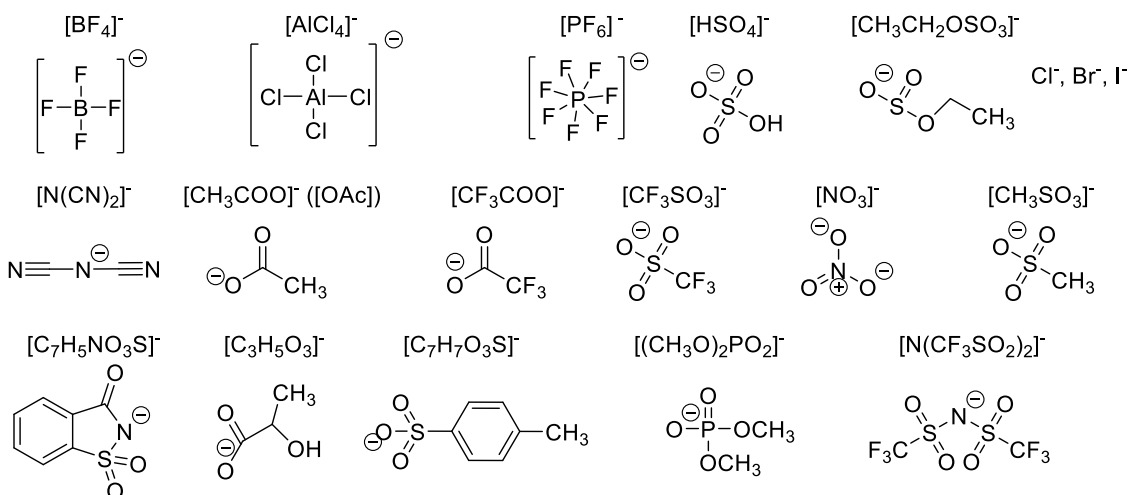


Figure A1.6. Common anions used ILs along with their structures adapted from [360,394,464].

Table A1.4. Literature on the use of different IL for different lignocellulosic materials. ND: Not defined in the paper, H: High, M: Medium, L: Low, and V: Vary

Biomass	IL	Biomass (wt.%)	Temp. (°C)	Time (hour)	Effect on fractions			Ref.
					Cellul.	Hemicell.	Lignin	
Eucalyptus	[EMIM][OAc]	3-5	120-160	4-12	H	H	V	[168,171,377]
	[EMIM][OAc] +DMSO (2:3)	15	140	2	No influence of DMSO components dissolution			[465]
	[EMIM][OAc] + H ₂ SO ₄ 1.2%	3	160	3	H	H	L	[218]
	[AMIM][Cl] & [BMIM]Cl	5	120-130	1-4	H	H	L	[466]
	[BMpy][Cl]	5	120	0.16-1.00	H	ND	ND	[219]
	[TEA][H ₂ SO ₄]	10	150	1	H	H	H	[467]
	(CIL): PIL [Pyrr][AC]: AIL [BMIM][Cl]	5-30	100	10	H	H	H	[468]
Pine wood	[EMIM][OAc]	3	160	12	H	H	M	[377]
	[BMIM][HSO ₄]	10	120	22	H	H	M	[184]
	[DMBA][HSO ₄]	10-20	150-170	1.3-1.5	H	H	M	[201,469]
Mixed Softwood	[BMIM][Cl]	5	130	15	H	H	ND	[217]
	[BMIM][OAc]	5	100	15	H	H	ND	[470]
Spruce wood	Torrefaction with [BMIM][OAc]	5	100-280	0.13-0.33	H	ND	L	[471]
Wheat Straw	[EMIM][OAc]	3-5	120-160	1.5-6	H	H	H	[172,205,472]
	[Ch][Lyss]	5	90	1	H	M	M	[473]
Rice straw	[EMIM][OAc]	100 mg/ml	120	24	H	ND	ND	[204]
	[EMIM][OAc]-DMSO(1:1)-MW	50 mg/ml	110	50 watts 1min	H	H	M	[474]
Rice hulls	[EMIM][OAc]	10	110	8	H	H	H	[215]
Corn stover	[EMIM][OAc]	3	110-160	3	H	H	M	[167,357]
	NaOH+[BMIM][Cl]+HCl	10	90-130	0.5-1	H	H	H	[475]
	NaOH+[BMIM][Cl]	5	25-130	2-24	M	M	H	[476]
	[Bmpy][Cl]	5	120	0.3-1	L	ND	ND	[219]
Bagasse	[BMIM][Cl]+1.2%HCl	10	130	0.5	H	L	L	[477]
	[Etid][For]	10	90	2	ND	ND	M	[478]
	[BMIM]Cl+ Org	10	130	1.5	H	High	low	[479]
Miscanthus	[H ₃ N(CH ₂) ₂ OH][OAc]	10	150	3.5	H	H	H	[174]
	[BMIM][HSO ₄]	10	120	22	H	H	H	[184]
	[DMBA][HSO ₄] Et	10	170	1.33	H	H	H	[469]
	[DMBA][HSO ₄]	20	150	2	ND	ND	M	[201]
	[BMIM][HSO ₄]+H ₂ O ₂	10	120	1	ND	ND	M	[480]
Coffee husk	[TEA][H ₂ SO ₄]	10	120	8	H	H	H	[360]
	[DIPEA][Ac]	5	120	4	H	H	H	[481]
Empty Fruit Bunch (EFB)	[BMIM][Cl]	3:1 (IL: EFB)	150	2.5	ND	ND	M	[198]
Oil Palm frond (OPF)	[BMIM][Cl]	4-12	80-120	0.5-3	V	V	V	[207]

Appendix 2 (Material and Methods)

Table A2.1. Physiochemical properties of macro-reticular ionic exchange resins [415,482–484].

Catalyst	IER-15	IER-35	IER-45	IER-70	IER-252	IER-275	IER-482
% Cross-linking	High	High	Low	Low	Medium	High	Low
Moisture Content ^a (%)	49.52	53.72	47.89	50.76	76.00	70.40	70.47
Swelling Degree ^b (%)	67.94	103.23	113.66	116.62	97.18	80.19	140.60
Sulphonation	C	O	C	C	O	O	C
Co-polymer	Styrene-divinylbenzene						
Matrix	Macroreticular						
Functional Group	SA	SA	SC	SC	SA	SA	SC
Physical Form Colour (Spherical, opaque beads)	Light Grey	Dark Grey	Black	Dark Brown	Dark Grey	Dark Grey	Black
Ionic Form	Hydrogen						
Acid Sites (mmol g ⁻¹) ^c	4.70	5.20	2.95	2.55	5.40	5.20	2.70
Water Retention (%)	52-57	51-57	51-55	53-59	54-58	51-59	48-58
Max Temperature (°C)	120	150	170	190	130	130	190
Particle Diameter (µm)	600 – 850	700 – 950	<355	<425	425-1200	425-1200	425-1200
Acid strength measured as average Adsorption Enthalpy (kJ mol ⁻¹)	-110 ± 3	-117 ± 2	Not available	-117 ± 2	-115 ± 3	-119 ± 1	-116 ± 3

(a) measured by drying at 105 °C, (b) measured by Equation 2.1, and (c) measured by back titration.
SA: Sulfonic acid, SC: Sulfonated-Chlorinated, C; Conventionally sulfonated, O: Over sulfonated.

Table A2.2. ATR-FTIR operational parameters

Parameter	Value
Number of Scans	64
Resolution	4 cm ⁻¹
Data spacing	0.482 cm ⁻¹
Final format	Absorbance
Atmospheric Interaction	Automatic atmospheric suppression
Background handling	Collect background after every 120 min.
Detector	MCT-A
Beam Splitter	KBr
Source	Infrared
Range	4000-400 cm ⁻¹

Table A2.3. XRD operational parameters

Parameters	Value
Angle	Wide 10-80°, 2θ
Step-size	0.02°/sec
Voltage & Current	40 kV & 40 mA
Detector	LYNXEYE
Scan mode	Continuous Power Spectral Density (PSD) Fast
Tube & Radiation	Anode copper & Cu-K α 1
Wavelength	0.15406 nm

Appendix 3 (Evaluation of Ionic Exchange Resins for Acid Hydrolysis)

Table A3.1. Ultimate analysis for IER70 fresh, ethanol washed-dry, and after pretreatment.

IER	C	H	S	N
Fresh-IER70	38.29 ± 3.90	4.01 ± 0.19	6.62 ± 0.24	0.11 ± 0.02
Ethanol-Wash-IER70	37.36 ± 4.71	3.77 ± 0.11	6.09 ± 0.26	0.15 ± 0.04
Used-IER70-1B	40.79 ± 0.29	4.39 ± 0.04	6.43 ± 0.09	0.44 ± 0.03
Used-IER70-2B	39.54 ± 0.30	4.09 ± 0.12	6.40 ± 0.18	0.40 ± 0.07
Used-IER70-3B	39.51 ± 0.37	4.11 ± 0.07	6.13 ± 0.52	0.20 ± 0.07
Used-IER70-4B	40.37 ± 1.18	4.10 ± 0.09	6.05 ± 0.25	0.12 ± 0.01

Table A3.2. Higher heating value (HHV) of raw material and pretreated pulp.

Raw Material	HHV (MJ/kg)
MIS48	16.01
P-IER00-0B	15.32
P-IER70-1B	15.66
P-IER70-2B	16.05
P-IER70-3B	16.46
P-IER70-4B	15.29
P-IER35-1B	16.36
P-IER35-2B	16.34
P-IER35-3B	16.20
P-IER35-4B	16.41

Table A3.3. pH of 20 mL Deionize water for different number of baskets.

Number of Baskets	Amberlyst 70	Amberlyst 35
0	6.44 ± 0.11	6.44 ± 0.11
1	3.33 ± 0.01	3.54 ± 0.02
2	3.15 ± 0.01	3.35 ± 0.00
3	3.01 ± 0.00	3.26 ± 0.01
4	2.87 ± 0.01	3.21 ± 0.00

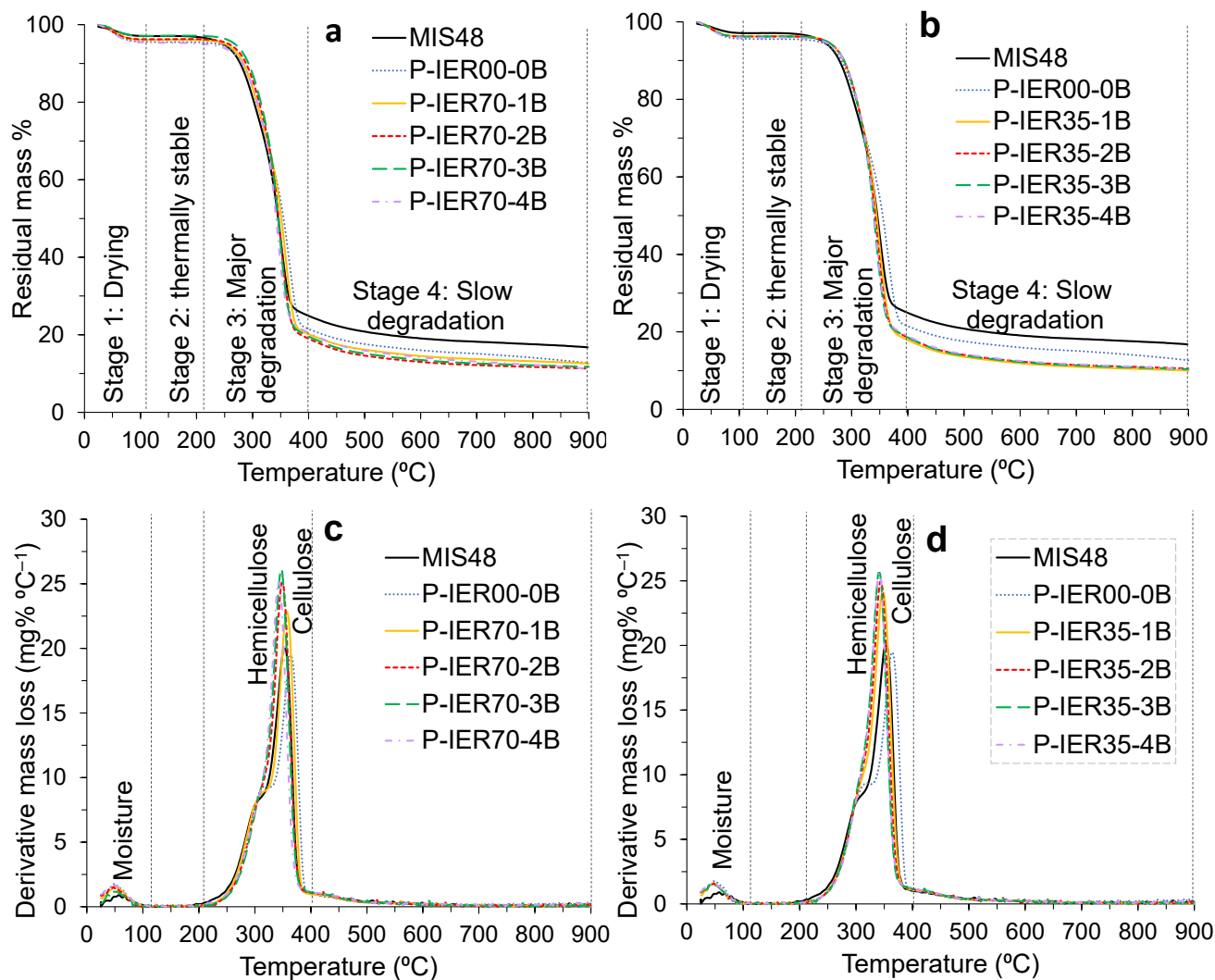


Figure A3.1. TGA and DTG thermograms under an (N₂) inert environment for MIS48 and the pretreated pulp with different IER loadings: (a) IER70 TGA; (b) IER70 DTG; (c) IER35 TGA; (d) IER35 DTG.

Table A3.4. TGA-DTG for raw material-pulp-treated IER under an inert atmosphere.

Material	1 st DTG (°C)	DTG (wt.% °C ⁻¹)	Mass loss (wt.%)	2 nd DTG (°C)	DTG (wt.% °C ⁻¹)	Mass loss (wt.%)
MIS48	303.8	8.1	20.6	355.5	20.0	61.7
P-IER00-0B	316.4	9.3	25.2	364.6	19.5	60.5
P-IER70-1B	297.0	7.6	14.8	356.5	22.9	56.4
P-IER70-2B	296.5	7.1	13.0	347.6	25.1	52.1
P-IER70-3B	297.0	8.4	15.2	346.6	26.1	51.4
P-IER70-4B	297.0	7.0	14.7	341.9	25.2	50.4
P-IER35-1B	296.6	7.7	14.1	347.8	24.1	55.3
P-IER35-2B	297.0	7.8	13.9	345.7	24.9	55.0
P-IER35-3B	297.0	8.0	14.0	342.3	25.6	54.1
P-IER35-4B	297.0	7.6	13.8	342.3	25.6	53.4

Table A3.5. TGA-DTG for raw material-pulp treated IER under oxidative atmosphere.

Material	1 st DTG (°C)	DTG (wt.% °C ⁻¹)	Mass loss (wt.%)	2 nd DTG (°C)	DTG (wt.% °C ⁻¹)	Mass loss (wt.%)	3 rd DTG (°C)	DTG (wt.% °C ⁻¹)	Mass loss (wt.%)
MIS48	296.3	10.9	28.5	325.6	16.2	50.0	454.0	4.9	88.6
P-IER00-0B	305.5	11.7	27.3	329.3	31.8	52.0	448.5	3.6	89.6
P-IER70-1B	292.6	9.4	17.4	323.8	36.1	50.1	496.1	3.1	90.9
P-IER70-2B	283.5	7.7	12.1	318.3	35.5	47.3	494.3	2.8	91.2
P-IER70-3B	285.3	7.1	12.1	318.1	34.7	46.0	499.8	3.0	92.6
P-IER70-4B	278.0	6.3	11.2	314.6	31.4	44.5	496.1	3.1	90.4
P-IER35-1B	292.6	10.7	17.0	320.1	37.7	50.1	494.3	2.7	92.5
P-IER35-2B	292.6	11.1	17.5	318.3	35.6	48.8	496.1	2.8	92.4
P-IER35-3B	292.6	11.1	18.5	316.5	34.8	46.3	496.1	2.9	92.8
P-IER35-4B	292.6	11.9	20.0	316.5	34.1	49.4	494.3	2.8	92.6

Table A3.6. Crystallinity Index (*CrI*) using area deconvolution and peak fit values.

Material	CrI (%) Area Deconvolution	CrI (%) Fit
MIS48	54.58	72.04
P-IER00-0B	61.05	77.99
P-IER70-1B	58.32	76.25
P-IER70-2B	59.73	77.30
P-IER70-3B	61.10	77.65
P-IER70-4B	59.94	78.11
P-IER35-1B	59.58	77.77
P-IER35-2B	60.47	78.56
P-IER35-3B	58.50	78.68
P-IER35-4B	57.31	76.59

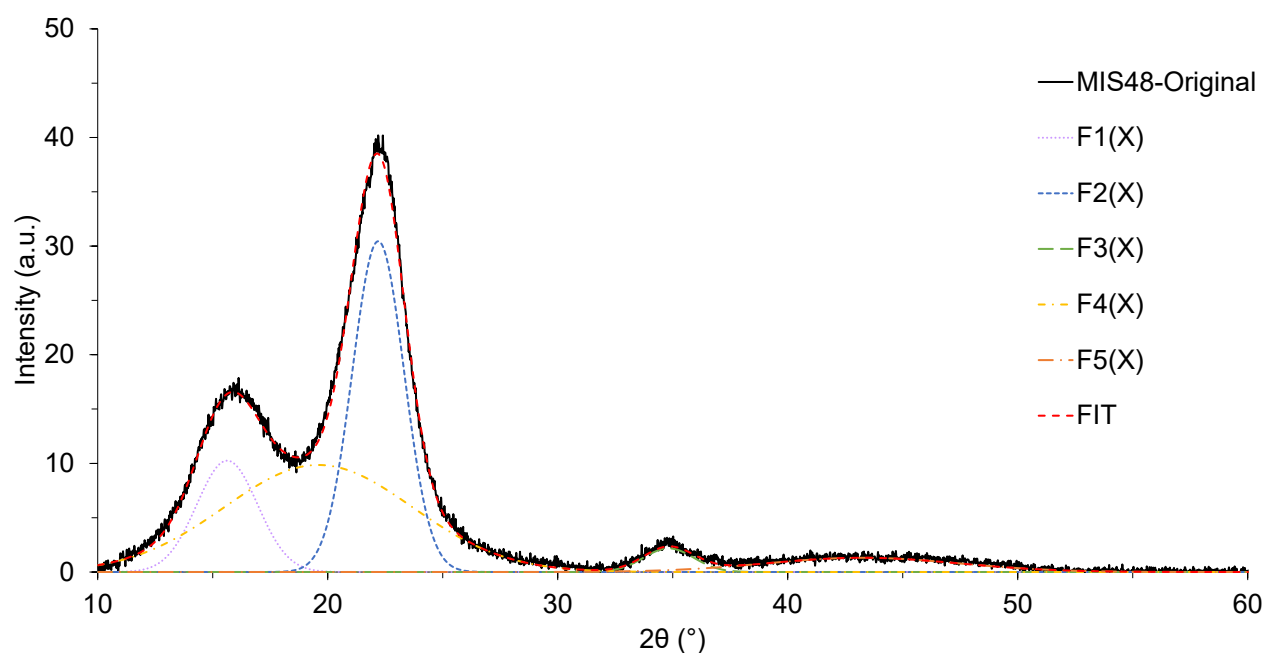


Figure A3.2. XRD diffractogram: Original after background subtracted, deconvoluted, and peak fit. F1(X), F3(X) and F4(X) deconvolution of crystalline peaks, F2(X) and F5(X) deconvolution of amorphous peaks, and FIT fitting curve.

Table A3.7. ATR-FTIR spectral wavenumber and band assignment

Wavenumber cm^{-1}	Band Assignment
3400-3200,	OH, stretching vibrations
3793-3012, ~3565, ~3346	OH, groups of alcohols and intermolecular bonds
~2870	-CH stretching of the aliphatic structure
3012-2800	-CH stretching vibrations due to methyl & methylene
~2918	-C-H stretching of cellulose
~2849	-C-H stretching of lignin
2140-2100, ~2143	$\text{C}\equiv\text{C}$ bond stretching mono substitution
~1730	C=O in ketone, ester, carboxylic acid, and unconjugated xylan
~1747	C=O stretching due to unconjugated ketones and ester groups
1700-1500	aromatic ring stretching in lignin
~1655	C=O stretching vibration in conjugate p-substituted aryl ketone group
~1646	OH, absorbed water deformation vibrations with C=O stretching vibrations
~1634	C=O stretching vibrations and benzene stretching rings
~1429	aromatic skeletal combined with C-H in-plane deformation and stretching
~1230	C-O stretching
980-960, ~984	C=C bending
~901	C-H deformation of ring valence vibration
850-700	aryl C-H and/or aryl C-O groups
725-680	cis and meta-aromatic distributions

Table A3.8. Crystallinity Index (*Crl*) using area deconvolution and peak fit values.

Material	<i>Crl</i> (%) by Area	<i>Crl</i> (%) Fit
MIS48	54.58	72.04
P-IER70-2B	59.73	77.3
P-HCl (IER70-2B)	60.08	78.06
P-H ₂ SO ₄ (IER70-2B)	56.91	75.45
P-IER35-2B	60.47	78.56
P-HCl (IER35-2B)	59.01	78.51
P-H ₂ SO ₄ (IER35-2B)	58.11	77.55

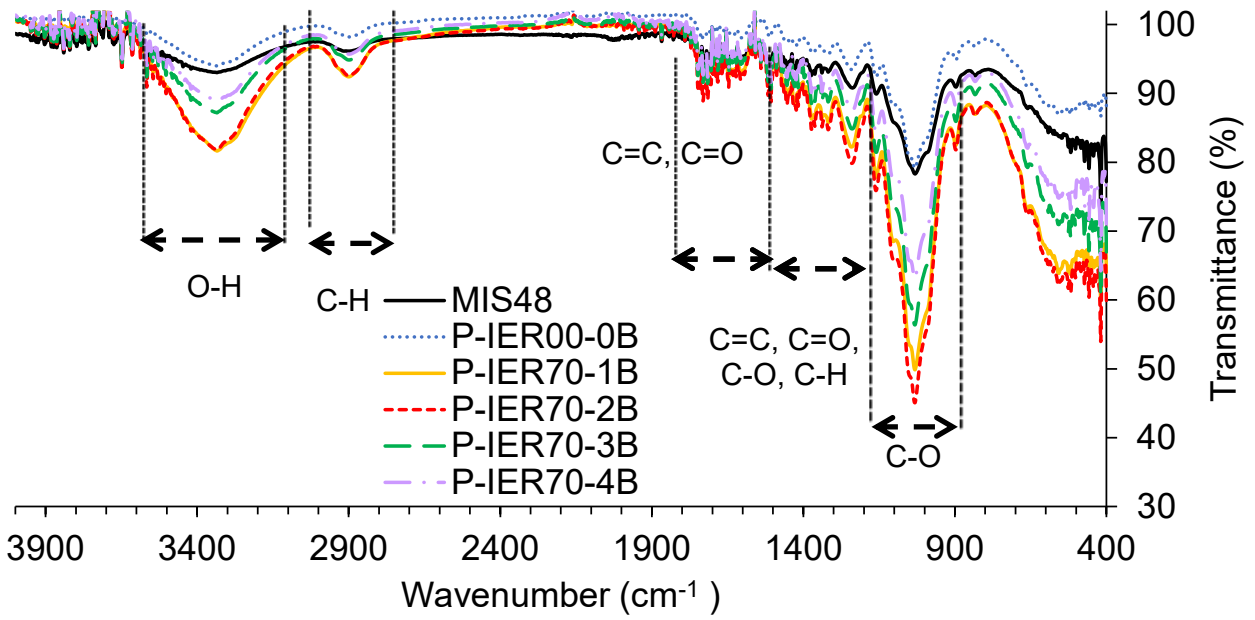


Figure A3.3. ATR spectral wavelength range 4000-400 cm^{-1} for MIS48 and IER70 treated pulp.

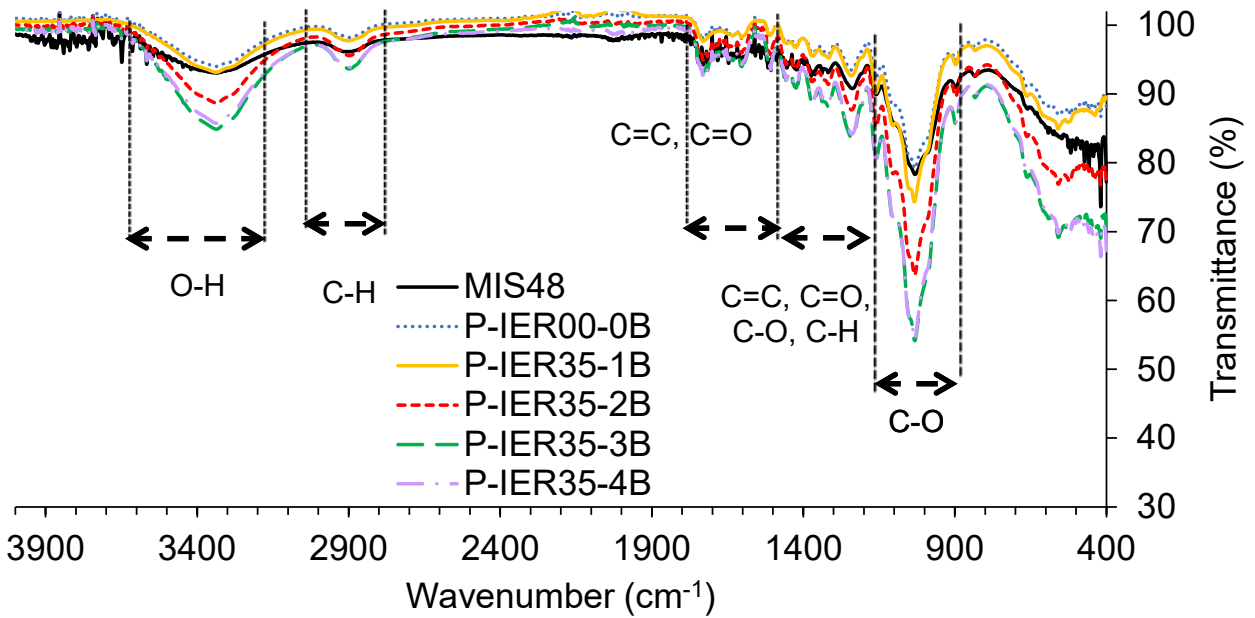


Figure A3.4. ATR spectral wavelength range 4000-400 cm^{-1} for MIS48 and IER35 treated pulp.

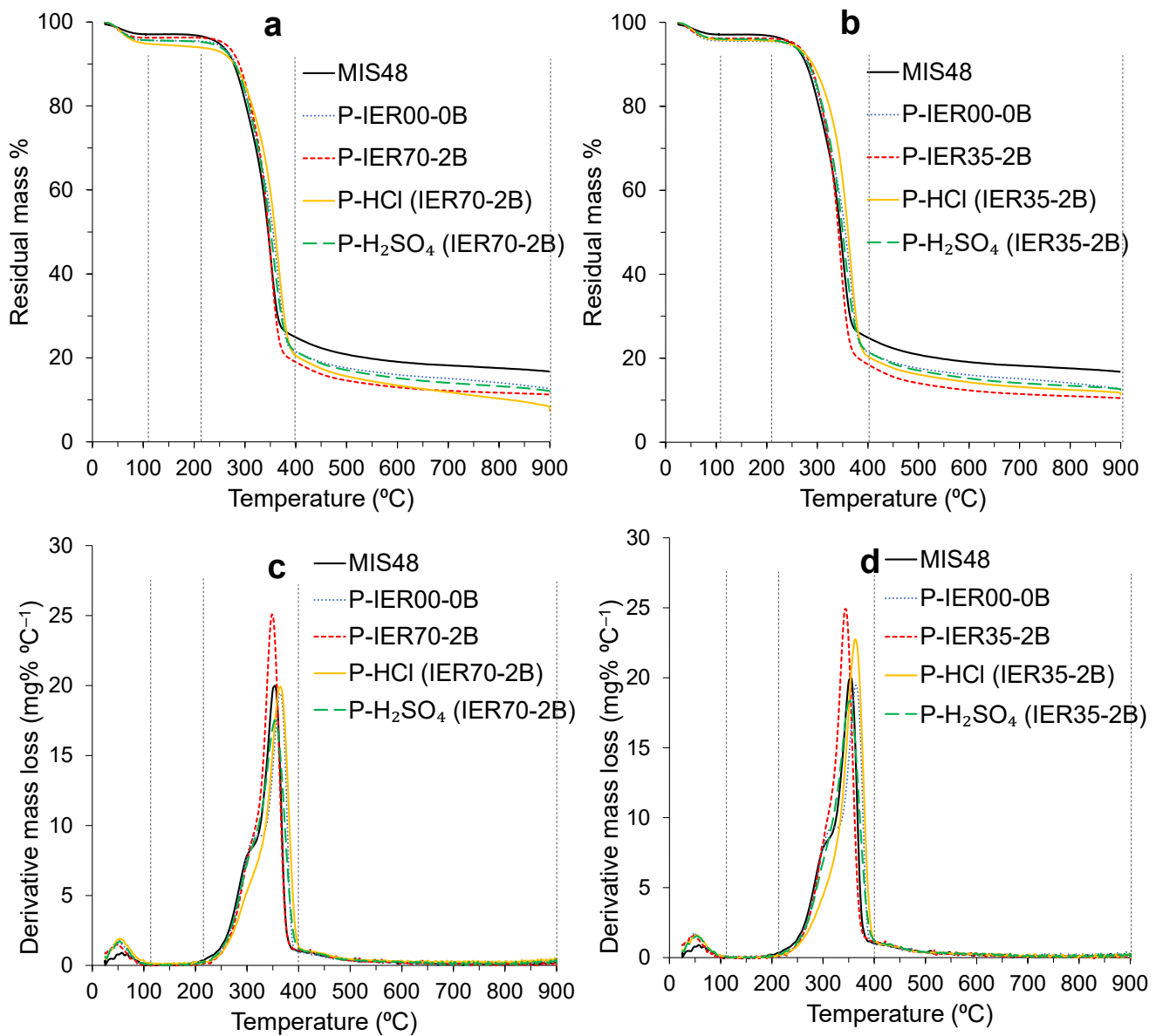


Figure A3.5. Thermogravimetric analysis of biomass and pulp under (N₂) inert conditions. Comparative of hydrolysis for two baskets of IER with mineral acid hydrolysis using equivalent proton concentration: (a) TGA IER70 and equivalent, (b) TGA IER35 and equivalent, (c) DTG IER70 and equivalent, and (d) DTG IER35 and equivalent.

Appendix 4 (Evaluation of Ionic Exchange Resin and Ionic Liquid mixtures for lignocellulosic biomass fractionation)

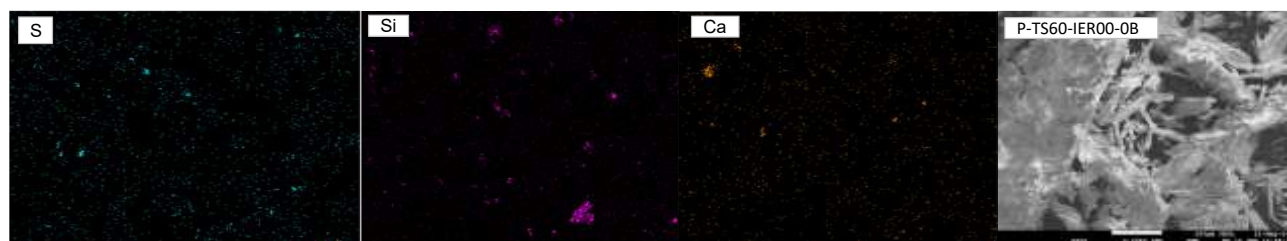


Figure A4.1. EDX colour mapping for pulp, after IL-TS60-IER00-0B: S (Sulphur), Si (Silica), Ca (calcium), and pulp

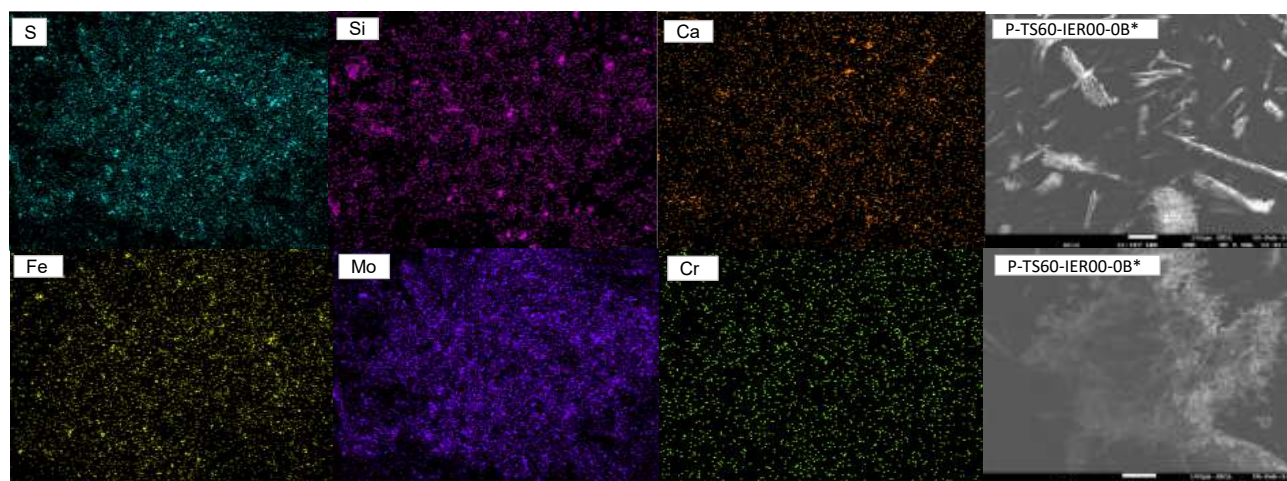


Figure A4.2. EDX colour mapping for pulp, after IL-TS60-IER70-2B: S (Sulphur), Si (Silica), Ca (calcium), (Fe) Iron, (Mo) Molybdenum (Cr) chromium and pulp. (* Baskets dissolved)

Table A4.1. Ultimate analysis (wt.%) of raw material (MIS16) and pulp for IL-TA-IER70.

Sample	N	C	H	S
MIS16	0.47 ± 0.01	43.87 ± 0.14	6.05 ± 0.06	0.00 ± 0.00
P-TA40	0.35 ± 0.01	42.97 ± 0.03	6.04 ± 0.07	0.00 ± 0.00
P-TA40-IER70	0.86 ± 0.11	43.80 ± 0.05	6.07 ± 0.10	0.00 ± 0.00
P-TA80	0.37 ± 0.00	42.98 ± 0.04	5.97 ± 0.12	0.00 ± 0.00
P-TA80-IER70	0.38 ± 0.01	43.27 ± 0.05	6.06 ± 0.07	0.00 ± 0.00

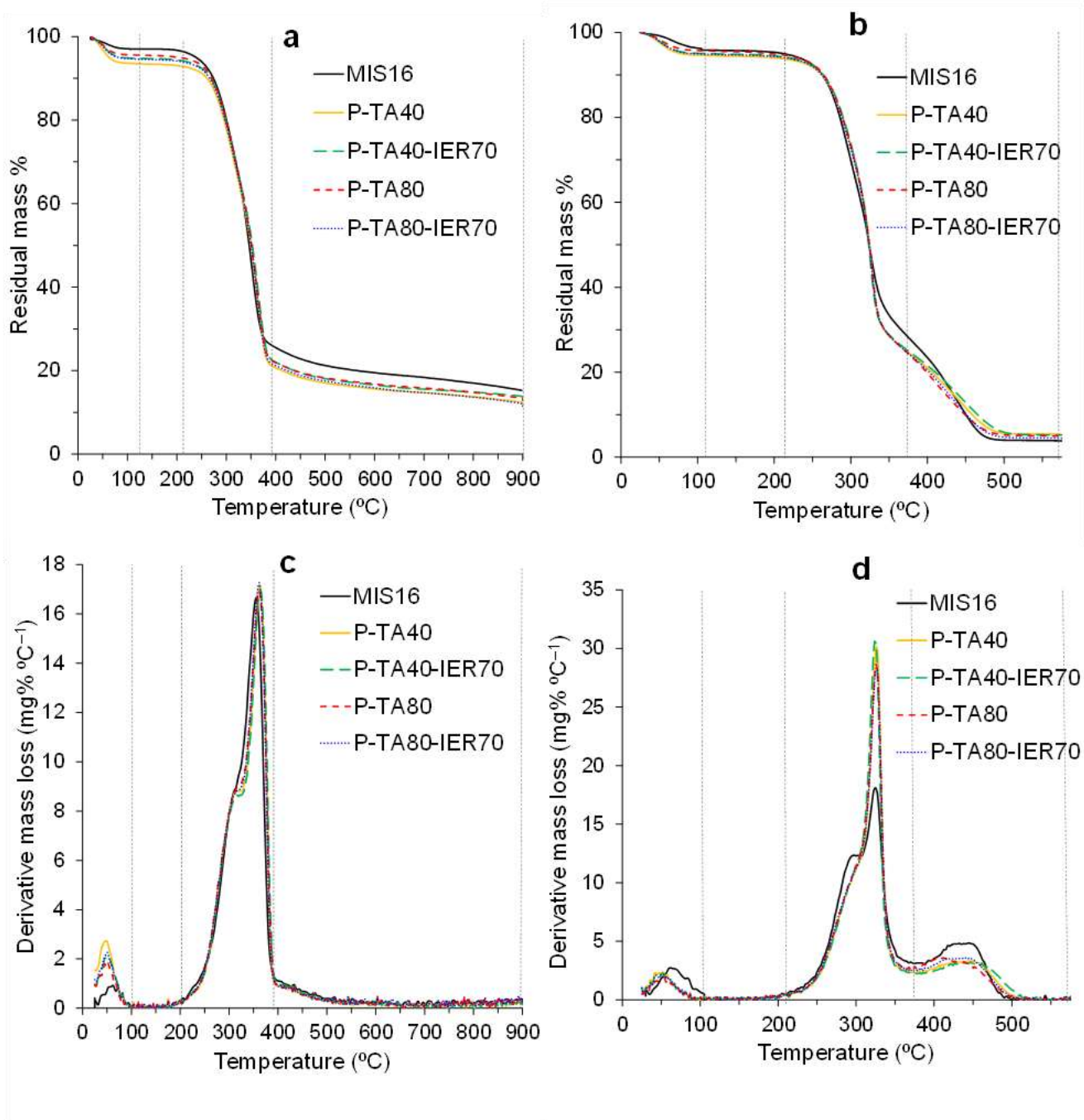


Figure A4.3. TGA-DTG curves under (N₂) inter conditions for biomass, pulp treated with IL-TA-IER70, (a, c) under nitrogen and (b, d) under air at different IL concentrations.

Table A4.2. TGA-DTG peak temperatures-mass loss for raw material-pulp treated IL-TA-IER70 under inert conditions.

Material	1 st DTG (°C)	DTG (wt.% °C ⁻¹)	Mass loss (wt.%)	2 nd DTG (°C)	DTG (wt.% °C ⁻¹)	Mass loss (wt.%)
MIS16	309.0	8.8	24.4	355.5	16.6	59.0
P-TA40	311.1	8.7	27.5	362.1	17.2	61.3
P-TA40-IER70	316.8	8.6	28.8	362.1	16.9	58.7
P-TA80	314.0	8.8	27.7	362.1	16.8	61.1
P-TA80-IER70	305.5	8.5	23.7	362.1	17.3	61.7

Table A4.3. TGA-DTG peak temperatures-mass loss for raw material-pulp treated IL-TA-IER70 under air.

Material	1 st DTG (°C)	DTG (wt.% °C ⁻¹)	Mass loss (wt.%)	2 nd DTG (°C)	DTG (wt.% °C ⁻¹)	Mass loss (wt.%)	3 rd DTG (°C)	DTG (wt.% °C ⁻¹)	Mass loss (wt.%)
MIS16	295.0	12.3	26.4	325.0	18.1	51.0	445.0	4.9	88.5
P-TA40	292.6	9.9	22.2	325.6	30.1	52.3	450.3	3.3	88.4
P-TA40-IER70	292.6	10.0	21.6	323.8	30.6	50.9	454.0	3.1	87.9
P-TA80	294.5	10.4	23.1	325.6	28.7	52.6	443.8	3.3	87.1
P-TA80-IER70	292.6	9.9	22.7	325.6	28.4	52.7	441.1	3.6	87.9

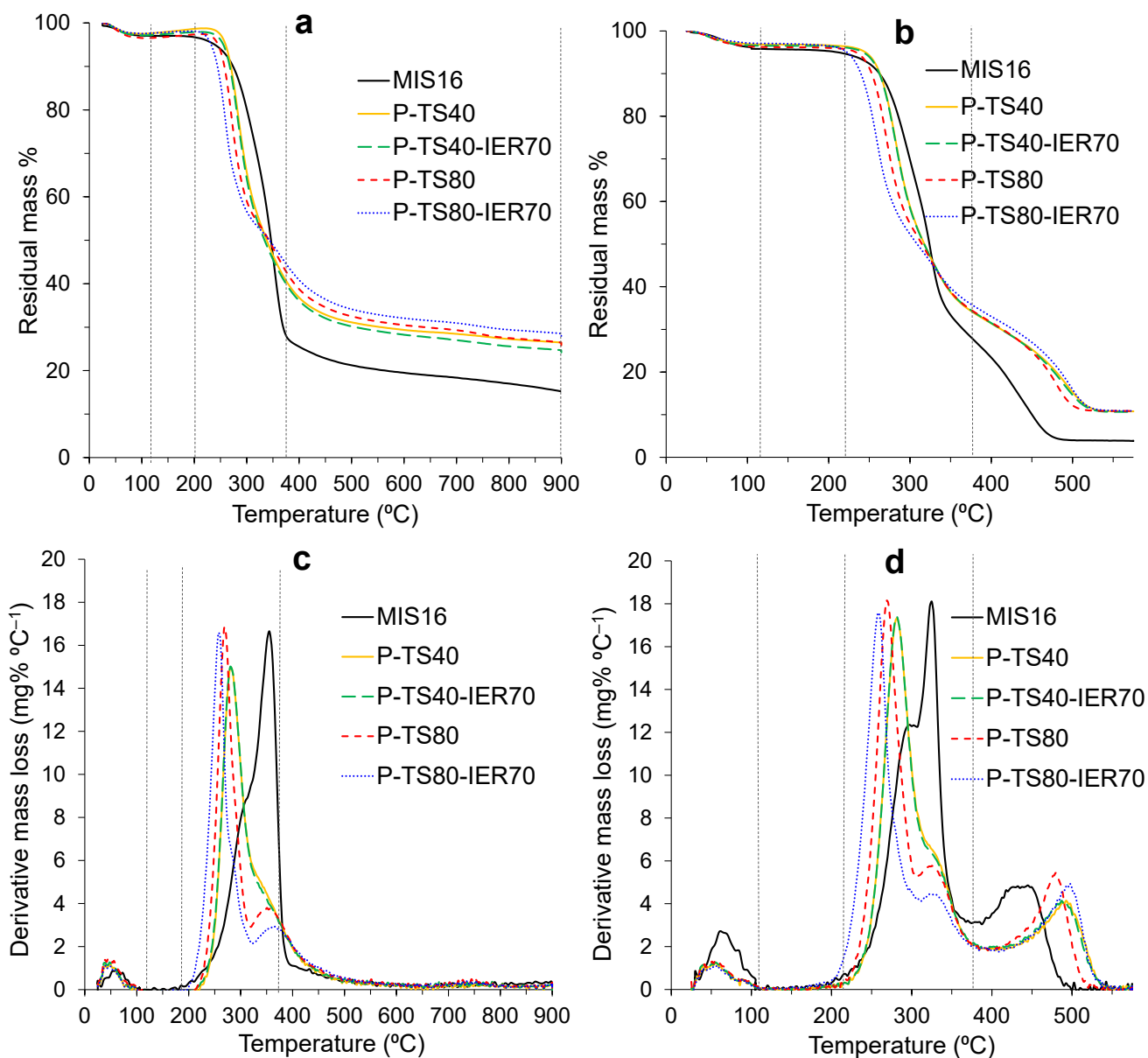


Figure A4.4. TGA-DTG curves under inter conditions for biomass, pulp treated with IL-TS-IER70, (a, c) under nitrogen and (b, d) under air at different IL concentrations.

Table A4.4. TGA-DTG peak temperatures-mass loss for raw material-pulp treated IL-TS-IER70 inert conditions.

Material	1 st DTG (°C)	DTG (wt.% °C ⁻¹)	Mass loss (wt.%)	2 nd DTG (°C)	DTG (wt.% °C ⁻¹)	Mass loss (wt.%)
MIS16	309.0	8.8	24.4	355.5	16.6	59.0
P-TS40	280.0	15.0	18.0	-	-	-
P-TS40-IER70	280.0	15.0	19.5	-	-	-
P-TS80	268.7	16.8	19.2	356.5	3.8	53.2
P-TS80-IER70	257.3	16.6	20.4	362.2	2.9	53.2

Table A4.5. TGA-DTG peak temperatures-mass loss for raw material-pulp treated IL-TS-IER70 under air.

Material	1 st DTG (°C)	DTG (wt.% °C ⁻¹)	Mass loss (wt.%)	2 nd DTG (°C)	DTG (wt.% °C ⁻¹)	Mass loss (wt.%)	3 rd DTG (°C)	DTG (wt.% °C ⁻¹)	Mass loss (wt.%)
MIS16	295.0	12.3	26.4	325.0	18.1	51.0	445	4.9	88.5
P-TS40	281.7	17.3	25.1	334.8	5.8	56.7	498	3.5	85.1
P-TS40-IER70	281.7	17.4	25.5	331.2	6.0	55.3	496	3.3	86.1
P-TS80	268.8	18.2	22.8	325.7	5.8	53.7	480	5.4	82.7
P-TS80-IER70	257.8	17.6	24.2	329.3	4.4	55.3	498	4.9	83.5

Appendix 5 (Evaluation of Triethyl ammonium hydrogen sulphate with different Ionic Exchange Resins and Lignocellulosic Feedstocks)

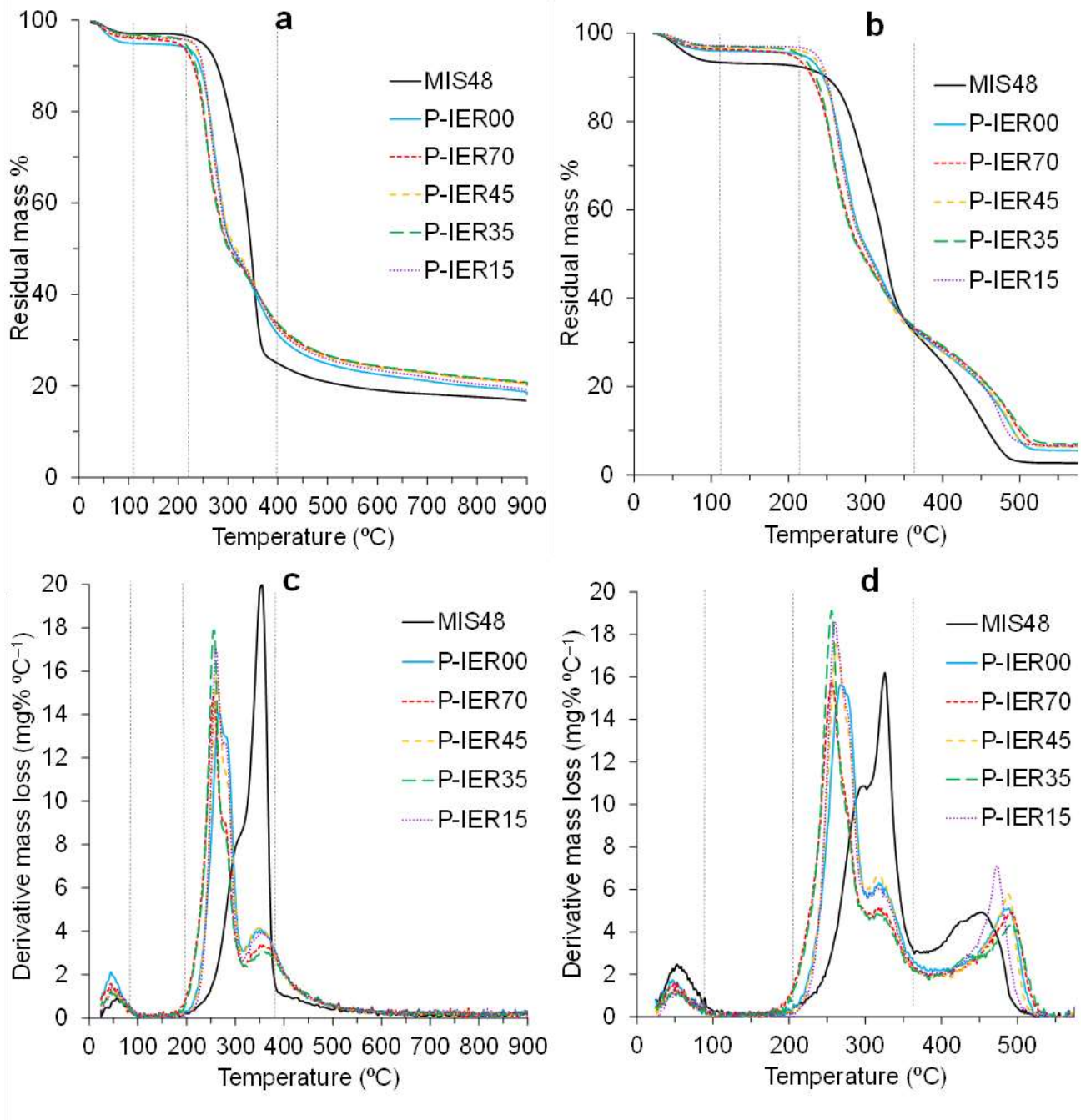


Figure A5.1. Comparison of TGA-DTG curves for raw material, benchmark pulp obtained from pretreatment with only TS80, and pulps obtained from pretreatment with TS80 + different Amberlyst IERs. (a) TGA under inert conditions, (b) TGA in air, (c) DTG for inert conditions and (d) DTG under air.

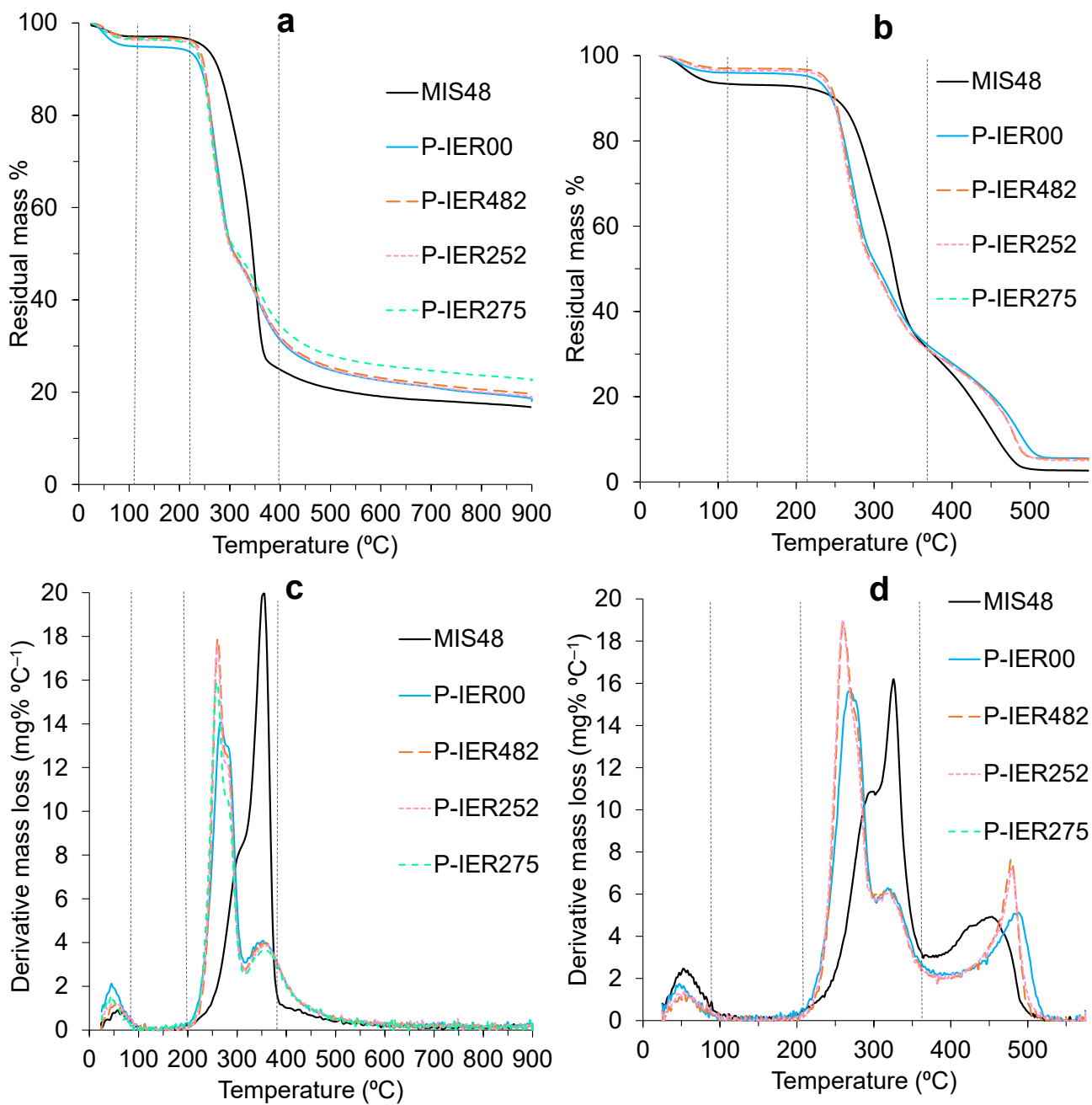


Figure A5.2. Comparison of TGA-DTG curves for raw material, benchmark pulp obtained from pretreatment with only TS80, and pulps obtained from pretreatment with TS80 + different PuroLite IERs. (a) TGA under inert conditions, (b) TGA in air, (c) DTG for inert conditions and (d) DTG under air.

Table A5.1. TGA-DTG peak temperatures-mass loss for raw material-pulp treated TS80 treatment with different IERs under inert conditions.

Material	1 st DTG (°C)	DTG (wt.% °C ⁻¹)	Mass loss (wt.%)	2 nd DTG (°C)	DTG (wt.% °C ⁻¹)	Mass loss (wt.%)	3 rd DTG (°C)	DTG (wt.% °C ⁻¹)	Mass loss (wt.%)
MIS48	303.8	8.1	20.6	355.5	20.0	61.7	-	-	-
P-IER00	268.6	14.1	25.3	282.8	12.9	36.6	359.3	4.0	60.9
P-IER70	257.3	14.7	26.1	280.0	9.0	41.3	367.8	3.3	61.4
P-IER45	263.0	15.8	21.3	280.0	11.3	35.1	353.6	4.2	58.2
P-IER35	257.3	18.0	26.0	280.0	8.5	42.2	367.8	3.0	61.3
P-IER15	260.1	17.0	18.9	282.8	12.4	38.3	359.3	3.9	59.7
P-IER482	260.1	18.0	18.1	282.8	12.3	38.2	356.5	4.0	59.5
P-IER252	260.1	17.6	20.1	282.8	12.0	39.3	362.1	3.9	61.2
P-IER275	260.1	15.9	21.2	282.8	10.4	38.4	359.3	3.7	58.2

Table A5.2. TGA-DTG peak temperatures-mass loss for raw material-pulp treated TS80 treatment with different IERs under oxidative conditions.

Material	1 st DTG (°C)	DTG (wt.% °C ⁻¹)	Mass loss (wt.%)	2 nd DTG (°C)	DTG (wt.% °C ⁻¹)	Mass loss (wt.%)	3 rd DTG (°C)	DTG (wt.% °C ⁻¹)	Mass loss (wt.%)
MIS48	296.3	10.9	28.5	325.6	16.2	50.0	454.0	4.9	88.6
P-IER00	270.6	15.6	28.0	322.0	6.2	56.0	488.8	5.1	89.1
P-IER70	257.8	15.6	27.4	320.1	4.9	57.0	494.3	4.9	88.5
P-IER45	261.5	17.5	21.0	320.1	6.6	56.5	490.6	5.6	89.5
P-IER35	256.0	19.1	25.6	320.1	4.8	57.3	494.3	4.4	87.7
P-IER15	261.5	18.6	20.9	320.1	6.0	56.0	472.3	7.1	85.9
P-IER482	259.6	18.8	18.8	320.1	6.2	56.8	477.8	7.6	88.3
P-IER252	259.6	19.0	20.9	322.0	6.0	57.9	380.6	2.1	70.5
P-IER275	261.5	17.9	23.8	322.0	5.7	57.3	499.8	4.0	88.7

Table A5.3. TGA-DTG shoulders-mass loss for raw material-pulp treated TS80 treatment with different IERs under oxidative conditions.

Material	1 st DTG (°C)	DTG (wt.% °C ⁻¹)	Mass loss (wt.%)
MIS48	296.3	10.9	28.5
P-IER00	274.3	15.2	31.4
P-IER70	268.8	11.4	36.5
P-IER45	274.3	14.1	33.6
P-IER35	270.6	10.5	38.8
P-IER15	274.3	14.6	33.8
P-IER482	274.3	14.7	34.0
P-IER252	272.5	14.5	34.0
P-IER275	276.1	12.8	37.4

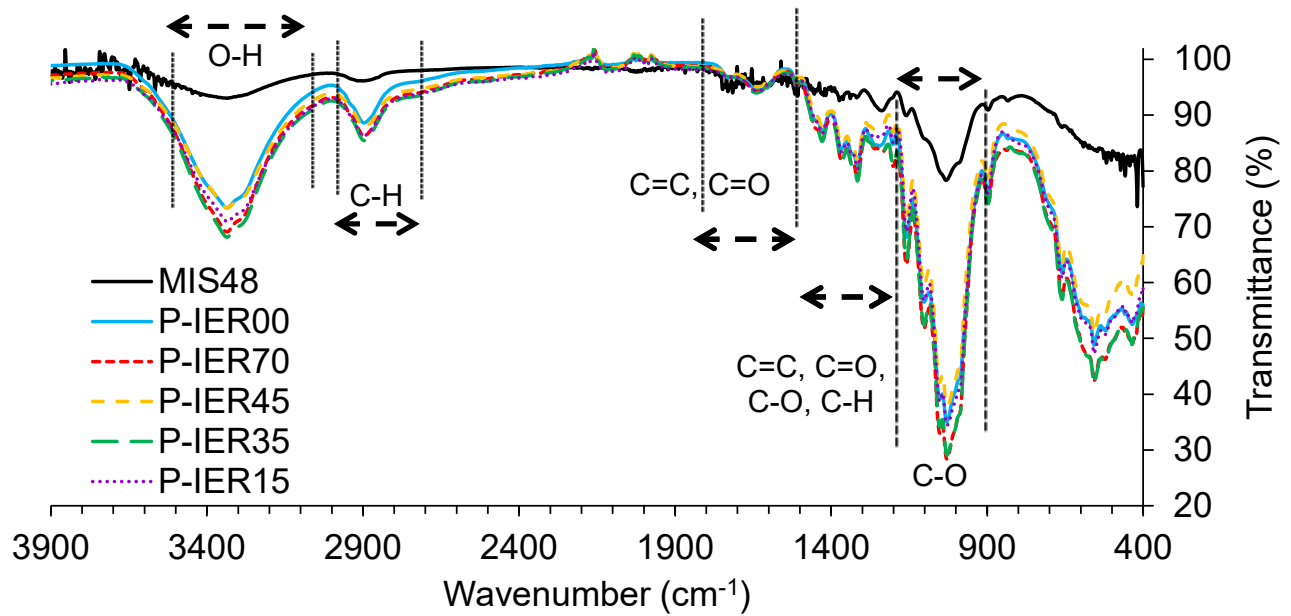


Figure A5.3. ATR spectral wavelength range 4000-400 cm^{-1} for raw material-pulp treated TS80 treatment with different Amberlyst IERs.

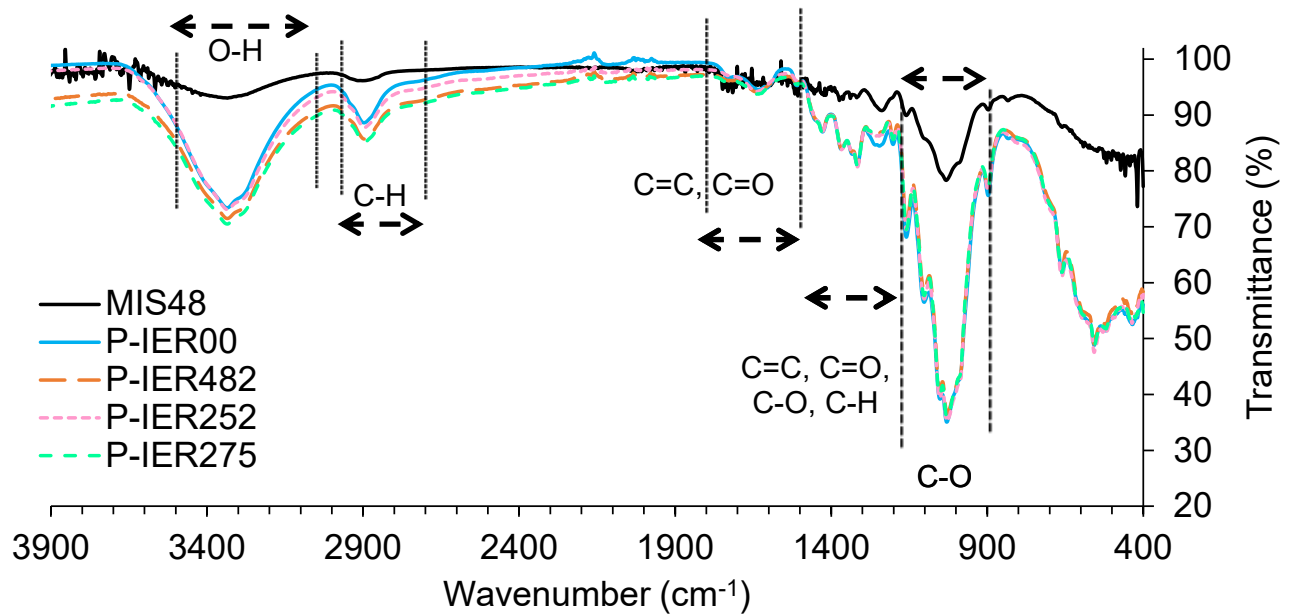


Figure A5.4. ATR spectral wavelength range 4000-400 cm^{-1} for raw material-pulp treated TS80 treatment with different Purolite IERs.

Table A5.4 Proximate analysis (wt.%) of raw materials for different particle size ranges.

Material	Moisture Content (%)	Volatile Content (%)	Ash Content (%)	Fixed Carbon (%)
MIS16	4.20 ± 0.03	78.01 ± 0.26	6.30 ± 0.43	11.49 ± 0.65
MIS48	3.21 ± 0.05	81.76 ± 0.91	3.36 ± 0.34	11.67 ± 0.51
BSG16	4.09 ± 0.16	78.07 ± 0.85	9.88 ± 0.07	7.96 ± 0.07
BSG48	2.62 ± 0.21	74.87 ± 0.15	16.81 ± 2.21	5.70 ± 2.40
PB16	7.70 ± 0.14	58.78 ± 0.46	5.14 ± 0.18	28.38 ± 0.70
PB48	6.77 ± 0.25	62.50 ± 1.03	3.76 ± 0.20	26.97 ± 0.76

Table A5.5. Ultimate analysis (wt.%) of raw materials and different particle size ranges.

Sample	C	H	S	N
MIS16	43.87 ± 0.14	6.05 ± 0.06	0.00 ± 0.00	0.47 ± 0.01
MIS48	44.98 ± 0.17	6.09 ± 0.08	0.00 ± 0.00	0.43 ± 0.05
BSG16	46.14 ± 0.06	6.81 ± 0.06	0.25 ± 0.01	4.87 ± 0.06
BSG48	47.78 ± 1.10	6.68 ± 0.08	0.08 ± 0.00	4.87 ± 0.75
PB16	49.14 ± 0.22	5.23 ± 0.01	0.00 ± 0.00	0.82 ± 0.02
PB48	50.16 ± 0.16	5.61 ± 0.14	0.00 ± 0.00	0.52 ± 0.01

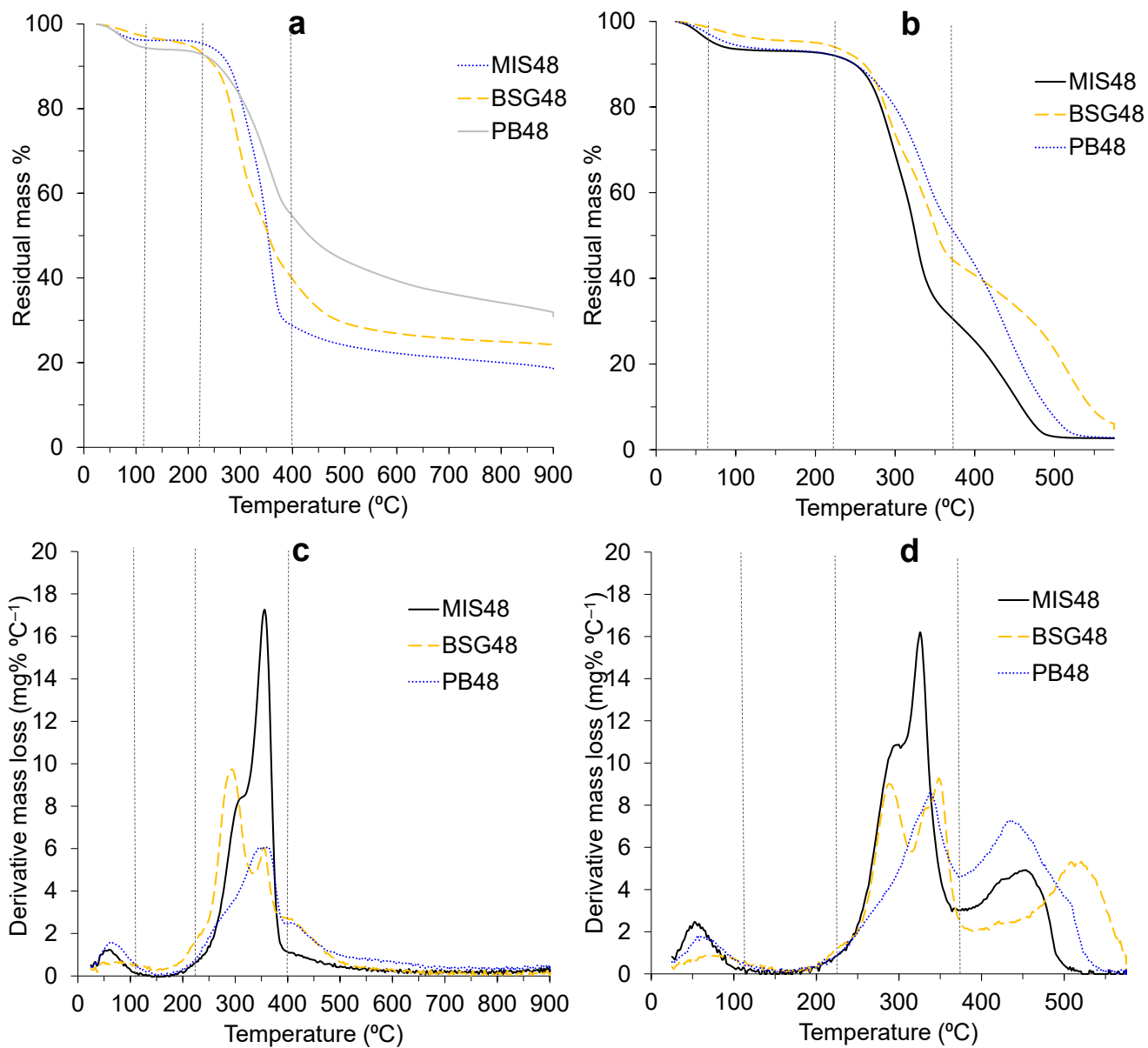


Figure A5.5. TGA-DTG curves under inert (a, c) and air (b, d) conditions for different lignocellulosic materials particle size 425-800 μm .

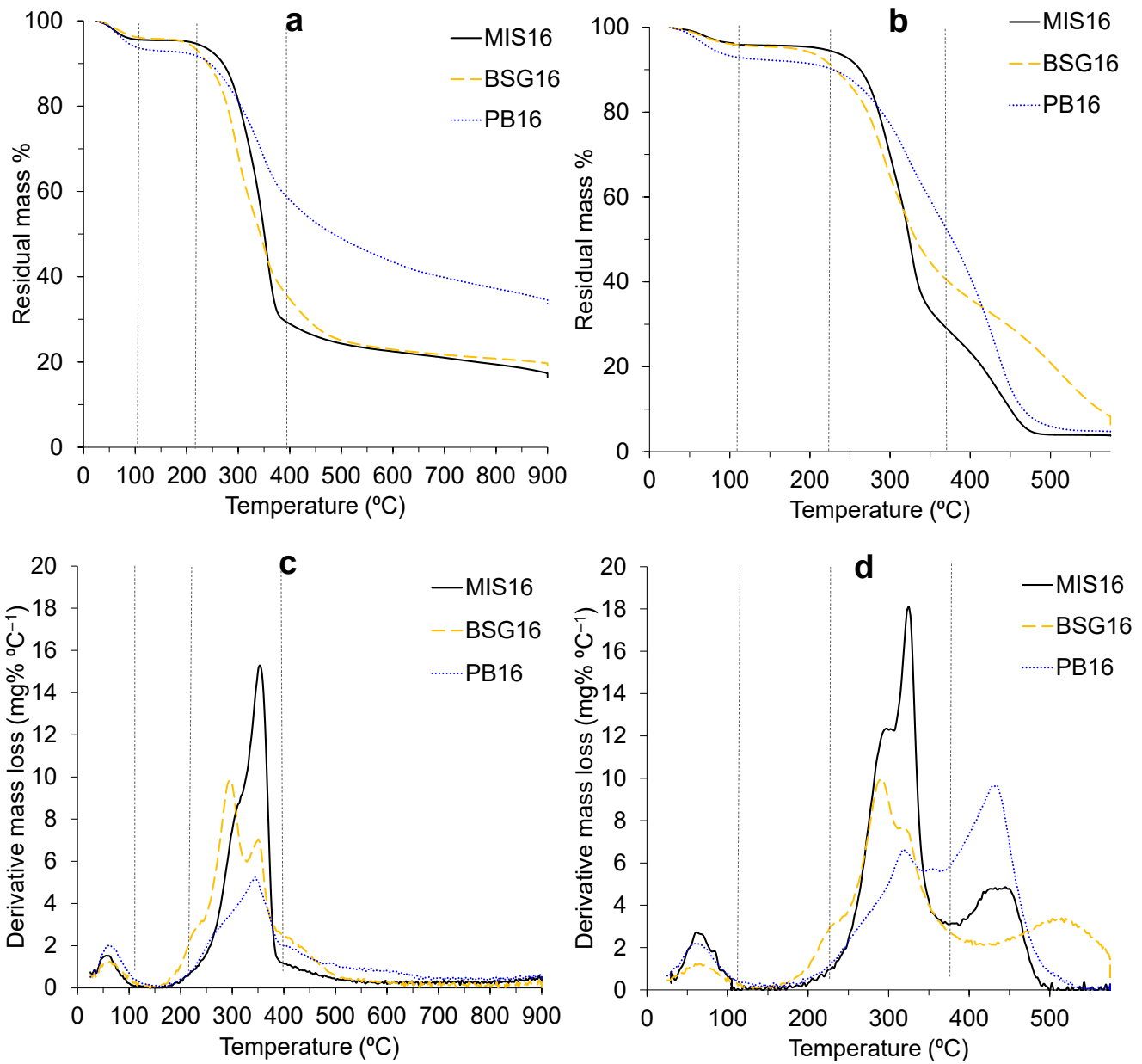


Figure A5.6. TGA-DTG curves under nitrogen (a, c) and air (b, d) conditions for lignocellulosic materials with particle sizes <106 μm .

Table A5.6. TGA-DTG peak temperatures-mass loss for different lignocellulosic materials particle size <106 μm under nitrogen.

Material	1 st DTG (°C)	DTG (wt.% °C ⁻¹)	Mass loss (wt.%)	2 nd DTG (°C)	DTG (wt.% °C ⁻¹)	Mass loss (wt.%)	3 rd DTG (°C)	DTG (wt.% °C ⁻¹)	Mass loss (wt.%)
MIS16	311.2	8.7	24.2	353.7	15.3	52.8	-	-	-
MIS48	303.8	8.1	20.6	355.5	20.0	61.7	-	-	-
BSG16	226.2	2.7	8.4	297.0	9.8	30.9	350.8	7.0	54.1
BSG48	294.2	9.7	26.6	353.7	6.0	49.7	413.2	2.6	62.4
PB16	274.3	2.9	13.9	345.2	5.3	30.6	410.3	1.9	43.3
PB48	268.7	2.6	11.4	350.8	6.1	32.1	401.8	2.4	45.7

Table A5.7. TGA-DTG peak temperatures-mass loss for lignocellulosic materials particle size 425-800 μm and <106 μm under air.

Material	1 st DTG (°C)	DTG (wt.% °C ⁻¹)	Mass loss (wt.%)	2 nd DTG (°C)	DTG (wt.% °C ⁻¹)	Mass loss (wt.%)	3 rd DTG (°C)	DTG (wt.% °C ⁻¹)	Mass loss (wt.%)
MIS16	301.8	11.5	28.3	333.0	16.8	52.6	417.3	5.2	81.4
MIS48	296.3	10.9	28.5	325.6	16.2	50.0	454.0	4.9	88.6
BSG16	290.8	10.0	29.8	322.0	7.6	45.6	520.0	3.4	83.0
BSG48	289.0	9.0	20.6	349.5	9.2	47.8	510.8	5.2	80.0
PB16	320.2	6.6	29.9	356.8	5.7	43.0	433.8	9.7	76.4
PB48	338.5	8.6	35.8	435.7	7.3	70.3	509.0	3.3	94.3

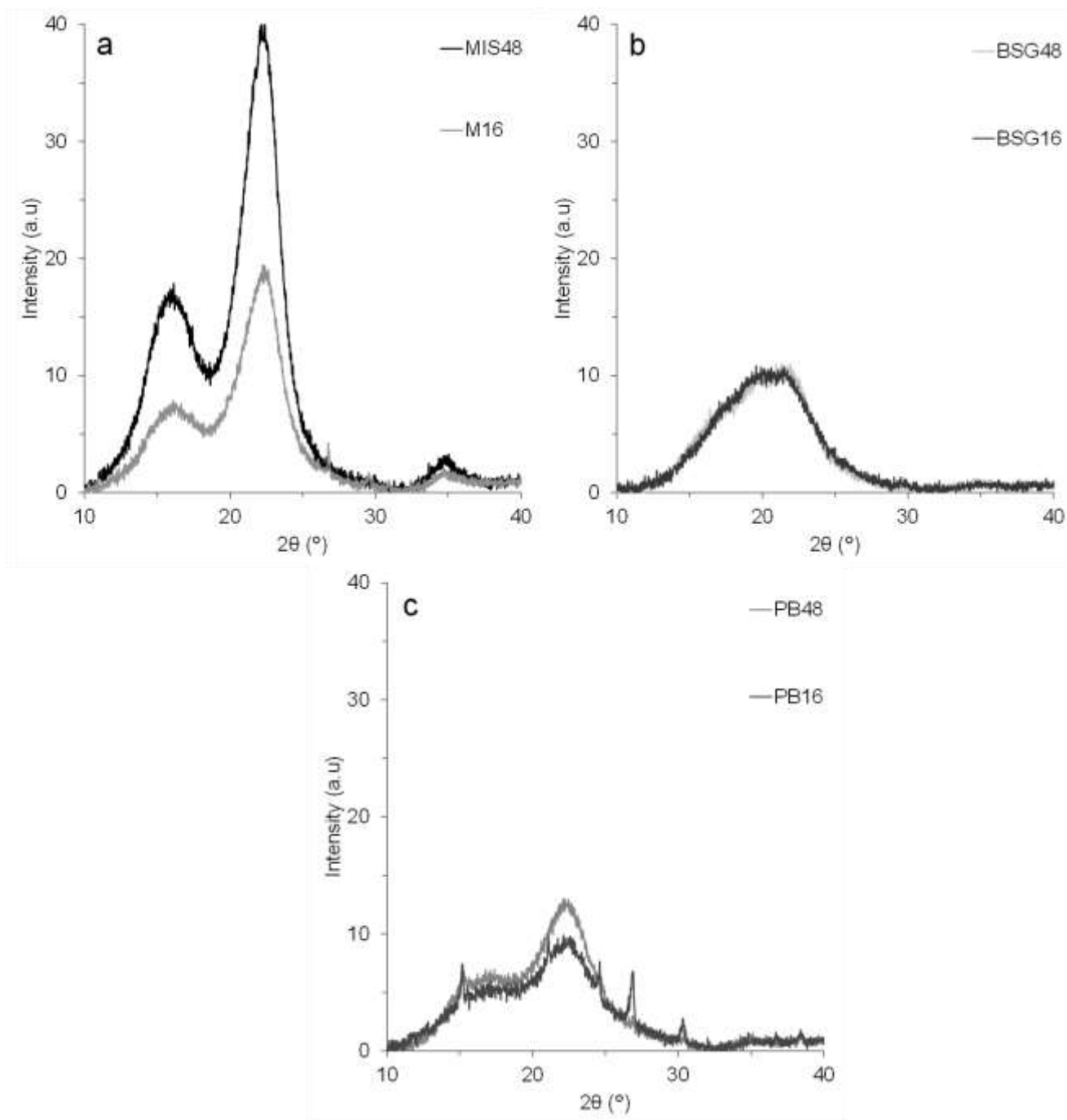


Figure A5.7. XRD diffractogram for lignocellulosic materials with different particle sizes 425-800 μm , <106 μm , MIS (a), BSG (b) and PB (c).

Table A5.8. XRD diffractograms for lignocellulosic materials in different particle size ranges.

Material	<i>CrI</i> (%) Original	Crystallite size (nm)
MIS16	75.71	3.1
MIS48	76.7	3.2
BSG16	36.69	1.2
BSG48	36.36	1.1
PB16	58.15	2.5
PB48	61.05	2.6

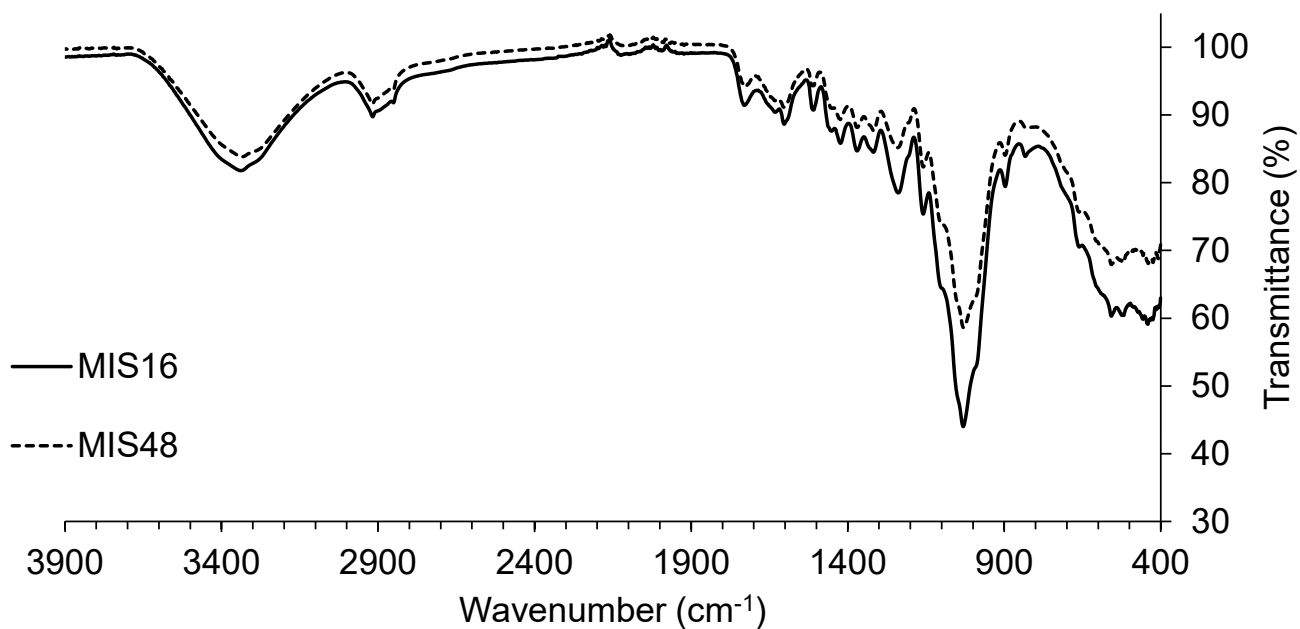


Figure A5.8. ATR wavelength range 3900-400 cm⁻¹ for MIS106 and MIS48.

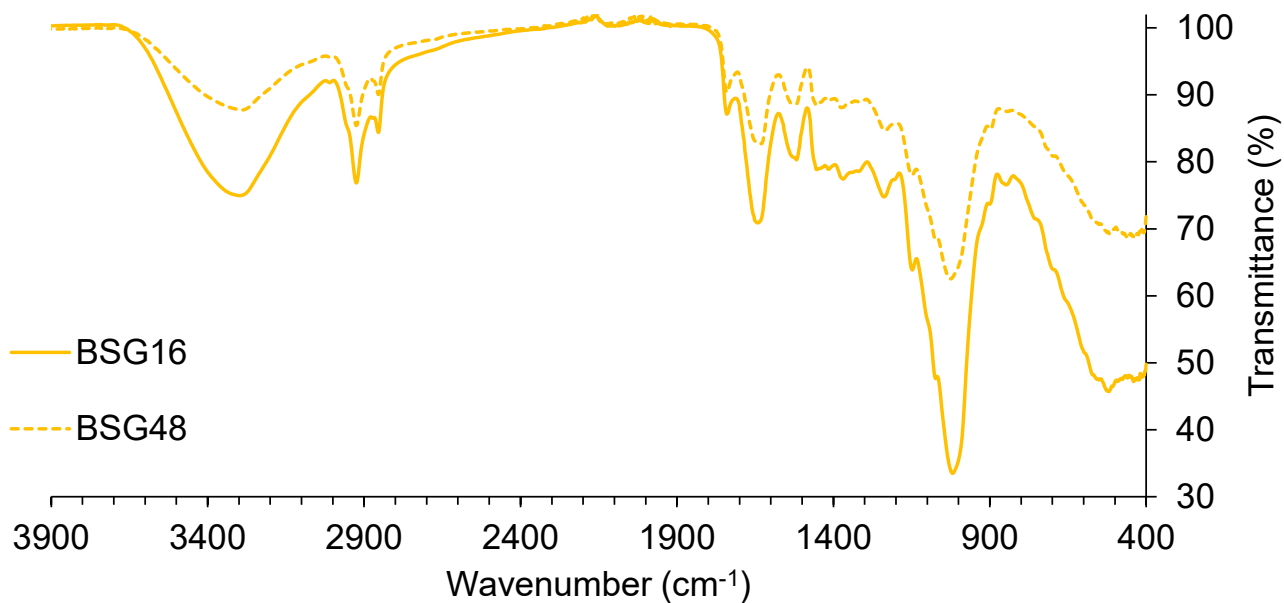


Figure A5.9. ATR wavelength range 3900-400 cm^{-1} for BSG106 and BSG48.

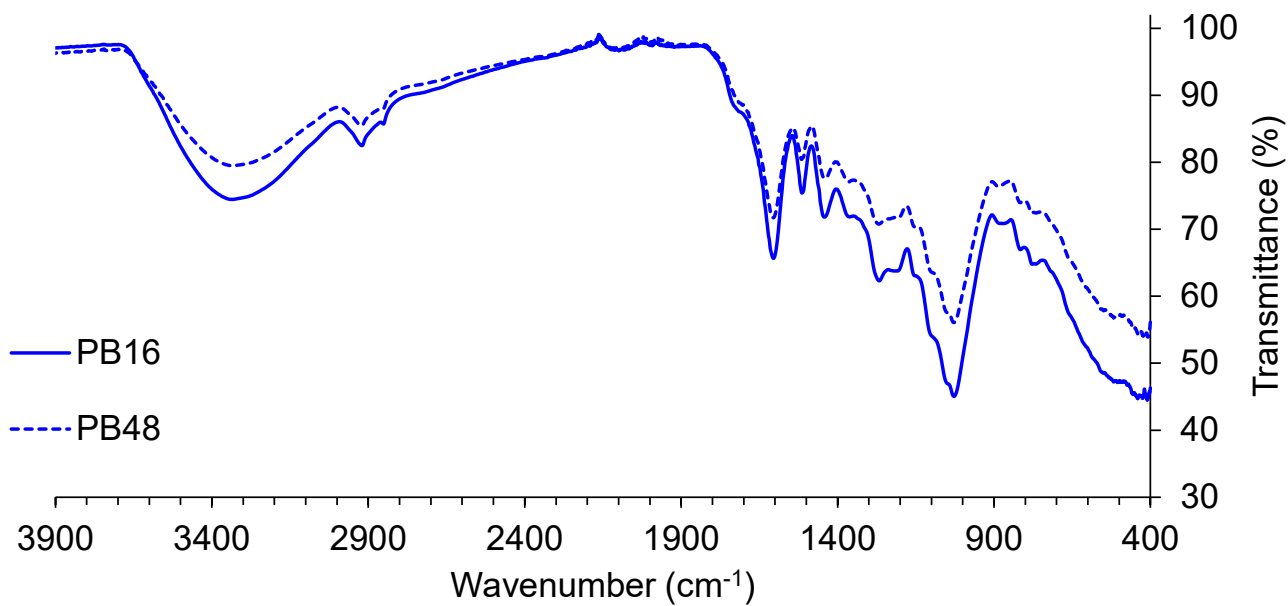


Figure A5.10. ATR wavelength range 3900-400 cm^{-1} for PB16 and PB48.

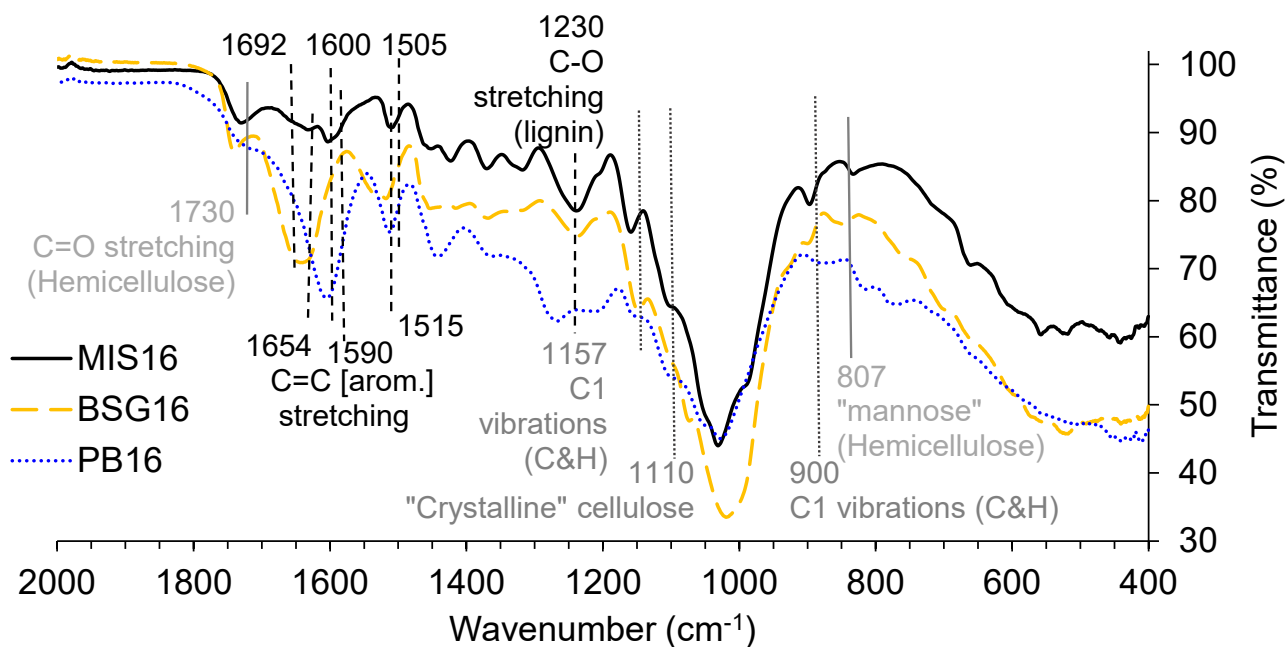


Figure A5.11. ATR wavelength range 2000-400 cm^{-1} for raw materials particle size $<106 \mu\text{m}$.

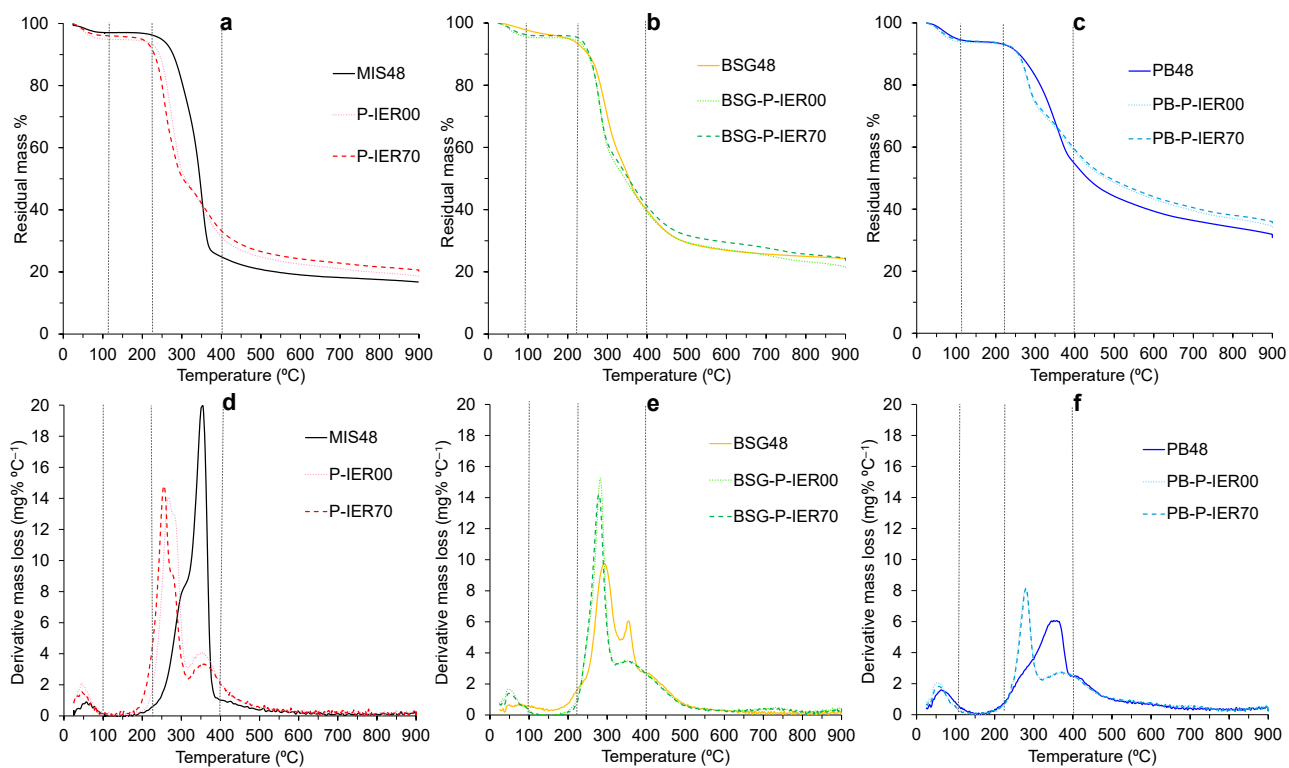


Figure A5.12. TGA-DTG curves under inert conditions for lignocellulosic materials, treated with TS80-IER70 for materials M48 (a, d), BSG48 (b, e) and PB48 (c, f).

Table A5.9. TGA-DTG peak temperatures-mass loss under inert conditions for lignocellulosic materials, treated with TS80 and IER70 for materials.

Material	1 st DTG (°C)	DTG (wt.% °C ⁻¹)	Mass loss (wt.%)	2 nd DTG (°C)	DTG (wt.% °C ⁻¹)	Mass loss (wt.%)	3 rd DTG (°C)	DTG (wt.% °C ⁻¹)	Mass loss (wt.%)
MIS48	303.8	8.1	20.6	355.5	20.0	61.7	-	-	-
P- IER00	268.6	14.1	25.3	282.8	12.9	36.6	359.3	4.0	60.9
P-IER70	257.3	14.7	26.1	280.0	9.0	41.3	367.8	3.3	61.4
BSG48	294.2	9.7	26.6	353.7	6.0	49.7	413.2	2.6	62.4
BSG-P-IER00	282.8	15.3	28.0	365.0	3.4	54.4	-	-	-
BSG-P-IER70	280.0	14.2	25.8	365.0	3.4	52.5	-	-	-
PB48	294.2	3.4	15.9	350.8	6.1	32.1	401.8	2.4	45.7
PB-P-IER00	277.2	8.0	17.3	370.7	2.7	37.0	-	-	-
PB-P-IER70	280.0	8.2	17.9	382.0	2.7	37.9	-	-	-

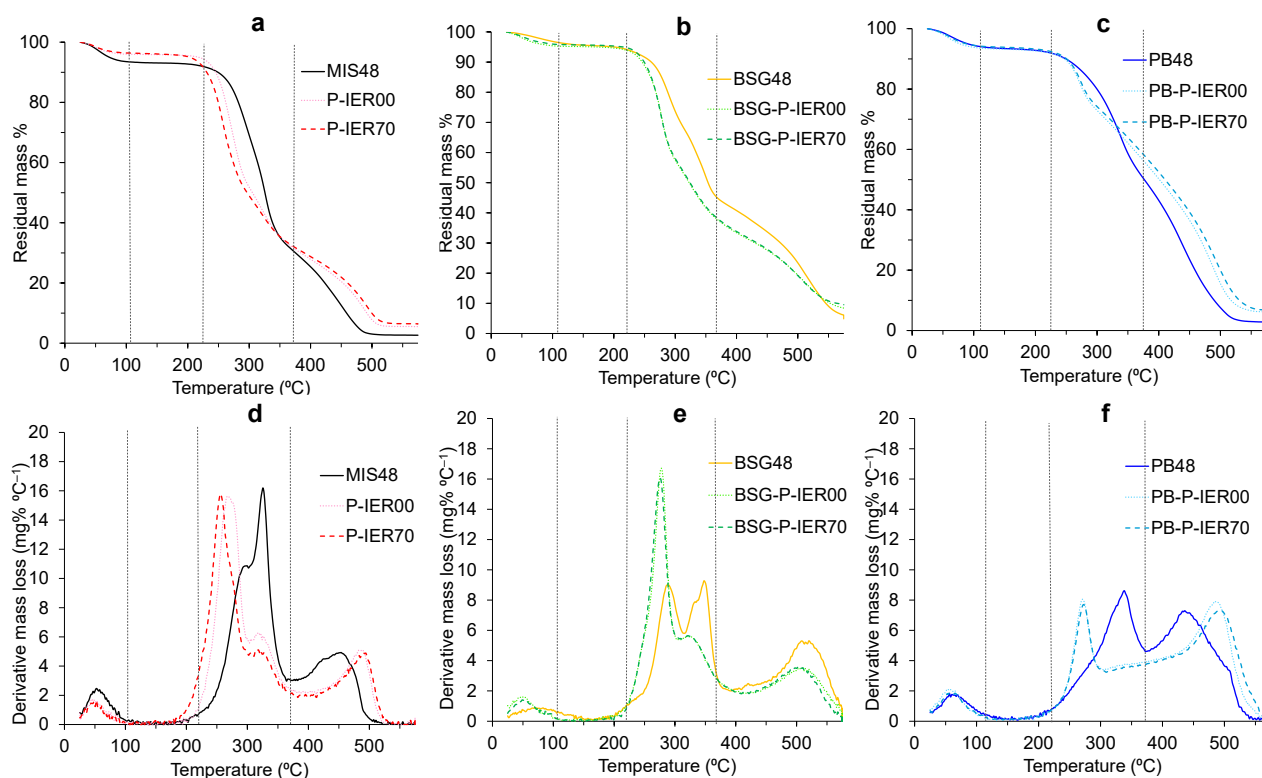


Figure A5.13. TGA-DTG curves under oxidative conditions for lignocellulosic materials, treated with TS80 and IER70 for materials M48 (a, d), BSG48 (b, e) and PB48 (c, f).

Table A5.10. TGA-DTG peak temperatures-mass loss under oxidative conditions for lignocellulosic materials, treated with TS80 and IER70 for materials.

Material	1 st DTG (°C)	DTG (wt.% °C ⁻¹)	Mass loss (wt.%)	2 nd DTG (°C)	DTG (wt.% °C ⁻¹)	Mass loss (wt.%)	3 rd DTG (°C)	DTG (wt.% °C ⁻¹)	Mass loss (wt.%)
MIS48	296.3	10.9	28.5	325.6	16.2	50.0	454.0	4.9	88.6
P- IER00	270.6	15.6	28.0	322.0	6.2	56.0	488.8	5.1	89.1
P-IER70	257.8	15.6	27.4	320.1	4.9	57.0	494.3	4.9	88.5
BSG48	289.0	9.0	20.6	349.5	9.2	47.8	510.8	5.2	79.9
BSG-P-IER00	278.0	16.7	28.3	325.7	5.6	51.0	510.8	3.5	82.9
BSG-P-IER70	276.2	16.1	27.0	323.8	5.6	49.9	505.3	3.5	81.9
PB48	338.5	8.6	35.8	435.7	7.3	70.3	509.0	3.3	94.3
PB-P-IER00	270.7	8.1	17.4	483.3	7.9	76.8	-	-	-
PB-P-IER70	272.5	7.7	17.0	494.3	7.3	77.5	-	-	-

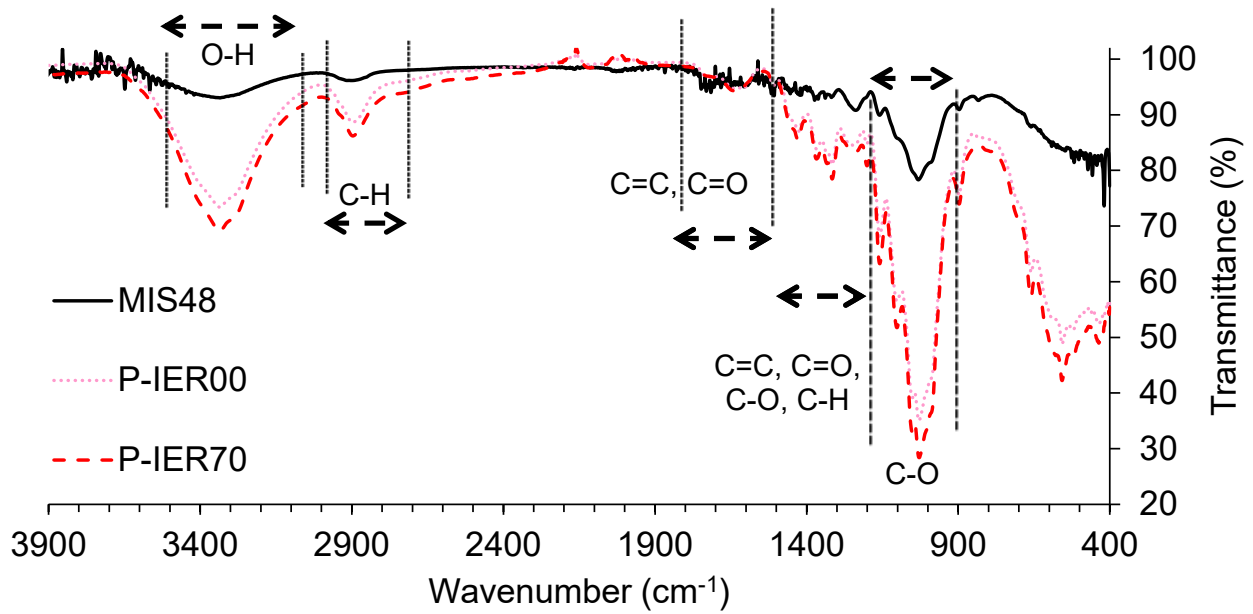


Figure A5.14. ATR-FTIR for MIS48, pulp TS-IER70 treatment range 3900-400 cm^{-1}

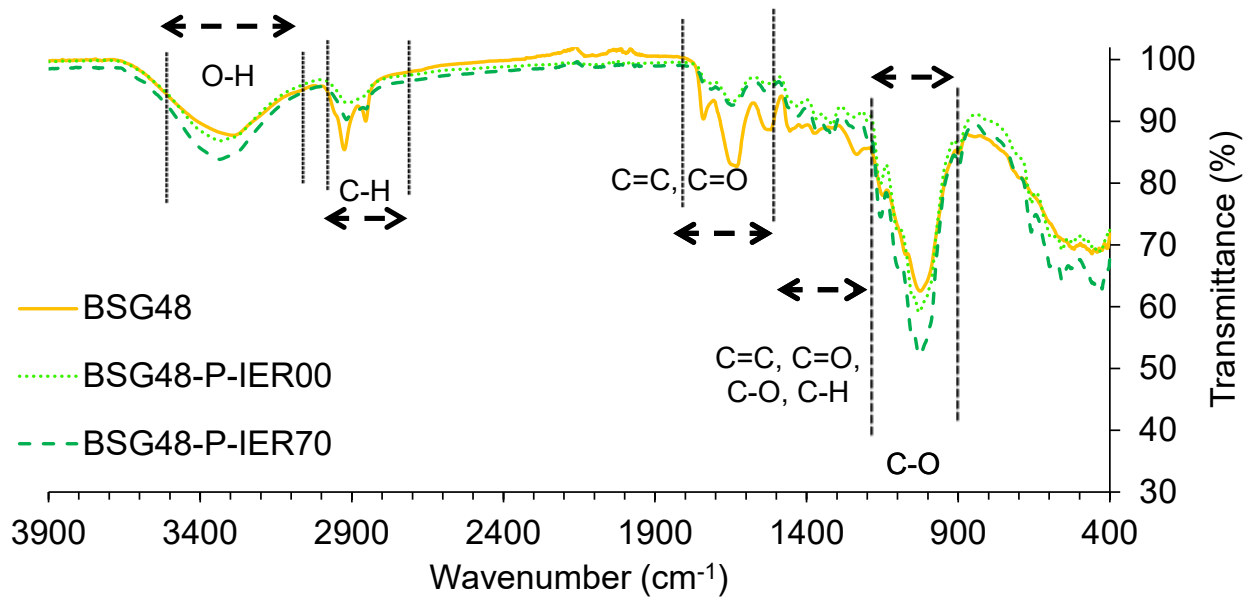


Figure A5.15. ATR-FTIR for BSG48, pulp TS80-IER70 treatment range 3900-400 cm^{-1} .

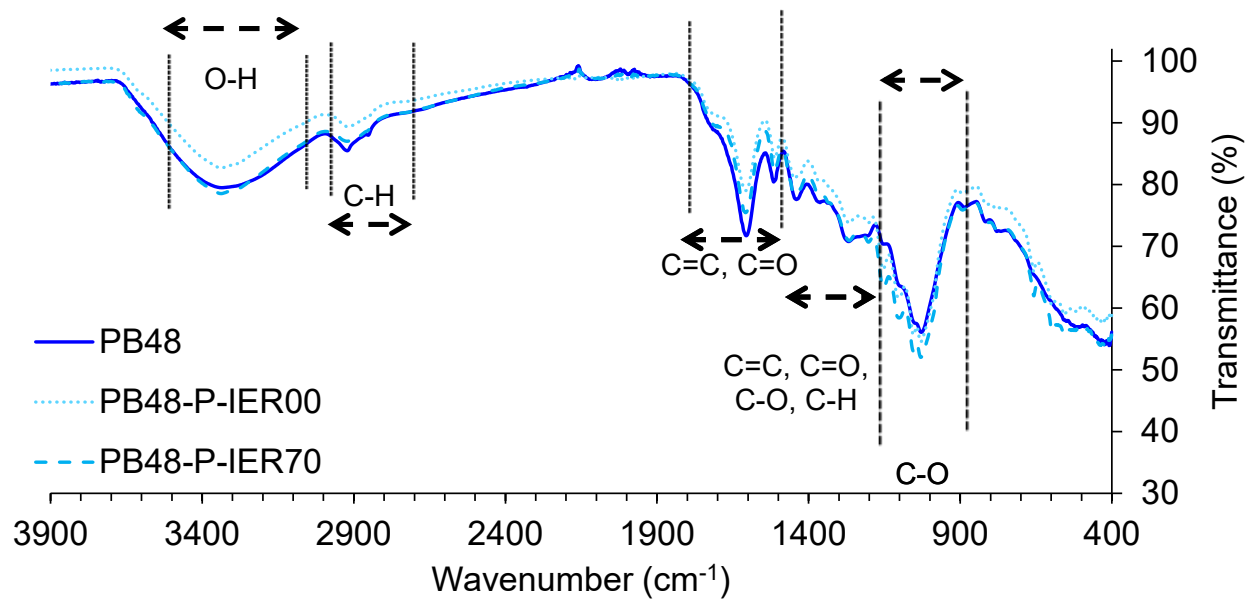


Figure A5.16. FTIR-ATR for PB48, pulp TS80-IER70 treatment range 3900-400 cm^{-1} .

